University of Southampton

Engineering and the Environment

PROGRESSIVE COLLAPSE MITIGATION USING CMA IN RC FRAMED BUILDINGS

Ben Punton

December 2014

Thesis for the degree of Doctor of Philosophy

Supervisors: Prof. S. Moy & Dr. M. Byfield

Abstract

Mitigation of progressive collapse after an initial failure has become a primary concern of engineers in recent years. Often alternative load paths are sought to redistribute load from the damaged area. It has been recognised for some time that the omission of compressive membrane action (CMA), also termed ‘arching action’, can lead to a significant underestimation of load capacity. An investigation has been conducted to ascertain whether the additional load carrying capacity from CMA can provide an inherent alternative load path to aid robustness.

A series of scaled specimens with industry standard detailing have been designed for an experimental investigation. Reinforced concrete elements were modelled in the double span scenario once an intermediate column has been removed. The test rig used allows the central support to be removed followed by the application of a point load applied at midspan; the system is determinate including measurement of the horizontal reaction. Subsequent to the flexural response two modes of membrane action are induced, initially compressive until tensile membrane extends load capacity at high values of deflection. The response during the latter tensile phase is outside the scope of this research.

Comparisons of experimental data with analytical methods inclusive of CMA have demonstrated that whilst conservative the method by Merola (2009) provides a reasonable prediction. This method has been utilised in a study of a series of flat slab structures with a range of column spacings. The inherent restraint stiffness provided by the surrounding slab and frame has been quantified using FEA and has allowed for the extent to which CMA can improve the robustness of a structure to be determined.

Acknowledgements

Professor Stuart Moy's expertise and willingness to provide support has been invaluable to the completion of this thesis.

I would like to express my gratitude to Peter Smith. Peter was a fellow PhD student at the university conducting a 'Robustness Assessment of Framed Buildings'. A focal and novel part of his research was testing to investigate the tensile membrane action or 'Catenery Action' developed in reinforced concrete structures in the damaged state. Peter and I have collaborated in the design and construction of the test rig used by the two of us. As such experimental results have been used in both of our theses, the differentiating feature of the two is that work presented in this thesis focuses on the compressive phase of behaviour, whilst Smith, P. P. (2014) contains results and analysis based on the tensile phase of response. A more detailed description of the collaboration between the author and P. Smith is outlined in the introduction to Chapter 3. His hard work, motivation and technical input throughout the experimental programme to overcome problems and delays have been invaluable. I would like to extend this gratitude to all the laboratory technicians for their technical advice and support.

Declaration

I Ben Punton declare that the thesis entitled "Progressive Collapse Mitigation using CMA in RC Framed Buildings" and the work presented in the thesis are both my own, and have been generated by me as the result of my own original research.

I confirm that where the thesis is based on work done by myself jointly with others, I have made clear exactly what was done by others and what I have contributed myself; namely collaboration on the experimental investigation.

Part of this work has been published as:

Punton et al. (2011)

Table of Contents

List of Tables

List of Figures

Nomenclature

Abbreviations

ALS	Accidental loading state
CMA	Compressive Membrane Action
CV	Coefficient of Variance
DLF	Dynamic Load Factor
DIF	Dynamic Increase Factor
FOS	Factor of Safety
RC	Reinforced Concrete
VBIED	Vehicle-Bourne Improvised Explosive Device
WWII	World War II

Latin Letters

a	Portion of half depth measure from the centreline no longer in contact with the support, McDowell et al. (1956)
a_1	The depth of section available for arching, Christiansen (1963)
A	Cross sectional area
ALS^{BS}	Accidental loading defined by BS:8110:1997
ALS^{EN}	Accidental loading defined by Eurocode 2
ALS^{GSA}	Accidental loading defined by GSA guidelines
A_s, A'_s	Area of tension and compressive steel reinforcement
b	Width of cross-section
C_C	Additional compressive force per unit width due to arching, Christiansen (1963)
C_1, C_2	Concrete compressive force at section 1 and 2 respectively, where 1 refers to hogging section and 2 refers to sagging section (Merola)

d	Effective depth, distance from the compressed face of the concrete to the centroid of the tension steel
d'	Distances from the compressed face of the concrete to the centroid of the compression steel
d_1	Half of the depth of arching section, Rankin and Long (1997)
d_o	Half the section depth, McDowell et al. (1956)
e_c	Strain associated with the crushing strength of the masonry material, McDowell et al. (1956)
E_c	Short-term static elastic modulus of concrete
f_c	Constant average compressive stress, Christiansen (1963)
f_{cd}	Concrete design compressive strength
f'_c	Concrete cylinder compressive strength (0·8 × cube strength)
f_{ck}	Characteristic cylinder strength
f_{cu}	Crushing strength of concrete cube
f_y	Yield stress of steel reinforcement
f_{yk}	Characteristic yield strength of the steel, Merola (2009)
f_{ult}	Ultimate stress of steel reinforcement
f_{st}	Stress in tension steel – BS8110 parabolic stress block calculations
f_{sc}	Stress in compressive steel – BS8110 parabolic stress block calculations
F_{s1}, F_{s2}	Steel tensile force at section 1 and 2 respectively, Merola (2009)
F'_{s1}, F'_{s2}	Steel compressive force at section 1 and 2 respectively, Merola (2009)
G_k	Dead load
h	Overall depth of section
H, H_1, H_2	Axial force in a arch, horizontal compressive reaction at support
H_{max}	Maximum horizontal axial compressive force

I_g	The gross cross-sectional moment of inertia
k	Static moment coefficient, Rankin and Long (1997)
k_1	Axial restraint stiffness ratio, Merola (2009)
k_1,k_2	Constants for calculation of parabolic stress block BS8110:1997
K	Stiffness of elastic spring restraint, Rankin and Long (1997)
l_J	The length of yield line or its projected length onto the axis of rotation for that region, Johansen (1972)
l_n	The clear span from the face of the centre column to an edge column, Su et al. (2009)
L	Full span considered, between rigid restraint
L_{cf}	The point of contraflexure
L/d	Span to depth ratio
L_1	Test span from experimentation
L_e	Half span
L_o	Original single span
L_r	Half span of equivalent rigidly-restrained strip, Rankin and Long (1997)
m	The moment of resistance of the slab per metre run, used in the yield line theory.
M, M’	Sagging bending moment at mid-span and hogging bending moment at support
M_a	Arching moment capacity for elastic restraint, Rankin and Long (1997)
M_{ar}	Arching moment capacity for rigid restraint, Rankin and Long (1997)
M_b	Positive bending moment capacity ,Rankin and Long (1997)
$\overline{\overline{M_b}}$	Negative bending moment capacity, Rankin and Long (1997)
M_n	Bending moment at support, Yu and Tan (2011)
M_p	Bending moment at mid-span, Yu and Tan (2011)

M_r	Arching moment ratio, Rankin and Long (1997)
M_u	Integrated moment of resistance, Rankin and Long (1997)
M(u)	Arching moment for rigid restraint at a deflection parameter of u, McDowell et al. (1956)
M_{u1}, M_{u2}	Bending moment acting at mid-depth of section 1 and 2 respectively, Merola (2009)
M_y	The bending moment at which yielding of reinforcement occurs
N_J	Loads(s) acting within a particular region, Johansen (1972)
N_{u1}, N_{u2}	Membrane force acting at mid-depth of section 1 and 2 respectively, Merola (2009)
P	Applied point load
P'	Enhancement factor, ultimate load supported by CMA over reaction of failed column
P_a	Component of total load carried by arching, Rankin and Long (1997)
P_b	Component of total load carried by bending, Rankin and Long (1997)
P_E	Enhanced central point load
P_F	Predicted load form modified Merola method, with the application of empirical factor
P_{max}	Maximum applied point load in the compressive phase
P_p	Predicted enhanced ultimate load capacity, inclusive of CMA
P_R	Assumed reaction of removed column i.e. self weight of half span
P_t	Experimental ultimate load
P_u	Predicted ultimate load capacity
P(u)	Arching force per unit width of the beam, McDowell et al. (1956)
q	Uniformly distributed self weight
Q_k	Imposed load

r(u)	Moment arm shown in Figure 9, McDowell et al. (1956)
R	Geometric and material property parameter for arching, Rankin and Long (1997)
R_A, R_B, R_C, R_D	Experimental vertical reactions
S	In-plane lateral stiffness of the end support, Park and Gamble (2000)
S_o	Combined in-plane stiffness of slab and surround, Eyre (1997)
S_S	In-plane stiffness of slab strip, Eyre (1997)
t	Lateral movement at each end of sample, Park and Gamble (2000)
T, T'	Force per unit width in the compressive and tensile reinforcement respectively, Christiansen (1963)
T_1, T_2	Force per unit width in the compressive and tensile reinforcement respectively, Christiansen (1963)
u	Non-dimensional centre arching deflection parameter, McDowell et al. (1956)
w_{ALS}	Uniformly distributed accidental loading
w_F	Predicted ultimate uniformly distributed from modified Merola method
w_p	Uniformly distributed load per unit area at, and after ultimate load in theory which includes membrane stresses, Park (1964b)
x	Depth of neutral axis
x_1, x_2	Neutral axis depth at section 1 and 2 of the beam respectively, Merola (2009)
y'	The location of the centroid of the stress distribution along the contact area, McDowell et al. (1956)
y_o	Defined in Figure 2.12 (McDowell)

Greek Letters

α	Enhancement factor empirically derived to apply to the flexural strength, Su et al. (2009)
α_{cc}	Coefficient taking account of long term effect on the compressive strength,

	Merola (2009)
β_1	Defined in ACI 318-95, Park and Gamble (2000)
β	Coefficient defining the position of the intermediate plastic hinge
β	Empirical factor to be applied to the Merola method derived from testing by Punton & Smith
γ_c	Partial safety factor for concrete
γ_s	Partial safety factor for steel
γ_w	Density of concrete
δ	Mid-span deflection
δ_J	The vertical displacement of the load(s) N on each region expressed as a fraction of unity, Johansen (1972)
δ_{Hmax}	Mid-span deflection normalised at peak horizontal compressive force
δ_{Pmax}	Mid-span deflection normalised at peak applied load
δ/h	Mid-span deflection normalised by the section height
δ/h_{Pmax}	Normalised mid-span deflection normalised at peak applied load
δ/h_{Hmax}	Normalised mid-span deflection normalised at peak horizontal compressive force
ε	Axial shortening from elasticity, creep and shrinkage, Park and Gamble (2000)
η	Coefficient defining the effective strength, Merola (2009)
θ_J	The rotation of the region about its axis of rotation, Johansen (1972)
θ_{CMA}	The plastic joint rotation at the maximum applied load during the compressive phase.
θ_{pra}	The plastic joint rotation.

θ_y	The elastic yield rotation.
λ	Ratio of the compressive zone to the neutral axis depth, Merola (2009)
ρ	Reinforcement percentage
Δ	Mid-span deflection

Chapter 1: Introduction

Membrane forces are not considered in the approved design codes currently used in the UK. The purpose of the work presented in this thesis was to determine the extent to which the robustness of an RC framed building can be improved by the inclusion of Compressive Membrane Action (CMA) in structural analysis. The abnormal situation when a column is lost on the perimeter of a building which creates a double span scenario as the slab bridges the failed column has been studied. Flat slab structures were chosen as the focus of the study due to their increased popularity as the chosen structural solution by architects and engineers alike in the UK. A series of scaled restrained RC specimens were tested, and their enhanced load capacities through CMA were measured. Test results provided data at the span to depth ratios expected in the double span situation that facilitated comparisons with analytical prediction methods. Thus an assessment of industry standard flat slab structures was made and the feasibility of CMA providing an inherent alterative load path to support accidental loading was assessed.

1.1 **Progressive Collapse**

When designing a building the structural engineer must consider its ability to protect the users and contents in a variety of situations. The primary function of any designed structure is to be able to support the vertical and horizontal static (wind loading is usually treated as being pseudo-static) loads to which the building will be subjected during its lifetime. These include the self-weight of the structure, the loads imposed by the occupants and contents, the force of the wind and perhaps thermal loading. As stated in the Building Regulations, consideration must be made in the design process for the behaviour of the structure in the unlikely event that the building is damaged. In particular, the focus should be directed to the loss of primary loading elements that are fundamental to the integrity of the structure. The damage that is caused as a consequence may propagate collapse of surrounding elements culminating in the loss of an extensive proportion of the floor area. Such a collapse is usually termed as

'progressive' and can be devastating to a structure and out of all proportion to the instigating event which can be small relative to the extent of collapse.

The initial failure can be caused by an accidental event or by a deliberate act of vandalism or terrorism. The most famous example of progressive collapse being triggered by an accidental event is the collapse of Ronan Point, a 22-storey tower block in London, in 1968. A natural gas explosion in a flat on the 18th floor caused the loss of the exterior load bearing wall panel and consequently the collapse of the rest of the building above to the roof followed by the remainder of the building to the ground due to the weight of falling debris from above. This triggered the first requirement in the building codes for accidental loading to be considered in the design of multi storey buildings. The Building Regulations were changed in 1970 so that any building over five stories should not suffer from collapse disproportionate to an event of accidental local damage.

Since 1970 numerous events across the globe have influenced the agenda of building codes forcing increased measures of protection against deliberate acts to cause damage. Terrorist incidents from the bombing of the US Marine Corps HQ in Lebanon in 1983 to the attack on the Murrah Federal building in 1995 have used the VBIED, Vehicle-Bourne Improvised Explosive Device; or the "car bomb". These devices with charge weights ranging from 450kg equivalent TNT in a large car to 4500kg in a small box van (ATF Car Bomb Table (2014)) can be placed in close proximity to buildings and the consequent damage to the structure can be devastating. Whilst the blast wave can cause substantial superficial damage to the cladding and glazing of the building, it is the damage to key structural elements that is of greater concern and relevance to the research reported here. A car bomb is more than capable of destroying a perimeter column but it is the subsequent behaviour of the structure that will determine the extent of collapse. In the case of the Murrah Building for example, progressive collapse ensued causing the collapse of nearly half the floor space of the building and considerable loss of life.

1.2 **Mitigation Recommendations in Current Codes and Guidelines**

The current UK Building Regulations Part A state that for class 2B buildings (see chapter 2) an alternative load path method based on the instantaneous removal of key structural elements

can be employed to check against progressive collapse. Structural integrity is assessed with either the notional removal of key columns, beams supporting one or more columns, or a nominal length of load bearing wall. Alternative load paths have to be provided in a number of ways to provide robustness to the damaged structure. Masonry infill panels, usually considered non-load bearing, have proved to be effective examples of this as shown in buildings damaged by bombing in World War II. Compressive struts form in masonry panels once a primary element such as a column has been lost and allow load to be redistributed away from the localised failure by a cantilever effect. Truss systems, usually at the top of the building, are now common practice in the design of high rise buildings in combination with effective vertical tying to redistribute load. All of these techniques can be readily employed to provide robustness in the design of new structures. When these methods have not been included in the structure, alternative load paths are harder to find and more research is needed to find inherent ways for the structure to redistribute load.

1.3 **Membrane Action**

Modern codes of practice contain approved methods for the design of reinforced concrete buildings based on elastic or plastic material behaviour but they do not allow the designer to include the effects of membrane (in-plane) forces, even in an accidental load case. Bridge design codes in Northern Ireland and Canada do allow the utilisation of compressive membrane action, but care must be taken in doing so, Department of the Environment, Northern Ireland (1986), Ontario Ministry of Transport and Communications (1983). For compressive membrane forces to be induced in reinforced concrete slabs horizontal (longitudinal) restraint must be provided by the surrounding structure; the onset of cracking and transverse deflection results in a movement of the neutral axis and effectively the slab is jammed between the supports, producing an increase in the ultimate load (compared to the value calculated by conventional methods such as yield line analysis). This process is also described as ‘arching action’ or compressive membrane action. It has been recognised by researchers for some time that the omission of compressive membrane action (CMA) can lead to a significant underestimation of load capacity. The contribution of CMA was highlighted in the 1950’s when a series of tests on full scale buildings were carried out in South Africa by Ockleston (1955). It was found that the ultimate load could be enhanced by anything up to four times that

predicted using the Yield Line Theory developed by Johansen (1972). Since the early work by Ockleston (1955) a number of investigations have been carried out to understand CMA.

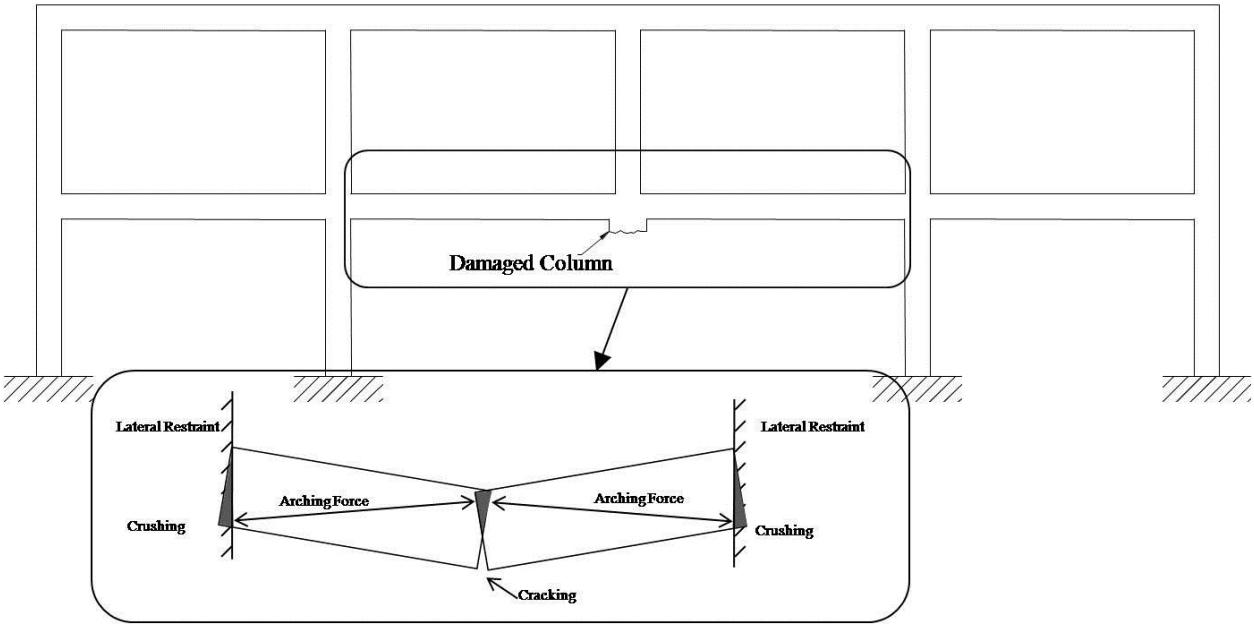

Figure 1.1: *Principle of compressive membrane action as an alternative load path.*

Extreme loading events such as blasts, either from high explosives or natural gas deflagration can cause the failure of exterior primary columns in framed buildings. In such situations the structure must have adequate robustness to prevent the onset of progressive collapse. There is a need for redundancy by the provision of alternative load paths, which could be provided for example by CMA developed because of the restraint of surrounding interior panels and shear walls. It has not yet been fully investigated whether CMA can provide sufficient additional load capacity such that it would allow the slab to span the damaged column under accidental loading conditions, Figure 1.1, in structural frames typical of those currently used in real structures. The effect of a column being lost at the edge of the building gives added complexity due to the variation of lateral restraint, particularly in flat slabs which are commonly used in construction today. The research reported here has entailed the investigation of the extent of CMA in reinforced concrete framed buildings which have lost a primary exterior column and an assessment of the feasibility and extent to which CMA can provide robustness. Of particular interest have been the benefits of CMA at the very large span to depth ratios that would be found in flat slabs following the loss of a column Other research

has been confined to smaller span to depth ratios so this research has made an original contribution to knowledge in this respect.

1.4 Aims and scope of the research

1.4.1 Aims:

1. To investigate the extent to which CMA can be mobilised in RC flat slab structures at the large span to depth ratios that would be found in flat slabs following the loss of a column.

2. To determine the feasibility and limitations of utilising CMA as an alternative load path and its ability to provide sufficient robustness to a structure by quantifying the range of column grid spacing that would allow accidental loading to be supported.

3. To assess the influence structural form has on the restraint stiffness provided and consequently on the development of CMA.

1.4.2 Scope:

The scope of the research dictates that only multi-storey RC commercial or office buildings that have glass/light weight cladding or open architecture have been considered. This is so that the structure must find internal emergency load paths rather than rely on masonry infill panels or cladding. The focus has been on exterior panels towards the centre of an edge of the building that have one edge unsupported; corner panels have not been considered. The phenomenon of CMA is closely related to that of tensile membrane action (TMA). TMA occurs after the compressive membrane phase once the slab has undergone significant deflection. There is also potential for load enhancement through this mechanism, however tensile membrane action is outside the scope of this investigation.

1.5 **Thesis Layout**

The thesis will present how the aims of the research have been achieved. The thesis is laid out in the following order:

Chapter 2 - Literature Review

A review of work that has been carried out since the 1950's examining the potential of CMA in various situations, including extensive numerical and experimental research to validate CMA prediction models. Focus is put on factors that affect CMA at the high span to depth ratios expected in the double span condition after removal of a column and instances of CMA being used as a robustness tool are also presented.

Chapter 3 - Experimental Study of CMA in RC Buildings

The literature review highlights the need for experimental data of restrained specimens at large span to depth ratios. A large scale experimental investigation has been devised to model two perimeter bays of an RC building with the loss of the central support. Specimens were developed with various span to depth ratios to represent the range of column spacings in typical flat slab structural frames. Longitudinal restraint was provided by a steel assembly and the specimens were loaded under displacement control until the end of CMA. (In fact loading was continued into the TMA stage and was continued until failure occurred by reinforcement fracture. However the TMA stage was the subject of a separate research programme)

Chapter 4 - Experimental Study Results and Analysis

Results from the experimental programme and analysis of those results are presented. The behaviour of the specimens under loading has been analysed and the influence of key factors such as the span to depth ratio and the percentage of reinforcement has been assessed. Key trends in results were identified and the load enhancement achieved through CMA has been assessed.

Chapter 5 – Predicting the Benefits of CMA

The prediction methods reported in Chapter 2 have been assessed against experimental testing to determine their accuracy. A prediction method has been chosen that provides a suitable degree of accuracy such that it could be used with confidence in predicting the behaviour of flat slabs in the double span condition following loss of a column.

Chapter 6 – Frame Assessment

Assessment of RC flat slab framed structures to determine the extent of CMA in emergency conditions. A parametric study has been conducted on a series of flat slab structures designed to the latest industry standards but with various column spacings. Analytical predictions of ultimate load inclusive of arching action have been made and compared with the accidental load case required by the design standards to determine whether CMA provides a safe alternative load path. The extent to which CMA improves the robustness of RC buildings has also been determined. In order to determine the impact of structural form on the restraint stiffness provided by the rest of the structure to the damaged region finite element analyses of various structural forms have been carried out and the results fed into the parametric study.

Chapter 7 – Conclusions and Recommendations

The findings from the thesis have been summarised and the recommendations based on research have been presented alongside recommendations for future research.

Chapter 2: Literature Review

2.1 **Introduction**

This chapter provides a background to the motivation for the research reported here. An overview of progressive collapse has been presented within which a series of case studies have been reviewed to highlight the structural mechanisms that have led to the onset of progressive collapse and conversely those that can aid robustness. In the light of these historical events several codes of practice currently in use, that have been developed to promote robustness, have been summarised in order to compare mitigation techniques. The concept of compressive membrane action (CMA) has then been introduced and a comprehensive review of prediction methods and experimental testing in this area has been presented. Finally the use of CMA in promoting robustness has been assessed.

2.2 **Progressive Collapse Background**

The concept of progressive collapse of a framed structure has been introduced below and to highlight its importance a review of example buildings that have suffered incidents with the potential to cause collapse has been conducted. Examples in which collapse occurred demonstrate through the severity of loss of life and building damage the need for engineers to design robust structures that are resistant to progressive collapse.

2.2.1 **Definitions**

"Progressive collapse - A situation where local failure of a primary structural component leads to the collapse of adjoining members which, in turn, leads to additional collapse", United States General Service Administration (2003)

The effect of failure of a small element in a structure has been observed in many cases to lead to the collapse of large parts or the entirety of a building. Whether a collapse can be described as disproportionate depends on the incident that triggered the collapse. For example if the blast

intensity was small relative to the size of the building or the element destroyed and resulted in a progressive collapse then the collapse can be described as disproportionate. (Nair 2006)

"Robustness – Ability of a structure or structural components to resist damage without premature and/or brittle failure due to events like explosions, impacts, fire or consequences of human error, due to its vigorous strength and toughness", United States General Service Administration (2003)

2.2.2 **Lessons from World War II Bombings**

Figure 2.1: *Front wall unsupported due to the unseating of a girder, Byfield (2006)*

During World War II (WWII) London was subjected to a persistent bombing campaign with aerial ordnance used ranging from 500 to 2000kg (1,000 to 4,000 lbs), Smith et al. (2010). Many structures sustained damage primarily from direct impact or detonation within close proximity. The behaviour of structures was observed and the findings were consolidated by Baker et al. (1948). Whilst many structures sustained local damage of varying degrees the onset of further progressive collapse was rare. The resistance of buildings to progressive collapse was attributed in part to the use of masonry panels. Many framed structures had masonry infill panels that were not load bearing but which segmented the structure. This gave the benefit of reducing the effect of blasts, but more significantly provided a series of alternative load paths. Once a primary structural element such as a column or girder was lost

compressive struts were formed in the masonry panels. This allowed for a cantilever effect to take place as load was redistributed away from the localised failure. As a result structures were noted to be able to resist collapse after considerable damage, Figure 2.1. With regards to progressive collapse resistance RC structures were also recorded to have performed well; this was attributed mainly to continuity within the structure. Flat slab structures were highlighted as outperforming fully framed structures due to the higher level of continuity provided, Smith et al. (2010).

2.2.3 **Ronan Point, 1968**

Figure 2.2: *Progressive collapse at Ronan Point, Pearson and Delatte (2005).*

Figure 2.3: *Close up of the damage at Ronan Point, Bussell and Jones (2010).*

The progressive collapse witnessed at the 22 storey block of flats at Ronan Point in Canning Town, East London has been frequently discussed with regards to awareness of progressive collapse of structures. Bussell and Jones (2010), Byfield (2006) and Khabbazan (2005) amongst others cite it as being a catalyst for change in the consideration and understanding of progressive collapse in the UK and subsequently across the world.

In May 1968 a match was struck on the 18th floor of Ronan Point which caused an accidental natural gas explosion. The construction consisted of large pre-cast concrete panels used for both wall and floor elements which had allowed rapid construction. This form of construction had been common practice since the 1950's. The technique essentially resulted in stacking precast apartments with each load bearing wall being placed on another to allow direct transfer of gravity loads. The explosion caused the failure of three load bearing walls removing support of the elements above which consequently led to the collapse of slab and wall panels up to the 22nd floor. A progressive collapse then ensued as the impact and weight of debris from collapsed floors caused the subsequent failure of floors below. The result was the loss of four lives and partial collapse of apartments from ground floor up to the roof as shown in Figure 2.2 and Figure 2.3.

The investigations that followed discovered that a poorly made connection from the gas supply to a cooker had degraded resulting in the gas leak. Whilst explosions from gas leaks were not uncommon in the UK, such extensive damage had not been experienced before. The report noted that an expected range of over-pressure from a gas explosion was 21-83kN/m^2 but the external wall may have experienced pressures of 34 – 42kN/m^2 over a very short time period; indicating that the blast therefore was not of an exceptionally large magnitude, Bussell and Jones (2010). The inquiry concluded that the structural system used was inherently dangerously susceptible to progressive collapse and no consideration had been made during the design phase for progressive collapse occurring.

Whilst the building complied with the design codes and building regulations in force at the time it was suggested that Ronan Point and towers like it were dangerously susceptible to collapse not only from an explosive triggering event but also through wind loading. The structure had been designed for wind loading below that to be expected for a multi-storey building. Collapse could have been brought on by strong winds causing the failure of load bearing walls, Pearson and Delatte (2005). It was also highlighted that the effects of fire on the building were not fully understood and the effect of thermal expansion causing premature collapse had not been considered.

The Building Regulations in the UK were amended in 1970 so that buildings of 5 storeys or more in height, formed with any structural material, had to be designed with consideration of

progressive collapse. It was required that consideration should be given to the behaviour of the structure with the notional removal of a primary structural element under emergency loading. The designer had to demonstrate that either the damage to the building was confined to the immediately adjacent floors and the lesser of 15% of the floor area or 750m^2. Alternatively key structural elements had to be designed to resist a nominal accidental load equivalent to 34 kN/m^2 over-pressure with reduced factors of safety for wind and imposed load. It was also recommended by the Institution of Structural Engineers that vertical and horizontal ties in both directions should be used, Bussell and Jones (2010).

As a result of the lessons learnt and legislation put in place directly after the incident at Ronan Point the consideration of the robustness of a structure and its resistance to disproportionate collapse is now an integral part of the design process. The requirements in the Building Regulations Part A are largely the same today and are discussed in detail later in this chapter.

2.2.4 **The Murrah Building, 1995**

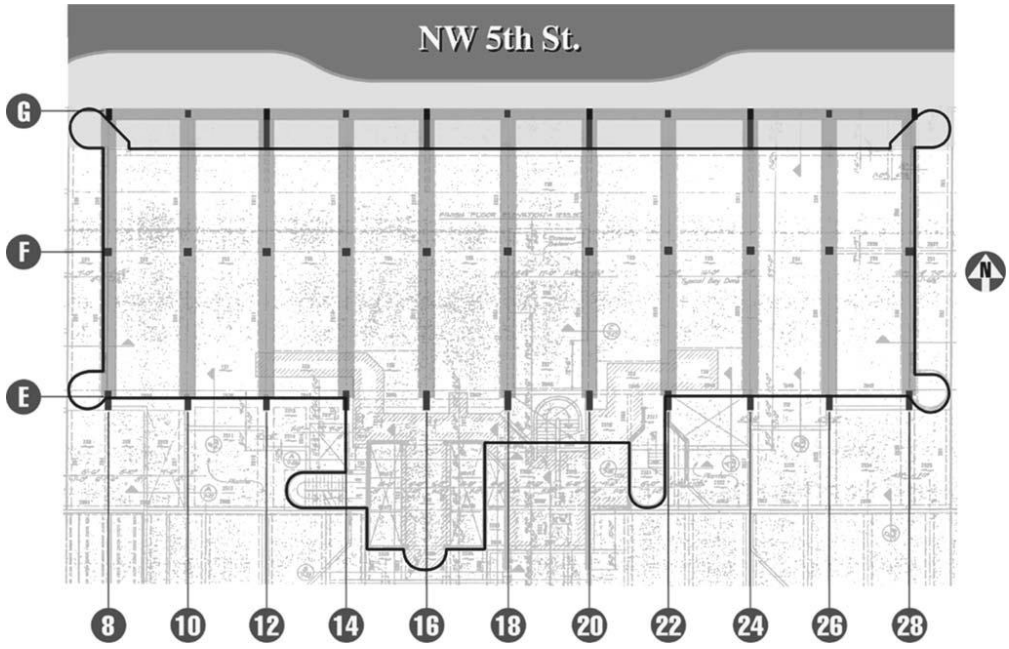

Figure 2.4: *Plan of Murrah Federal Building – Office Block, Osteraas (2006)*

The Alfred P. Murrah Federal Building in Oklahoma City, USA was a 9 storey reinforced concrete building constructed in the mid 1970's. The floor area was divided into a 6.1m x 10.7m grid of columns, with beams supporting one-way spanning slabs, as shown in Figure

2.4. Lateral strength was provided to the structure in the form of a series of shear walls and lift shafts. On the north elevation (the G Column line) a transfer beam was used to create the main architectural feature of the building of a recess between the ground and second floor. Alternate double storey height columns at twice the grid spacing to columns above the second floor were used. The function of the transfer beam was therefore to distribute the load from the higher floors where columns were spaced more closely to the more widely spaced columns below.

On April 19th 1995 a vehicle loaded with ammonium nitrate oil explosive was detonated approximately 5m from column G20. From analysis of the 8.5m diameter crater the charge size was thought to have been the equivalent of approximately 1800kg of TNT, Mlakar et al. (1998). The direct effect of the blast was the failure of column G20 in brisance, a process in which the shock wave produced was strong and fast enough to shatter the concrete. Adjacent columns G16 and G24 also failed in shear from the blast load. Progressive collapse was then induced as the transfer girder could not span the three failed columns and extensive lateral support was lost from the radiating blast. Around half the entire floor space, 10 out of 20 bays, of the nine story building collapsed.

Mitigation methods to reduce the extent of collapse have been looked at in depth. Sozen et al. (1998) suggested that improvement in shear reinforcement could have prevented the loss of G16 and G24, whilst increased continuity of reinforcement in the transfer beam might have helped the beam to span a single failed column. Detailing using seismic design methods might also have provided enough ductility to reduce the damage by 50% and allowed more of the structure to remain intact long enough for occupants to escape, Corley et al. (1998).

Ultimately the frame's lack of robustness caused the onset of progressive collapse, the perimeter frame was analysed and it was found that it could not support even its own self weight if one column was lost, Sozen et al. (1998). The open plan architecture meant that there were no alternative load paths provided through internal partitions and hence once three columns were lost the structure could not sustain itself. This case highlights the need for redundancy in a frame to provide alternative emergency load paths.

2.2.5 **World Trade Centre, 2001**

At 8:46am on September 11th 2001 American Airlines Flight 11, a Boeing 767-200ER with 87 people on board was flown at around 440mph into the north face of the north World Trade Centre tower in New York. The nose of the aircraft struck the 96th floor of the 110 storey tower. The impact damage of the plane entry extended between the 93rd and 99th floors. Then at 9:03am a second Boeing 767-200ER, United Airlines Flight 175 struck the south face of the south tower at around 540mph with 60 people on board. The entry damage of the plane stretched between the 77th and 85th floor. Each plane had an approximate weight at the time of impact of 124.3 tonnes. The impact of both planes caused extensive initial damage with exterior and core columns severed and many core columns and trusses stripped of their fire insulation. Both towers withstood the initial impact however the structural damage combined with intense fires which degraded material strength meant that eventually the structure near the impact load could not support the structure above. The impact and weight of the structure above caused progressive failures down to the ground floor. (National Institute of Standards and Technology NIST (2007))

Figure 2.5: *Layout of The World Trade Centre in Lower Manhattan,* National Institute of Standards and Technology NIST (2007).

WTC2 (the south tower) resisted collapse for around 55 minutes whilst WTC1 collapsed after around 1 hour and 45 minutes. A significant contributing factor to the delay before the onset of total collapse was the 'hat truss' that was installed at the top of each tower which allowed load distribution between the core and perimeter columns. This provided the structure with the ability to redistribute load from severed members to intact columns away from the impact points. The main reason for WTC2 collapsing more quickly was due to the greater damage caused to core columns. (National Institute of Standards and Technology NIST (2007))

2.3 **Mitigation Recommendations in Current Codes and Guidelines**

Events where localised damage caused progressive collapse of structures forced engineers to consider the robustness of their structural designs. The events at Ronan Point led directly to changes in the UK building codes, which can still be found in the current guidelines, Office of The Deputy Prime Minister (2004). Terrorist attacks on the US both in America and abroad led to several guidelines being published with recommendations for mitigating the potential for collapse in US federal, military and commercial structures. The events at New York in 2001 further reiterated the need for robustness in design for all new structures.

In the following sections modern codes of practice and guidelines have been reviewed and robustness recommendations summarised.

2.3.1 **Building Regulations Part A**

Requirement A3 in the current UK Building Regulations, which aims to reduce the sensitivity of buildings to disproportionate collapse, requires that *"The building is sufficiently robust to sustain a limited extent of damage or failure, depending on the class of the building, without collapse".* The regulations give requirements for a range of building classes. Commercial buildings commonly designed by structural engineers fall within classes 2 & 3, whilst class 1 buildings include houses not exceeding 4 storeys and agricultural buildings. An example of a class 2A building is a commercial (office) building under 5 storeys, whilst commercial structures of 5 or more storeys are classed as 2B. Any buildings that exceed the specified storey limit of 2A and 2B buildings, such as grandstands and buildings containing hazardous materials or processes fall into Class 3.

A building defined as class 3 is required to have a systematic risk assessment undertaken to identify all normal and abnormal hazards that can be reasonably foreseen throughout the lifetime of the building. Measures must then be taken to eliminate these risks and mitigate disproportionate collapse. In the case of blast these will often include provision for safe stand-off distances in the form of vehicle exclusion zones and bollards. Other such systems include blast resistant glass, blast resistant up-stands and layering the internal layout of the building. The building must also be designed as a class 2B structure.

It is recommended that Class 2A buildings are designed with horizontal ties whilst class 2B have to be detailed with both horizontal and vertical ties. In regards to the detailing of effective horizontal and vertical ties the regulations reference the relevant Eurocodes for the design of structures using masonry, steel and reinforced concrete. Steel structures must have connections designed for prescribed axial tie forces dependent on the beam spacing, floor loading and the position of ties (perimeter or external). For reinforced concrete structures the detailed rules laid out in the Eurcodes provide sufficient continuity through vertical and horizontal ties. Similar tying systems are used in buildings designed in seismic regions, with great success in resisting abnormal loading.

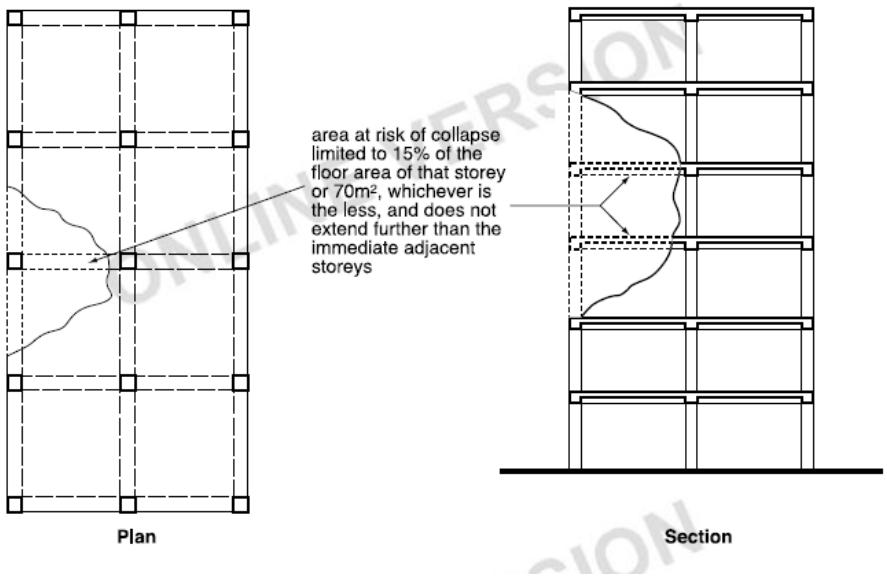

Figure 2.6: *Area at risk of collapse in the event of an accident.Office of The Deputy Prime Minister (2004)*

An alternative approach for class 2B buildings is to consider the alternative load path method based on the instantaneous removal of columns. The structural integrity is then assessed with the notional removal of columns, beams supporting one or more columns or a nominal length of load bearing wall. Upon the removal of a column it must be ensured that the area at risk of collapse is limited to 15% of the floor area or $70m^2$, whichever is the smaller, as shown in Figure 2.6.

If the extent of damage is assessed as being larger than the allowable limits then the elements that have been notionally removed must be designed as 'key elements'. A 'key element' is one that has been designed to withstand an accidental design over-pressure loading of $34kN/m^2$ in either the vertical or horizontal plane. This is a separate load case which has to be considered with a reduced combination of the characteristic loading, wind and imposed load, on the element. Any connecting members that provide stability to the key element i.e. bracing or intermediate beams that provide lateral restraint must also be designed as key elements. Key element design is commonly used in blast resistant design and is often applied to primary structural supports and the exterior of the building. It is also referred to as the specific local resistance method.

2.3.2 **Eurocodes**

As well as the guidelines outlined in the UK National Annex which are very similar to those of the UK Building Regulations, BS EN 1991-1-7:2006 gives recommendations for design against progressive collapse. The accidental design situations are divided into two strategies, one based on identified accidental actions and the other based on limiting the extent of localised failure. The first strategy involves three processes:

- Designing the structure to have sufficient minimum robustness
- Preventing or reducing the action e.g. protective measure
- Designing the structure to sustain the action

A degree of risk assessment is required with this strategy as the number and severity of actions must first be defined before it is determined whether actions can be prevented or if the structure can be designed to withstand the action. This may be a problematic approach for clients whose structures are susceptible to a large number of actions. Some localised damage

can be acceptable from a perceived action if the structure is designed with sufficient robustness such that it will not endanger the stability of the whole structure. This approach is undertaken more often for bridge structures.

The second strategy used more commonly for building structures is based on limiting the extent of localised failure and essentially details the requirements to ensure the Building Regulations Part A3 are adhered to through the following measures:

- Enhanced redundancy through alternative load paths
- Key element design to sustain the uniformly distributed load of 34 kN/m^2
- Prescriptive design and detailing rules to ensure integrity and ductility through tying measures.

2.3.3 **General Services Administration 2003**

Guidelines developed by the United States General Services Administration (GSA) on progressive collapse design and analysis, aimed at New Federal Buildings and modernization projects were published in 2003, United States General Service Administration (2003). The main purposes of these guidelines are to reduce the potential for progressive collapse either in new or existing Federal Office Buildings. In both cases the aim is to protect human life and the function and assets of the building.

The guidelines provide a series of flow charts that evaluate the potential for progressive collapse in a structure and provide a process for exemption from further consideration when a structure is deemed to be at low risk. The exemption process takes into account the structural form, occupancy and functional use of the building.

Once a structure has been deemed not to be exempt from further analysis to prevent progressive collapse the guidelines provide a series of analysis procedures with clear direction on the applicability of each one. A linear static or dynamic (quasi-static) approach is deemed to be a simplified analysis method and its use is limited to low-to-medium rise buildings. Such buildings are defined as being below 10 storeys in height. When buildings exceed this height,

contain atypical structural configurations or exhibit a complex response to a primary vertical element being removed it is recommended that a nonlinear procedure is employed.

An important point to note is that the analysis outlined in the guidelines looks to find only the potential for progressive collapse. The linear elastic procedure used is not capable of predicting the detailed response of a building when a primary vertical element is instantaneously removed.

With regards to reinforced concrete structures in particular it is recommended that structures are designed with redundant lateral and vertical force resisting systems so that alternate load paths are available in the event of failure of a structural element. Detailing of reinforcement should promote structural continuity and ductility so that elements are capable of spanning two full spans with particular reference to sufficient beam-to-beam continuity across columns. It is also recommended that structural members are designed to be capable of resisting load reversals. For example when a column is removed the hogging bending moments adjacent to the column are reversed and the original negative moment reinforcement is in the wrong position to resist the now positive bending moment.

Using the linear-elastic procedure the potential for progressive collapse is analysed for the loss of one column only at any particular instant. The loss of an external and internal column is considered separately. The frame is analysed for the instantaneous loss of one external column at or near the middle of the short and long sides of the building, and at a corner of the building. Internal considerations examine the loss of one column in one structural bay on the ground floor when it is to be used as an uncontrolled public area, such as a car park or retail area.

During analysis of the structure the correct way to instantaneously remove a column is shown in Figure 2.7. When considering dynamic loading the length of time for removal must also be taken into account.

Following analysis the elements found to have a potential for causing progressive damage or collapse based on the Demand-Capacity Ratio must be redesigned. This must be done so that the damage caused by the instantaneous loss of a primary vertical support is limited. These limitations are shown in Figure 2.8, United States General Service Administration (2003)

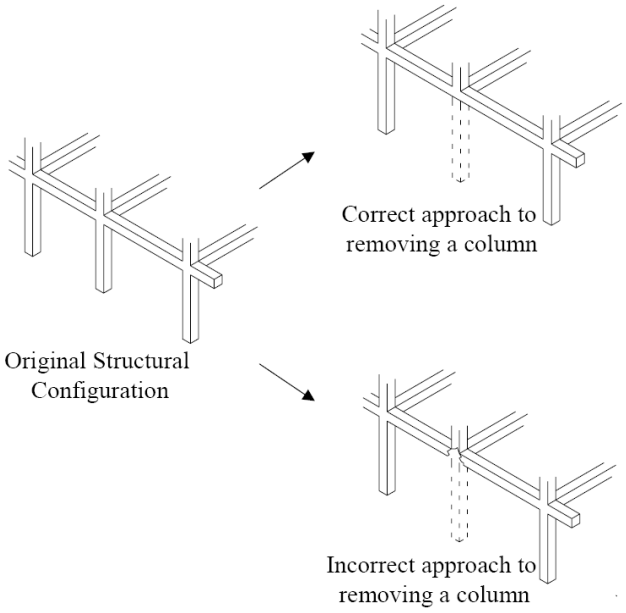

Figure 2.7: *Correct way to instantaneously remove a column during analysis, United States General Service Administration (2003)*

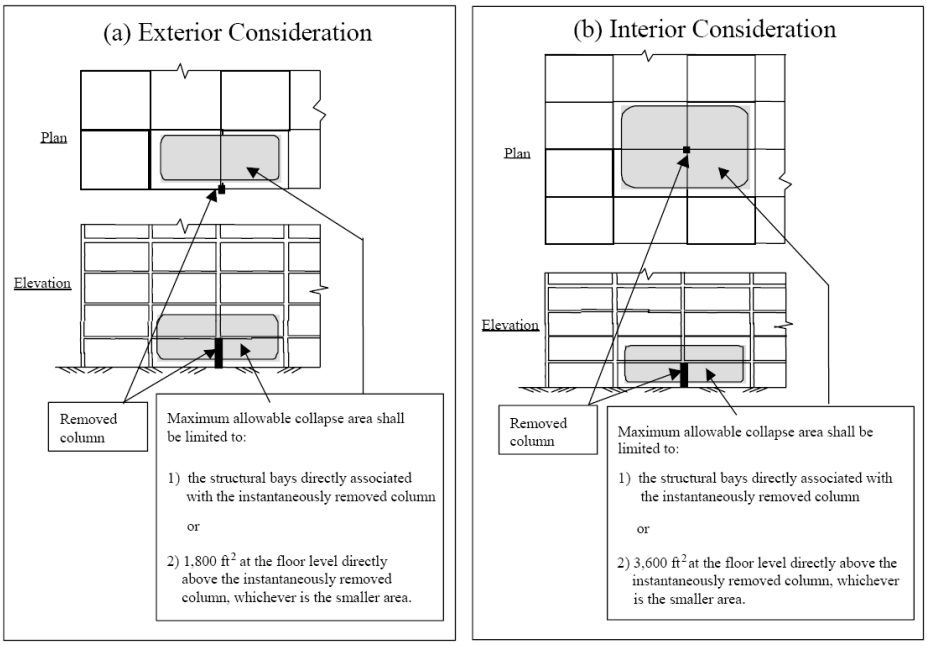

Figure 2.8: *Limitations to collapse, United States General Service Administration (2003)*

2.3.4 **American Department of Defense (DoD), UFC 4-023-03 (2009)**

The document produced by the Unified Facilities Criteria in the USA is for the purpose of reducing the potential of progressive collapse in new and existing Department of Defense (DoD) facilities, Department of Defense (2009). It requires all structures above 3 storeys to take measures to prevent progressive collapse. Two design approaches are set out, the direct and indirect design approaches. The direct approach considers resistance to progressive collapse during the design process:

- The alternative load path method, requiring the structure to bridge a missing element.
- The specific load resistance method, where parts of the building must resist a specific load or threat.

In the indirect design approach resistance is given through the provision of minimum levels of strength, continuity and ductility. Requirements of this approach include; good plan layout; integrated systems of ties; returns of walls; changing span directions of floor slabs; load-bearing interior partitions; catenary action of the floor slab; beam action of the walls; redundant structural systems; ductile detailing; additional reinforcement for blast and load reversal with regard to explosive loads.

When assessing the alternative load paths in a structure, similar to the GSA guidelines three analysis procedures are recommended; linear static, nonlinear static and nonlinear dynamic. There is also a similar approach with instantaneous column removal assumed from the middle of long and short span as well as corner column. Considerations also have to be made for accidental loading in the opposite direction to gravity loading.

2.3.5 **Summary**

In the codes of practice and guidelines reviewed there are common trends that indicate the different institutions across the world are in agreement in their advice to mitigate progressive collapse. Each requires some level of risk assessment to first determine the structural form, commonly this is dictated by the storey height or floor area. Then there is a requirement to determine the level of threat and consequently the extent of measures that needs to be considered. One measure is to employ a specific load resistance method in which a key

element is designed to withstand a pre-determined load that would prevent failure in an emergency scenario. Alternatively an analysis of the structure can be carried out once a primary vertical element is notionally removed, usually from the centre of the structure either internally or on the building's perimeter. The column is removed in an instantaneous manner such that no further damage of the structure is assumed. In this method alternative load paths must be provided by the structure such that sufficient robustness is provided to bridge the removed element. In reinforced concrete design it is recommended that vertical and horizontal tying is employed to aid the development of alternative load paths. The experimental programme which made up a significant part of the research reported here was based on the accidental situation resulting from the instantaneous removal of a perimeter column.

2.4 **Quantification of Accidental Loading**

International guidelines and codes of practice give provisions for loading exerted on a structure in the event of localised damage and exceptional emergency load cases. The situation under consideration is the loss of a perimeter column, the loading imposed on the structure after such an event caused by malicious or accidental means must be quantified for structural behaviour to be analysed. Various suggested emergency loading conditions from the guidelines and codes of practice have been reviewed and are summarised below.

2.4.1 **GSA**

GSA (2003) states that when analysing an existing structure the gravity load should be taken as:

$$\mathrm{ALS}^{\mathrm{GSA}} = \mathrm{DLF}(1.0\mathrm{G_k} + 0.25\mathrm{Q_k}) \qquad 2.1$$

Where:

DLF = 2.0

ALS: Accidental Load State

DLF: Dynamic Load Factor

G_k: Dead loading

Q_k: Imposed loading

2.4.2 **BS 8110:1997**

Clause 2.4.3.2 of Part 1 of the British Standard for the Structural Use of Concrete. considers the effects of exceptional loads or localised damage (BS 8110: 1997). When considering the stability of a structure after localised damage has occurred from excessive loading through misuse or accident the emergency loads to be considered are given as:

$$ALS^{BS} = \gamma_f G_k + {}^1/_3\,\gamma_f Q_k \qquad 2.2$$

γ_f (taken as 1.05) is the partial safety factor introduced to take account of unconsidered possible increases in load, inaccurate assessment of load effects, unforeseen stress redistribution, variation in dimensional accuracy and the importance of the limit state being considered. Thus

$$ALS^{BS} = 1.05G_k + 0.35Q_k \qquad 2.3$$

2.4.3 **Eurocodes**

BS EN 1990:2002+A1:2005 clause 6.4.3.3 provides the combination of actions for accidental design situations:

$$ALS^{EN} = \sum_{j\geq 1} G_{k,j} + P + A_d + \left(\psi_{1,1} \text{ or } \psi_{2,1}\right) Q_{k,1} + \sum_{i>1} \psi_{2,i}\, Q_{k,i} \qquad 2.4$$

The UK National Annex to Eurocode 0 – Basis of Design also provides guidance on accidental load combinations in Table NA.A1.3. The term P in equation 2.4 is a factor representing pre-stressing action; however pre-stressed elements are not considered in this research so P has been taken as 0. A_d deals with accidental action (fire or impact); however the situation considered here is after the event so A_d=0. $Q_{k,1}$ is the main accompanying variable action and $Q_{k,i}$ are other accompanying variable actions for example wind loading. Only the main accompanying variable action of the imposed load is considered which results in the following combination for accidental loading:

$$ALS^{EN} = G_k + \left(\psi_{1,1} \text{ or } \psi_{2,1}\right) Q_k \qquad 2.5$$

$\psi_{1,1}$ is the partial factor for frequent occurrence of a variable action and $\psi_{2,1}$is the factor for quasi-permanent occurrence. Frequent variable actions can be considered to be those

commonly imposed on the structure, for example personnel loading when the building is in use. Conversely quasi-permanent variable actions are those that could potentially be removed but are commonly in place throughout the lifetime of the structure, for example. partition walls and furniture (the building when not occupied by people). Table NA.A1.1 of the UK Annex (BS EN 1990:2002+A1:2005)) defines these two factors for different categories of imposed loadings applied to buildings. Categories A and B, domestic, residential and office areas respectively are considered here. For these categories $\psi_{1,1}$= 0.5 and $\psi_{2,1}$ = 0.3, giving two loading conditions:

$$ALS_1^{EN} = G_k + 0.5Q_k \quad 2.6$$

$$ALS_2^{EN} = G_k + 0.3Q_k \quad 2.7$$

2.4.4 **Application to Frame Analysis**

The various approaches in the quantification of loading to be imposed on a structure in the damaged state, which is termed an accidental loading condition, described herein have been assessed in Chapter 6. Along with a dynamic amplification factor an accidental loading state has been defined. This has been applied to a series of industry standard framed structures to analyse their response to the loss of a column with the inclusion of CMA.

2.5 **Yield Line Theory**

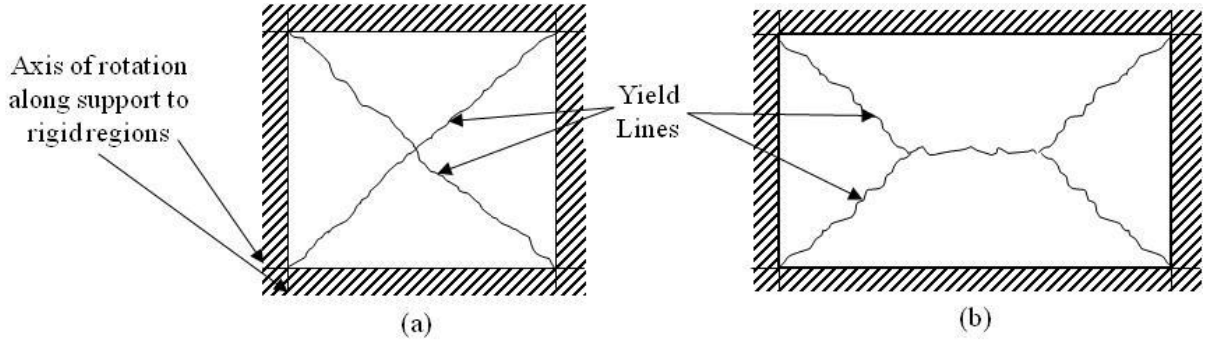

Figure 2.9: *Yield line patterns for restraint on all four sides of a square (a) and a rectangular slab (b).*

Numerous authors have based load enhancement against the ultimate load predicted through the yield line theory. Others have developed the theory with an inclusion of CMA to allow

prediction of load capacity of laterally restrained elements. It is therefore insightful to understand the principals behind yield line theory.

In the yield-line method the slab is divided into rigid regions joined by localised plastic regions (yield-lines). The analysis is carried out either by equating the work done by the external loading to the energy dissipated by plastic rotation at the yield lines, or by examining the equilibrium of the region bounded by the yield lines and slab edges. The collapse load obtained is an upper bound, thus the true collapse load is less than or equal to the load obtained, (Moy (1970)).

Johansen (1972) pioneered the Yield Line Theory that gave structural engineers a simple and reliable method for analysis and design of under-reinforced concrete slabs. It gave the designer an ultimate load analysis to provide either the moment at failure or the ultimate load. This allowed it to be used by numerous authors such as Park and Gamble (2000) to provide a basis of comparison for enhancement from Compressive Membrane Action. It is recognised by the British Standards Institution as an acceptable design method (BS 8110-1:1997 Clause 3.5.2.1). In slab design yield line patterns are postulated, as in Figure 2.9. A yield line can be envisaged as a crack in a reinforced slab across which the reinforcement bars have yielded and along which plastic rotation occurs, Kennedy and Goodchild (2004). The rigid regions rotate about the yield lines and pivot about their axes of rotation causing the supported loads to move, Kennedy and Goodchild (2004). Johansen (1972) produced a set of formulae for calculating the ultimate load for various one-way and two-way slabs with different restraint conditions. The positions of yield lines can be calculated or a pattern can be assumed for simplicity.

An alternative to using standard formulae is to work from first principles in what is known as the Work Method, Kennedy and Goodchild (2004).The theory is based on the concept that at failure the (virtual) energy absorbed in yield lines rotating is equal to the (virtual) work done in loads moving, Equation 2.8. In this plastic method elastic deformations are ignored. All deformations are assumed to be concentrated in the yield lines and slab deflections are calculated relative to a nominal maximum value of unity. The ultimate collapse load can then be calculated, giving an upper bound solution. To determine the minimum collapse load various yield line patterns need to be examined.

$$\sum(N_J \times \delta_J)\text{for all regions} = \sum(m \times l_J \times \theta_J)\text{for all yield lines} \qquad 2.8$$

Where:

N_J = loads(s) acting within a particular rigid region

δ_J = vertical displacement of the load(s) N_j on each region expressed as a fraction of unity

m = the moment of resistance of the slab across the yield line per metre run

l_J = the length of yield line or its projected length onto the axis of rotation for that region

θ_J = the rotation of the yield line resulting from rotation of the rigid regions about their axes of rotation

2.6 **Principles of Compressive Membrane Action**

The model in Figure 2.10(a) represents a two-way spanning slab. Along the yield lines the "Perspex" has been completely severed, giving four rigid portions, which make the model incapable of carrying load through bending or catenary action. When lateral restraint is given by a surrounding stiff diaphragm, as in Figure 2.10(b), compressive membrane forces develop allowing it to take a considerable amount of load through arching action, Ockleston (1958)

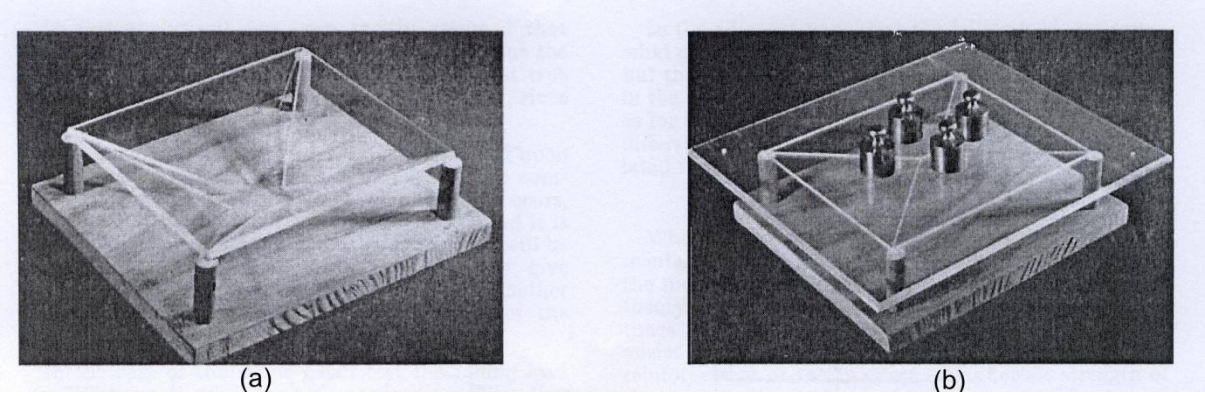

Figure 2.10: *Model demonstration of Arching Position Ockleston (1958)*

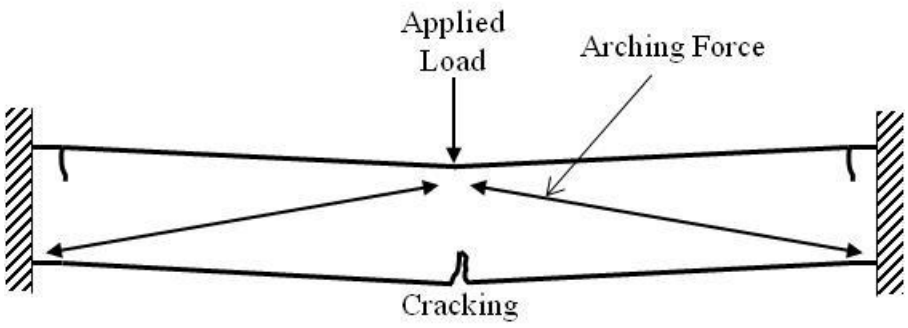

Figure 2.11: *Principle of compressive membrane action in laterally restrained reinforced concrete slabs*

There is a great difference in the stress-strain relationship in reinforced concrete when a section is in tension or compression. When load is applied to a beam or slab cracking can occur due to the relatively low tensile strength of concrete and the neutral axis migrates to the compressive zone of the concrete. With a relatively low percentage of reinforcement the neutral axis is moved close to the compressive face. The effect is accelerated if the reinforcement yields. This would normally cause in-plane expansion, but if in-plane lateral restraint is provided, by adjoining slabs or vertical supports, an internal arching effect is produced (Figure 2.11) , Peel-Cross et al. (2001). This can be thought of as a self induced pre-stress in the slab as all-round compression develops, Wood (1961). The compressive forces cause the neutral axis to move towards the mid-plane of the section. The compressive internal force is known as compressive membrane action (CMA) or arching action and the ultimate load capacity of longitudinally restrained reinforced concrete slabs and beams is enhanced by the development of arching action. Effectively the beam or slab is jammed between the edge restraints.

Compressive membrane action is greater and more likely to occur in lightly-reinforced elements or ones with low span to depth ratios as cracking will cause larger movements of the neutral axis, Wood (1961). It is also induced at relatively small deflections, the ultimate load in the compressive phase of behaviour is considered to occur at around 40-50% of the section depth (Wood (1961), Park and Gamble (2000)). The compressive strength of the concrete and the degree of lateral restraint provided directly affect the capacity produced by compressive membrane action, Lahlouh and Waldron (1992), Taylor et al. (2001).

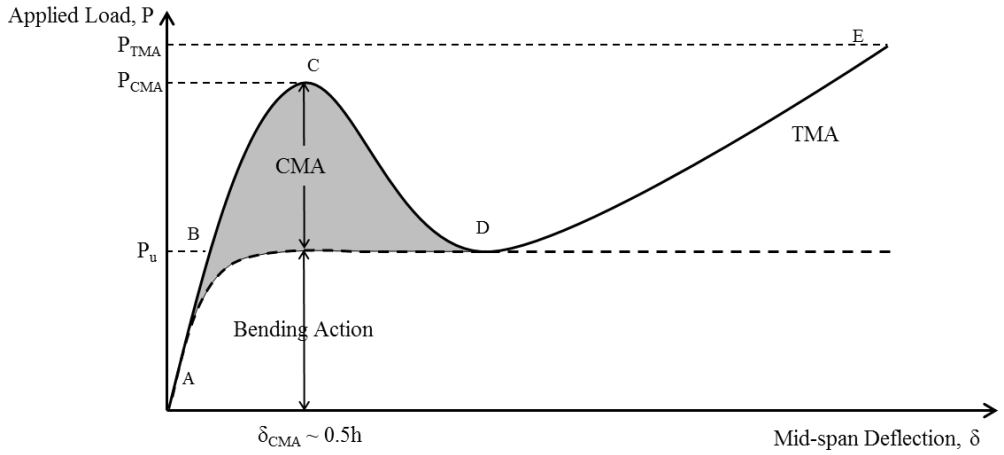

Figure 2.12 : *Idealised load vs. deflection curve for laterally restrained slabs*

When discussing laterally restrained one-way or two way spanning slabs it is illustrative to plot load against deflection, Figure 2.12. Initially at low loading the resistance is given by almost purely elastic bending action. As load is increased from A to C, at small deflections and with the onset of cracking at B, compressive membrane action begins to supplement the bending action. The peak enhanced ultimate load occurs at C. At this peak the steel reinforcement has yielded and the yield-line pattern has developed, Park (1964b). An unstable failure then occurs as the slab snaps through, Braestrup (1980). From C to D the compressive membrane forces decrease as the deflection increases and reduces the rise of the internal arch, Chattopadhyay (1981). At D the resistance from arching action is lost when deflection is equal to about the slab depth, Chattopadhyay (1981), the load has dropped to a minimum and cracking may extend through the entire depth of the slab, Park (1964b).

From point D in Figure 2.12 where the concrete has cracked throughout the depth, the concrete is incapable of carrying load and the load is mainly carried through the reinforcement bars acting as a tensile membrane. For a slab with a stiff surround the membrane forces change from compression to tension in the central region of the slab with a surrounding compression ring, Figure 2.13, which resists the inward movements of the slab edges. The extent of the slab acting under tensile membrane action will continue to spread until failure occurs through fracture of the reinforcement. In tests carried out by Park (1964a) and Wood (1961) it was found that in slabs with a high percentage of reinforcement or where the reinforcement was sufficiently ductile, the maximum load due to compressive membrane

action could be exceeded by the development of tensile membrane action. Tensile membrane action is an important mechanism because if the load drops quickly after reaching its peak at C, then the tensile membrane strength of the reinforcement could be sufficient to "catch" the load and prevent a catastrophic failure, Park and Gamble (2000).

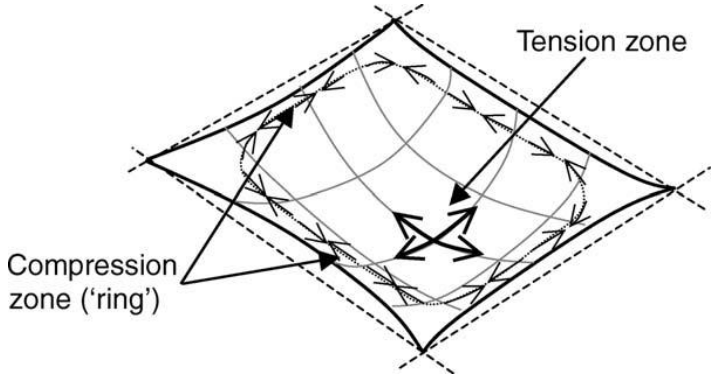

Figure 2.13: *Tensile membrane action in a concrete slab, Foster et al. (2004)*

2.7 **Early CMA Research**

Ockleston (1955) tested portions of a reinforced concrete framed Old Dental Hospital in Johannesburg, South Africa that was due for demolition. The ten-year old 30m square building was generally three storeys high. The series of tests carried out were the first significant full scale tests on a reinforced concrete frame building and were to become instrumental in bringing the potential of compressive membrane action to the forefront. Beams (610x305mm & 457x229mm) and both one-way (5m clear span) and two-way (4m x 5m) spanning slabs were tested to failure. It was found in all cases that cracking occurred at two to three times the design load and the slab eventually failed, when both the negative and positive reinforcement had yielded, at nearly four times the ultimate loads predicted by the yield-line method using the actual properties of materials from test samples. In the two-way spanning slab that was tested the conditions for CMA to occur were evident. Lateral restraint was provided by surrounding slabs restricting horizontal movement; deflections were small; slabs were lightly reinforced; cracking occurred at yield lines in the centre of the slab causing migration of the neutral axis. Ockleston (1958) later attributed these unexpected results of lightly reinforced slabs (0.04 to 0.24 %) to arching action.

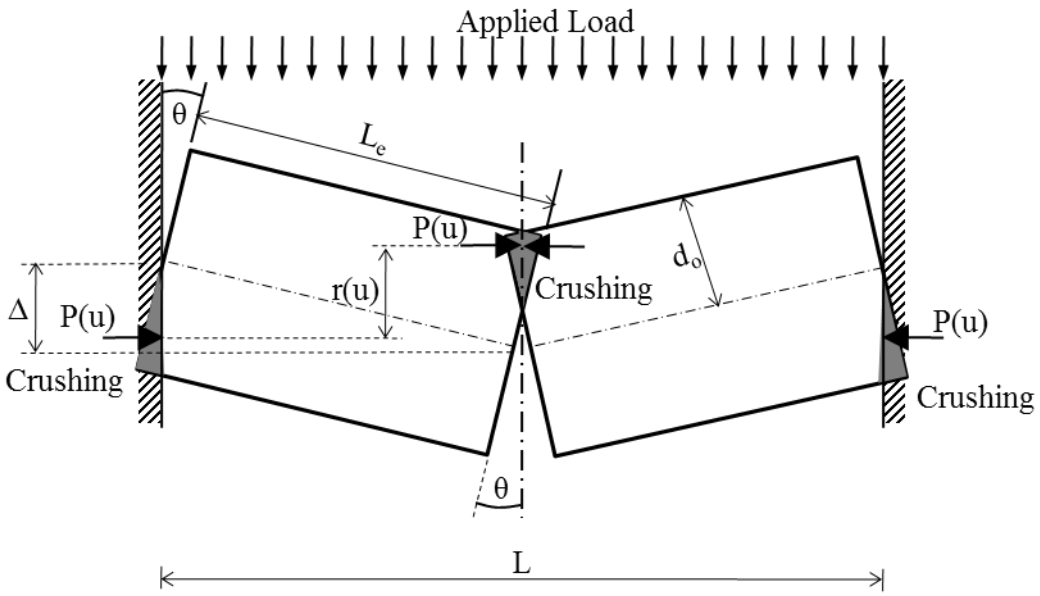

Figure 2.14: *Wall in deflected position, McDowell et al. (1956)*

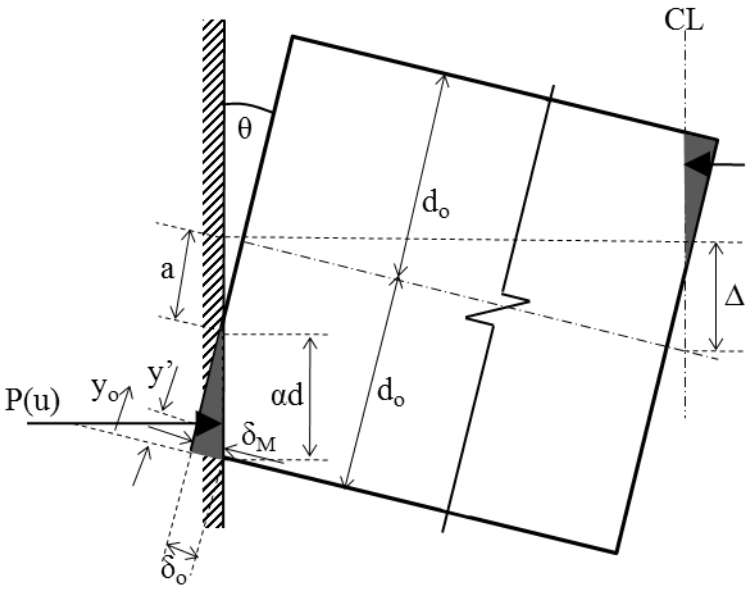

Figure 2.15: *Geometry at support, McDowell et al. (1956)*

McDowell et al. (1956) developed a theory of compressive membrane action based on observations made from testing of brick beams representing masonry walls butted up against supports which were essentially rigid. The arching action theory was at the time a bold change to the assumed way masonry walls resisted lateral forces. It was assumed that masonry was unable to withstand tensile stresses and in compression was idealised as a linear elastic-perfect

plastic material. Upon loading cracking occurred at mid-span, each half of the beam remained rigid and rotated about the mid-depth of the section at the end point and at mid-span. The contact areas at the ends and mid-span are equal and decrease with increased deflection and cracking. From the geometry shown in Figure 2.14 and 2.15 the decrease in contact area can be expressed by:

$$a = \frac{L_e}{2}\left(\frac{1-\cos\theta}{\sin\theta}\right) \qquad 2.9$$

The centre deflection is given in terms of the rotation by

$$\Delta = L\left(\frac{1-\cos\theta}{\sin\theta}\right) \qquad 2.10$$

Combining 2.9 and 2.10 gives

$$a = \frac{\Delta}{4} \qquad 2.11$$

The strain along any one fibre (a unit width strip across the section depth) is assumed to be linear with maximum at the bottom of the contact area and zero at the top. The distribution of strain along the contact area or, from Figure 2.15, the distribution of strain with respect to y_o, can be found using Equation 2.12, where R is a non-dimensional variable, e is the strain at the contact end and e_c is the strain associated with the crushing strength of the masonry material.

$$\frac{Re}{e_c} = u\left(1 - \frac{y_o}{d_o} - \frac{u}{2}\right) \qquad 2.12$$

Where

$$R = \frac{e_c L_e^2}{4d_o^2} \text{ and } u = \frac{\Delta}{2d_o}$$

The expression for R above is based on elastic behaviour. The strain along the contact area is assumed to increase linearly with the midspan deflection. There will therefore be a force at the contact area which increases almost linearly to a maximum value and then reduces to zero once the crushing strength has been reached. The stresses along the contact area at mid-span and end points of the beam can be represented by the arching force per unit width of the beam P(u). This is a function of the non-dimensional midspan deflection, u. This force depends on the value taken for R, which represents whether the section undergoes an elastic or plastic state of stress throughout the deflection history. The moment of resistance due to arching can then be defined as the moment due to arching forces:

$$M(u) = r(u)P(u) \qquad 2.13$$

$$r(u) = 2d_o(1 - u - \frac{y'}{d_o}) \quad 2.14$$

From static considerations, values for M(u) and P(u) were calculated for different values of R. The arching moment of resistance can be expressed as the moment ratio M_r:

$$M_r = \frac{4M(u)}{s_c d_o^2} = 4\left(1 + \frac{R}{2} + \frac{3u^2}{4} - 2u - \frac{R^2}{3u^2}\right) \quad 2.15$$

It was found that this method gave a close correlation with tests carried out at Massachusetts Institute of Technology, McDowell et al. (1956). Experiments on brick beams showed fixed end beams had three to six times the load carrying capacity of simply supported beams, when subjected to lateral loading.

The theory was based on the assumption that the principal resistance to lateral loads came from the compression force in the masonry panel. This was an idealisation and, coupled with the assumptions of the stress-strain properties of masonry, gave limitations to the theory in relation to its application to masonry, even though favourable comparisons were made with the experimental data. This approach to the calculation of arching forces was later used in the analysis of reinforced concrete elements by Rankin and Long (1997)

2.8 **CMA Theories**

2.8.1 **Deformation Plastic Theory**

It was widely agreed by Wood (1961), Christiansen (1963) and Park (1964b) that Johansen's yield line method gave a good prediction of the ultimate load in cases where membrane forces were insignificant. It has been shown however in testing by Wood (1961), Ockleston (1958), Christiansen (1963) and Park (1964b) that in one-way and two-way laterally restrained slabs the ultimate load is in excess of that predicted by Johansen (1972). The development of CMA in the slab gives considerably higher ultimate moments at the yield lines, Park (1964b). Thus neglecting compressive membrane action in appropriately restrained slabs would appear to be very conservative. The term 'Deformation Plastic Theory' groups together work taking a similar approach to predicting the enhanced load due to CMA by developing the work of Johansen (1972) to include compressive membrane forces and providing rigorous formulae for predicting the enhanced ultimate strength of the slab. The basis of these approaches is the

assumption that the total strain in the material is used. Plastic hinges are then assumed to form at the yield line and the remaining portions of the slab can be considered to be rigid.

Christiansen (1963) carried out analysis based on a beam which represented a one-way spanning slab and developed formulae for predicting the ultimate load due to arching. Integral to this was the value for a_1 in Figure 2.16, which was the depth available for arching, which could be found by equating the outward movement of the support with the lengthening due to rotation minus the elastic and plastic shortenings of the beam half, as in Equation 2.16. This essentially provides a value for the amount of the section which is available to provide a compressive strut once the forces in the section have been balanced.

$$a_1 = h - \Delta - \frac{(T_1 + T_2 + 2C_C)}{f_c} \qquad 2.16$$

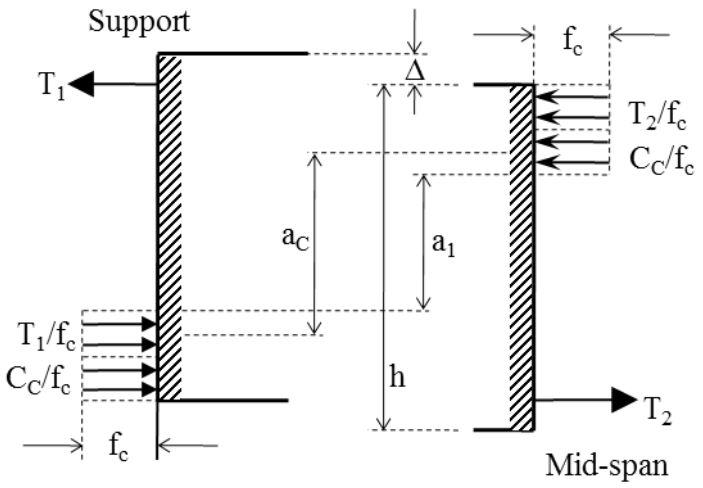

Figure 2.16: *Horizontal forces at support and at mid-span, Christiansen (1963)*

Tests were carried out on reinforced concrete beams laterally restrained by a steel frame. Beams were 152.4mm (6") wide and 76.2mm (3") deep with 6.4mm (one quarter inch) diameter mild steel reinforcement. Results from these tests showed a good correlation between predicted load and actual load due to arching. Two-way spanning slabs were also investigated. In both series of tests the maximum load was not reached until the deflection was higher than predicted, this was explained by additional bending near the hinges due to increased compression, Johansen (1972).

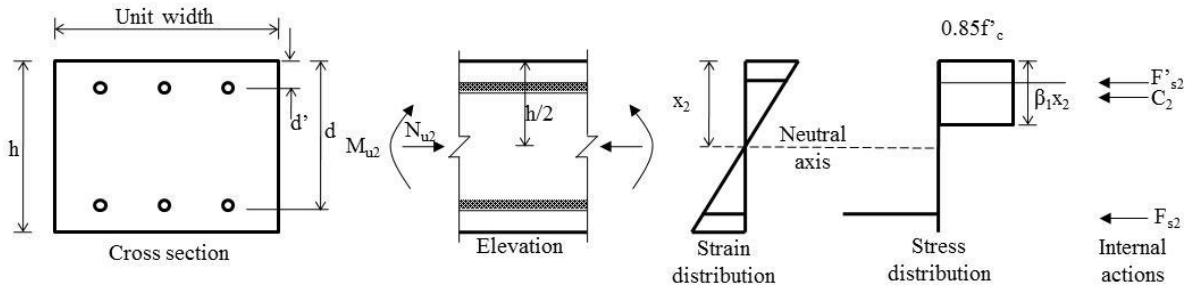

Figure 2.17: *Conditions at a section on a yield-line, Park (1964b), Park and Gamble (2000)*

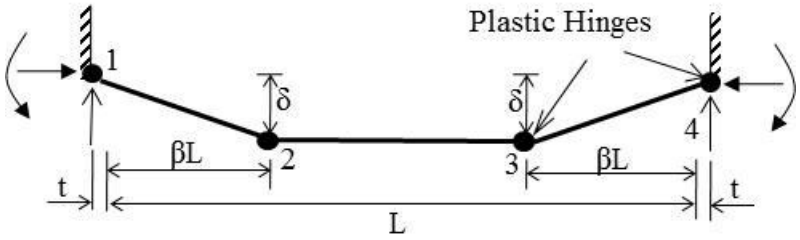

Figure 2.18: *Collapse mechanism of a strip with ends restrained against rotation and all translation, Park (1964b), Park and Gamble (2000)*

Park (1964a) contributed to the field with a series of papers in the 1960's. His first paper in 1964 concentrated on tensile membrane action which is not applicable to this thesis . In the same year Park (1964b) developed the yield-line theory to include compressive membrane stresses. Later Park and Gamble (2000) extended this work into formulae that were more easily manipulated and applied. The section at the sagging yield line under consideration is shown in Figure 2.17, with the assumed stress and strain distributions and the subsequent internal actions. At each plastic hinge shown in Figure 2.18 it is assumed that the tension steel has yielded, the tensile strength of concrete is neglected and no strain hardening of the steel occurs.

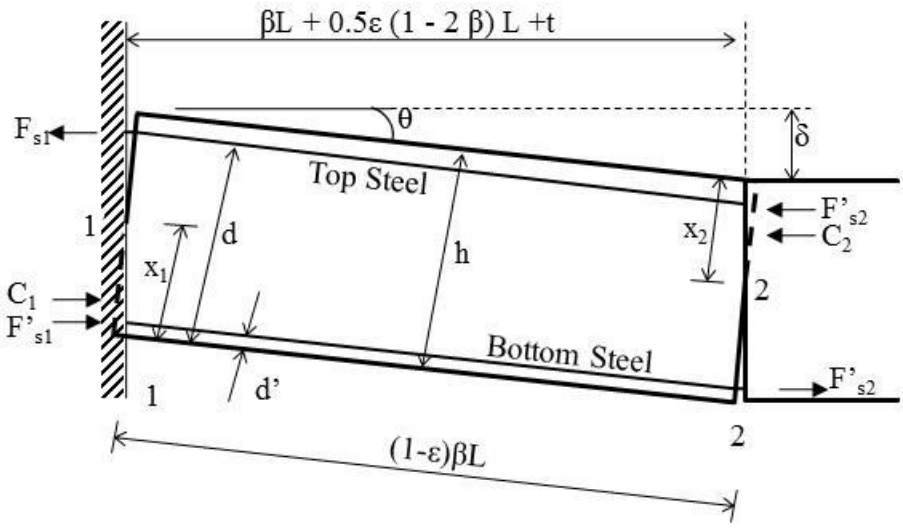

Figure 2.19: *Internal actions at yield sections of the end portion of a strip between yield sections 1 and 2, Park and Gamble (2000)*

The axial shortening from elasticity, creep and shrinkage was taken into account as one combined component of strain, ε, and was assumed to be constant across the entire section as the membrane force was constant. The shortening of the middle strip, the strip between the two yield points to the right of point 2 in Figure 2.19, was then given by;

$$\varepsilon(1-2\beta)L \tag{2.17}$$

due to symmetry the shortening of the outer strips is

$$0.5\varepsilon(1-2\beta)L \tag{2.18}$$

The change in length can be found by looking at the collapse mechanism of the strip (Figure 2.18), and a more detailed look (Figure 2.19) shows the change in dimensions of the end strip, the distance between 1 and 2. When θ and ε are assumed to be small, the change in length is shown by the geometry to be;

$$x_1 + x_2 = h - \frac{\delta}{2} - \frac{\beta l^2}{2\delta} - \left(\varepsilon + \frac{2t}{L}\right) \tag{2.19}$$

For equilibrium the membrane forces at each end of the strip must be equal. Where, C_1 and C_2 are the concrete compressive forces, F'_{s1} and F'_{s2} are the steel compressive forces and F_{s1} and F_{s2} are the tensile forces in the steel (all in terms of a strip of unit width). Therefore,

$$C_1 + F'_{s1} - F_{s1} = C_2 + F'_{s2} - F_{s2} \tag{2.20}$$

The concrete compressive stress block defined in ACI 318-77 (1997) was adopted allowing for the compressive force in the concrete to be defined as:

$$C_1 = 0.85f'_c\beta_1 c' \tag{2.21}$$

$$C_2 = 0.85f'_c\beta_1 c \tag{2.22}$$

Where $\beta_1 = 0.85$ for $f'_c < 30\ N/mm^2$and was reduced by 0.008 per each $1\ N/mm^2$increase in f'$_c$ but $\beta_1 \geq 0.65$, and

$$x_1 - x_2 = \frac{F_{s1} - F_{s2} - F'_{s1} + F'_{s2}}{0.85f'_c\beta_1} \tag{2.23}$$

Solving 2.19 and 2.23 simultaneously gives:

$$x_1 = \frac{h}{2} - \frac{\delta}{4} - \frac{\beta_1 L^2}{4\delta}\left(\varepsilon + \frac{2t}{l}\right) + \frac{F_{s1} - F_{s2} - F'_{s1} + F'_{s2}}{1.7f'_c\beta_1} \tag{2.24}$$

$$x_2 = \frac{h}{2} - \frac{\partial}{4} - \frac{\beta l^2}{4\delta}\left(\varepsilon + \frac{2t}{L}\right) - \frac{F_{s1} - F_{s2} - F'_{s1} + F'_{s2}}{1.7f'_c\beta_1} \tag{2.25}$$

Where

$$\varepsilon + \tfrac{2t}{L} = \tfrac{n_u}{hE_c} + \tfrac{2}{L}\tfrac{n_u}{S} = \left(\tfrac{1}{hE_c} + \tfrac{2}{LS}\right)\left\{0.85f'_c\beta_1\left[\tfrac{h}{2} - \tfrac{\delta}{4} - \tfrac{\beta l^2}{4\delta}\left(\varepsilon + \tfrac{2t}{L}\right) + \tfrac{F_{s1}-F_{s2}-F'_{s1}+F'_{s2}}{1.7f'_c\beta_1}\right] + F'_{s2} - F_{s2}\right\} \tag{2.26}$$

Therefore:

$$\varepsilon + \frac{2t}{L} = \frac{\left(\frac{1}{hE_c} + \frac{2}{LS}\right)\left\{0.85f'_c\beta_1\left[\frac{h}{2} - \frac{\delta}{4} - \frac{F_{s1} - F_{s2} - F'_{s1} + F'_{s2}}{1.7f'_c\beta_1}\right] + F'_{s2} - F_{s2}\right\}}{1 + 0.2125\frac{f'_c\beta_1\beta L^2}{\delta}\left(\frac{1}{hE_c} + \frac{2}{LS}\right)} \tag{2.27}$$

The resultant membrane force acting at mid depth N_{u2} shown in Figure 2.17 at position 2 can then be found as well as the resisting moment M_{u2} about the mid-depth axis:

$$N_{u2} = C_2 + F'_{s2} - F_{s2} \tag{2.28}$$

$$M_{u2} = C_2(0.5h - 0.5\beta_1 x_2) + F'_{s2}(0.5h - d') + F_{s2}(d - 0.5h) \tag{2.29}$$

Similarly for position 1:

$$N_{u1} = C_1 + F'_{s1} - F_{s1} \tag{2.30}$$

$$M_{u1} = C_1(0.5h - 0.5\beta_1 x_1) + F'_{s1}(0.5h - d') + F_{s1}(d - 0.5h) \tag{2.31}$$

However for equilibrium:

$$N_{u1} = N_{u2} = N_u \quad 2.32$$

The sum of moments about the mid depth at one side of the yield section is for a point load:

$$M_{u1} + M_{u2} - N_u\delta = \frac{P_P L}{4} \quad 2.33$$

And for a uniformly distributed load:

$$M_{u1} + M_{u2} - N_u\delta = \frac{w_P L^2}{8} \quad 2.34$$

Putting Equations 2.34 and 2.35 in terms of load gives:

$$P_P = 4 \times \frac{(M_{u1} + M_{u2} - N_u\delta)}{l} \quad 2.35$$

And:

$$w_P = 8 \times \frac{M_{u1} + M_{u2} - N_u\delta)}{L^2} \quad 2.36$$

Where δ is a given increment of midspan deflection. By increasing δ in set increments the corresponding value for load can be calculated and plotted against the deflection to show the load-deflection behaviour.

Tests were carried out on slab samples with all four edges fully restrained to give a comparison with the developed method and the theoretical predictions gave a conservative estimate of the ultimate loading. Experimental data showed that the central deflection at ultimate loading could be taken as 0.4 to 0.5 of the slab depth regardless of the span/depth ratio. This confirmed work by Wood (1961). The value for deflection at ultimate load was found to be approximately 0.33h for a simply supported short edge and 0.4h for a simply supported long edge (the short edge is the shorter dimension of a rectangular bay). It was therefore suggested that a value of 0.4h should be used when using theoretical equations.

Roberts (1969) developed a theory based on the rigid-plastic approach. Tests were carried out to verify the theory of compressive membrane action which provided a prediction for the ultimate load. Slab strips were tested to represent one-way spanning slabs. Beams were 0.229m wide, 1.461m in length and 0.076m deep. Reinforcement used was 4.8mm diameter mild steel. Longitudinal restraint to samples was given by a large concrete frame cast for the purpose. Whilst some success has been found using formulae such as those of Park and Roberts, with accurate prediction of arching loads from the tests of Wood (1961) and Park

(1964b), a discrepancy was also noted. Christiansen (1963) found that the calculated deflection when compressive membrane action was at a maximum was grossly underestimated. Results from Roberts (1969) supported this. Christiansen (1963) put this discrepancy down to possible additional bending near the hinges due to increased compression.

An important conclusion was that the restraint provided did not need great stiffness to develop the enhanced collapse load. When the stiffness of the restraint was equal to the stiffness of the beam it was found to only reduce the enhanced load by 10% compared to when the restraint stiffness was eleven times greater than that of the beam.

Long (1975) first developed a two-part approach, in which the components of bending and arching were calculated separately and then summed, for predicting the punching shear strength of flat slabs at interior columns, which took into consideration the interaction of the flexural and shear effects. Later Kirkpatrick (1984) carried out 20 tests on 1/3 scale models of the M-beam bridge deck panels of Clinghan's Bridge, over the Tullinskey Cut River in County Down in Northern Ireland, with the aim of reducing the spacing of the beams to create a more cost-effective slab. It was concluded that codes of practice at the time were conservative, results showed a good correlation with the prediction method based on Long (1975) below a span to depth ratio of 15 and when 0.5% reinforcement was required. Even at low levels of load, CMA forces play an important part in controlling crack development in the slab.

Rankin and Long (1987) developed the two-phase approach of Long (1975) into a method for predicting the punching strength of conventional slab-column specimens. With codes of practice varying in the Britain and the USA, the aim was for a simplified formula that could be easily used in design. In Rankin et al. (1991) CMA was looked at further in regards to laterally restrained slabs in cellular concrete structures. In previous research the three-pinned arch analogy had been used to find a critical value of deflection for failure of the slab. Due to the complex nature of concrete the critical deflection at failure was not a constant function of the slab depth. A rational treatment of arching action was therefore proposed which did not rely on knowledge of the critical deflection at failure.

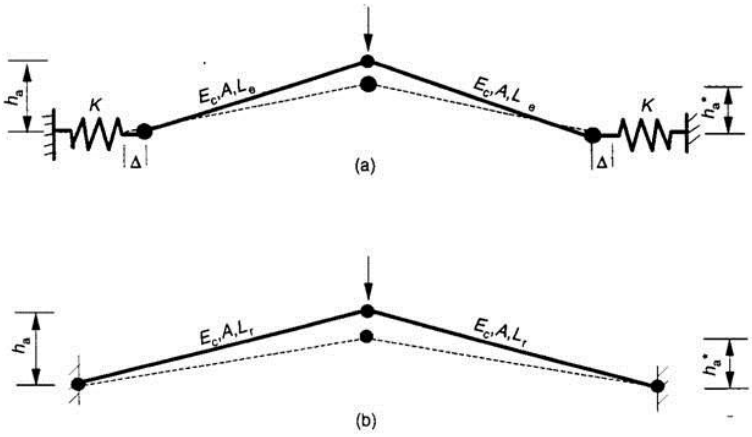

Figure 2.20 *Equivalent three-hinged arches (a) Elastically-restrained arch; (b) Rigidly-restrained arch Rankin and Long (1997)*

Rankin and Long (1997) presented an overview and summary of previous work on formulae for CMA in laterally restrained slab strips. The formulae derived by McDowell et al. (1956) in Equation 2.12 for R and u, and the value for the moment ratio M_r was developed by finding the root of the quadratic equation formed from the derivatives of Equations 2.37 and 2.38 (as given by McDowell et al. (1956)) giving a value for u and providing a direct method for predicting the maximum arching resistance without the need for the critical deflection.

$$\frac{8u}{3R}\left(1-\frac{5u}{4}\right)\left(1-\frac{u}{2}\right)^2 = 0 \qquad 2.37$$

$$4\left(1+\frac{R}{2}+\frac{3u^2}{4}-2u-\frac{R^2}{3u^2}\right) = 0 \qquad 2.38$$

Hence the moment ratio M_r can be found and then the maximum arching moment of resistance M_a:

$$M_r = 4.3 - 16.1\sqrt{(3.3\times10^{-4}+0.1243R)} \qquad 2.39$$

$$M_a = \frac{M_r 0.85 f'_c d_1^2}{4} \qquad 2.40$$

To account for the lateral restraint not being completely rigid a three pin arch analogy with linear elastic 'spring' restraints was employed as in Figure 2.20(a). It can be shown through equilibrium considerations that the load-deflection response of the laterally restrained arch in Figure 2.20(a) can be represented by the rigidly restrained arch in Figure 2.20(b) with an equivalent leg length defined by:

$$L_r = L_e \left[\frac{E_c A}{K L_e} + 1\right]^{1/3} \quad 2.41$$

Thus the flexible and rigid arching moment capacities can be related using the calculated equivalent leg length:

$$M_a = M_{ar} \frac{L_e}{L_r} \quad 2.42$$

Using this method it was found that for a slab strip with an in-plane stiffness equal to the restraint stiffness the arching moment was between around 50% and 80% of the moment for a completely rigid restraint. This was increased to between 75% and 90% for a restraint stiffness equal to three times the in-plane stiffness of the slab strip.

The sagging bending moment capacity M_b, assuming a plastic collapse mechanism can be calculated using the formula from Mattock et al. (1961) with all safety factors removed:

$$M_b = \rho f_y d^2 \left(1 - 0.59 \frac{\rho f_y}{f'_c}\right) \quad 2.43$$

The hogging bending moment capacity, $\overline{M_b}$, can be calculated using the same equation with the equivalent top reinforcement ratio $\bar{\rho}$. The bending and arching loads, P_b and P_a respectively, can then be calculated separately and added together to give the enhanced load, P_p. This is based on the assumptions that the maximum arching moment develops after yielding of the reinforcement and the bending deformation necessary to cause yield can be neglected.

$$P_b = k(M_b + \overline{M_b}) \quad 2.44$$

$$P_a = kM_a \quad 2.45$$

$$P_p = P_b + P_a \quad 2.46$$

Where for a strip under uniform loading:

$$k = \frac{8}{L}$$

The proposed method was used to predict the ultimate loads from previous testing by Chattopadhyay (1981), Christiansen (1963), Birke (1975) and Roberts (1969). The load comparisons gave strong correlations giving accurate results (Rankin and Long (1997)) as shown in Figure 2.21.

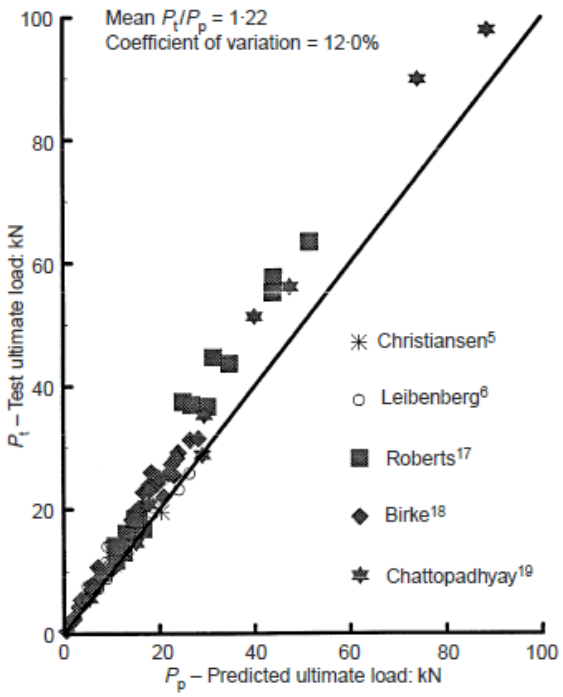

Figure 2.21: *Correlation of predictions with test results, Rankin and Long (1997).*

Taylor et al. (2001) presented research investigating the possibility of utilising compressive membrane action to reduce the amount of reinforcement needed in concrete deck slabs in bridges. Their aim was to reduce the amount of corrosion to reinforcement and so reduce the deterioration and high costs of maintenance and repair to bridges. Testing on full scale slabs was carried out as well as analysis to predict failure loads of concrete specimens of different compressive strengths. From the fifteen tests carried out the theory for CMA was extended to include concrete strengths of up to 100 N/mm^2. Comparisons led to modifications to the stress-strain block in Rankin and Long (1997) producing more accurate results for high strength concrete. Results showed that with the CMA component increased by higher concrete strength the reinforcement levels could indeed be reduced in bridge decks. The theory also showed good correlation for slabs with span to depth ratio of less than 15, with a near rigid restraint.

Peel-Cross et al. (2001) carried out a full-scale experimental study of composite metal decking / concrete floor slabs in the Building Research Establishment's Large Building Test Facility (LBTF) at Cardington, where the contribution of compressive membrane action to the load

carrying capacity was examined. Tested panels exhibited strength enhancements of 80% and 50% over predicted values from the yield-line theory. Comparisons were also made to the method of Rankin and Long (1997). An important point raised in this work was the difference in results between interior panels and edge or corner panels. A greater enhancement was found in the interior panels which was put down to the increased lateral restraint in these panels. Interior panels could also be represented by slab strips whereas further investigation was needed for edge and corner panels which were harder to represent.

Ruddle et al. (2003) conducted a combined experimental and analytical investigation into the effect of arching action on the ultimate strength of reinforced concrete rectangular and T-section beams. Their method, based on Rankin and Long (1997), was used for predicting enhanced flexural and shear capacities. Results from 50 tests were used to validate results with span to depth ratios of 6.3 and 12.7 and a scale of ¼. Research showed that the formulae of Rankin and Long (1997) could be used for rectangular and T-section beams. This indicated that arching action could also improve the serviceability performance of such beams.

2.8.2 **Flow Theory**

It is important to first note the difference between the deformation and flow theories. Braestrup (1980) carried out an extensive review and defined the difference to be that in the deformation theory the total strains in the materials are used whereas flow theory is based upon strain increments. The flow theory therefore examines the movement of the neutral axis with respect to time increments. The strain rates corresponding to stress rates can then be calculated. The rate of external work done by the applied load is equated to the rate of internal work dissipated in the yield lines, the membrane forces are then found and plotted against deflection. Braestrup (1980) cited flaws in deformation theory and advocated the use of the flow theory.

The behaviour of reinforced concrete remains elastic up to the yielding of the steel reinforcement and then plastic behaviour governs the deformation. When plastic deformations are large in this post yield phase the geometry of the section and even small changes in geometry from plastic deformations can be of significant importance in relation to arching action in reinforced concrete. If analysis is based on the undeformed geometry results can be

very inaccurate. Kemp (1967) and particularly Morley (1967) recognised these flaws in the conventional yield-line theories in post-yield behaviour. Both authors developed an upper bound solution based on yield criteria and calculated ultimate loads inclusive of membrane action in accordance with strain rate dependent energy dissipation at yield lines. A kinematical approach for deformed slabs was used by Janas (1968) to analyse slabs in the post yield phase. The following conclusions, which are common to other authors adopting the same approach, were drawn:

Central deflection was found to be twice as great in deformation theory as opposed to the flow theory. This is in agreement with discrepancies expressed in previous work on the deformation theory by Christiansen (1963) and Roberts (1969). These findings were attributed to the fact that in deformation theory the concrete is assumed to assert its compressive stress even during unloading. A greater problem that Braestrup (1980) found with deformation theory was that it predicted the membrane force to decrease very slowly with increasing deflection. This contradicted experimental data as well as predicted results from the flow theory.

It has been shown that flow theory gives more accurate results for the unstable failure that occurs after the maximum compressive membrane force has been reached, highlighting the drawbacks of deformation theory in this part of the loading process, Braestrup (1980). Kemp et al. (1989) confirmed this stating that deformation plastic theory using total strain was appropriate for the loading process as the compressive membrane force is increasing and could therefore predict the peak load, whilst flow theory should be employed for a more accurate prediction of the unloading process where the compressive membrane force is decreasing.

Eyre (1990, 1997, 2000) agreed with this approach and looked to clarify and define the point at which transfer between the approaches should take place, and developed formulae for each approach. Eyre (1990) used slab strip analysis in a similar way to previous authors, but with the allowance for different areas of tensile and compressive reinforcement. The assumptions made were also similar: the tensile strength of concrete was neglected, the concrete was assumed to be perfectly plastic in compression, no strain hardening of steel occurred, the regions between yield points remained rigid and straight. It was also assumed that incremental strains were linearly distributed over the depth of the section and that the neutral axis was defined as the limit of compression in the section, Eyre (2000).

The method of modelling the elastic effects from the combination of axial elastic stiffness, shrinkage and construction tolerances using an end gap ξL and an initial deflection Δ_{o1} is shown in Figure 2.22. It should be noted that the value for the neutral axis $(\mu_2 h)$ is in brackets as it only refers to the neutral axis under the total strain flow rule. To deal with the issue of in-plane longitudinal stiffness, the stiffness of the restraint at the support, point 3, is combined with the stiffness of the slab S_s to give a combined surround stiffness S_o, the slab elements are then considered to be rigid.

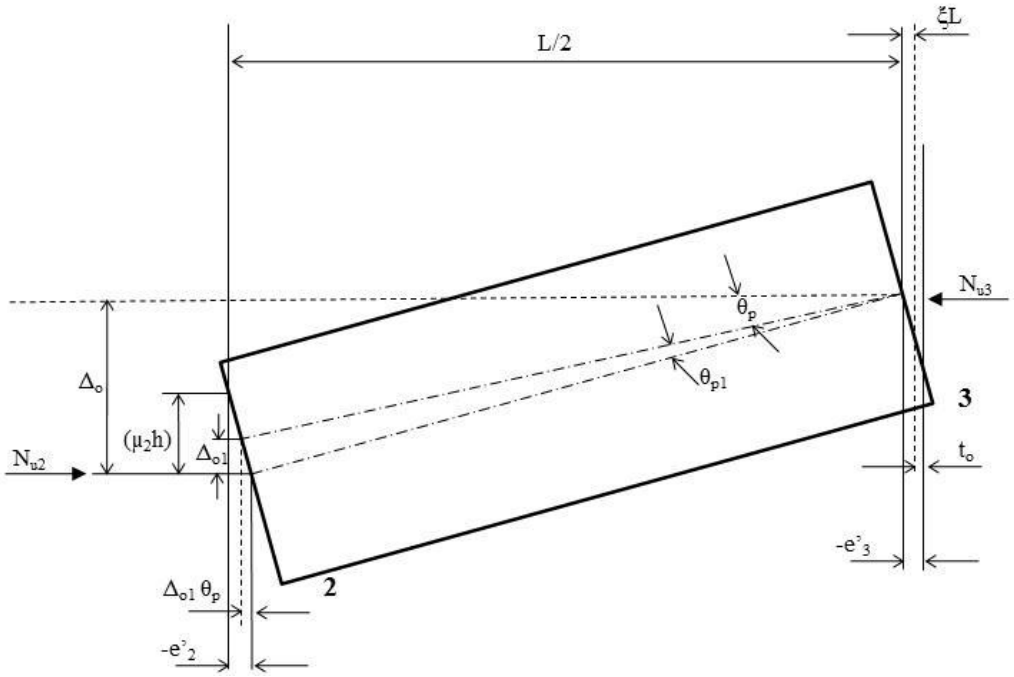

Figure 2.22: *Half-strip element with initial deflection and gap, Eyre (1990)*

Equations were formulated to define the depth of the neutral axis using the strain-rate flow theory and for the total strain. The non-dimensionalised membrane force n_o was defined as:

$$n_o = \frac{\bar{\alpha} - \frac{\delta + \delta_i}{2} - \frac{\bar{\bar{\xi}}}{(\delta + \delta_i)}}{1 + \frac{1}{\bar{S}(\delta + \delta_i)}} \qquad 2.47$$

Where:

$$\bar{\alpha} = \frac{1}{2}\left(\frac{\alpha}{\beta} + 1 - \gamma\right)$$

and $\alpha = \mu_0 / z_o$ = pure flexure neutral axis altitude / pure flexure lever arm; γ = ratio of tension reinforcement support / span; β = depth of centroid of compressive block under pure flexure / pure flexure lever arm; δ = deflection; δ_i is the non-dimensional deflection; $\bar{S}$ = non-dimensionalised stiffness; $\bar{\xi}$ = end gap.

Eyre (1990) made the interesting point that for the case where there is zero gap, $\bar{\xi} = 0$, his equation to define the non-dimensionalised membrane force n_o (Equation 2.47) when considering the total strain, becomes the same as that derived by Christiansen (1963) when looking at two-way spanning rectangular slabs. Also when Equation 2.47 is considered where the initial deflection is equal to zero, $\delta_i = 0$, $\gamma = 0$, it degenerates to the simply supported restrained strip formula in Roberts (1969).

For the point of transition between the two approaches Eyre (1990) concluded that in rigid-plastic systems with a gap both methods gave the same predictions during increasing membrane force, and so the transition from total strain to strain rate could conveniently occur when the deflection corresponds to the maximum compressive membrane force. However in elastic-plastic systems the predictions in the increasing membrane force stage were different. It was noted that tracing of the neutral axis must be unique and the correct method in the increasing membrane stage was the total strain approach. Once the maximum membrane force was reached, the values of the deflection and load were valid as the initial conditions for the strain-rate flow rule, which then accurately predicted the decrease of the compressive membrane force.

The peak applied load always occurred before the maximum membrane force was reached and both were correctly predicted using a total strain rule, Eyre (1990).

2.9 **Key Factors**

Lahlouh and Waldron (1992) conducted a series of tests to validate predictions from a finite element analysis model. This work allowed identification of key factors that have a significant influence on the enhancement produced by CMA.

Three identical slabs of 150mm thickness, 300mm width and 2.5m length were tested. Vertical members were cast at each end of the slab to provide longitudinal restraint, the level of restraint was varied by altering the thickness of the vertical walls, (100mm, 200mm and 300mm) all being 1.8m high and 300mm wide. The slab strips were under-reinforced with a reinforcement ratio of 0.54%. Main reinforcement was 8mm in diameter with 6mm shear reinforcement, for both slabs and walls. A 1:2:4 mix was used with a 10mm aggregate and a water to cement ratio of 0.54.

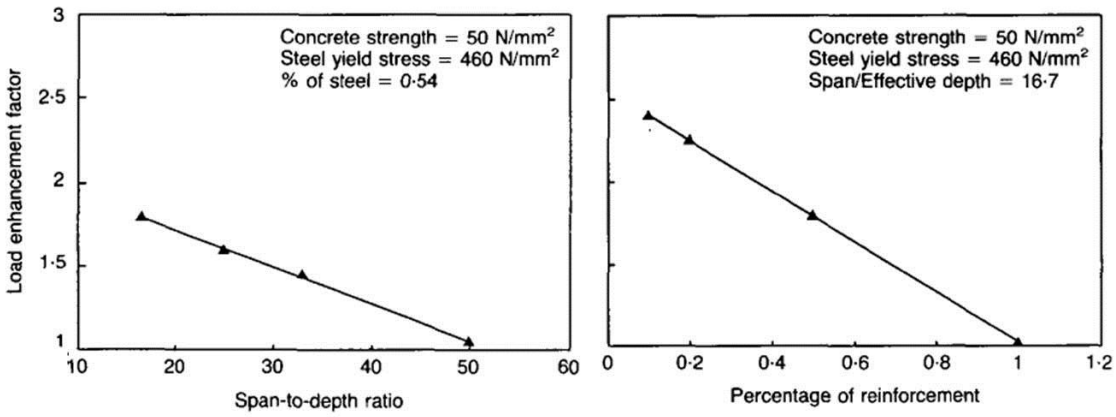

Figure 2.23: *Plots of load enhancement factor due to arching action against span-to-depth ratio and percentage of reinforcement , Lahlouh and Waldron (1992)*

The extent of load enhancement through arching action was shown to be closely related to the span to depth ratio and reinforcement percentage. With an increase in reinforcement percentage the enhanced load factor, which is the factor by which the load has been increased due to CMA, falls almost linearly as the available concrete becomes progressively more utilized in balancing the tensile steel stresses generated by bending and so the concrete capacity available to resist additional membrane forces decreases, Figure 2.23. Therefore for CMA an increase in reinforcement percentage can be detrimental as it reduces the slab's ability to induce compressive membrane forces. With respect to span to depth ratio again there was a linear relationship with the load enhancement factor decreasing as the span to depth ratio was increased, Figure 2.23. As the arch becomes shallower it is unable to resist as much applied load before snap-through occurs and applied loading falls.

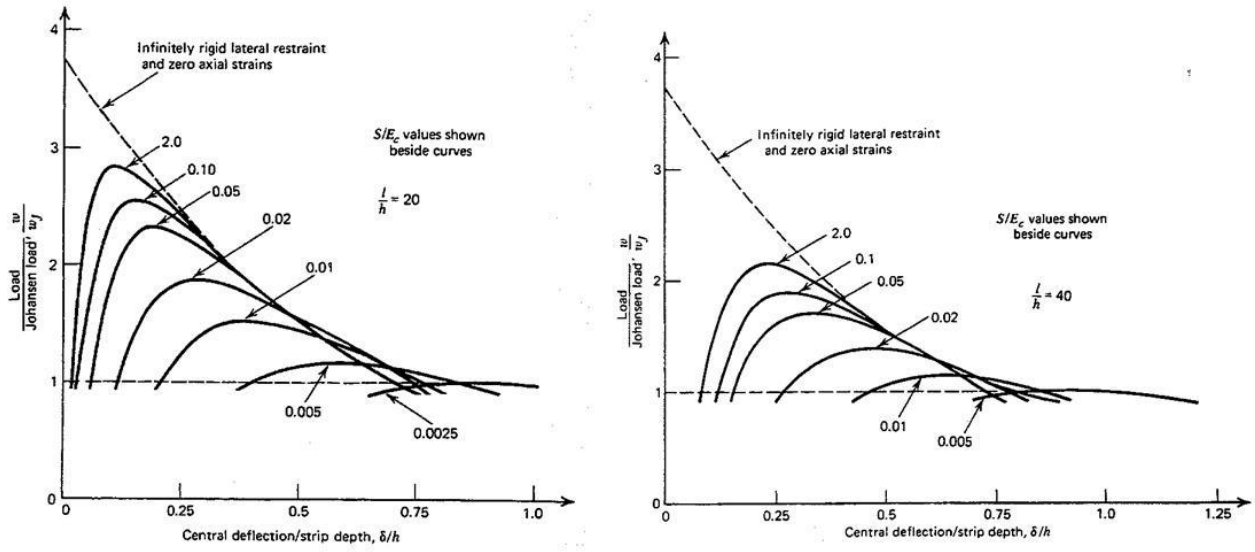

Figure 2.24: *Effect of lateral stiffness and span to depth ratio on CMA, Park and Gamble (2000)*

Results also showed that with increased end restraint there was greater compressive membrane action and thus a higher load carrying capacity. Park and Gamble (2000) applied their method to concrete slab strips of span to depth ratios of 20 and 40 with a range of surround stiffness, Figure 2.24. It was found that at a span to depth ratio of 20 with restraint stiffness equal to the slab stiffness an enhancement of around 2.5 times the load predicted by yield line theory could be achieved. It was noted that the increase in enhancement by making the surround significantly stiffer was not great. Whereas at a span to depth ratio of 40 the effect of increasing the restraint stiffness was much more influential. It was concluded that slab strips at small span to depth ratio were less sensitive to outward movements than slab strips with large span to depth ratios. It was also noted that the restraint stiffness does not necessarily need to be excessive to produce membrane action close to that with a completely rigid restraint.

2.10 **CMA as a Robustness Tool**

Su et al. (2009) tested 12 axially restrained reinforced concrete beams with the objective of determining the enhancement from CMA under transverse (bending) loading in order to further the understanding of robustness of RC structures. The specimens were designed to simulate two bays of a structure, Figure 2.25 shows column stubs cast at each end with an additional stub at mid span representing the removal of the central support. The supports at

each end of the specimen were encastré with full vertical, horizontal and rotational restraint. Additional support was provided at midspan of the specimen using roller bearings on the sides of the beam to prevent any torsion effects. Three factors that were shown to significantly influence the enhancement from CMA included the percentage of reinforcement, the span to depth ratio and the loading rate; testing was divided into three series, A, B and C respectively. Specimens varied in length to give a range of span to depth ratios of 4.08 to 9.08, reinforcement percentage varied from 0.55 to 1.30%. Whilst the loading rate was kept constant for A and B series tests the rate was varied for the C series to represent the instantaneous removal of a column due to explosion.

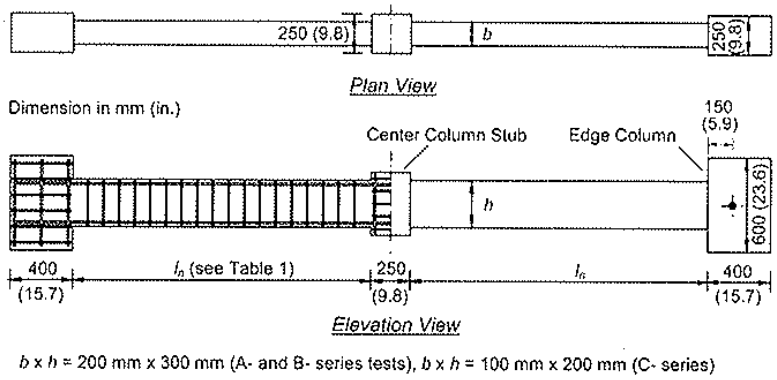

Figure 2.25: *Test Sample Layout with Reinforcement Detail, Su et al. (2009)*

Results showed that the cracking load was reduced as the span to depth ratio was increased due to the increased self weight of the sample. Thus the combination of increased span and self weight causes the moment to exceed the concrete cracking moment earlier. Yielding of reinforcement first occurred at mid span followed by yielding at the supports at the peak load which occurred at between $\delta/h = 0.16$ and 0.34. The horizontal force continued to increase and the maximum compressive reaction occurred at between $\delta/h = 0.29$ and 0.50. Almost all specimens exhibited the transition from compressive arching action to tensile catenary action. At failure δ/h ranged between 0.66 and 1.44 and the ultimate load under catenary action measured at the fracture of the top reinforcement was lower than the compressive arch capacity. The C series showed that the effect of different loading rates was negligible.

The value of δ/h at peak horizontal force gave an indication of the deflection at which snap-through occurred. This was important as it marked the limit of CMA and indicated the

deflection limit which would allow full utilisation of CMA. Previous authors, for example Wood (1961) and Park (1964b), had also suggested values of δ/h at snap-through which agreed with those suggested by Su et al. (2009)..

Whilst it was shown that the flexural capacity of the section was enhanced at the supports and mid-span by 66% and 150%, respectively, the axial force in the section reduces the load carrying capacity due to the P-Δ effect. It was therefore found that in each specimen the maximum vertical load was reached well before the maximum bending moments occurred at critical points of the section and thus the specimen could still resist significant bending moments after peak load had been achieved. A double curvature deformed shape was therefore maintained until reinforcement fracture at midspan under catenary action, supporting the earlier suggestion by Park and Gamble (2000) that catenary action can act beneficially to "catch" the sample once maximum load due to CMA has been achieved.

Comparisons made between predictions using conventional plastic analysis and the experimental ultimate values showed an enhancement factor ranging from 1.53 and 2.63, increasing as the span to depth ratio decreased. The experimental results were then used to validate a proposed theoretical model which was a modification of the method proposed by Park and Gamble (2000) for the use of axially restrained beams. Their proposed enhancement factor was derived empirically to apply to the flexural strength and is shown in Equation 2.48. Since it is empirical further investigation is needed before it can be used with confidence in wider application.

$$\alpha = 2.4\left(1 - \frac{\rho}{3}\right)\left[1 + \frac{5}{\left(\frac{l_n}{h}\right)^2}\right] \qquad 2.48$$

Su et al. (2009) advocated the use of CMA over catenary action to resist progressive collapse as considerable deformation is required for the ultimate capacity from Catenary action to exceed CMA. Since the deformation limit depends on the ductility of the reinforcement, the prediction of enhanced loading due to catenary action can be uncertain since ductility cannot always be guaranteed.

Su et al. (2009) indicated that enhancement dropped with increased span to depth ratio, with the span to depth ratios tested being 4.08, 6.12 and 9.08. At 9.08 an enhancement factor of 1.54 was found. At full scale the specimens would equate to spans of approximately 5m and 10m which are not unrealistic for deep beam sections. The application of a structural element of this nature is limited with use only in specific cases such as transfer beams where column spacing is changed. Beams with such dimensions are not common in standard design for office/commercial buildings. At emergency span after removal of a column, beams are likely to have much greater span to depth ratios and so whilst the study gives a positive insight into using CMA to support transverse loading it is not conclusive for greater span to depth ratios.

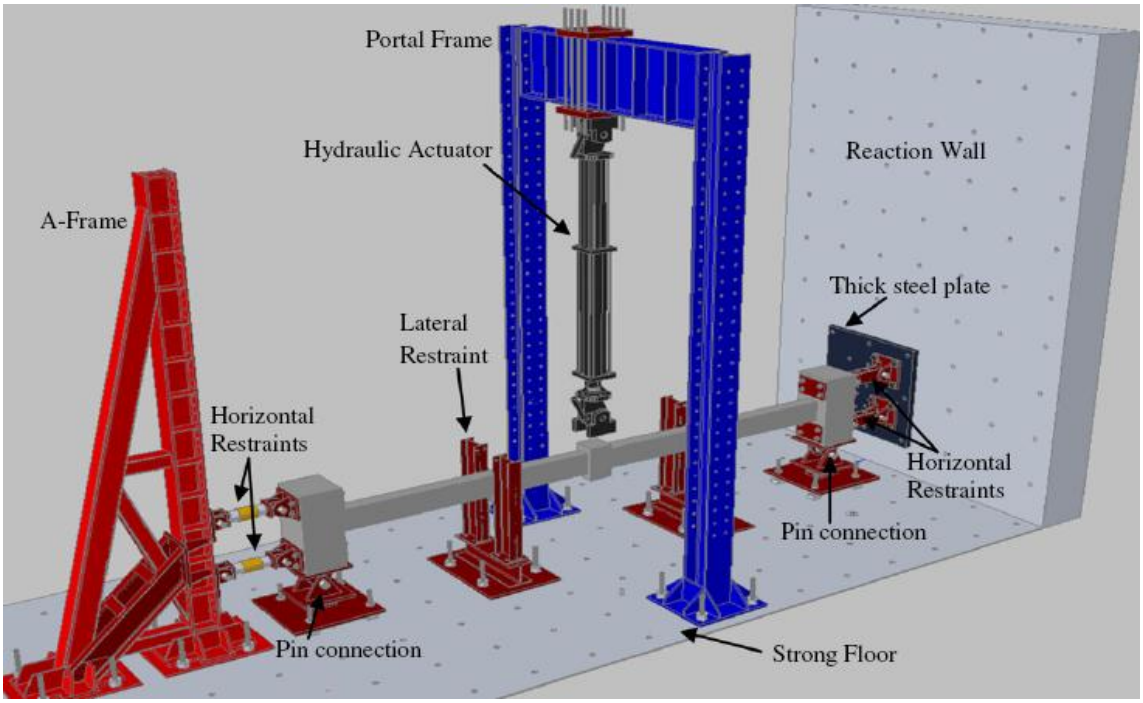

Figure 2.26: *Schematic of test rig, Yu and Tan (2011).*

Similar research was carried out in China by Yu and Tan (2011), in which two half scale samples were tested to investigate the effect of reinforcement detailing (standard or seismic) on structural behaviour. Design of samples was based on the assumption that the central column in the longest side of the building was removed, reflecting the assumption that this point of the structure is most vulnerable due to ease of accessibility. A five storey structure with 6m column spacing was designed to ACI 318-05 with seismic and non-seismic detailing. Scaled samples from these designs were detailed with 0.49% tension reinforcement at the

middle of the double span, creating a span to depth ratio of 25. High yield deformed bar with a yield stress of 511 N/mm^2 and concrete with a compressive strength of 31.2 N/mm^2 were used. To provide sufficient end anchorage samples were constructed with column stubs at each end along with a column stub at mid-span. Lateral restraint to model the undamaged surrounding structure was provided by a steel frame at one end and a reaction wall at the other. A schematic of the test rig can be seen in Figure 2.26. The focus of the experimental investigation was to extend knowledge as to whether catenary action can provide an alternative load path as it is not included in current British and American guidelines on progressive and disproportionate collapse. Further to this a component based finite element analysis was proposed to predict behaviour with the inclusion of membrane action. The extent of arching action (called Compressive Arch Action (CAA)) that was induced was recorded and analysed. The peak applied load supported by CMA was compared to an accidental loading, calculated in accordance with UFC 4 023-03. As the process of load redistribution once a column is lost is dynamic in nature to equate the scenario to a static procedure a dynamic increase factor (DIF) was required. This was calculated based on the UFC 4 023-03 as 1.1 in the compressive phase. It was demonstrated that accidental loading of 38.73 kN slightly exceeded the load capacity through CMA, 38.20 kN, equating to a factor of safety equal to 0.99. Indicating that the compressive arch marginally falls short of having the capacity to support the load conditions expected in the event of column loss.

Yu and Tan (2011) indicated that the supported load can be calculated by:

$$P = \frac{4\left(M_p + M_n - N\Delta\right)}{L} \qquad 2.49$$

Where M_p is the moment at mid-span, M_n is the moment at the support, N is the horizontal compressive force, Δ is the mid-span deflection and L is the double span. It was observed that whilst the axial compressive force caused an increase in the bending moment in the section at mid-span and the support, and consequently an increase in the load supported, when deflection was increased the N-Δ effect resulted in a decrease in load carrying capacity. The effect also caused the peak applied load to occur before the peak horizontal force.

The limitation to the experimentation conducted was that the test span to depth ratio was low in comparison with legislation in current UK design codes. It also ignored the effect of the

slab which whilst being at a higher span to depth ratio would contribute to load carrying capacity and progressive collapse resistance in the compressive and tensile phases of behaviour.

In recent years there have been further examples of the use of small scale experimental testing combined with the development of finite element analysis to investigate the use of membrane action to prevent progressive collapse. Dat (2011) adopted the concept of an instantaneous removal of a column from an explosion and noted that the axial force carried by the lost column must be redistributed within milliseconds within the structure. All slabs above the lost column deflect identically and dynamically causing two notable increases to the internal forces from firstly the double span effect as the slab bridges the failed column and the span doubles, and secondly the existing loads are increased by the dynamic effect of the column loss by a factor up to 2.0. The identification of these two effects is common throughout all research into the use of membrane action as a robustness tool.

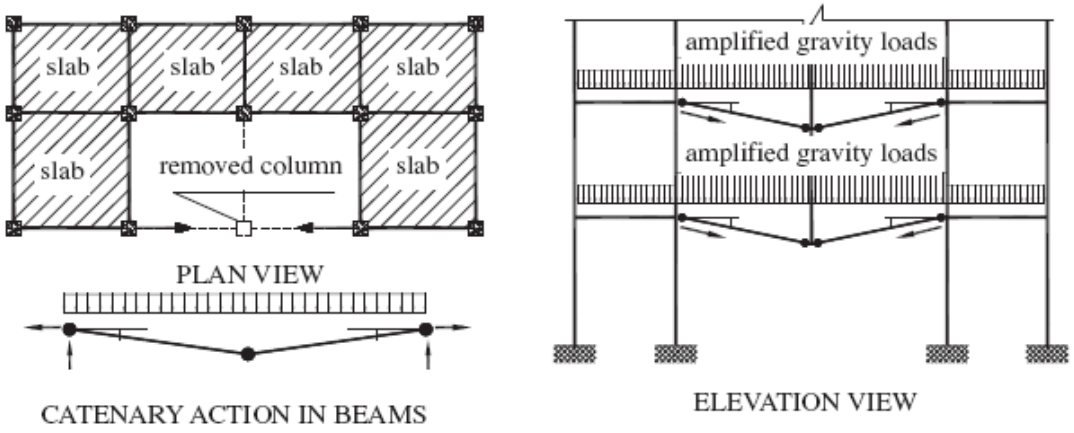

Figure 2.27: *Catenary action following loss of an external midspan column, Dat (2011)*

Dat (2011) highlighted that the focus of previous studies from the likes of Yi et al (2008) and Sesani (2007) had shown that when a midspan column is lost tensile membrane (catenary) action can be an effective mechanism to prevent progressive collapse due to the very strong diaphragm provided by the in-plane slabs (Figure 2.28). However, in order for catenary action to be beneficial in mitigating collapse when a penultimate internal or external column is lost, a compressive ring within the slab is required to provide restraint (Figure 2.28).

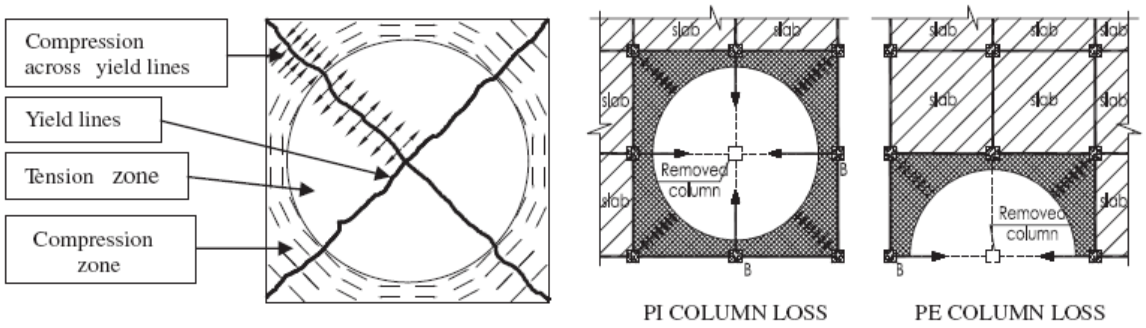

Figure 2.28: *Membrane action in a slab from penultimate internal or external column loss, Dat (2011).*

The results from the ¼ scale experimental testing accompanied by numerical analysis demonstrated that it is feasible for catenary action within unrestrained slabs to provide sufficient enhancement to prevent collapse. Load enhancement was shown to be up to double the flexural strength. Dat (2011) advocated the further development of experimental testing over finite element analysis. This was due to the shortcomings of FEA in predicting behaviour in the final failure modes and the modelling of localised behaviour such as concrete crushing, torsional failure of perimeter beams due to slab hogging moments and the fracture of bottom reinforcement at larger deformation.

Bailey (2001) had previously studied membrane action within unrestrained composite floor slabs subject to high displacement during fires and through a simplified analytical design method, which was based on the yield line patterns observed in large scale testing, and also found that tensile membrane action could successfully prevent progressive collapse.

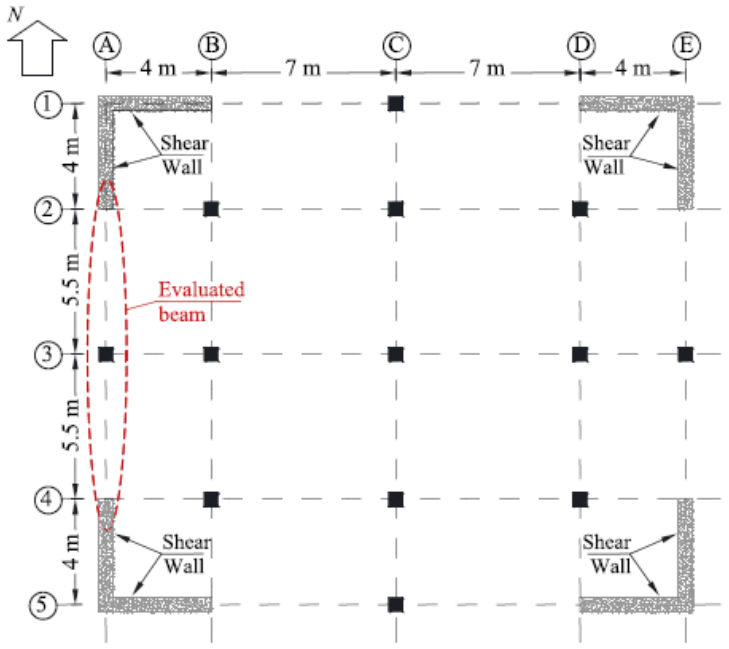

Figure 2.29: *Floor plan of model building for experimental investigation, FarhangVesali (2013)*

Rather than focusing on membrane action within the slab FarhangVesali et al. (2013) decided that one of the primary mechanisms for preventing progressive collapse in longitudinally restrained RC beams is the enhancement of both capacity and stiffness from CMA. Six 2/5th scale RC assemblies based on the perimeter beam of a seven-story building designed to current Australian building codes of practice were tested. The floor plan of the model building is shown in Figure 2.29 which highlights that the longitudinal restraint to the beam is provided by the shear walls. The main variables in the experimental programme were the longitudinal reinforcement and the shear link arrangement. The simplicity of the test rig in providing restraint (Figure 2.30) resulted in a fixed boundary condition that could be accurately modelled in numerical analysis. Test specimens were 180mm deep providing a test span to depth ratio of 26. Load was applied via a displacement controlled actuator at mid-span to a column stub within the RC assembly at a rate of 0.1 mm/sec.

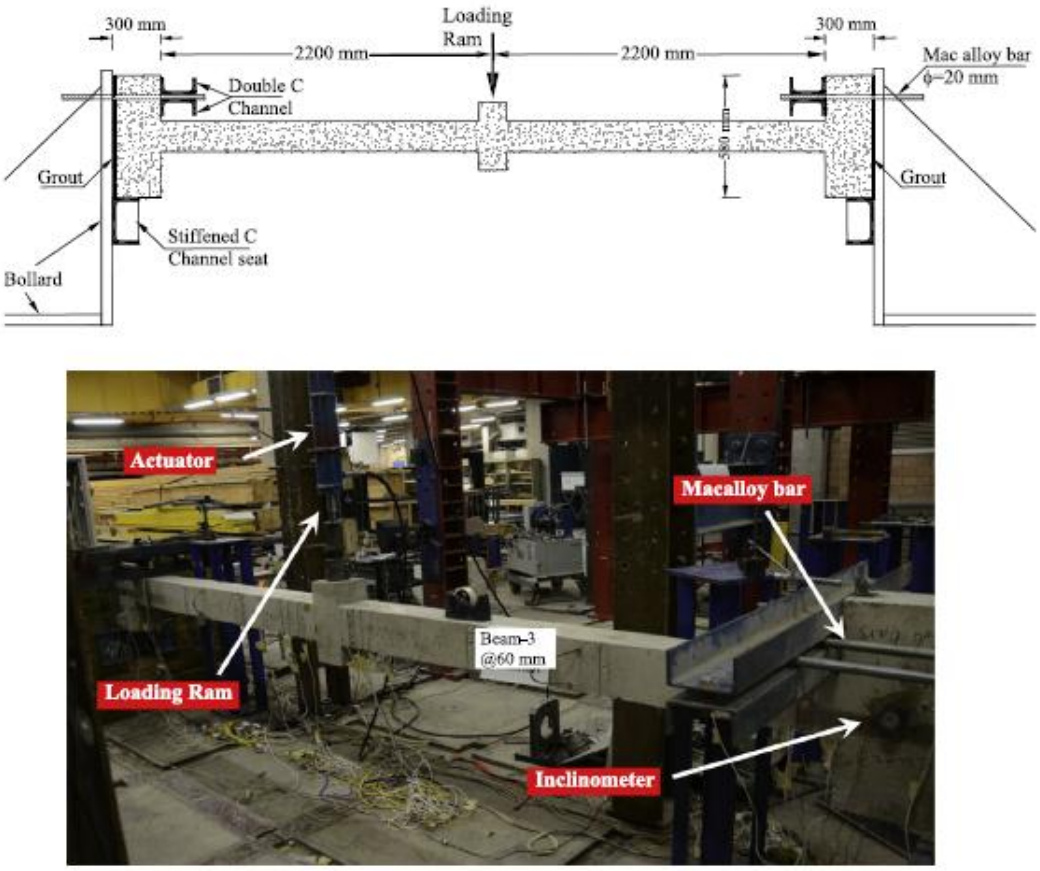

Figure 2.30: *Experimental setup, FarhangVesali (2013)*

Readings from strain gauges on the hogging steel reinforcement in the top of the section at the supports showed that the tensile strain had exceeded the yield strain of the reinforcement. Consequently slip in the anchorage length occurred indicating strain penetration into the beam end-support. It was concluded that neglecting this effect could lead to an overestimation of initial stiffness and ultimate load capacity.

Results indicated that the longitudinal reinforcement ratio has only a minor effect on the load capacity of restrained RC elements. More influential is the concrete compressive strength. The experimental results were used to modify the numerical analysis method devised by Valipour et al. (2013) and provided accurate predictions of the full load-deflection behaviour and peak load of the test specimens.

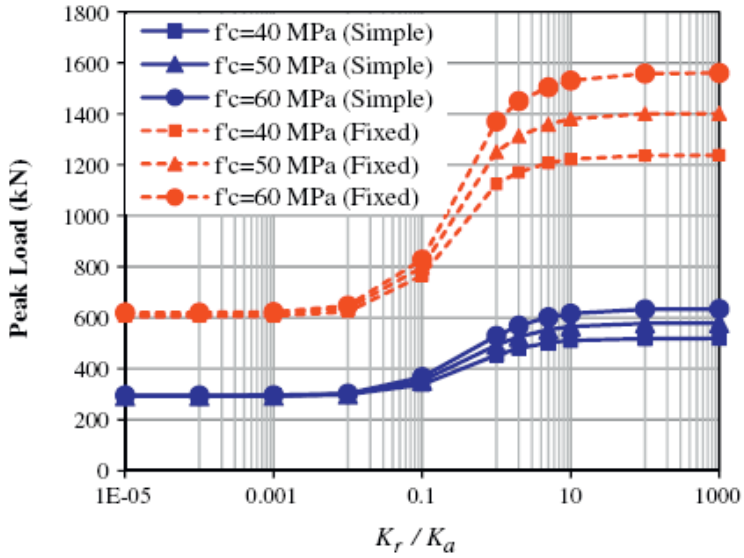

(a)

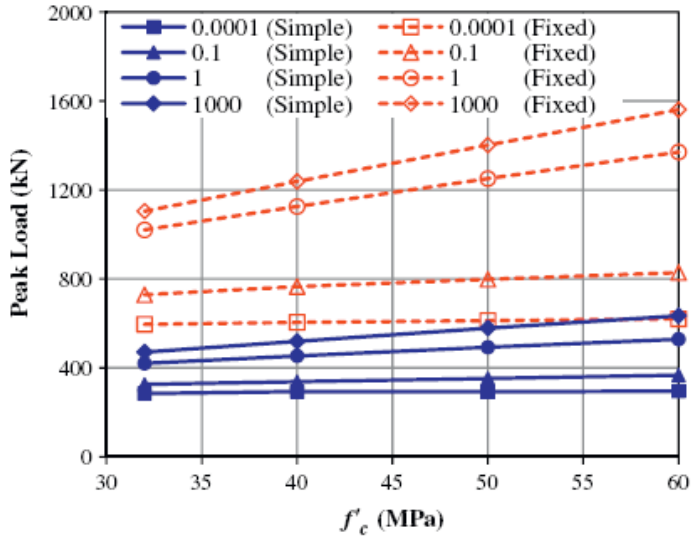

(b)

Figure 2.31: *(a) Peak load versus support longitudinal stiffness ratio (K_r/K_a) for beams with different f'_c values and different end supports, i.e. simple and fixed, (b) peak load versus the compressive strength of concrete for beams with different longitudinal stiffness ratio (K_r/K_a) and different end supports, i.e. simple and fixed, Valipour et al. (2013)*

Valipour et al. (2013) presented the devlopment of a generic nonlinear compound frame model which was applied to the investigation of CMA in reinforced concrete beams. The model accounted for cracking and crushing of the concrete, yielding of the reinforcement and was

able to account for the compressive softening of concrete. The model was verified against previous experimental data, albeit at low span to depth ratios, and it was found that the effect of the support stiffness and concrete compressive strength was important in predicting the member response. To further investigate these results a parametric study was undertaken. The results from beams with a span to depth ratio of 15 loaded at mid-span are shown in Figure 2.31. The stiffness ratio, K_r/K_a, was defined as the ratio of restraint stiffness K_r to the axial stiffness of the beam. Results indicated that the relationship between concrete compressive strength and load enhancement was almost linear. It was also shown that if the stiffness ratio exceeds 10 the beam can be considered to have fully fixed restrainsts whilst if the stiffness ratio is below 0.01 the effect of arching action is negligible.

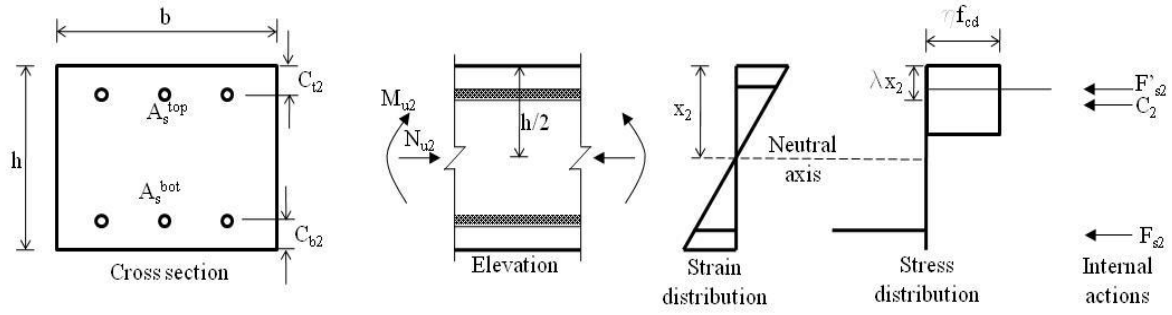

Figure 2.32: S*tress distribution at yield point, Merola (2009)*

Merola (2009) investigated the requirements to prevent progressive collapse set out in the current codes and regulations that govern the construction of reinforced concrete buildings in Europe and the UK. An integral part of the work was the development of a full load-deflection model for reinforced concrete inclusive of both compressive and tensile membrane action. To model the CMA behaviour Merola (2009) modified the method devised by Park and Gamble (2000), as had Su et al. (2009). The modification was to adopt the stress block described in EC2 (EN 1992-1-1:2004) as depicted in Figure 2.32. The compressive forces C_1 and C_2 can thus be written in accordance with EC2 as:

$$C_1 = \eta f_{cd} \lambda x_1 b \qquad 2.50$$

$$C_2 = \eta f_{cd} \lambda x_2 b \qquad 2.51$$

Where the concrete design compressive strength f_{cd} was defined as:

$$f_{cd} = \frac{\alpha_{cc} f_{ck}}{\gamma_c} \quad 2.52$$

and,

λ is the ratio of the compressive zone to the neutral axis depth

η is the coefficient defining the effective strength

b is the breadth of the beam

α_{cc} is the coefficient taking account of long term effects on the compressive strength and of unfavourable effects resulting from the way the load is applied, given in the UK National Annex as 0.85.

f_{ck} is the characteristic cylinder strength

γ_c is the partial safety factor for concrete given as 1.2 for the accidental design situation in EC2 (EN 1992-1-1:2004) clause 2.4.2.4.

The neutral axes at sections 1 and 2, x_1 and x_2 (Equations 2.24 and 2.25 above) were modified to become:

$$x_1 = \frac{h}{2} - \frac{\delta}{4} - \frac{\beta L^2}{4\partial}\left(\varepsilon + \frac{2t}{L}\right) + \frac{F_{s1} - F_{s2} - F'_{s1} + F'_{s2}}{\eta f_{cd} \lambda b} \quad 2.53$$

$$x_2 = \frac{h}{2} - \frac{\delta}{4} - \frac{\beta L^2}{4\partial}\left(\varepsilon + \frac{2t}{L}\right) + \frac{F_{s1} - F_{s2} - F'_{s1} + F'_{s2}}{\eta f_{cd} \lambda b} \quad 2.54$$

When the reinforcement is equal top and bottom the tensile forces are defined as:

$$F_{s1} = F'_{s1} = A_s \frac{f_{yk}}{\gamma_s} \quad 2.55$$

$$F_{s2} = F'_{s2} = A_s \frac{f_{yk}}{\gamma_s} \quad 2.56$$

The membrane force N_{u2} and bending moment acting at mid-depth as described in Section 2.6.1 can be re-written as:

$$N_{u2} = C_1 + F'_{s2} - T \quad 2.57$$

$$M_{u2} = C_2\left(0.5h - 0.5\frac{\lambda}{2}x_2\right) + F'_{s2}(0.5 - d') + F_{s2}(0.5h - d') \quad 2.58$$

As in Park and Gamble (2000) the sum of moments about the mid depth at one side of the yield section relates the central deflection of the beam to the load carried in the following equation:

$$M_{u1} + M_{u2} - N_u\delta = P\beta L \tag{2.59}$$

With Merola's (2009) modification, Equation 2.27 becomes:

$$\varepsilon + \frac{2t}{l} = \frac{\left(\frac{1}{bhE_c} + \frac{2}{LS}\right)\left\{\eta f_{cd}\lambda b\left[\frac{h}{2} - \frac{\delta}{4} - \frac{F_{s1} - F_{s2} - F'_{s1} + F'_{s2}}{\eta f_{cd}\lambda b}\right] + F'_{s2} - F_{s2}\right\}}{1 + \left(\eta f_{cd}\lambda b\frac{\beta L^2}{4\,\partial}\right)\left(\frac{1}{bhE_c} + \frac{2}{LS}\right)} \tag{2.60}$$

Similar assumptions were made for the stiffness parameter S as in Park and Gamble (2000). The assumption that the effects of creep and shrinkage strains can be neglected was also maintained and it was considered that this would result in at most a 10% inaccuracy in the results.

To validate this modification Merola (2009) made comparisons with previous testing by Taylor et al. (2001), Roberts (1969) and Lahlouh and Waldron (1992). Results showed good correlation with experimental data following similar trends to findings from Park and Gamble (2000). It should be noted that no significant difference was found between predictions from Merola (2009) and Park and Gamble (2000). Merola concluded that his proposed method provided an adequate prediction of the compressive phase. However both methods were validated through comparisons with testing at low span to depth ratios. Clarification of the effectiveness of the methods at high span to depth ratios is still needed.

An insightful part of the research carried out by Merola (2009) was the definition of the reinforcement failure criteria for both the compressive and tensile phase. It was highlighted that the proposed method of prediction assumed that both top and bottom reinforcement remained intact through the compressive phase into the tensile phase, however this may not be the case and fracture could occur at different phases of the loading. This is by far the most novel part of the research, the ability to accurately predict the failure of reinforcement is imperative when modelling the load deflection behaviour of reinforced concrete.

A parametric study was conducted on an isolated beam restrained both axially and rotationally. The study used the developed theoretical model to examine each factor in turn whilst keeping the others constant, dimensions of the beams were based on realistic designs. The span to depth ratio ranged from 10 to 30 and reinforcement from 0.5 to 2%. This study confirmed earlier work from Rankin and Long (1997), Park and Gamble (2000) and Taylor et al. (2001) that the key parameters affecting CMA are the span to depth ratio, axial restraint stiffness and the concrete compressive strength.

A series of frames designed according to EC2 (BS EN 1992-1-1:2004) were then studied with the notional instantaneous removal of a column. A parametric study was not carried out but a series of realistic framed designs were investigated. It is also of note that only the beams of the frames were considered in the analysis, any additional membrane strength given by the one way spanning slabs was neglected. Beams had span to depth ratios ranging from 15 to 25 over emergency (double) spans of 10, 14 and 18 metres.

The study predicted the load carrying behaviour of reinforced concrete frames inclusive of membrane action and steel fracture criteria and showed that robustness can be achieved with the minimum tie requirement in BS 8110-1:1997 Clause 3.12.10. The study advocated the use of Grade C reinforcement and recommended that the area of bottom reinforcement should be increased to that of the requirement for a 10 storey building. The study yielded a number of useful insights, the first being that it was feasible that CMA could be used to enhance robustness in a framed building with a realistic structural design. The work developed a means to predict fracture of reinforcement that was novel and essential for a full prediction of load deflection behaviour.

The limitations to Merola's method appear to be that only beams were tested in the frames, no contribution from slabs was included. The consequence of this was that the emergency span to depth ratio was limited to 30. This excluded the higher emergency span to depth ratios in two way spanning flat slab structures. In such instances continuous elements are commonly designed with a limiting span to depth ratio of 26, with the ability to increase this to around 30 in some cases (BS 8110-1:1997 Table 3.9). Thus in an emergency span situation it is likely that span to depth ratios will be in the range of 50 to 60. Merola (2009) also stated the need for reliable testing inclusive of membrane forces for comparison with theoretical models of

realistic structures. It was also recommended that further work was needed to quantify the amount of damage that would be inflicted on a structure when using the instantaneous removal of a column assumption.

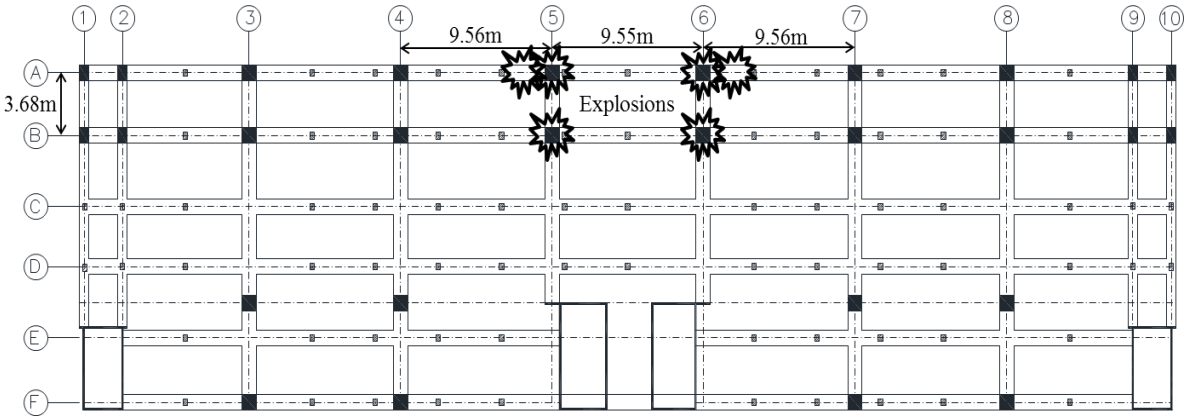

Figure 2.33: *First floor plan of RC Crowne Plaza hotel, Sasani (2011)*

Whilst the current codes of practice and guidelines considered in Section 2.2 of this Chapter recommend the instantaneous removal of a single column and consequent analysis of alternative load paths in the structure, Sasani (2011) considered the more severe scenario created from a terrorist blast. The 11 storey RC Crowne Plaza hotel located in Houston, Texas was built in 1973 and was due for demolition when it was made available for full scale experimental testing. After the experiment was concluded the building was demolished by implosion. Through explosive charges 4 adjacent columns (two internal and two perimeter) and two beam segments of the hotel were removed as shown in Figure 2.33. This resulted in a situation where first storey beams had to span two failed columns creating a span to depth ratio of 14.37. In the event of losing the columns severe cracking and yielding of reinforcement caused the expansion of the beam through the axial compression and arching action (CMA) which was induced. Sasani (2011) called this mechanism ‘beam growth’. The expansion of the beam was restrained primarily by the in-plane action of the floor system and additionally through the frame. This resulted in small vertical deflections (46mm) creating optimum conditions for arching action. The increase in the beam yield moment by about 38% was attributed to CMA, which in addition to the Vierendeel (frame) action of the floor slab of the frame prevented progressive collapse of the structure. This full scale testing presented a clear indication that in certain situations CMA can aid mitigation of progressive collapse.

Sasani (2007) carried out a similar full scale study during demolition of the reinforced concrete framed University of Arkansas Medical Centre dormitory which had been constructed in 1958. The 10-storey structure comprised transverse beams supporting one-way spanning slabs at a span of 6.71m producing an emergency span of 13.42m and a span to depth ratio of 66.11. Controlled explosives destroyed the central ground floor perimeter column representing sudden column removal through localised damaged with no effects from air blast. At the first floor directly above the failed column the measured vertical deflection was only 6.6mm. The deflection on each floor was almost identical which was attributed to the large axial stiffness of the columns. No additional structural elements failed due to the initial column failure, with only cracking recorded but no yielding of reinforcement, hence the structure successfully resisted progressive collapse.

2.11 **Conclusions**

Early studies compared the enhancement found from CMA to ultimate load predictions from the yield line method developed by Johansen (1972), whilst more recent studies made comparisons to the ultimate load from the flexural response based on the analysis methods outlined in modern codes of practice. The enhancement factor, the maximum load inclusive of arching action over the predicted value exclusive of membrane forces, ranged from 1.5 up to 4.0. The difference in enhancement can be attributed to variations in factors that have been highlighted to have a significant effect on CMA:

- Percentage of Reinforcement
- Span to Depth Ratio
- Restraint Stiffness

With reference to the scope of the current work the factors of most pertinence are the span to depth ratio and the restraint stiffness. It is widely agreed, as illustrated by Lahlouh and Waldron (1992) in Figure 2.23, that with increasing reinforcement percentage the enhancement from CMA decreases. In flat slabs the percentage will be dependent on the design span with a notable difference between the column and middle strip as well as interior and exterior bays. In most design situations flat slabs can be considered to have a low percentage of reinforcement and potentially should have significant load enhancement from CMA.

The influence of the span to depth ratio follows a similar trend, in that with increasing span to depth ratio the benefit from arching action decreases. The extent of this detrimental effect is open to question. Taylor et al. (2001) have suggested that a span to depth ratio of 15 can be thought of as the limiting value at which any beneficial enhancement can be achieved, whilst Park and Gamble (2000) indicated that an enhancement factor of up to 2.0 could still be obtained at a span to depth ratio of 40. There is still doubt about the benefits of CMA at high span to depth ratios.

Results from Roberts (1969) supported by Park and Gamble (2000) showed that whilst the benefits from CMA reduced as the lateral restraint stiffness reduced, the effect was not as dramatic as the effects of reinforcement percentage and span to depth ratio on enhancement.

Roberts (1969) found that the enhanced load fell by just 10% when the restraint stiffness was equal to that of the test beam compared to when the restraint stiffness was 11 times greater than the test beam. This was encouraging for CMA in the emergency span situation and was reflected by results from Merola (2009) where enhancement was still achieved at relatively low levels of restraint stiffness.

The prediction methods reviewed share similarities in their approach, for example the use of a simplified collapse mechanism of the slab. Amongst these the methods developed by Park and Gamble (2000) and Rankin and Long (1997) were similar with both utilising total deformations and strains. Park and Gamble (2000) gave a prediction of the full load deflection behaviour based on the calculation of the concrete shortening and support movement at assumed increments of mid-span deflection. However Rankin and Long's method was based on a simplified version of McDowell et al. (1956) with the use of a 3 pin arch analogy which only gave the maximum enhanced load at maximum deflection. Both methods have been validated against experimental testing, albeit at small span to depth ratios.

In reviewing the use of total strains or strain rates in predicting the membrane force deflection relationship many authors, especially Eyre (2000), have concluded that it is appropriate to use the total strain when predicting the maximum membrane force. As it is the maximum membrane force that is of interest when assessing the benefits of CMA in an emergency span situation, only prediction methods using the total strain approach will be looked at further.

The method of Park and Gamble (2000) was altered by Su et al. (2009) and Merola (2009) specifically for the use of CMA as a robustness tool. Neither method however included the influence of the slab, concentrating on the beams of the frame. Su et al. (2009) focused on deep beams with low span to depth ratios, which has limited application to common design practice, but did validate predictions of emergency spans with experimental testing. Merola (2009) looked at realistic structural frames but again only focussed on the beams restricting the span to depth ratio in the emergency span to 30. Both gave great insight into the feasibility of utilising CMA as a robustness tool, as did the full scale testing carried out by Sasani (2009), they pointed to the need to quantify the contribution of continuous slabs in the emergency damage situation.

The previous researches conducted with the aim of addressing the shortcomings of codes of practice by neglecting the potential for CMA to provide an alternative load path share similarities in the assumption made in modelling the scenario of column loss. To assess a structures resistance to progressive collapse all adhere to the key element removal approach suggested in numerous guidelines and codes of practice as reported in Section 2.3. In the analytical and scaled experimental investigations key element removal was achieved by the instantaneous removal of a column and assessment of arching action induced in the resulting double span. These approaches were not extended to include structures such as flat slab buildings in which very high span to depth ratios would occur following the removal of a column. It is in light of this that further experimental data is required to allow for a prediction method to be validated and then used with confidence in this context. Thus the experimental programme which forms the major part of this research has been concerned with investigating CMA at very high span to depth ratios.

Chapter 3: Experimental Study of CMA in RC Buildings

3.1 **Introduction**

The findings from the review of previous literature demonstrated that the focus of the majority of work undertaken in the field of compressive membrane action has been in the application of the well known load enhancement found in restrained RC elements at low span to depth ratios in instances such as bridge design. For the developed theoretical prediction methods to be employed in the situation created when a column is lost from the perimeter of a building structure it was concluded that there is insufficient experimental data to facilitate validation of the methods at large span to depth ratios. A large scale experimental investigation has thus been devised to model two perimeter bays of an RC building with the loss of the central support.

In the early stages of the design process for the experimental apparatus and whilst devising the procedure for testing 6m long specimens it became evident that there were limitations in the possible scope due to the experimental facilities, time restrictions of the research period and lack of technical support. It came to light at this stage that another PhD student (Peter Smith) had as a focal point of his research a study into the behaviour of RC slabs in the tensile membrane phase, seeking to establish the load carrying capacity of the catenary action formed at larger deflections in the event of column loss. A novel aspect to his research was the planned experimental investigation but similar limitations were faced in the scope of the programme. To fulfil the aims of both projects a collaboration was formed with the focus of the research reported here being the compressive phase of behaviour in samples while the later tensile phase was examined by P.Smith. The design of the test rig was carried out by both parties as a result of joint brainstorming sessions with continued collaborative design development to ensure the test rig served the purpose of both research projects.

The aim of the devised experimental programme was therefore to model and quantify the behaviour of reinforced concrete buildings in the situation when a column has been lost. It was assumed that the column was notionally removed instantaneously and the behaviour of the structure was investigated by considering a double span situation. Lateral restraint that would have been provided by the surrounding intact structure was modelled by a steel test rig. The focus for the author was the early stages of behaviour where compressive membrane action was expected to be evident. The point after snap-through of the compressive arch when the load carrying capacity dropped off was taken as the end of relevant behaviour for this research project. At this point tensile membrane action became the mechanism supporting load, which was the focus of the research of P.Smith.

With two parties conducting the experimental programme in collaboration the design of test specimens was split so that the aims of each research project could be achieved. P.Smith designed 6 no. specimens to model edge beams and slabs from a conventional beam and slab building. In those specimens the parameter of interest was the percentage of reinforcement, the influence of which was investigated by detailing an incremental increase for each sample. The main focus of this research project was the behaviour of flat slab buildings and 6 no. specimens were designed at various span to depth ratios representing different column spacings in buildings. The influence of reinforcement was also investigated by having specimens which represented column slab strips with 0.4% and middle slab strips with 0.2% reinforcement.

It should be reiterated that the results from all 12 test specimens have been included in both pieces of research, the compressive phase is the focus of this research whilst the later tensile phase is the focus of research by P.Smith.

3.2 **Experimental Concept**

A generic 6 bay structural frame has been used as the basis upon which the experimental specimens have been modelled. It was assumed that the central perimeter column has failed through accidental or malicious means. For the purpose of this experimental investigation it was assumed that the column was removed instantaneously and the slab was not undamaged in the process. Dynamic effects of column loss have not been investigated, the behaviour of the

structure once the central support was lost has been determined based on a static response to load applied centrally. The adjacent structural bays to the damaged area were assumed to remain intact and provide lateral restraint to the double span slab section. It was also assumed that each floor acted independently of each other, with each individual floor plate acting to span the failed column. The two central external structural bays have been modelled in the experimental investigation. Figure 3.1 summarises the assumptions made.

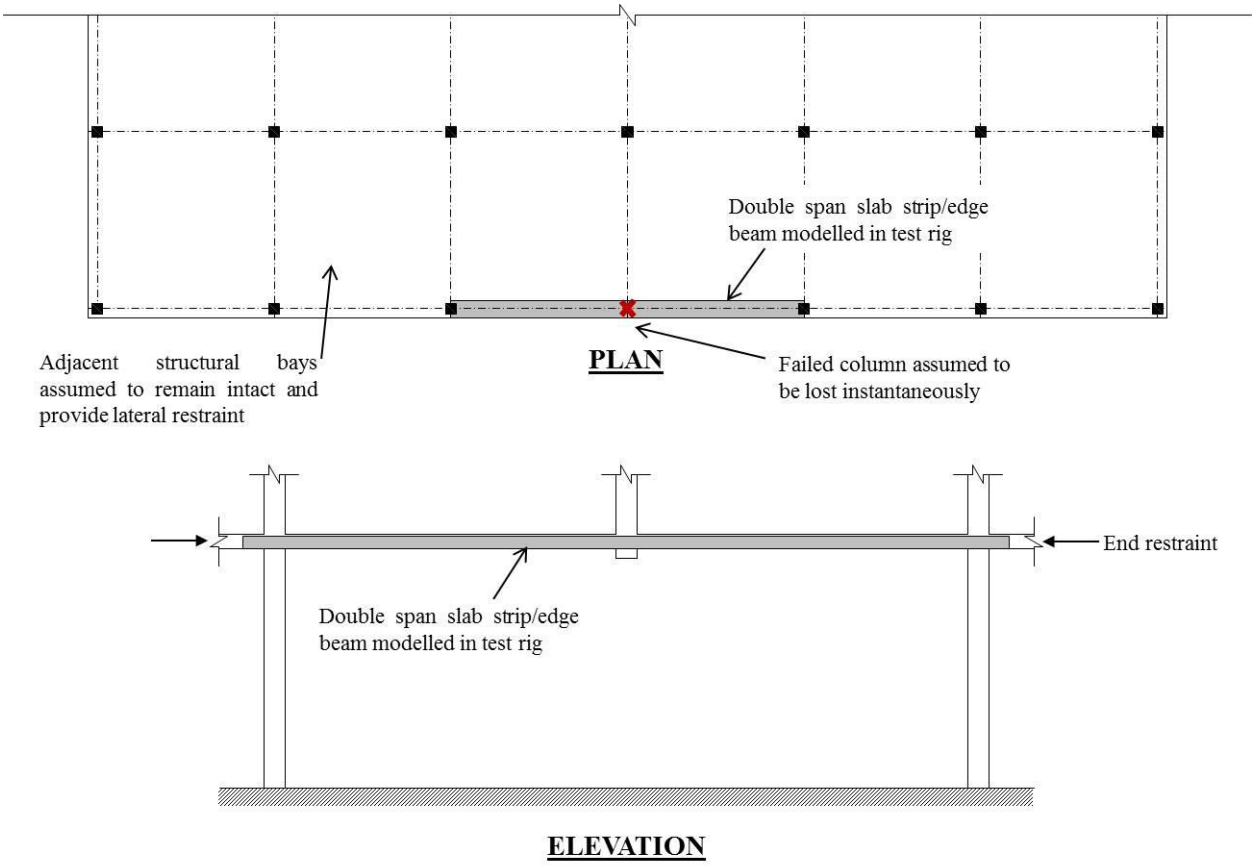

Figure 3.1: *Experimental concept simulating column loss*

It is worth pointing out that the behaviour described above is idealised and unlikely to occur in practice. In particular the loss of the column would only be instantaneous in the event of an explosion and would be accompanied by various dynamic effects. However it has been posed as a situation in which a large span to depth ratio would occur and it is the development of compressive membrane action at large span to depth ratios that is the focus of the research.

3.3 **Rig Set Up**

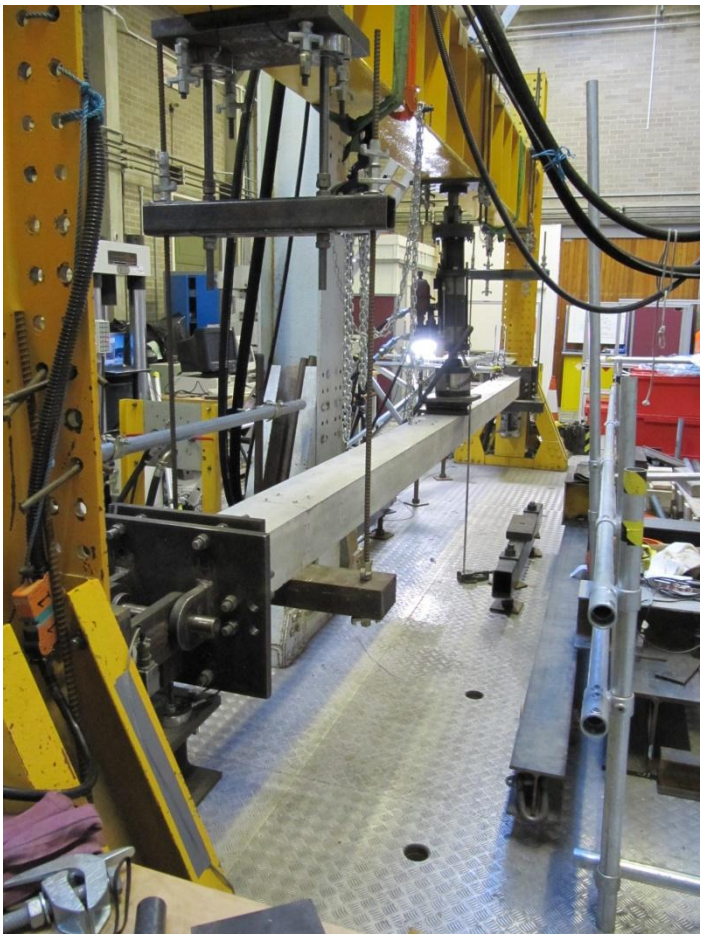

Figure 3.2: *Photograph of test rig with central support removed and load actuator lowered*

The design of the test rig shown in Figure 3.2 was undertaken to allow the behaviour of restrained RC samples to be investigated. The system devised provided three primary vertical reactions that model two structural bays supported by three columns. Vertical reactions at these locations were provided by steel hangers that were supported by the girder of the H-frame, as shown in Figure 3.3. A system of strain gauges and strain gauge based load cells measured the vertical reaction at locations A, B, C, D and M. The end detail that provided connectivity of the RC specimen to the steel H-frame also provided measurement of the horizontal reaction by load cells mounted on the face of a column of the H-frame.

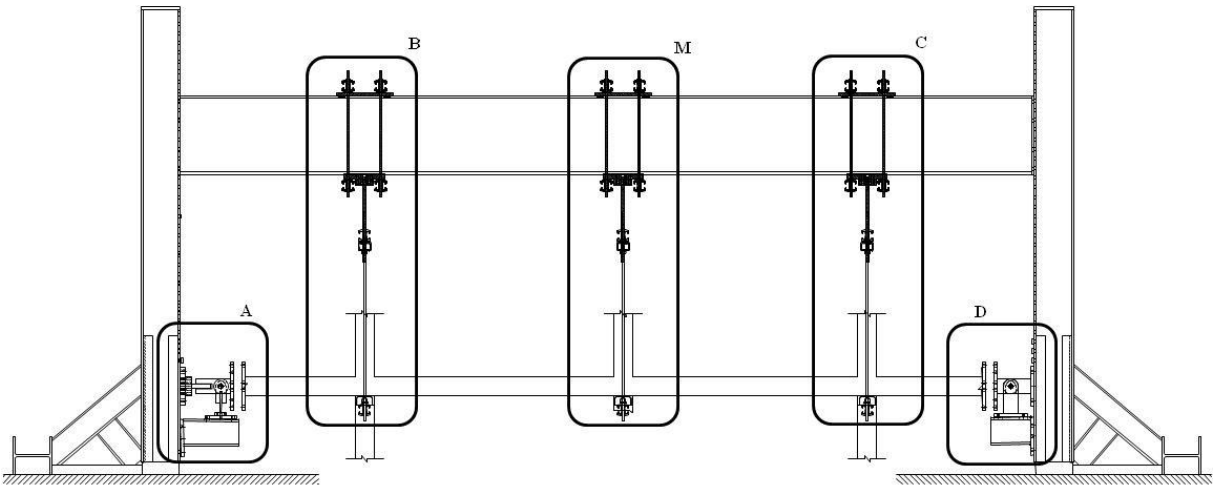

Figure 3.3: *Test rig representing 2 bay system with instantaneous removal of central column.*

3.3.1 **End Detail**

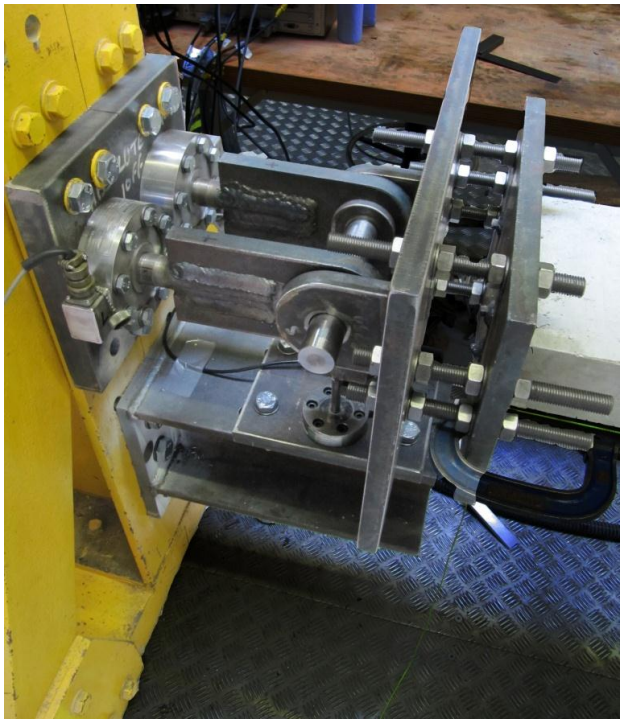

Figure 3.4: *Photograph of end detail connection to H-frame providing end restraint to RC sample and measurement of reactions via load cells*

The degree of rotation and restraint that is provided at the connection detail between the H-Frame and the specimen at points A and D in Figure 3.3 has a significant influence on the behaviour of the test sample and was designed to replicate realistic conditions. Figure 3.5 illustrates the three directions of movement at the end of the test specimens. Movements in the *x* and *y* directions were restrained and the forces in these directions were measured at point A. All specimens were reinforced symmetrically and loaded at midspan; therefore it was unlikely that there would be any significant movement in the *z* direction so no direct restraint was made. Rotation about the *z* axis was allowed, effectively creating a pin joint. This was more realistic than a fully restrained end detail which would have induced unrealistic end restraint moments on the specimen. The pin joint was located at the approximate position of the point of contraflexure of the adjacent bay of the continuous slab / beam considered.

The magnitude of the membrane force in the *x* direction (see Figure 3.5) was of particular interest. The data obtained from the applied load and measured reaction forces has allowed for greater analysis of the contribution from CMA.

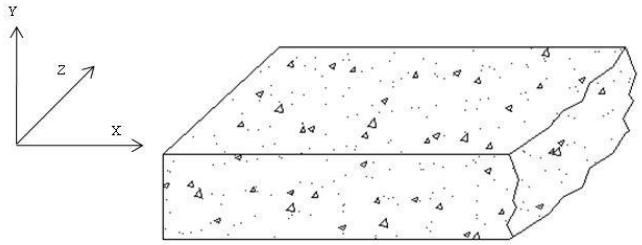

Figure 3.5: *Direction of movement of test specimens.*

The designed end detail is shown in Figure 3.6, Figure 3.7 and Figure 3.8. The connection between the concrete and the end plate was made by welding starter bars (with sufficient lap length to the main reinforcement) to the steel endplate. The weld was designed to resist the full tensile force capacity of a 12mm bar, the largest diameter of starter bar used. A fillet weld was made on the full circumference of each bar on both the inside and outside face of the steel endplate.

Indicated in the figures are the positions of the load cells. The capacity of each of the load cells measuring the force in the *x* direction was 222kN, giving a total 444kN load capacity in

both compression and tension. The load cells measuring the force in the *y* direction had a joint capacity of 50kN, in both compression and tension.

The pin joint was created by steel lugs with a steel axle passing through them, as shown in Figure 3.6 and Figure 3.7. The system restricted movement in the two directions, allowed rotation and ensured only minimal transverse forces were applied to the load cells, which could potentially have affected the accuracy of their readings. This will be discussed further later in the thesis.

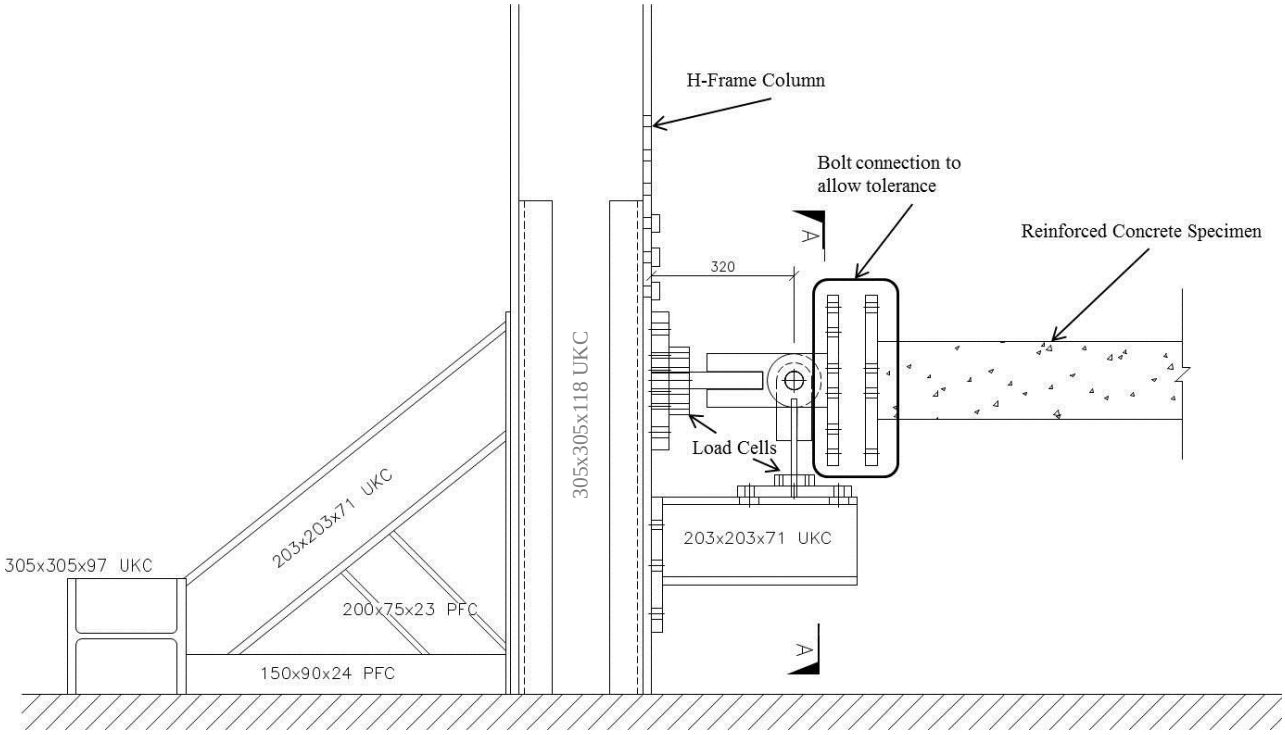

Figure 3.6: *Elevation of End Detail*

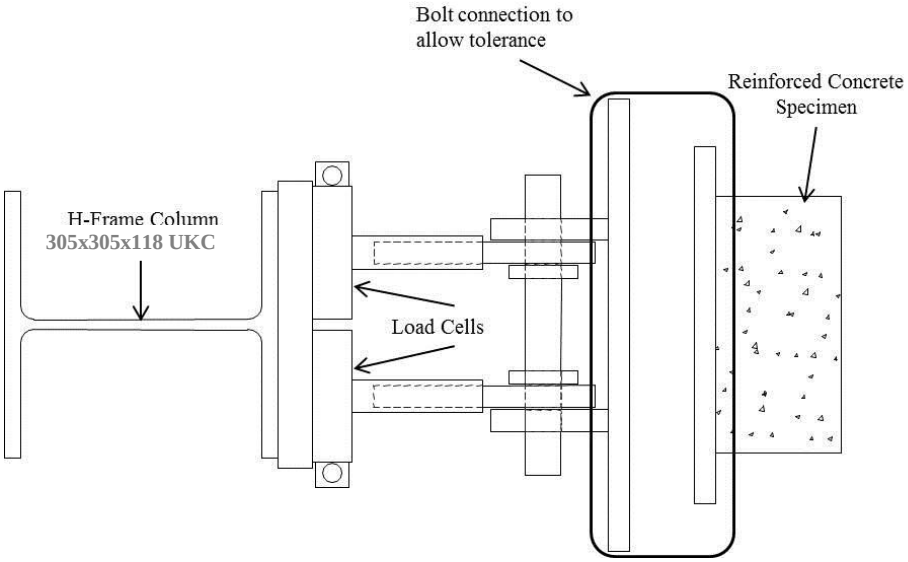

Figure 3.7: *Plan of End Detail*

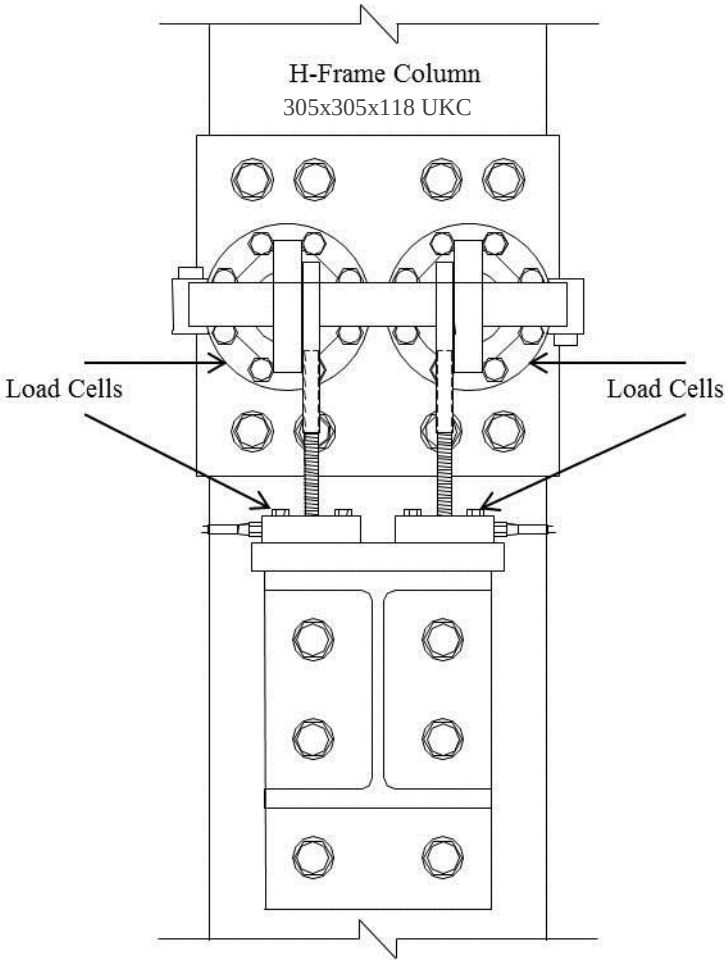

Figure 3.8: *Section A-A Figure 3.6, End Detail.*

3.3.2 **Hanger Design**

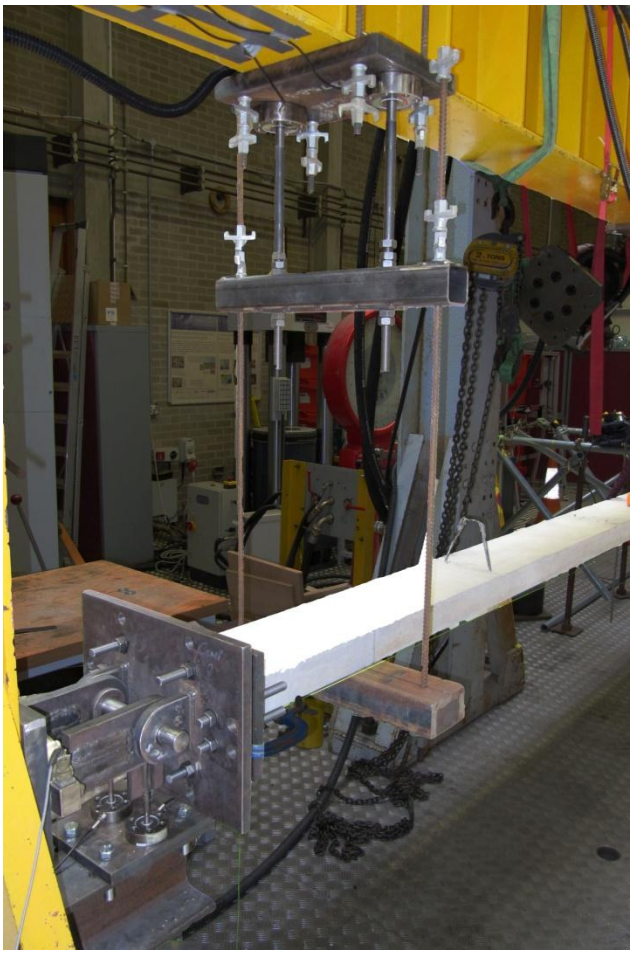

Figure 3.9: *Photo of hanger assembly with load cell arrangement*

The hanger supports at B and C, as shown in Figure 3.3 and Figure 3.9, could be moved to vary the length of span L_1, the clear span of the specimen after removal of the central support. This was taken into consideration when the support detail was designed. A hanger system utilising the girder of the H-Frame was specified. This included two load cells at B with a combined capacity of 100kN to measure the vertical reaction. The hanger detail, like the end detail, was designed to minimise any transverse force exerted on the load cells. It was important for the integrity of results that the load cells were kept flat and load was only applied perpendicular to the load cells.

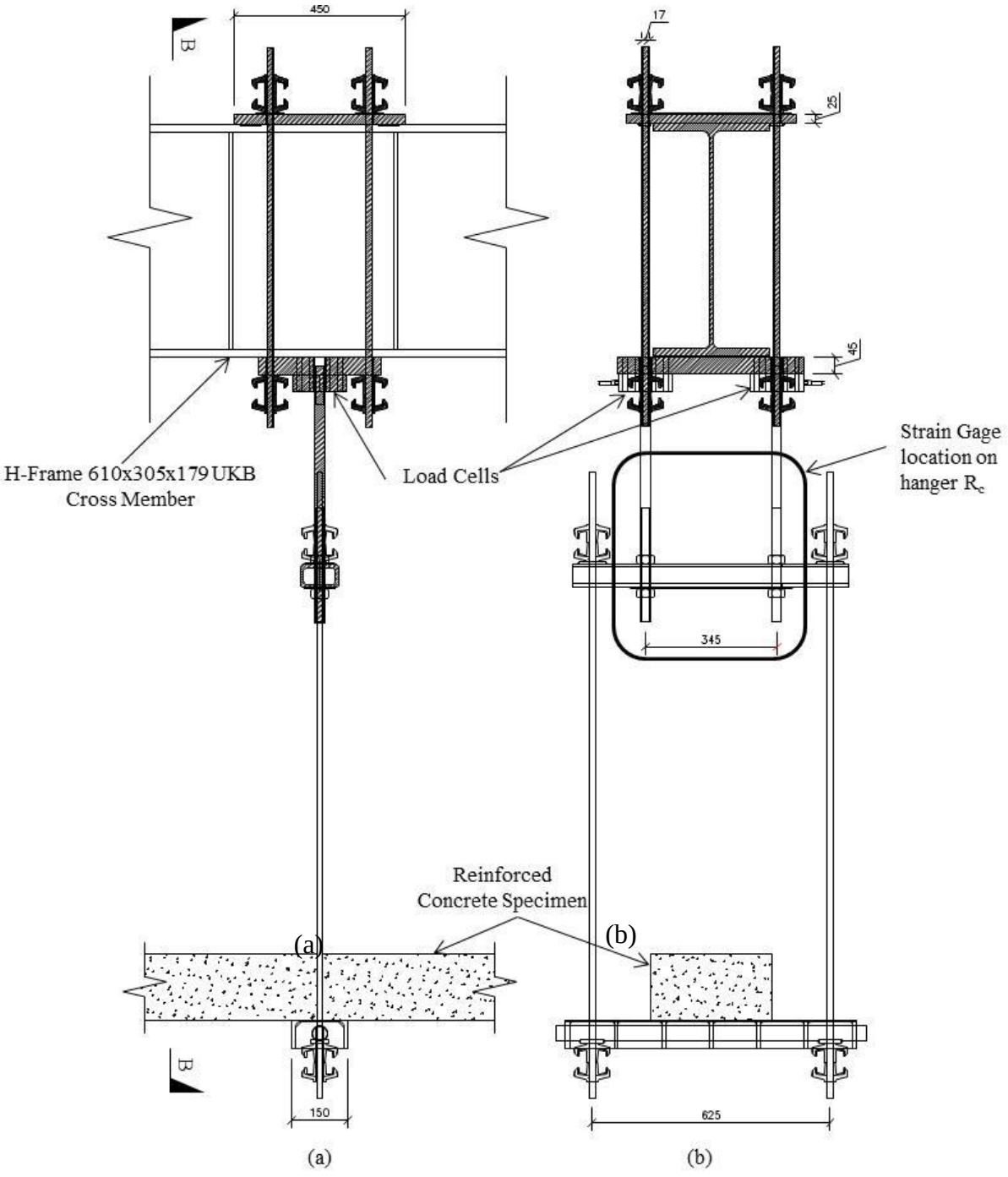

Figure 3.10: *(a) Elevation of Hanger Detail, (b) Section B-B of Hanger Detail*

The hanger at support C was identical except that the load cells were replaced with strain gauges. Two number strain gauges were applied on two opposite faces of each of the supporting rods, as highlighted in Figure 3.10.

All measurement equipment was subjected to rigorous calibration procedures. More photographs of the end detail and hanger assemblies can be seen in Appendix A.1.

3.3.3 **Displacement Measurements**

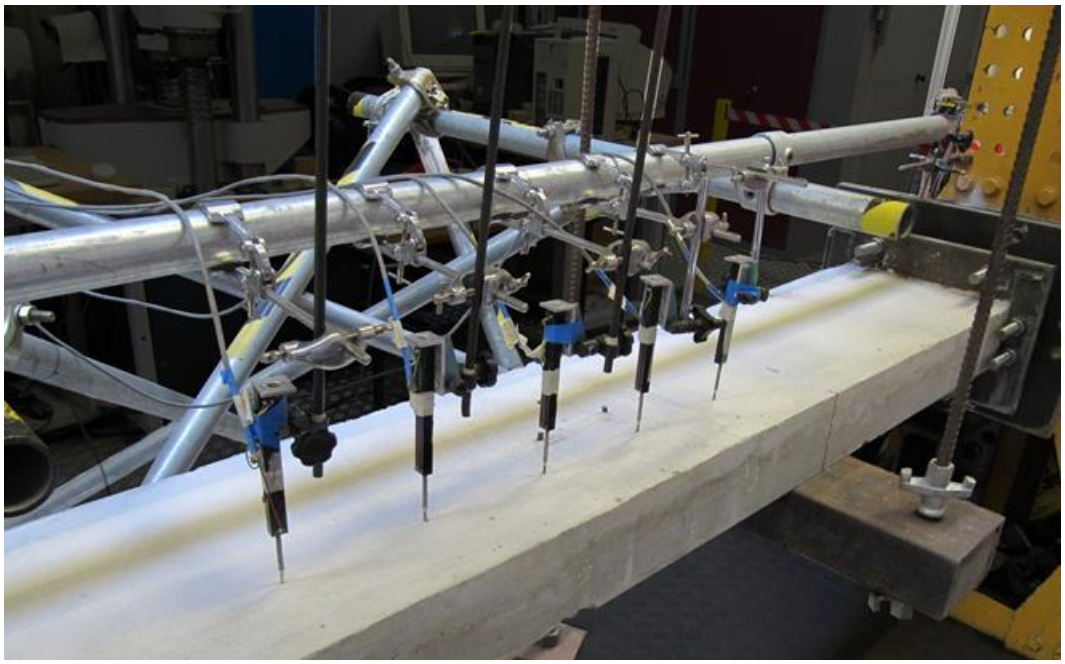

Figure 3.11: *The location of displacement measuring equipment*

In order to accurately determine end joint rotation a series of linearly variable displacement transducers (LVDT's) were placed at equal spacings from support C, as shown in Figure 3.11. The 100mm stroke LVDT's were calibrated to give a reliable measurement of vertical displacements. In addition to providing end joint rotation they served to verify the displacement reading given by the load actuator at mid-span and gave an indication of curvature of the specimen.

The displacement of the test rig caused by the horizontal reaction at the end detail was measured by a single LVDT at each column. The LVDT was supported by a free standing frame and was located on the outer flange of the H-frame column. The LVDT was placed in line with the connected end detail to record the direct response of the frame to the horizontal reaction. It was not possible to fix the LVDT to the back of the inside flange due to space restrictions from lateral bracing of the column this resulted in errors due to the bending of the front flange. From calculations based on assuming the half flange acts as a cantilever from the

web (considering the horizontal load acting over a one metre height of the column) the error has been estimated at 4%. In retrospect it would have been better to measure the horizontal movement of the specimen end plate.

3.4 Section Design

3.4.1 Material Properties

Bar Diamter [mm]	Yield Strength Re [N/mm2]	Tensile Strength Rm [N/mm2]	Tensile / yield strength ratio, Rm/Re	Total Elongation at Maximum Force [%]
8	554.80	674.20	1.22	16.00
10	512.80	603.80	1.18	15.50
12	527.30	612.20	1.16	15.00
16	842.40	642.80	1.19	11.40

Table 3.1: *Steel properties, Smith, P. P. (2014).*

To negate scaling effects the percentages of reinforcement for each specimen were taken from full scale designs and the bar diameters were reduced to fit the specimens. The top and bottom reinforcement was detailed for all specimens between 8 and 16mm in diameter. Steel reinforcement was specified with the notation H. In accordance with BS866:2005 this notation for diameters less that 12mm denotes grade B500A, B500B or B500C. For diameters greater than 12mm the notation H denotes grade B500B or B500C. Hence the specified reinforcement was high yield bar with a yield strength of 500 N/mm^2 with ductility of three possible grades A, B & C. The properties for all reinforcing steel used in the experimental specimens are shown in Table 3.1.

To ensure that experimental results were applicable to typical industry standard structures it was imperative that the properties of the smaller diameter bar used were comparable to those of the larger bar sizes frequently used in practice. To comply with minimum steel requirements all reinforcement for main bars used in flat slab design were 12mm or larger and so are grade B or C. BS 4449:2005 provides characteristic tensile properties for the three ductility reinforcement grades, shown in Table 3.2. Comparison of the tensile / yield ratio with the values from steel used in the experimental programme show that all sizes of reinforcement used were grade C, which is the most ductile. It is important to note that BS 4449:2005 states

that for diameter sizes below 8mm A_{gt} drops to just 1%. Therefore 6mm bars were not used as main reinforcement in any specimens to ensure that unrealistic brittle failures did not occur. However, shear links were detailed with 6mm or 8mm diameter bars. All bars were bent off site at a local steel fabricator.

	Yield Strength Re [N/mm^2]	**Tensile / yield strength ratio, R_m/R_e**
B500A	500	1.05
B500B	500	1.08
B500C	500	≥ 1.15, < 1.35

Table 3.2: *Characteristic tensile properties as defined in Table 4 BS4449:2005*

It is normal practice for concrete cube strength to be specified at 28 days. Concrete structures are designed on the basis of the concrete characteristic strength to allow for the variability of the material. Concrete cube strength follows a normal distribution and statistically 5% of cube strengths would fall below the characteristic strength. The normal distribution is centred on the mean cube strength and when considering the design of a concrete mix the target mean strength is commonly used. A small scale concrete mixer was used throughout the experimental programme. This gave poor control over the concrete quality and thus greater material variability compared to a ready mix batch from a concrete plant. To ensure that the required characteristic strength was achieved a higher target design strength was needed to allow for the expected higher standard deviation of the concrete strength.

The concrete compressive strength is an important parameter and has been shown to have a significant effect on behaviour in the compressive membrane phase Lahlouh and Waldron (1992), Taylor et al. (2001). The specimens modelled a building in a damaged state which was assumed to have lost a column through accidental or malicious means. An investigation has been conducted into historical examples of buildings that have suffered damage through malicious attacks (such as from car bombs) to determine the age of the structure at the time of attack. Examples shown in A.12 indicate that buildings had an average age of 20 years before sustaining damage. Therefore it was assumed that the modelled structure was at least 5 years old and the target compressive mean strength was designed to reflect this. To achieve this a C35/45 concrete mix was used. This had a design mean strength (58.1 N/mm^2) similar to the

predicted strength of a 5 year old concrete designed to a C30/37 mix (56.4 N/mm^2). Full details of the calculations for the prediction of the development of concrete compressive strength with age are shown in Appendix A.2. As scaled specimens with small reinforcement diameters were used, a 10mm aggregate was used throughout to comply with BS8110.

The mean concrete cube strength achieved was found to be 57.9 N/mm^2 less than 0.5% different from the target 5 year strength. However the set of results had a coefficient of variation of 16.2%. The distribution of cube strength is shown in Figure 3.12, together with the target design strength. The level of variation reflects the unpredictable nature of the concrete mix process (temperature and weather effects from different pour dates). Appendix A.2. shows the full set of cube test data.

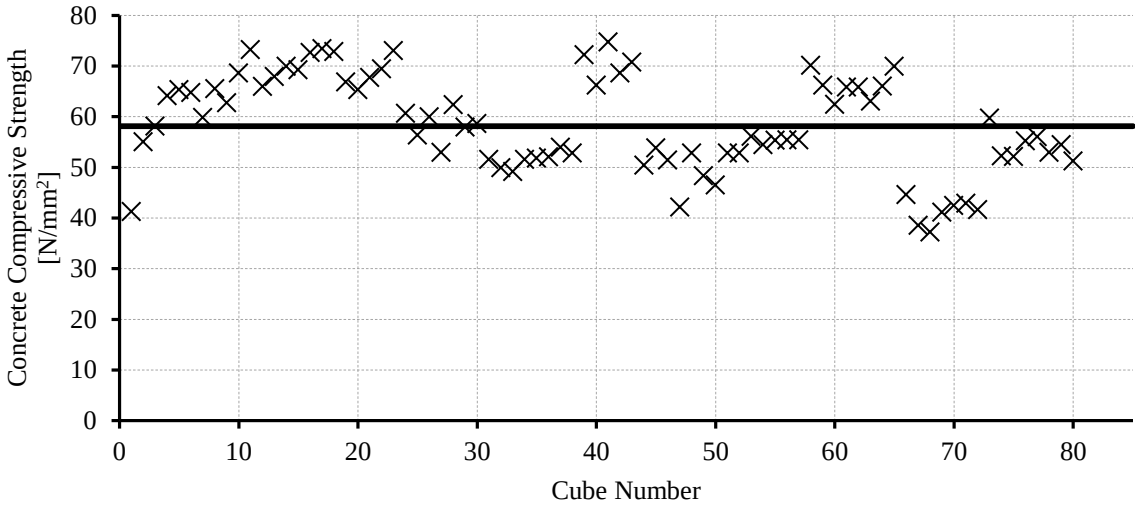

Figure 3.12: *Distribution of cube strength compared with target design strength.*

3.4.2 **Flat Slab Structures**

RC flat slab construction is often used for 5 to 10m spans, over 10m would require post-tensioning which has not been considered in this research, TCC (2006). When designing to BS 8110 the span to depth ratio is limited to 26 for a continuous slab however a higher span to depth ratio can be used (Clause 3.4.6.3 and Table 3.10). Practically in design the span to depth ratio would not be much greater than 30, and so the upper limit for the damaged building would be 60, (double the span). For the flat slab specimens the span to depth ratio was the main parameter of interest, and the range used was from 30 to 60 in increments of 10.

From the economical designs of flat slab structures given in Appendix A.3, in which structures have been designed for a range of spans between 5 and 9m, an average value of reinforcement percentage can be taken for the column and middle strips of the slab. These averages have been used as a constant in the experimentation with 4 samples representing a column strip with ρ_s = 0.4% and 3 samples representing a middle strip with ρ_s = 0.2%. By setting ρ_s as a constant, a quantifiable comparison could be made of the compressive membrane action load enhancement from different span to depth ratios; and additionally the comparative performances of the column and middle strips could also be assessed.

Slab No.	**L_1 [mm]**	**L_1/d [mm]**	**h [mm]**	**b [mm]**	**d [mm]**	**ρ_s [%]**	**ρ'_s [%]**	**f_{cu} [N/mm^2]**
C1	4050	31.64	160	320	128	0.49	0.49	62.89
C2	4320	40.00	140	320	108	0.44	0.44	70.09
C3	4550	50.00	118	320	91	0.35	0.35	69.17
C4	5000	60.24	110	320	83	0.38	0.38	47.21
M2	4720	40.00	145	320	118	0.21	0.21	57.50
M3	3900	50.00	105	320	78	0.20	0.20	51.57
A	5000	66.67	90	275	75	0.24	0.24	54.60

Table 3.3: *Section properties of flat slab samples.*

The focus of the section design was to scale two bays of a flat slab structure such that it spanned between the two stanchions of the H-Frame. The scale was roughly 1:3 although this varied due to the increase in span to depth ratio. A percentage of tension reinforcement was then assumed as close as possible to the target values of 0.4% or 0.2%, however the restrictions of size of rebar and the set span to depth ratio resulted in discrepancies from the target values. Bar spacing and cover were specified in accordance with BS 8110. The minimum cover to be provided for 10mm aggregate is 15mm to the shear links (Table 3.4 BS 8110). The maximum spacing of the tension reinforcement was restricted and in no circumstances did it exceed the values specified in BS 8110 Clause 3.12.11.2. Specimen details are shown in Table 3.3.

Specimen A has been used for two purposes. The reinforcement percentage and span to depth ratio allowed it to be considered as a specimen that represents a middle strip of a flat slab structure and also a one way spanning slab in a conventional framed structure. It provides a middle strip specimen at the highest span to depth ratio considered and a slab specimen at the

lowest percentage of reinforcement considered; hence it could have been named in either series as M4 or S3 respectively. Sample A was reinforced to Arrangement 1 from Figure 3.13.

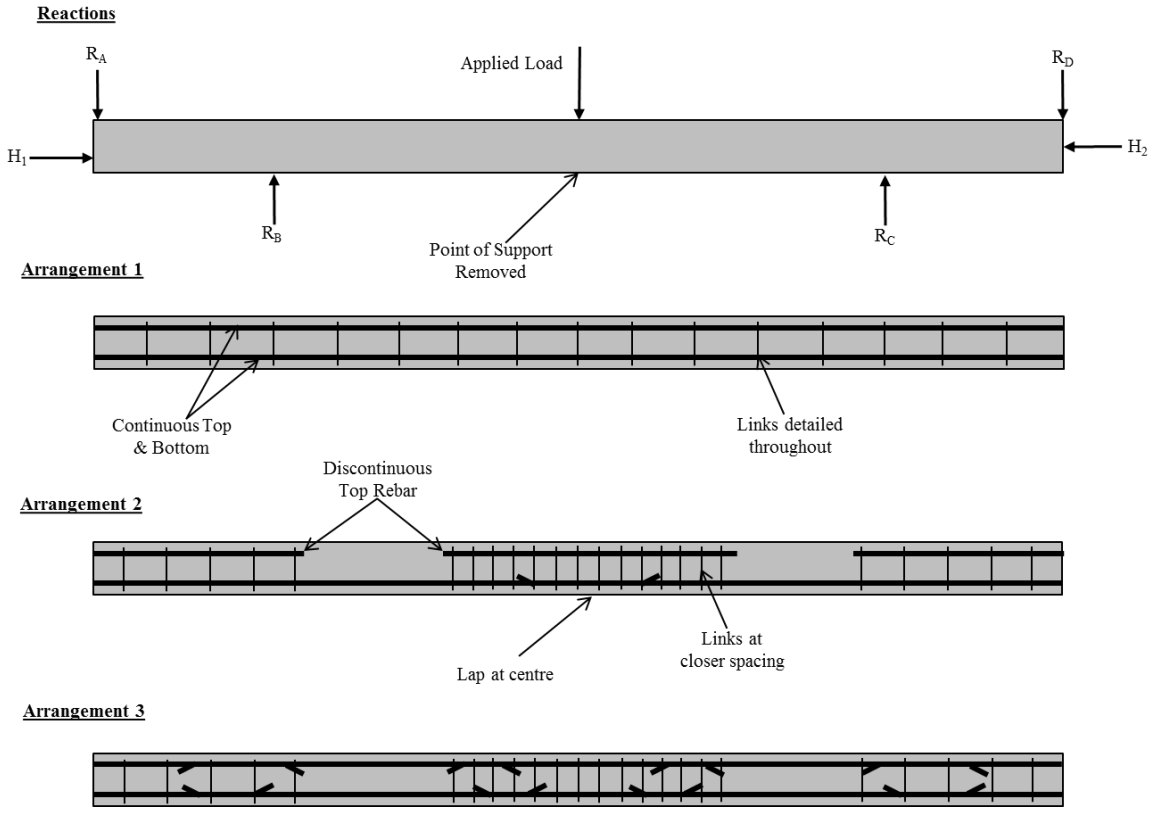

Figure 3.13: *General Arrangement of Reinforcement.*

Reinforcement is required in hogging areas of the RC section, and has been specified to be equal to the tension reinforcement. Due to the small scale spans of the flat slab specimens both sagging and hogging reinforcement was continuous for the entire length of the specimen for ease of fabrication. The general arrangement of reinforcement used for all flat slab specimens is shown as Arrangement 1 in Figure 3.13. It is not uncommon in flat slab construction that both top and bottom reinforcement continues throughout the span, however the percentages of reinforcement would be different.

Shear checks were carried out in accordance with BS:8110, and minimum shear resistance was provided in the form of shear links, which for ease of construction were placed around both the top and bottom steel, as in beam construction. Links were 8mm diameter high yield bars

spaced at 200mm centres throughout the specimen. Detailed reinforcement schedules and drawings for all flat slab specimens can be found in Appendix A.4.

3.4.3 **Conventional Framed Structures**

For the purposes of this research a conventional framed structure is defined as one that contains a system of one way spanning slabs that distribute load to main beams; edge beams located at the perimeter support a portion of slab loading and additional façade loads. Since perimeter column loss was the key driver the elements that have been scaled and tested are the edge beam and slab. Their design was carried out by Smith, P. P. (2014) based on a four storey generic structure designed to BS 8110 in Higgins and Rogers (1998). In the research carried out by Smith, P. P. (2014) the specimens have been used to investigate the effects of Catenary Action in RC structures, but the results for the compressive membrane action phase of behaviour have been utilized in the current research. Using the generic structure ensured that detailing was similar to that commonly used in UK practice. The original full scale span was 5m; this was modelled at half scale to produce a span of 2.5m and a double span during loading of 5m. The span to depth ratio has been kept constant and equal to the original design, with the depth being scaled accordingly. The same material properties as for the flat slab specimens were used. Reinforcement was detailed as shown by Arrangement 2 in Figure 3.13 for slab specimens and Arrangement 3 for edge beam specimens reflecting the design from the generic structure. The parameter that was varied was the percentage of main reinforcement. The original percentage of reinforcement was incrementally increased by Smith, P. P. (2014) to investigate its effect on Catenary Action but has been used here to focus on the relationship between reinforcement percentage and CMA. Specimen details are shown in Table 3.4, the percentage of reinforcement displayed is that detailed at the centre of the double span, at the point of loading.

Shear reinforcement was detailed using links that were fixed around both top and bottom steel as in the flat slab samples. The diameter of the shear links varied from 6 to 8mm diameter. As shown in Figure 3.13 the spacing of links in the centre cage was decreased to ensure that a shear failure did not occur, as a failure in this manner was thought not to reflect the behaviour of the full scale structure.

For comparison purposes the details of the flat slab specimens have been appended to Table 3.4.

Slab No.	L_1 [mm]	L_1/d [mm]	h [mm]	b [mm]	d [mm]	ρ_s [%]	ρ'_s [%]	f_{cu} [N/mm^2]
A	5000	66.67	90	275	75	0.24	0.24	54.60
S2	5000	66.67	90	275	75	0.49	0.49	70.48
S3	5000	66.67	90	275	75	0.73	0.73	49.33
E1	5000	34.97	175	225	143	0.31	0.70	66.15
E2	5000	34.97	175	225	143	0.47	1.05	41.19
E3	5000	34.72	175	320	144	0.51	1.31	54.21
C1	4050	31.64	160	320	128	0.49	0.49	62.89
C2	4320	40.00	140	320	108	0.44	0.44	70.09
C3	4550	50.00	118	320	91	0.35	0.35	69.17
C4	5000	60.24	110	320	83	0.38	0.38	47.21
M2	4720	40.00	145	320	118	0.21	0.21	57.50
M3	3900	50.00	105	320	78	0.20	0.20	51.57

Table 3.4: *Section properties of conventional framed samples, with flat specimen details added for comparison.*

3.5 **Rig Stiffness**

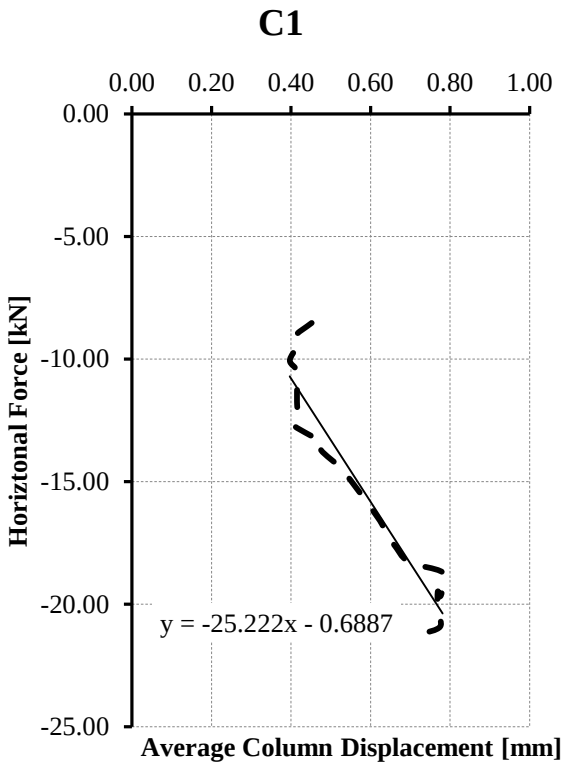

Figure 3.14: *Calculation of rig stiffness for specimen C1*

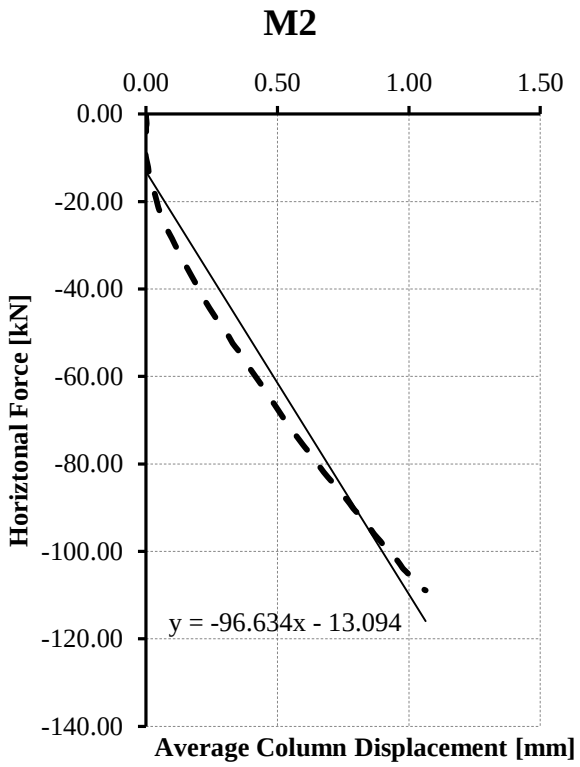

Figure 3.15: *Calculation of rig stiffness for specimen M2*

To determine the stiffness of the test rig a LVDT was placed on an independent frame at the position of the horizontal force at both columns. The outward thrust from the loaded specimens caused displacement in the columns which was measured by the LVDT. The measured displacement from the two columns was averaged and plotted against the horizontal force for each specimen. The linear relationship between the two provides the stiffness of the test rig. Examples of this calculation are shown in Figure 3.14 and Figure 3.15. The gradient of the line shown in the two figures is the calculated rig stiffness.

As previously noted the test rig was an existing piece of apparatus at the University that was modified for the purposes of this research. Due to restricted resources preliminary testing to determine the stiffness of the rig could not be carried out. The results of the first test conducted (on specimen C1), shown in Figure 3.14, provided an initial value for the stiffness of the rig of 25 kN/mm. To facilitate quantitative comparisons of restraint stiffness the axial

stiffness ratio, k_1, has been defined in Chapter 5. From analysis of the stiffness provided by a series of flat slab structures designed to BS:8110 in Chapter 6 values of k_1 ranged from 0.40-2.00 depending on the placement of structural cores. The results of the test rig for specimen C1 produced a k_1 value of 0.06, significantly lower than the values found for flat slab structures. Consequently the rig was modified to provide an increase in the provided stiffness by introducing a steel buttress system fixed to the laboratory strong floor and welded to the columns, as shown in Figure 3.16. All other specimens in the experimental programme were tested with the additional support. The average measured stiffness for the remaining specimens was 105 kN/mm. The corresponding average k_1 value was 0.41 making the test rig stiffness comparable to a framed structure, albeit at the lower end of the range.

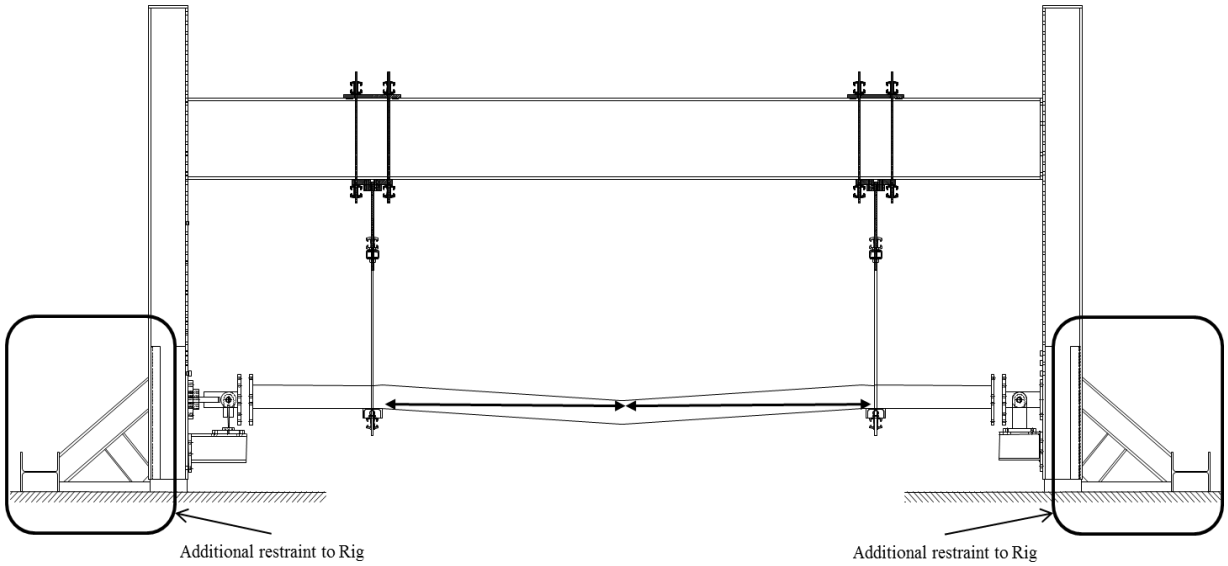

Figure 3.16: *Additional restraint stiffness provided to test rig.*

3.6 **Experimental Setup Procedure**

Prior to testing each specimen a sequence of processes was carried out to ensure that the specimen was correctly placed in the test rig such that measured reactions matched theoretical values. The setup procedure has been split into phases for clarity. At each phase sample M2 has been used as an example to demonstrate the comparison of measured and theoretical reactions.

3.6.1 **Phase 1**

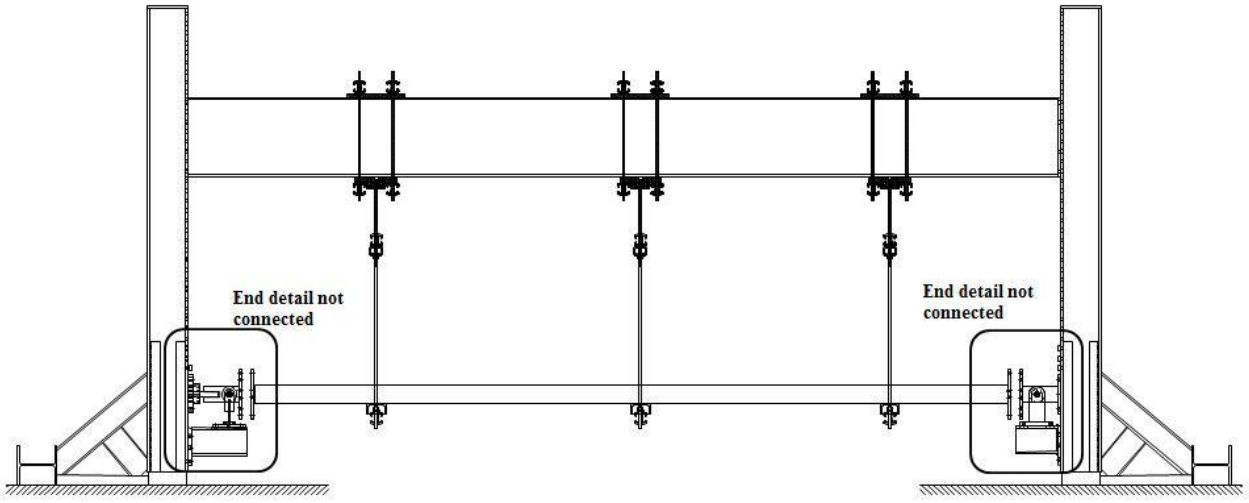

Figure 3.17: *Sample in test rig at phase 1*

Initially the sample was placed so that it was supported by the three hangers only. The end details were not connected with the axle omitted so there was no reaction at the end detail as shown in Figure 3.17. The full self weight of the sample including the point load from the endplates was supported by the three vertical reactions from the hangers as shown in the free body force diagram in Figure 3.18. Theoretical values of these reactions were calculated using the structural analysis software Oasys GSA. The self weight of the sample was calculated using measured cube densities but the weight of steel reinforcement was ignored which has contributed to small discrepancies between measured and theoretical values. A comparison of reactions for the example sample M2 is shown in Table 3.5. There is a good correlation for phase 1 of the procedure. It should be noted that the difference between calculated theoretical values for R_B and R_C arise from a small difference in the length from hanger to end detail which is a result of only one end having load cells. The magnitude of each reaction was altered by adjusting the level of the hanger support via Dywidag GEWI Threadbars that screw onto the vertical tie rods, as shown in Figure 3.19. The reaction was equalled across North and South (see Figure 3.19) to ensure that the specimen was square in the test rig and loading of the specimen would not induce torsion. At the end of this phase the sample was level under its own self weight and the system was balanced.

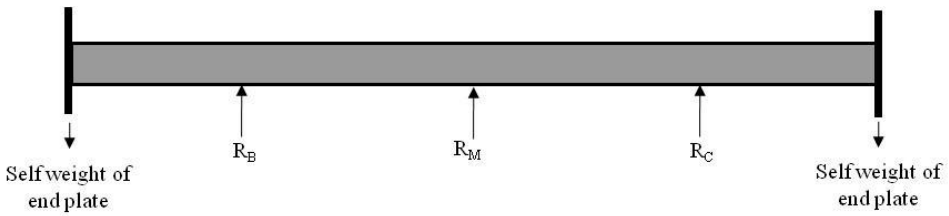

Figure 3.18: *Free body force diagram for the sample at phase 1*

Phase 1			
	R_B [kN]	**R_M [kN]**	**R_C [kN]**
Theoretical	2.302	2.558	2.265
Measured	2.223	2.440	2.286
Phase 2			
Theoretical	2.398	2.539	2.398
Measured	2.409	2.516	2.457

Table 3.5: *Comparison between theoretical and measured reactions for the setup procedure*

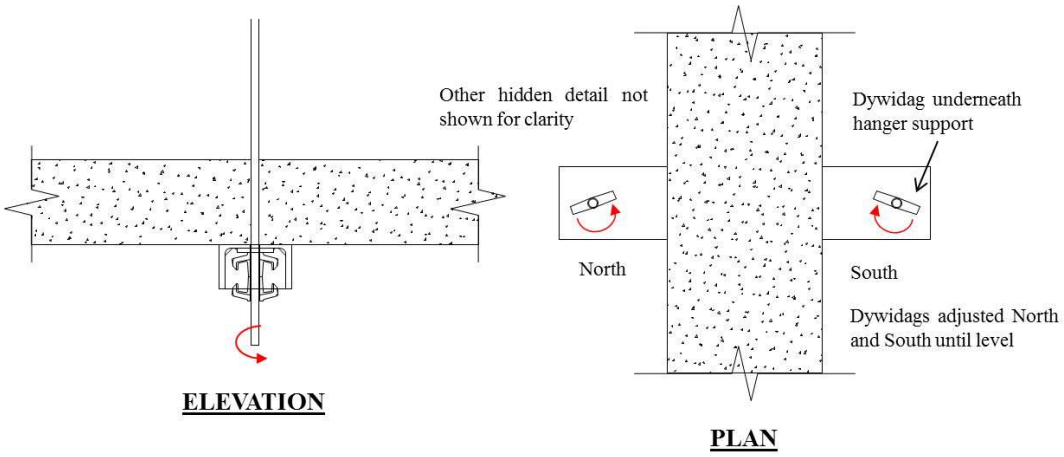

Figure 3.19: *Arrangement at each hanger to allow sample to be levelled*

3.6.2 **Phase 2**

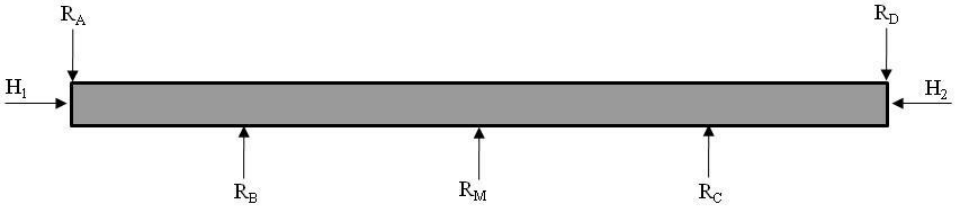

Figure 3.20: *Free body force diagram for the sample at phase 2*

The axle was then inserted into the end detail and the bolts highlighted in Figure 3.21 to the base plate of the end detail were tightened down. The load cells measuring the vertical reaction at point A (designated R_A) were set so that when the bolts were tightened a pre-load

was induced in them. The purpose of this slight pre-load was to ensure that the load cells remained in tension throughout the whole testing process. If there had been a transition between tension and compression there would have been a loss in data. Tightening down the end details with the pre-load required the reactions at the hangers to be adjusted. They were adjusted to match an equivalent 6 bay system (the section dimensions of the specimen over 6 bay lengths) calculated using Oasys GSA; these reactions are shown in the graphical extract in Figure 3.22. The good correlation between theoretical and measured reactions for phase 2 is shown in Table 3.5. The position of the reaction R_A on the equivalent 6 bay model occurs at roughly the point of contraflexure and as such the shear force at this point is close to zero which is modelled in the test rig.

At the end of this phase the specimen modelled the 2 central bays of the 6 bay structure under its own self weight. No pre-load was applied to the system to model any imposed load on the structure.

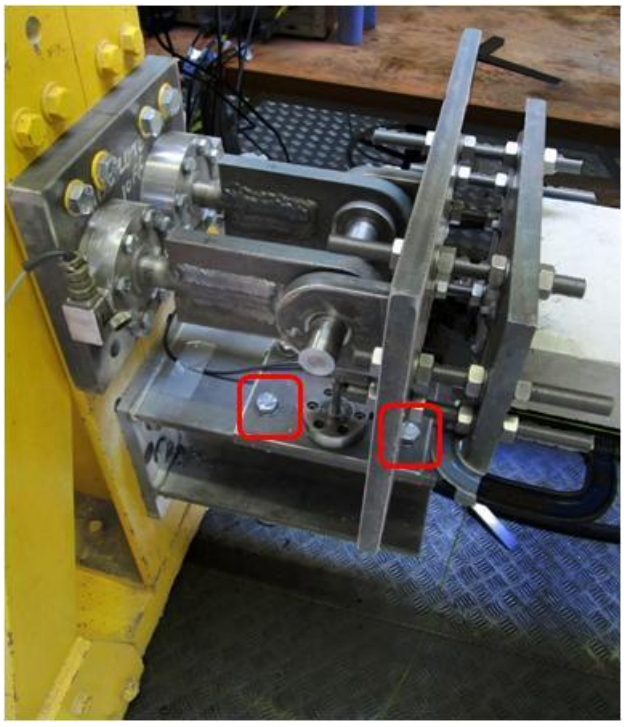

Figure 3.21: *Photo of end detail with highlighted bolts tightened during this phase*

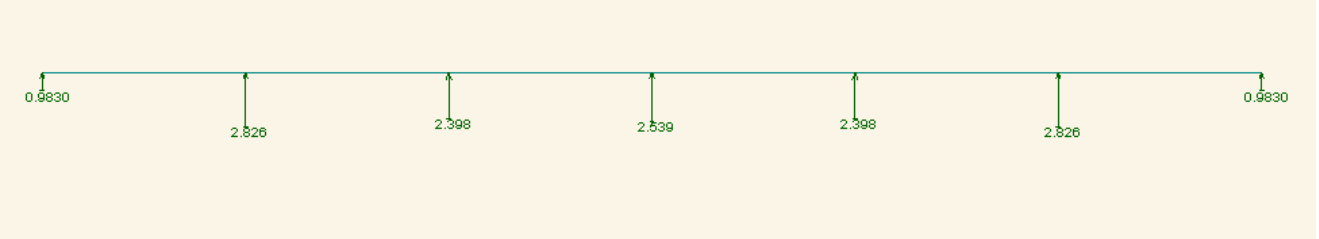

Figure 3.22: *Extract from Oasys GSA of 6 bay equivalent of sample M2 under self weight only*

3.6.3 **Phase 3**

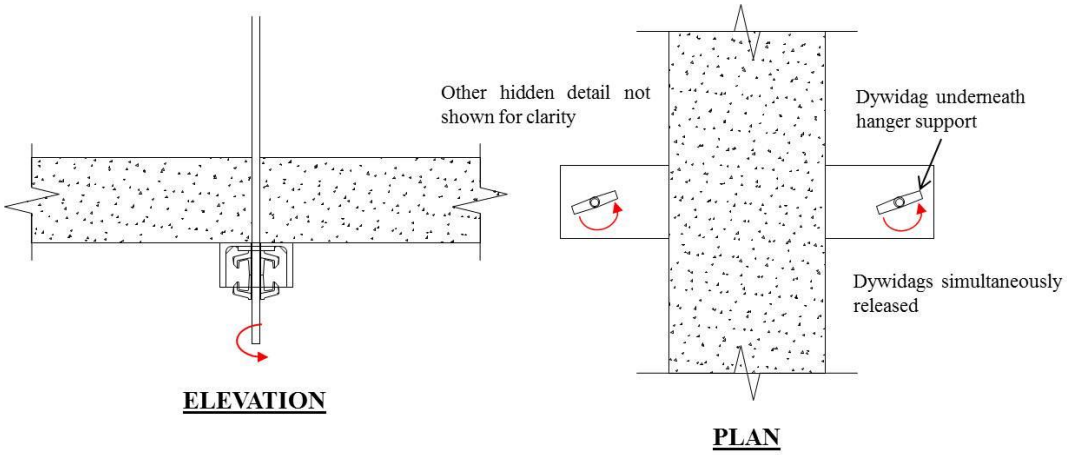

Figure 3.23: *Arrangement allowing the removal of the central hanger*

To model the loss of the central perimeter column the middle hanger was removed. This was done by simultaneously loosening the Dywidag Threadbars underneath the central cross support as shown in Figure 3.23. This allowed the central hanger to be removed almost instantaneously. The self weight load was redistributed from the central support to the other supports, for specimen M2 the reactions after removal of the central hanger are shown in Table 3.6. The almost symmetrical distribution of load shown is typical of all the other samples indicating a balanced system prior to the removal of the central support. The total vertical reaction induced in the two end details is also shown, where the reaction at D (designated R_D) was assumed to be equal to R_A. It can be seen that the total load at the end of phases 2 and 3 are very similar.

	R_B [kN]	R_M [kN]	R_C [kN]	$R_A + R_D$ [kN]	Total Load
Phase 2	2.409	2.516	2.457	0.000	7.382
Phase 3	5.760	0.000	5.880	-4.320	7.320

Table 3.6: *Redistribution of load after the removal of the central hanger*

3.7 Testing Procedure

At the start of the testing procedure the load actuator was lowered into position as shown in Figure 3.24. The LVDT's were then also moved into position as shown in Figure 3.11. The load actuator was positioned over the sample, two 150mm wide plates with a transverse round bar between were positioned on top of the midspan of the sample. The round bar ensured that the jack force was applied vertically.

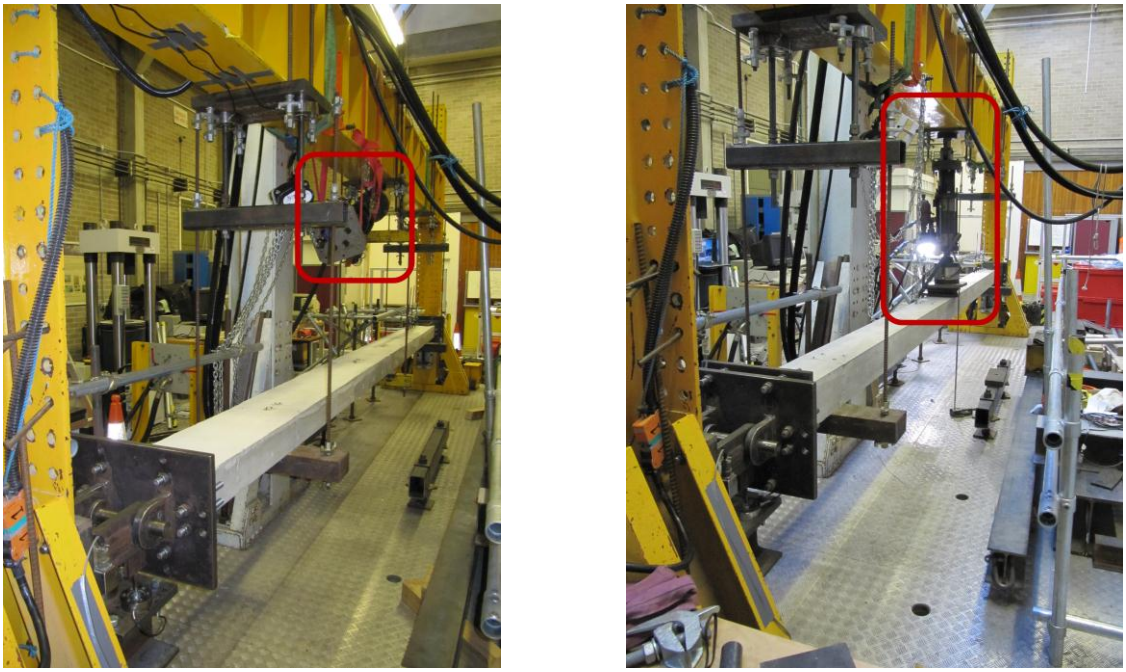

Figure 3.24: *Photographs showing the central hydraulic actuator being lowered into position for loading the specimen.*

Figure 3.25: *Loading arrangement at the centre of the specimen*

The specimen was then loaded at mid-span with the actuator displacement set at a rate of 1 mm/sec. Actuator movement was stopped whenever it was necessary to reset instruments. The maximum stroke of the actuator was 150mm, and when the actuator reached this limit the sample was strapped down with 4x1 ton capacity straps to RHS sections which were attached to the strong floor. This arrangement is shown in Figure 3.26. Once the load was released from the actuator and taken by the straps a 150mm high steel I-Section packer was bolted to the load actuator. The actuator was then positioned back over the sample and load was released from the strapping. Measurements of displacement were recorded to ensure loading recommenced at the same load and displacement. This procedure was repeated each time the maximum stroke of the actuator was reached until the end of the test.

Actuator displacement was continued until a maximum load had been applied to the specimen. It was then continued beyond the end of compressive membrane action into the tensile membrane action (catenary) phase. Behaviour in that phase has been reported separately by Smith, P. P. (2014).

Figure 3.26: *Strapping down arrangement at the limit of the actuator's stroke*

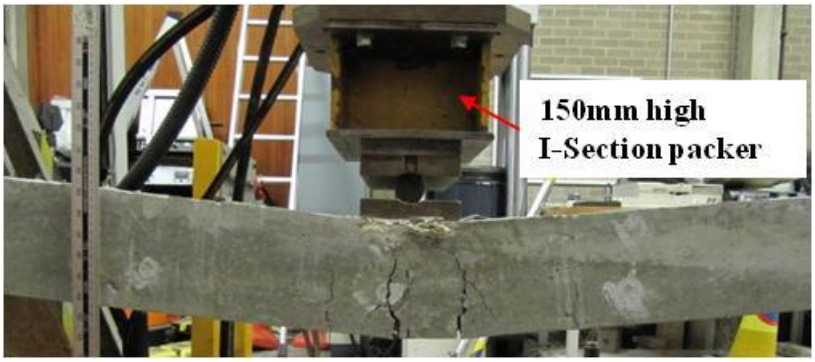

Figure 3.27: *150mm steel I-Section packer to the load actuator*

Chapter 4: Experimental Study Results and Analysis

4.1 **Introduction**

The results from the experimental programme have been analysed to determine the key trends in results, with particular interest in the extent of load enhancement achieved through the mechanism of compressive membrane action (CMA). The influences of key factors, such as the percentage of reinforcement and span to depth ratio, as defined for each specimen in the previous chapter have been assessed to provide an insight into the behaviour of restrained RC elements at the exceptional spans that would result from the loss of a column (called the double span scenario in the previous chapter).

4.2 **Specimen Behaviour**

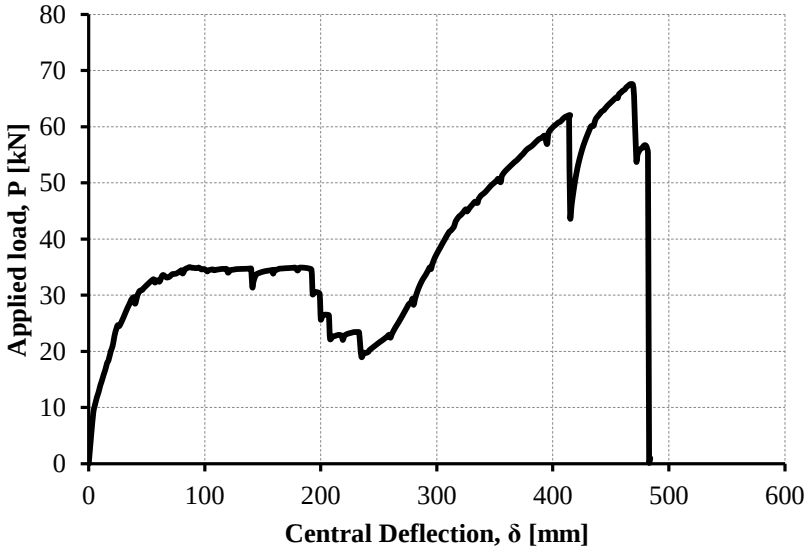

Figure 4.1: *Load-deflection graph for specimen C1*

Figure 4.1 shows the applied load versus central deflection graph for specimen C1 which is typical of the graphs for each specimen. Initially the graph was a straight line which represented the pre-cracking stage. At just under 10kN load the gradient reduced as cracking occurred but the graph remained a straight line. At 25kN load the graph became non-linear and reached a first maximum at about 35kN load. The applied load remained roughly constant as deflection increased and then dropped away to a minimum value of about 19kN at a deflection of about 235mm. During this phase of behaviour the horizontal force induced in the specimen had been compressive as can be seen in Figure 4.2. Above 200mm deflection the horizontal force became tensile. The initial phase has been called compressive membrane action (CMA) (when the horizontal force was compressive) and the latter phase tensile membrane action (TMA). The initial phase is the focus of this research, while the second phase is the focus of the research reported by Smith, P. P. (2014).

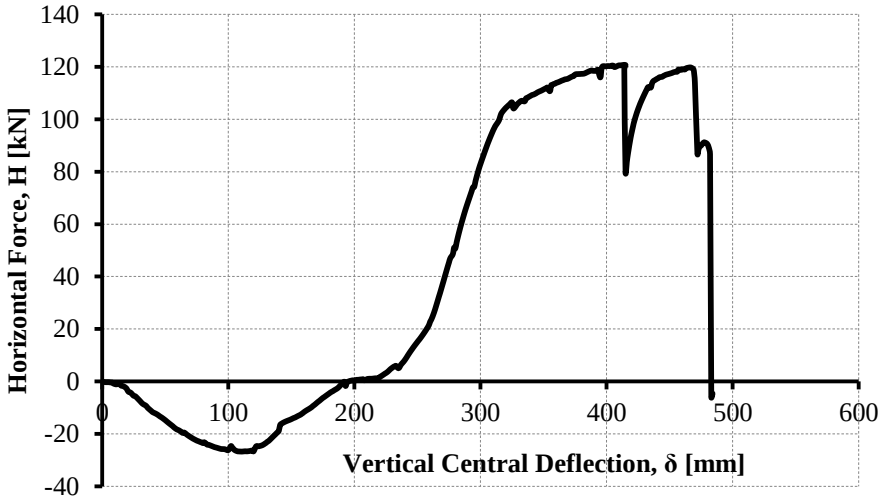

Figure 4.2: *Horizontal force-deflection graph for specimen C1*

The magnitude of the horizontal force and the relative compressive and tensile magnitudes varied between specimens. The arching action associated with CMA increased the maximum load above the value predicted by yield line or plastic bending theory. This load enhancement has been one of the focuses of this research.

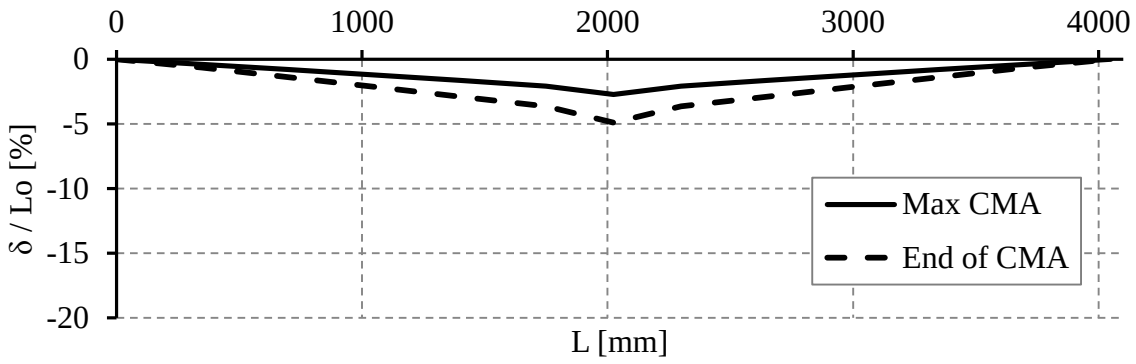

Figure 4.3: *Deflected shape of specimen C1* during compressive phase.*

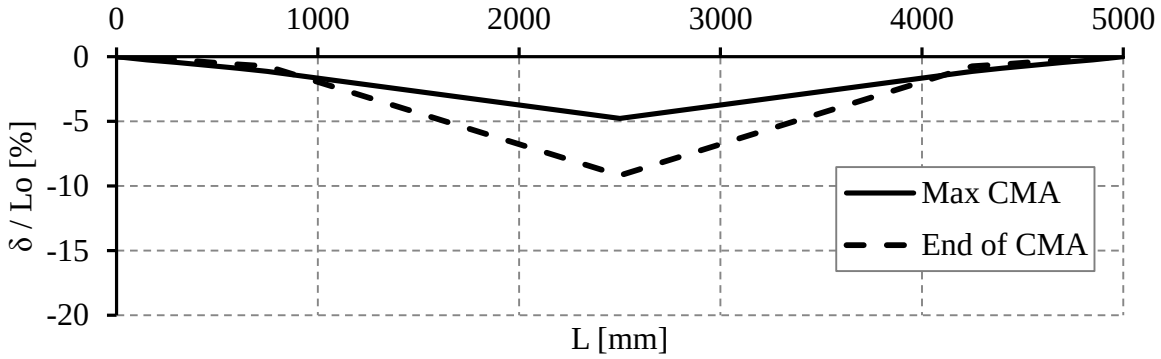

Figure 4.4*: Deflected shape of specimen E1 during compressive phase.*

At low loads the deflected shape of the specimen was a smooth curve as would be expected in a beam in bending. The deflected shapes of specimens C1* and E1 have been plotted from recorded values in Figure 4.3 and Figure 4.4 respectively and the photo in Figure 4.5 shows specimen C1* at the end of the CMA phase. Photos of each specimen during testing are shown in Appendix A.6. Deflection along the specimen has been captured at the point of maximum compressive force, H_{max}, and at the point of transition from compressive to tensile membrane action denoted as: End of CMA. In the early stages of loading all specimens exhibited a similar response, with increased deflection cracking occurred at mid-span and the supports. At higher loads all specimens, apart from the edge beam series, formed 'plastic' hinges at mid-span and the supports and remained in the large part straight between the hinges until the end of the compressive phase. In the edge beam specimens after the fracture of bottom tension steel at mid-span the two halves of the specimen behaved as cantilevers over the supports as rotation began to occur at the curtailment of the top hogging reinforcement over the support. This lead to a change in the deflected shape as shown in Figure 4.4. In each

instance this effect occurred after the peak compressive force and became predominant towards the end of the compressive phase as the mechanism of load support changed from arching to catenary.

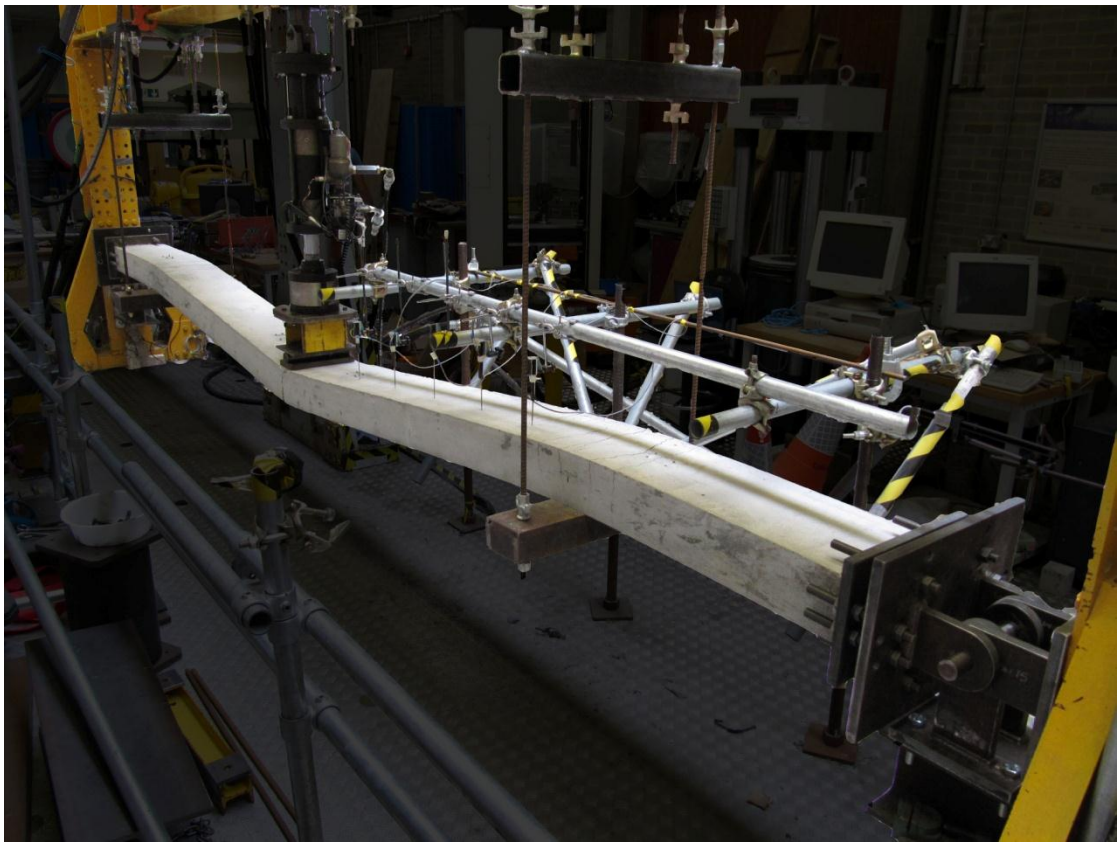

Figure 4.5: *Loaded specimen C1* at approximately the end of CMA phase (δ=200mm).*

In four specimens fracture of reinforcement occurred during the compressive phase after the peak load had been reached, in all instances the fracture was of the bottom tensile steel at mid-span. In all but one case the reinforcement fracture coincided with a rapid drop in load and the end of the compressive phase. Specimen E1 was the exception; fracture of reinforcement occurred in two locations first at mid-span and then the top steel at the support (point C) at the end of the compressive phase. Where the rapid drop in load occurred due to failure of reinforcement, the specimen was "caught" as TMA developed and with increased deflection the specimen was able to support further loading. It should be noted that in no instance did the snap through of the compressive arch lead to a sudden unstable failure.

Complete failure of specimens occurred at high deflection during the tensile membrane phase. Failure of flat slab specimens detailed with the continuous reinforcement designated arrangement 1 in Figure 3.13 in all but one case occurred at mid-span. Fracture of reinforcement occurred first in the bottom steel at mid-span then top steel at the supports and finally top steel at mid-span. Whilst TMA was able to support higher applied load than CMA it was not as predominant in flat slab specimens as it was in the specimens that modelled conventional framed structures.

Slab and edge beam specimens detailed with reinforcement arrangements 2 and 3 (Figure 3.13) respectively exhibited far greater catenery effects. Both types of arrangement allowed for the load path to change as fracture of reinforcement occurred resulting in a noticeable change in the deflected shape as observed initially in specimen E1, see Figure 4.4. A detailed examination of behaviour in the tensile phase and the final failure mechanism is described in Smith, P. P. (2014).

4.3 **Results**

Specimen No.	**Peak Load during CMA P_{max} [kN]**	**Normalised deflection at P_{max}, δ/h_{Pmax}**	**Horizontal Reaction at P_{max} [kN]**	**Maximum Horizontal Reaction, H_{max}**	**Normalised deflection at H_{max}, δ/h_{Hmax}**
C1	35.00	0.54	24.68	26.76	0.69
C2	23.45	0.70	44.80	48.04	0.79
C3	10.53	1.05	1.87	4.63	0.81
C4	7.76	1.12	-0.15	10.20	0.67
M2	16.91	0.52	94.24	110.07	0.79
M3	8.16	0.52	53.61	69.03	0.84
E1	26.28	0.44	57.56	75.90	0.68
E2	33.59	0.52	30.33	36.12	0.66
E3	50.72	0.65	72.15	79.45	0.80
A	3.09	1.51	-0.24	5.81	0.70
S2	6.22	0.70	0.00	0.52	0.43
S3	9.32	1.37	0.83	7.61	0.88

Table 4.1: *Summary of Experimental Results.*

A summary of the experimental results is displayed in Table 4.1. Snap-through is defined as the point at which the compressive arch can no longer sustain the increasing applied load and the data in Table 4.1 allows for an investigation into snap-through and the point at which it

occurs. In specimens where CMA is prominent and significant horizontal force is produced, snap-through can result in an obvious rapid drop off in applied load.

Two types of behaviour have been identified from consideration of the deflection at the peak applied load: the first was found when the peak load occurred at a deflection greater than the specimen depth, or a normalised deflection (δ/h) greater than 1.0. In these specimens the compressive force in the arch was low, and the arch provided little resistance to the applied load resulting in no rapid drop off in load when snap-through occurred; the load continuously increased with deflection. The load deflection curve of each specimen is shown in Appendix A.5, but as shown in the load deflection curve in Figure 4.6, specimen A exhibited this type of behaviour. It can be seen in Figure 4.7 that specimens exhibiting this behaviour had high span to depth ratios (50 – 66). At higher span to depth ratios the arch was shallow and significant compressive thrust was not induced.

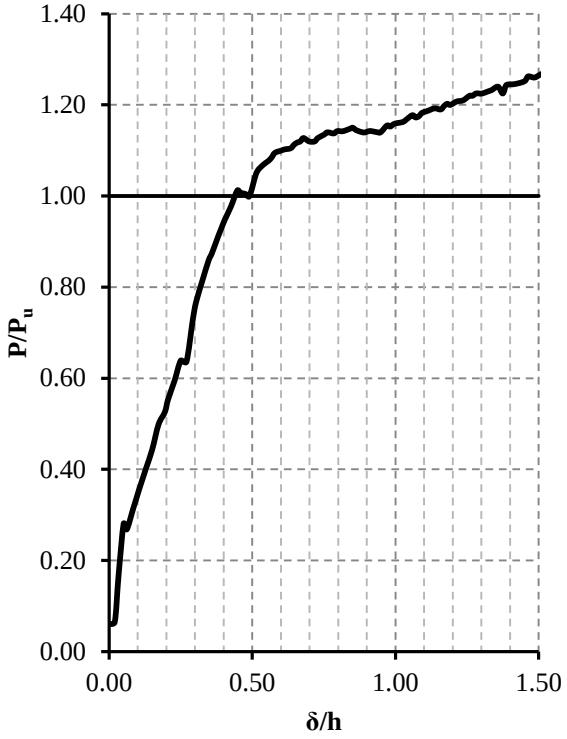

Figure 4.6: *Load deflection curve for specimen A.*

In the second type of behaviour the specimens did exhibit a rapid load reduction at snap-though. In these specimens snap through occurred when δ/h at P_{max} was less than 1.0. In these

specimens the average deflection was 0.58h with a range of 0.44h to 0.70h. This is slightly higher than the 0.4h to 0.5h suggested by Park and Gamble (2000) and Wood (1961) (see the Literature Review), although previous testing was not carried out at the high span to depth ratios considered here. This finding indicates that specimens with very high span/depth ratios can undergo more deflection in the compressive stage before maximum applied load occurs at snap-through than previously thought.

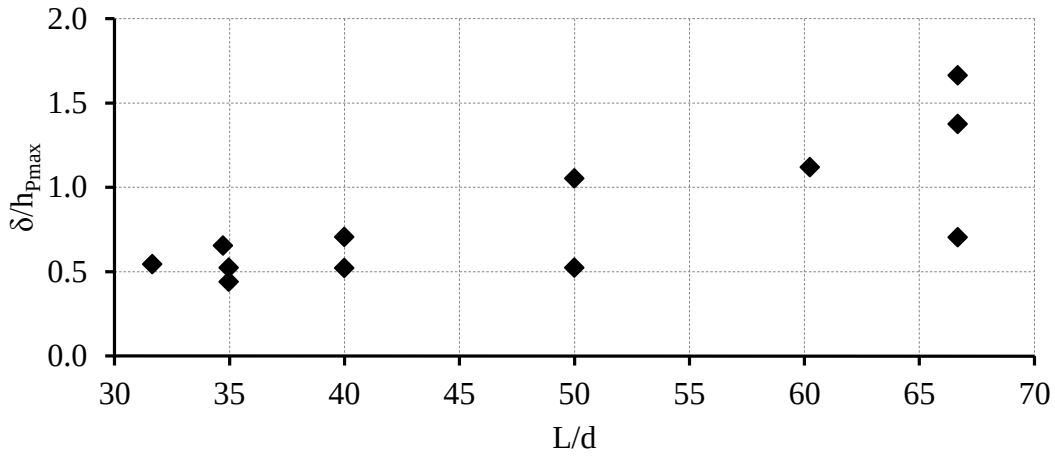

Figure 4.7: *Influence of span to depth ratio on deflection when peak applied load is considered.*

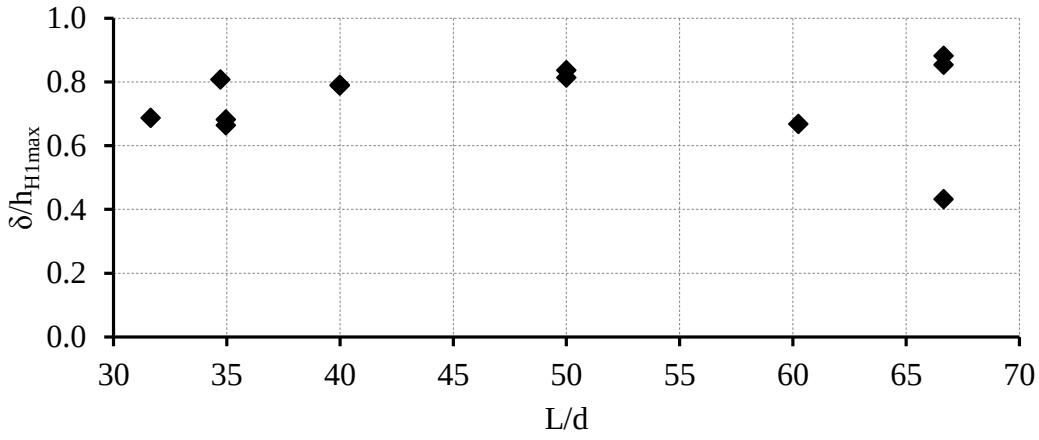

Figure 4.8: *Influence of span to depth ratio on deflection when peak horizontal reaction is considered.*

Two types of behaviour can also be identified when considering the differences between values of deflection at peak applied load and maximum horizontal force. In specimens where a clear drop off in applied load occurred at snap-through ($\delta/h < 1.0$) peak applied load was closely followed, with increased deflection, by maximum horizontal force. Specimens where P_{max} occurred at a normalised deflection above 1.0 exhibited maximum horizontal force at a lower value of deflection. This further indicates that at high span to depth ratios once the compressive arch reaches its maximum load carrying capacity there was no drop off in central

load. The values of δ/h at maximum horizontal force H_{max} are comparable for all specimens as displayed in Figure 4.8, with a range of 0.43 to 0.88 and an average value of 0.74. Table 4.2 summarises the above discussion and identifies the behaviour type of each specimen.

Specimen No.	H at P_{max}/H_{max}	δ at P_{max}/δ at H_{max}	Behaviour type
C1	0.92	0.78	1
C2	0.93	0.89	1
C3	0.40	1.30	2
C4	-0.01	1.67	2
M2	0.86	0.66	1
M3	0.78	0.62	1
E1	0.76	0.65	1
E2	0.84	0.79	1
E3	0.91	0.81	1
A	-0.04	2.16	2
S2	0	1.63	1
S3	0.11	1.56	2

Table 4.2: *Summary of specimen behaviours*

The test results indicate that the arch in a restrained specimen will produce a maximum compressive thrust at an average deflection of 0.74h. Whether the load carrying capacity drops rapidly and significantly near this peak depends on the span to depth ratio. The results also indicate that for slabs with L/d greater than 50 it is unlikely that there will be any drop off in load because of the small compressive thrust induced in the slab. However restraint stiffness and percentage of reinforcement will also affect slab behaviour.

4.4 Enhancement Assessment

To determine the extent of the beneficial effect from CMA it is insightful to consider the enhancement above the predicted behaviour from conventional plastic/yield line theory, in which membrane effects are ignored. Previous authors, Rankin and Long (1997) and Park and Gamble (2000), have based their assessment of enhancement on the bending moment developed above the conventional ultimate bending moment capacity. When load on the specimen is increased cracking occurs at mid-span followed by yielding of the reinforcement and a 'plastic' hinge is formed. With increased load, further hinges form at the supports and a three hinge collapse mechanism is achieved. It is assumed that collapse occurs in flexure and the slab has sufficient capacity to prevent failure through shear. Normally the ultimate moment of resistance (or 'plastic moment') at the hinges is taken as that defined by Mattock et al. (1961) in Equation 2.43. However this ignores the compression reinforcement and all

specimens in the experimental programme had a significant amount of compression steel which must be considered in the moment capacity calculation.

To determine the yield moment (M_y) and the moment of resistance (M_u) of a doubly reinforced concrete section the parabolic concrete stress block from BS:8110: Part 3 has been assumed, as shown in Figure A.7.1. Removing all safety factors and assuming that the tensile steel stress is limited to the yield stress f_y the ultimate bending moment capacity (moment of resistance) M_u, can be calculated from the following process and is ultimately given by Equation 4.5.

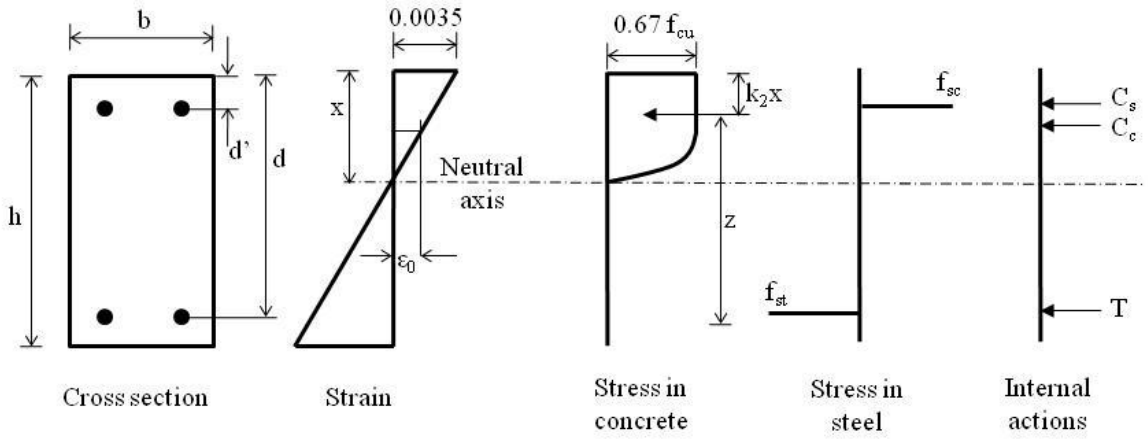

Figure 4.9: *Conditions of stress and strain assumed at the ultimate limit state (BS 8110-3:1985 Appendix A Figure 1)*

Equilibrium of axial forces is found from:

$$N = C_c + C_s - T \tag{4.1}$$

$$N = k_1 bx + A'_s f_{sc} - A_s f_{st} \tag{4.2}$$

Where the concrete compressive force C_c at failure is given by:

$$\frac{0.67 f_{cu} bx}{0.0035}\left(0.0035 - \frac{\varepsilon_0}{3}\right) = k_1 bx \tag{4.3}$$

Where ε_0 can be taken as:

$$\varepsilon_0 = 2.4 \times 10^{-4}\sqrt{f_{cu}} \qquad 4.4$$

Taking moments about the mid-depth on the section gives

$$M = k_1 bx\left({}^{h}/_{2} - k_2 x\right) + A'_s f_{sc}\left({}^{h}/_{2} - d'\right) + A_s f_{st}(d - h/2) \qquad 4.5$$

Where:

$$\left[\frac{\left(2 - {}^{\varepsilon_0}/_{0.0035}\right)^2 + 2}{4\left(3 - {}^{\varepsilon_0}/_{0.0035}\right)}\right] x = k_2 x \qquad 4.6$$

The compressive and tensile stresses in the reinforcing steel can be determined from the strain once a value of neutral axis, x, has been assumed:

$$\varepsilon_{sc} = \frac{0.0035}{x}(x - d') \qquad 4.7$$

$$\varepsilon_{st} = \frac{0.0035}{x}(d - x) \qquad 4.8$$

$$f_{sc} = \varepsilon_{sc} E_s \qquad 4.9$$

$$f_{st} = \varepsilon_{st} E_s \qquad 4.10$$

Equations 4.9 and 4.10 are based on elastic behaviour of the steel. If yield has occurred the steel stress is limited to the yield stress f_y.

The neutral axis position is determined by trial and error, the value of *x* being adjusted until the axial force *N* in Equation 4.2 is equal to zero.

The above analysis is based on the concrete achieving a strain of 0.0035 at failure. In reality the strain at failure varies with concrete strength (Hognestad, Hanson and McHenry (1956)) but this is ignored in BS8110.

In order to provide a detailed explanation of the procedure for assessing the enhancement provided through CMA the calculations for specimen M3 are presented in detail. The

specimen cross-section and other properties were given in Table 3.2. ; L_1 = 3.9m, h = 105mm, b = 320mm, d = 78mm, $\rho = \rho' = 0.2\%$, f_{cu} = 51.57N/mm^2, L/d = 50. The specimen was reinforced according to arrangement 1 in Figure 3.13.

Using Equations 4.1 to 4.10, and since $A_s = A'_s$, the moment capacity of the specimen at mid-span (M_u) and at support (M'_u) are both equal to 2.82 kNm.

The ultimate load that causes the assumed collapse mechanism when considering the conditions in the tests is defined as:

$$P_u = \frac{4\left(M_u + M'_u - \frac{qL^2}{8}\right)}{L} \qquad 4.11$$

Where q is the uniformly distributed self-weight of the specimen. Equation 4.11 is identical to that employed by previous authors including Merola (2009) except for the addition of a term for the self-weight of the specimen, since at higher span to depth ratios the effect of self-weight is more significant and cannot be neglected.

The load capacity of M3 was thus found from:

$$P_u = \frac{4\left(2.82 + 2.82 - \frac{0.77 \times 3.9^2}{8}\right)}{3.9} = 4.29\ kN$$

The load enhancement factor used here is defined as the measured applied load P over the predicted ultimate load, P/P_u. For specimen M3 the maximum applied load was 8.16 kN hence the load enhancement was 8.16/4.29 = 1.90.

The effect of axial restraint on the internal forces of the specimen is complex. Whilst as shown in previous literature and experimental studies the axial force produced in longitudinally restrained RC elements can increase the flexural strength, the axial compression force also creates a second order destabilising moment as the specimen deflects at mid-span, commonly referred to as the P-Δ effect. As can be seen from Equations 2.35 and 2.36 any load enhancement from an enhancement in moment capacity is offset by the effect of the moment $N_u\delta$.

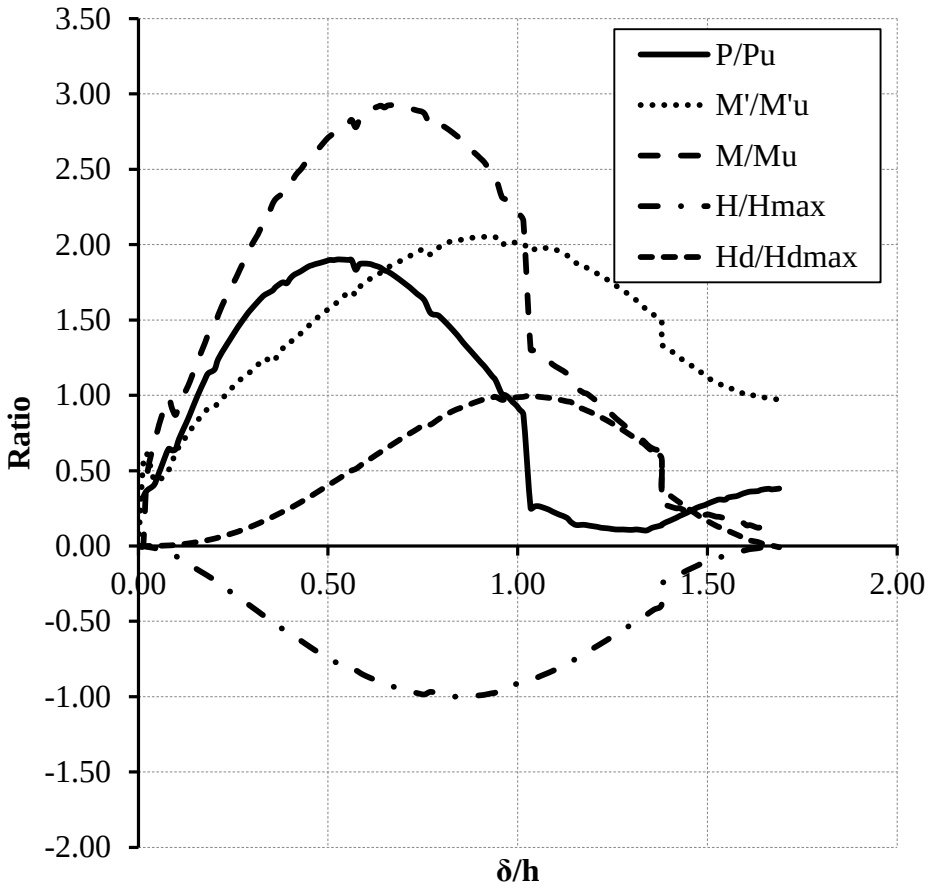

Figure 4.10: *Normalised bending moments, applied load, horizontal force and second order effect for specimen M3.*

To illustrate the effect of this second order component Figure 4.10 shows the response of vertical load P, the mid-span calculated moment M, the calculated support moment M', and the horizontal reaction H as the mid-span deflection δ is increased. The vertical load P has been normalised using the predicted load capacity P_u, the mid-span and support moments have been normalised using the calculated moment capacities M_u and M'_u, and the horizontal force has been normalised using the maximum horizontal force. The response shown covers only the compressive membrane phase.

The values for M and M' have been calculated from the measured reactions using the following formulae:

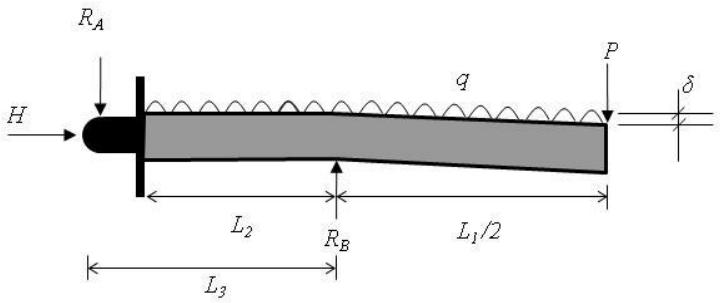

Figure 4.11: *Free body diagram for the calculation of the mid-span moment*

$$M = R_A\left(\frac{L_1}{2} + L_3\right) + \frac{q\left(\frac{L_1}{2} + L_2\right)^2}{2} - R_B\frac{L_1}{2} - H\delta \qquad 4.12$$

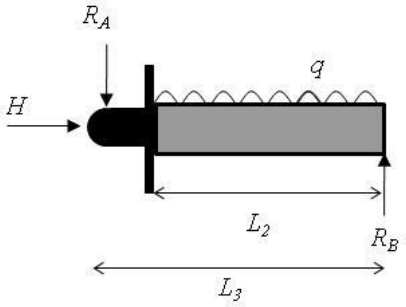

Figure 4.12: *Free body diagram for the calculation of the support moment*

$$M' = R_A L_3 + \frac{q(L_2)^2}{2} \qquad 4.13$$

Figure 4.10 shows that the axial force reduced the load carrying capacity through the second order P-Δ effect. As a result the peak load was reached prior to the peak bending moments at mid-span and support. The second order effect was generally found not to reduce the supported load below the predicted plastic analysis load capacity, with the exception of specimen E3 which only achieved 91% of the predicted load in the compressive membrane action phase. The reduction in load carrying capacity below the predicted value in specimen E3 cannot be attributed exclusively to the second order effect but it is clearly very significant. The component Hδ from the calculation of the mid-span moment has been shown in Figure 4.10 normalised against its maximum value, further indicating that there is a decrease in load enhancement as this second order component increases.

As can be seen in Figure 4.10 the flexural bending capacity was increased at mid-span by about 200% and by about 100% at the support. The average of the two was still greater than the load enhancement. There was still significant flexural strength at the end of the CMA phase which allowed the specimen to resist any sudden failure through the transition into TMA. The results found are similar to those in Su et al (2009).

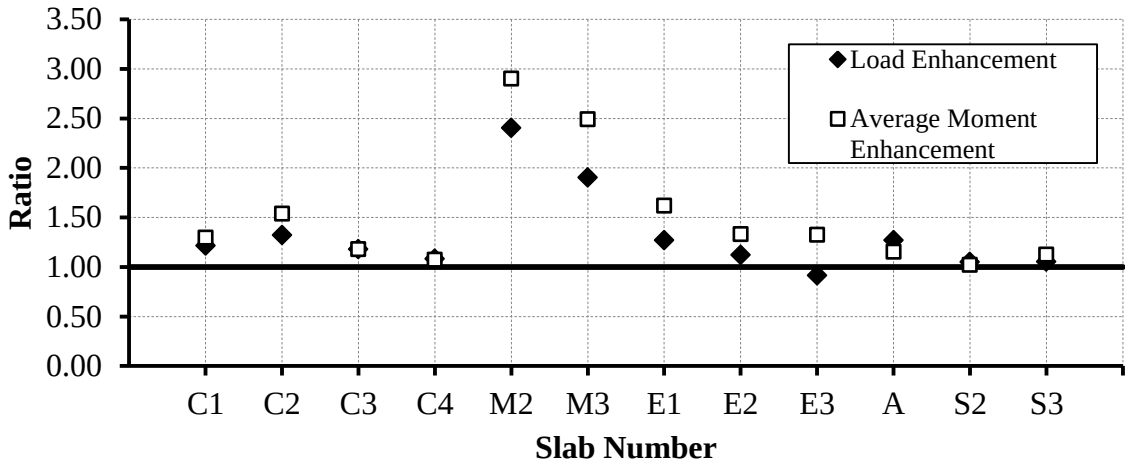

Figure 4.13: *Enhancement through CMA of experimental specimens*

The peak load enhancements (P/P_u) and average moment enhancements for all the specimens in the experimental programme are shown in Figure 4.13. As with the example specimen M3 all but one specimen produces a higher average moment enhancement than load enhancement. The development of moment and applied load with mid-span deflection for all samples is presented in Appendix A.5. Whilst all but one specimen reached their predicted load capacity, significant load enhancement through CMA was limited only to specimens M2 and M3 from the flat slab set of specimens. These two specimens which model the middle strip of a flat slab had the smallest percentage of tensile reinforcement of all specimens tested.

4.4.1 **Flat Slab Specimens**

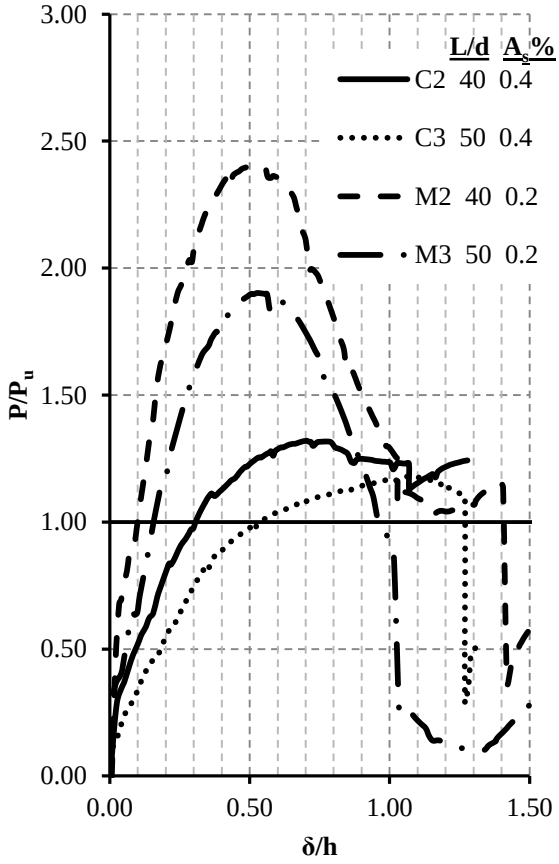

Figure 4.14: *Comparison of applied load for flat slab specimens.*

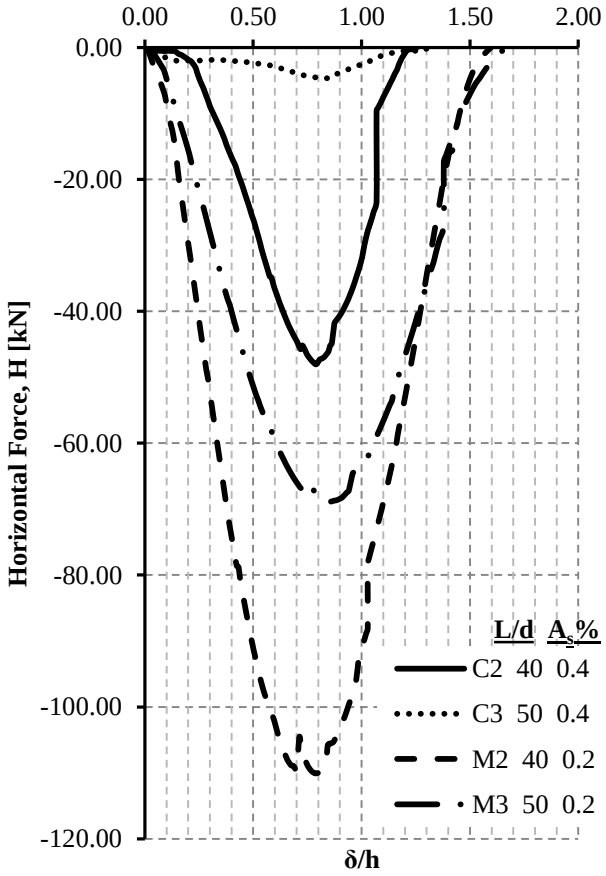

Figure 4.15: *Comparison of horizontal force for flat slab specimens.*

A comparison of the applied load and the measured horizontal force between the two column strips and two middle strips has been made and is displayed in Figure 4.14 and 4.15. This allows for a direct comparison of differences in behaviour at span to depth ratios of 40 and 50 as well as due to a change of reinforcement percentage from 0.2% to 0.4%. C2 and M2 had a span to depth ratio of 40 whilst C3 and M3 had a span to depth ratio of 50. Column strips (C2 and C3)had 0.4% reinforcement whilst middle strips (M2 and M3)had 0.2% reinforcement.

From the load enhancement curves shown in Figure 4.14 there is a clear relationship between enhancement and percentage of reinforcement. The greatest load enhancements were produced from the specimens detailed with the lowest percentages of reinforcement. This indicates that the modest increase in area of reinforcement did not result in an increase in load capacity and more was gained from CMA which was more predominant at low reinforcement percentage.

When assessing the effect of span to depth ratio for both column and middle strip specimens the enhancement fell as the span to depth ratio increased. Although even when L/d = 50 for the middle strip significant enhancement was found. This relationship is reflected in the variation in compressive thrust presented in Figure 4.15. It can be seen that the horizontal force reduced when span to depth ratio increased, an effect that was more significant at the highest percentage of reinforcement considered.

4.4.2 **Conventional Framed Specimens**

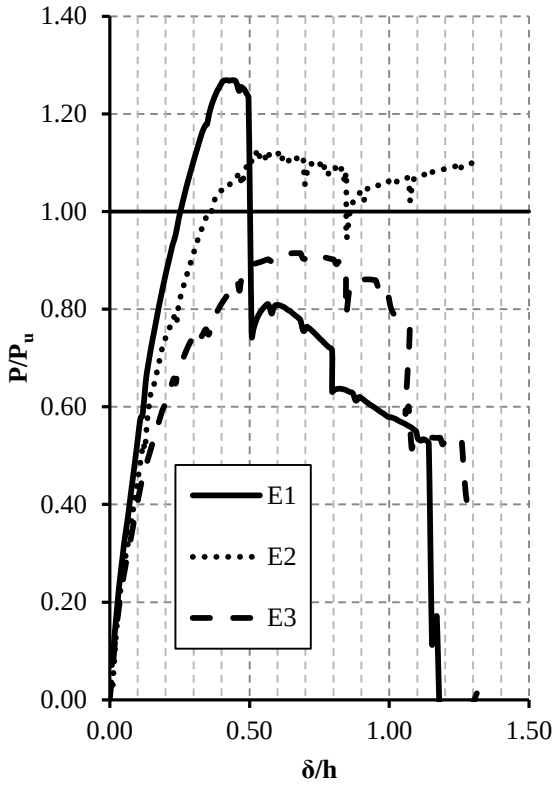

Figure 4.16: *Comparison of applied load for edge beam specimens.*

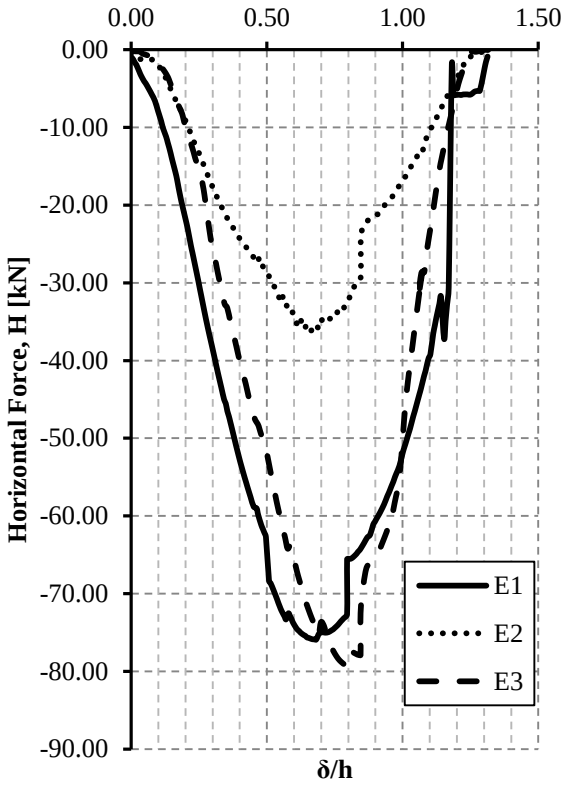

Figure 4.17: *Comparison of horizontal force for edge beam specimens.*

A direct comparison of the influence of percentage reinforcement at a constant span to depth ratio can be made by assessing the total moment enhancements and horizontal reactions of the three edge beam specimens (Figure 4.16 and 4.17). Results show that the moment enhancement fell with increase in percentage of reinforcement, echoing predictions from the Literature Review (Figure 2.20 by Lahlouh and Waldron (1992)). Whilst the horizontal compressive force was found to drop when the percentage of reinforcement was increased

from specimen E1 to specimen E2. Specimen E3 developed a horizontal force similar to that of E1 probably due to the change in cross sectional area as the section width increased from 225mm for specimens E1 and E2 to 320mm for specimen E3, allowing a higher compressive thrust to be induced.

4.4.3 **Influence of Key Factors**

The influence of span to depth ratio on load enhancement is displayed in Figure 4.18. It can be seen that the results are split into two groups; the middle strip specimens with lower reinforcement (M2 & M3) have a consistently high enhancement factor. The remainder of the specimens show a weak trend that at higher span to depth ratios the enhancement factor reduces. This trend is also implied by the two 'M' series specimens. The percentage of reinforcement is a more influential parameter showing a clearer trend in results. Figure 4.19 demonstrates a clear trend that with increasing percentage of reinforcement moment enhancement falls. This relationship is best highlighted by the Edge Beam series specimens (E1, E2 & E3); in Figure 4.19 it can be seen that as the reinforcement percentage is increased the enhancement factor falls. The results therefore confirm theories cited in previous literature, Park and Gamble (2000) & Roberts (1969), that restrained slab elements with smaller span to depth ratios but more influentially lower percentages of reinforcement produce the optimum conditions for load enhancement through CMA.

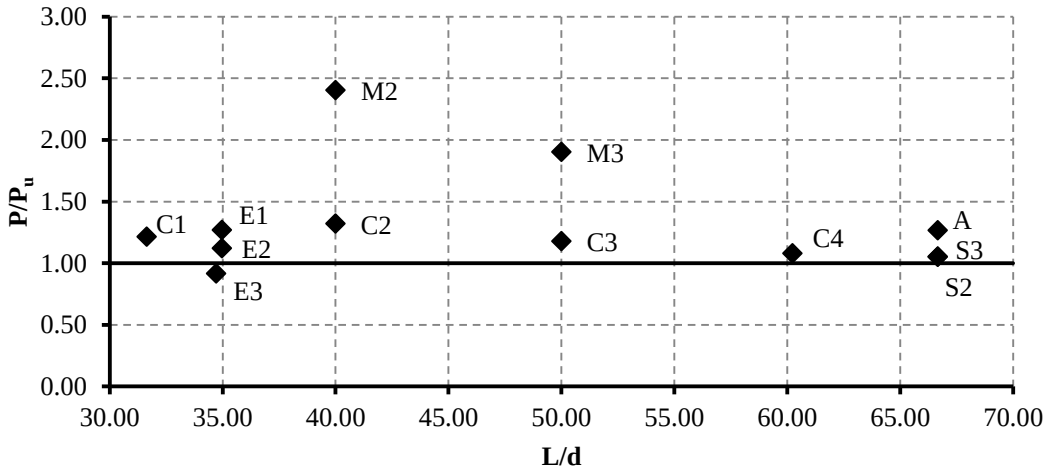

Figure 4.18: *Relationship of load enhancement and span to depth ratio.*

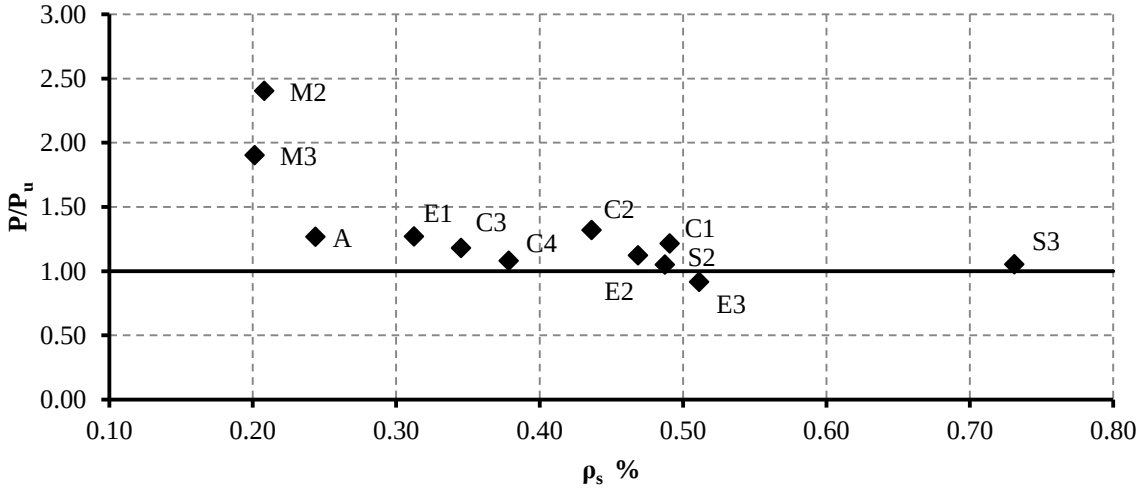

Figure 4.19: *Relationship of load enhancement and percentage of tension reinforcement.*

4.5 **Conclusions**

A total of 12 RC specimens that model flat slab and conventionally framed structures have been tested at span to depth ratios ranging from 30 to 66 and percentage of tension reinforcement ranging from 0.2% to 0.7 %. Longitudinal restraint was provided by a steel H-frame, with additional stiffening, providing a stiffness of 105000 N/mm. From the behaviour observed during testing and the measured reactions and calculated bending moments the following conclusions from the experimental test results can be made.

Snap-through that caused a drop off in central load was found to occur at an average normalised deflection (δ/h) of 0.58 which was slightly higher than the values suggested in previous literature. It was demonstrated that some specimens did not exhibit a reduction in supported load at snap-through and in such cases it was more insightful to analyse the peak horizontal compressive force which allowed direct comparison of all specimens. The average normalised deflection at the maximum horizontal force had a value of 0.74. Specimens that did not produce a clear peak of applied load had high span to depth ratios.

Load enhancement was really significant only in specimens with low levels of tension reinforcement; namely in specimens M2 and M3 which had reinforcement percentages of 0.2% even though these specimens still had relatively high span to depth ratios of 40 and 50 respectively. All other specimens but one reached the predicted ultimate load but did not significantly exceed it, although the average enhancement was 17%. The peak applied load occurred at a lower deflection than the peak moment, which was attributed to the second order Pδ effect that occurs with the induced compressive axial force. At the end of the compressive phase of behaviour the specimens still had sufficient flexural strength to prevent any sudden failure from occurring so that after the compressive phase it was possible to increase the applied load through frame and catenary action.

It was problematic to determine the limitations to load enhancement in terms of span to depth ratio alone when percentage of reinforcement and the restraint stiffness of the test rig had a significant influence. The longitudinal restraint stiffness provided by the test rig was comparable to that reported by Taylor (2000), however it is a factor of 10 lower than the stiffness generated in other reported research, Su et al (2009) & Christiansen (1963). This relatively low value of rig stiffness along with high span to depth ratios helps explain lower

enhancement values than might have been expected on the basis of previous test results. The level of stiffness provided was however comparable to values provided by realistic frames as discussed in Chapter 5. From the load enhancement factor it was found that reinforcement percentage had a more significant effect on enhancement than span to depth ratio. However even at a span to depth ratio of 66 a load enhancement factor above 1.0 was still achieved. The significant load enhancement produced at span to depth ratios of 40 and 50 indicates that there is the potential for a slab in the double span situation due to loss of column to carry load through compressive membrane action.

Chapter 5: Predicting the Benefits of CMA

5.1 **Introduction**

The prediction methods of Rankin & Long (1997) and Merola (2009) discussed in the literature review have been assessed herein to determine their accuracy. These methods were identified in the literature review as being accurate when compared to test data, albeit at low span to depth ratios. Both methods are based on a similar approach. A simplified collapse mechanism is used and the total deformations and strains of samples are utilised rather than the use of strain rates. This chosen approach was concluded in the literature review to be the most appropriate (over the strain rate approach) when the maximum load carrying capacity is the focus of the study as it is in this research. As total strains are considered the equations are consequently simpler. This allows them to be applied to a parametric study and hence a frame assessment.

Although Merola's method is capable of predicting the load and deflection at the point of reinforcement fracture, it was only used to predict the peak load, because, in the tests under consideration, reinforcement fracture did not occur prior to the attainment of the peak load.

Two prediction methods have been used to predict failure loads for the test specimens resulting in ratios of test against predicted failure loads (P_t / P_p). These ratios were analysed statistically to select the more accurate method for predicting the behaviour of the specimens tested by the author at high span to depth ratios. By employing this method a parametric study was conducted to determine the ability of slab strips to support self weight in the double span scenario. The limitations in utilizing this approach in further predictions have been evaluated. Factors that are significantly influential in the enhancement from CMA have also been assessed.

5.2 **Comparative Study of Experimental Results**

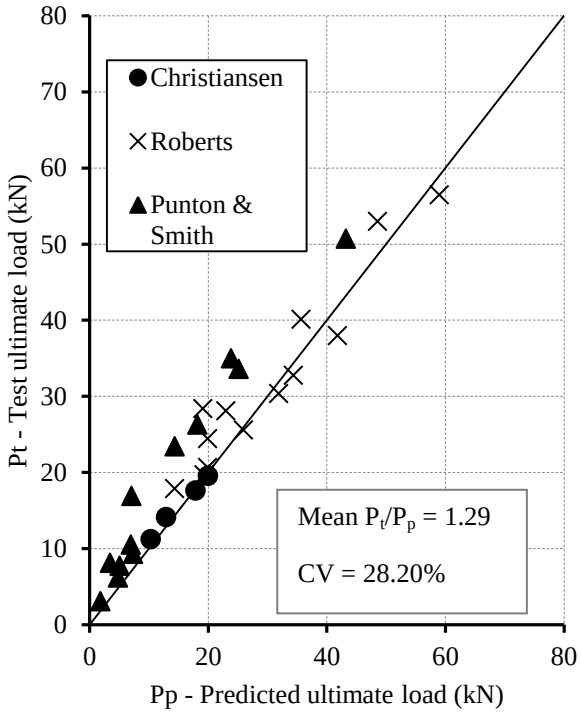

Figure 5.1: *Comparison of Rankin & Long predicted values with test results.*

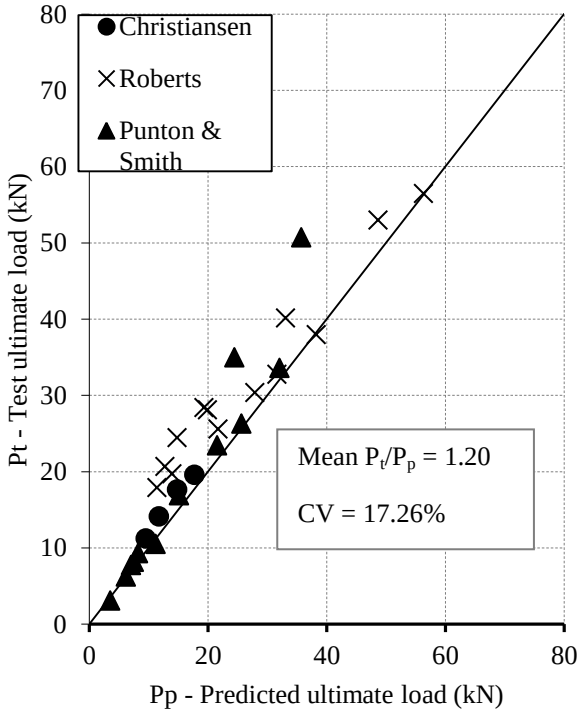

Figure 5.2: *Comparison of Merola predicted values with test results.*

Comparisons of predicted ultimate loads for a series of previous experimental studies (Christianson (1963), Roberts (1969)) as well as the test data produced by the author (labelled Punton & Smith) have been carried out for the two prediction methods and the results are shown in Table 5.2 and graphically in Figure 5.1 and Figure 5.2. Summarised specimen section properties and ultimate test load are shown in Table 5.1. Full details are given in Appendix A.8. These data have also been presented in Figure 5.3 and Figure 5.4 as graphs of the ratio of test to predicted load against span to depth ratio. This allows an assessment of the relationship between prediction accuracy and span to depth ratio.

For each prediction method the average value of the ratio of test to predicted load has been calculated. A value above 1.0 represents an underestimation of failure load by the prediction method and conversely a value below 1.0 means an overestimate. The coefficient of variance (CV) has also been presented; this is a normalised measure of the dispersion of a probability distribution. It is defined as the standard deviation over the mean expressed as a percentage and gives an indication of the spread of results and is thus a measure of variability. A lower percentage indicates a closer spread of results.

Rankin and Long (1997) provides less accurate results overall from the two methods considered with a mean P_t/P_p of 1.29, (an underestimation of failure load), and a CV of 28.20%. With regards to the test results from Punton & Smith at the high span to depth ratios that are more pertinent to slabs in emergency conditions it yielded a mean P_t/P_p of 1.59 (CV = 23.63%), representing an underestimate of 60%. From Figure 5.3 it can be seen that the method tends to underestimate load prediction at all span to depth ratios considered. Whilst the spread of predictions was moderately consistent for predictions of data from literature, discrepancies occurred with the Punton & Smith test results.

The Merola (2009) method also produced a general underestimation of load carrying capacity. As shown in Figure 5.2 the mean P_t/P_p was 1.20, lower than Rankin & Long, and the coefficient of variance was 17.26%. This indicates that overall the Merola method gives a closer spread of results with a higher accuracy in predicted values. For the Punton & Smith test results the mean P_t/P_p was 1.10 and the coefficient of variance was 14.32%. The closer spread of results is demonstrated graphically in Figure 5.4. Hence for the Punton & Smith test

results the Merola predictions were more accurate and less variable (mean P_t/P_p of 1.10 and CV of 14.32%) than those from Rankin & Long (mean P_t/P_p of 1.59 and CV of 23.6%).

Author	Slab No.	f_{cu} [N/mm^2]	k_1	A_s [%]	A'_s [%]	L/d	P_t [kN]
Christiansen	1	34.27	2.35	0.62	NA	27.42	11.25
	2	32.27	2.02	0.62	NA	22.85	14.15
	3	28.20	1.85	0.62	NA	19.19	17.66
	4	39.02	1.57	0.62	NA	19.19	19.57
Roberts	RB10	50.40	21.28	0.56	NA	33.16	28.39
	RB11	24.70	30.40	0.56	NA	33.16	17.90
	RB12	32.80	26.38	0.74	NA	33.16	24.45
	RB13	30.20	27.49	0.74	NA	33.16	19.72
	RB14	49.70	21.43	0.74	NA	33.16	28.11
	RB15	24.10	30.77	0.93	NA	33.16	20.67
	RB17	53.30	20.69	0.93	NA	33.16	25.57
	RB18	27.00	19.51	0.58	NA	21.02	32.78
	RB19	28.70	18.92	0.58	NA	21.02	40.12
	RB20	47.90	14.65	0.58	NA	21.02	52.99
	RB21	18.10	23.83	0.92	NA	21.02	30.39
	RB22	30.20	18.45	0.92	NA	21.02	37.97
	RB23	56.30	13.51	0.92	NA	21.02	56.49
Punton & Smith	C1	62.89	0.06	0.49	0.49	31.64	17.50
	C2	70.09	0.29	0.44	0.44	40.00	11.73
	C3	69.17	0.36	0.35	0.35	50.00	5.26
	C4	47.21	0.51	0.38	0.38	60.24	3.88
	M2	57.50	0.33	0.21	0.21	40.00	8.45
	M3	51.57	0.40	0.20	0.20	50.00	4.08
	A	54.60	0.68	0.24	0.24	66.67	1.54
	S2	70.48	0.60	0.49	0.49	66.67	2.99
	S3	49.33	0.71	0.73	0.73	66.67	4.66
	E1	66.15	0.39	0.31	0.70	34.97	13.14
	E2	41.19	0.49	0.47	1.05	34.97	16.80
	E3	54.21	0.30	0.51	1.31	34.72	25.36

Table 5.1: Summary of Test Specimen Properties

Author	Slab No.	P_t [kN]	R&L [kN]	Merola [kN]	R&L Pt/Pp	Merola Pt/Pp
Christiansen	1	11.25	10.34	9.51	1.09	1.18
	2	14.15	12.91	11.71	1.10	1.21
	3	17.66	17.87	14.77	0.99	1.20
	4	19.57	19.97	17.73	0.98	1.10
Roberts	RB10	28.39	19.14	19.31	1.48	1.47
	RB11	17.90	14.37	11.37	1.25	1.57
	RB12	24.45	19.95	14.77	1.23	1.66
	RB13	19.72	19.35	13.93	1.02	1.42
	RB14	28.11	22.99	19.90	1.22	1.41
	RB15	20.67	19.93	12.72	1.04	1.62
	RB17	25.57	25.98	21.71	0.98	1.18
	RB18	32.78	34.39	31.61	0.95	1.04
	RB19	40.12	35.68	33.06	1.12	1.21
	RB20	52.99	48.59	48.64	1.09	1.09
	RB21	30.39	31.93	27.88	0.95	1.09
	RB22	37.97	41.85	38.26	0.91	0.99
	RB23	56.49	59.02	56.30	0.96	1.00
Punton & Smith	C1	35.00	23.84	24.45	1.47	1.43
	C2	23.45	14.35	21.53	1.63	1.09
	C3	10.53	6.96	11.16	1.51	0.94
	C4	7.76	5.11	7.03	1.52	1.10
	M2	16.91	7.09	15.12	2.38	1.12
	M3	8.16	3.48	7.50	2.35	1.09
	A	6.22	4.80	6.17	1.29	1.01
	S2	9.32	7.35	8.23	1.27	1.13
	S3	3.09	1.87	3.5	1.65	0.88
	E1	26.28	18.17	25.61	1.45	1.03
	E2	33.59	25.16	32.05	1.34	1.05
	E3	50.72	43.23	35.71	1.17	1.42

Table 5.2: Test Results and Predicted Values

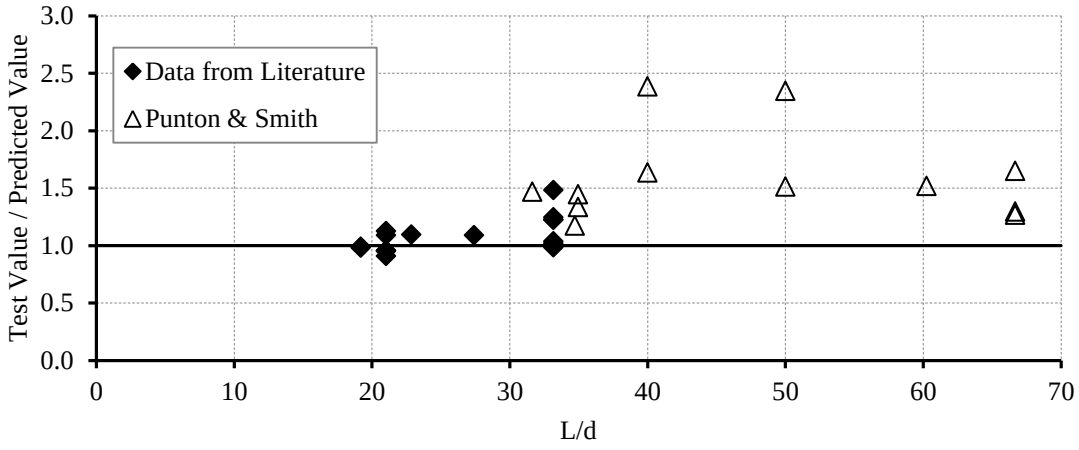

Figure 5.3: *Experimental and predicted loads by Rankin & Long against L/d.*

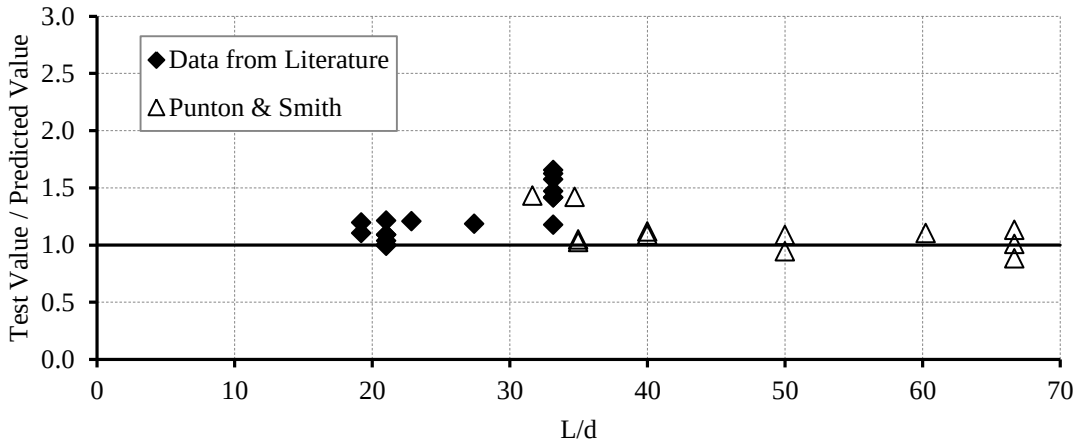

Figure 5.4: *Experimental and predicted loads by Merola against L/d.*

From Figure 5.3 and Figure 5.4 it can be seen that the experimental data for restrained RC specimens obtained from the previous literature reviewed has been expanded by the research reported here to cover high span to depth ratios. It has been shown that of the two methods considered the predicted values from the Merola method provide the better correlation at high span to depth ratios. Consequently the Merola method will be used to assess the capacity of restrained slabs in the double span conditions which arise from the loss of a column. The method has been shown to provide a consistent underestimation of load capacity which will provide a conservative assessment of enhancement through CMA in double span conditions. It also provides a value for the development of horizontal compressive thrust with mid span

deflection. This is particularly useful when assessing the restraint stiffness of adjacent floor slabs and has been employed in this fashion in the frame study conducted in Chapter 6.

5.2 **Enhancement Factor**

To quantify the beneficial effect of CMA an enhancement factor P', defined in Equations 5.1 and 5.2, has been introduced. The ultimate load capacity of a slab strip inclusive of CMA P_F from the Merola method has been normalised by dividing it by the double span self-weight of the strip P_R. Thus the ratio $\frac{P_P}{P_R}$ gives an indication of the ability of the strip to resist load in excess of its self-weight. Hence if $P' = 1.0$ the slab strip is only able to support its own self weight and any additional loading would be expected to cause the slab to fail. Clearly $P' > 1.0$ indicates that the strip can carry more than just the self weight and $P' < 1.0$ indicates that the strip is incapable of carrying its own weight.

$$P' = \frac{P_P}{P_R} \tag{5.1}$$

$$P_R = \gamma_w bhL \tag{5.2}$$

Where γ_w is the concrete density and L is the double span after column removal.

5.3 **Influence of Percentage of Tension Reinforcement**

The Rankin and Long method (1997) has been employed to investigate the relationship between the quantity of tension reinforcement and the enhancement provided by CMA. Of particular interest was the finding from previous literature (Lahlouh and Waldron (1992) and Taylor et al. (2001)) that an increase in tension reinforcement decreases the load carrying capacity of any compressive arch induced. The purpose of using the Rankin and Long method for this investigation was that the method provides separate values of bending and arching strength. In the two-phase approach of Rankin and Long the total enhanced load P_p is equal to the sum of the arching component P_a and the bending component P_b. This allows for the contribution of each to be quantified and assessed. Although the Merola method was shown to more accurate the Rankin and Long method is employed here for a standalone study to investigate the influence of the quantity of tension reinforcement on enhancement from CMA.

A full description of the Rankin and Long method (1997) used in this section and an example calculation are given in Appendix A.9.

A study has been conducted to determine when the arching component no longer makes a significant contribution to the total enhanced load when the percentage of reinforcement is varied. The reinforcement percentage has been progressively increased for a 0.3m deep 1m wide slab strip for a range of span to depth ratios. In Figure 5.5 the component of the failure load due to arching action has been expressed as a percentage of the total enhanced load and plotted against the percentage of reinforcement. Figure 5.5 shows that there is a rapid decrease in the contribution from arching action (CMA), indicating that as the reinforcement percentage increases there is more to be gained from the increase in the bending moment capacity of the section. This is confirmed in Figure 5.6 which shows that the enhancement factor P' increases with the percentage of reinforcement.

The results also give an indication of the effect of reinforcement percentage in the double span (accidental column loss) situation when the original span to depth ratio is doubled. By comparing the curves for L/d ratios of 20 and 40 and those for L/d ratios of 30 and 60 in Figure 5.5 it can be seen that the arching component percentage is reduced by approximately half when the span to depth ratio is doubled. This relationship is maintained up to high reinforcement percentages and all curves converge on a value close to zero. It can therefore be said that in accidental conditions the contribution from the arching component reduces by approximately 50%. Such a direct relationship cannot be drawn when considering the enhancement factor P' as shown in Figure 5.6. In this case as the span to depth ratio doubles the arching component halves whilst the self-weight doubles resulting in a reduction of P' much greater than 50% at double span. Figure 5.7 shows that the load carried through bending also reduces by 50% as the span to depth ratio is doubled.

Table 5.3 summarises the results shown in the graphs in Figures 5.5 to 5.7. It has been demonstrated that the contribution from arching action decreases with increased percentage of reinforcement, a reduction that is doubled in the double span emergency situation. The relationship of enhancement factor with reinforcement is more complex as the section reaches a point where more load can be supported through flexural strength than CMA. The additional

self-weight loading adds to the detrimental effect of less arching action at high values of reinforcement and span to depth ratio.

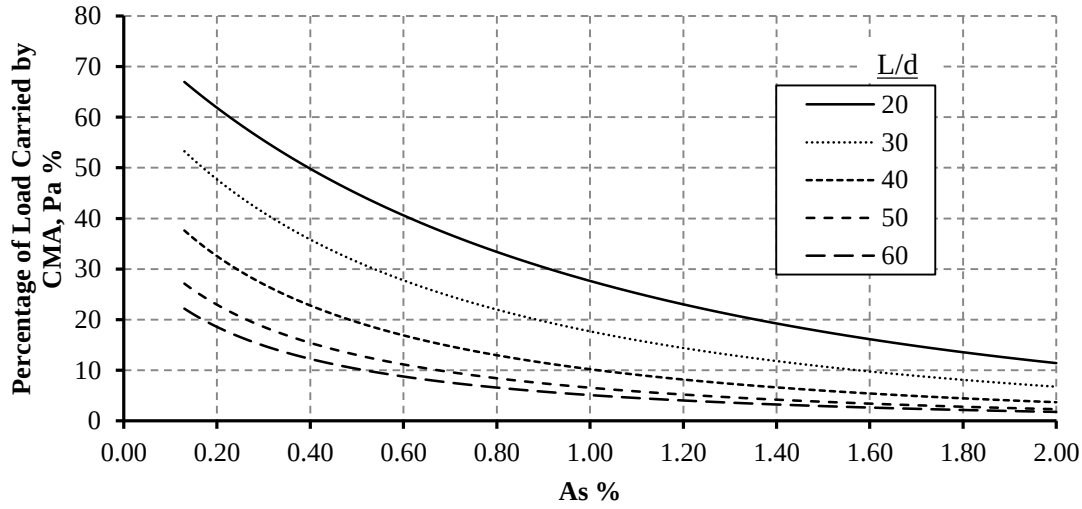

Figure 5.5: *Effect of reinforcement percentage on arching component of failure load at various span to depth ratios.*

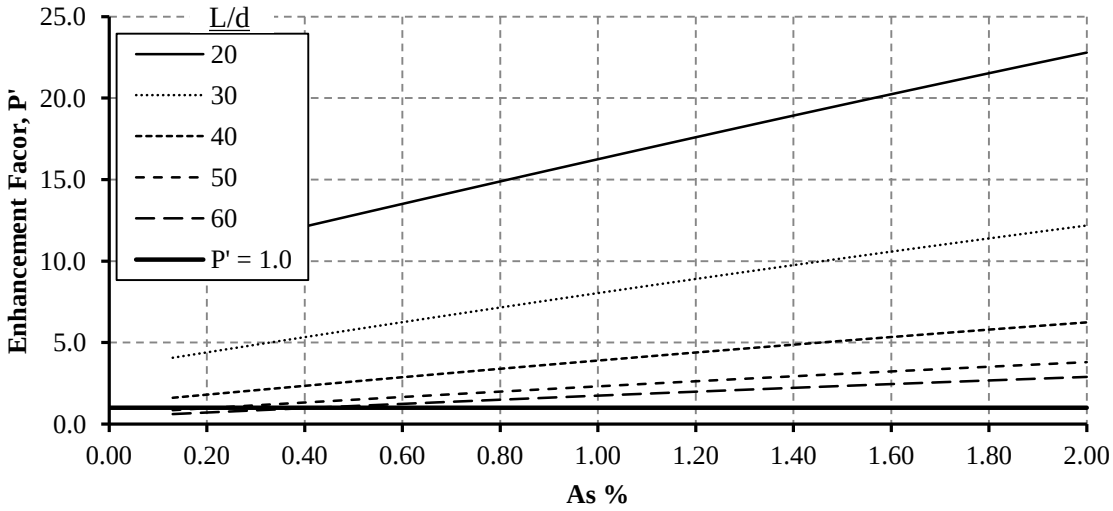

Figure 5.6: *Effect of reinforcement percentage on the enhancement factor at various span to depth ratios.*

Original Span L_o [m]	Double Span L [m]	L/d	A_s [%]	A'_s [%]	Pa [kN]	Pb [kN]	Pp [kN]	% of Pa to Pp	P'
3.00	6.00	22.06	0.20	0.20	47.73	29.44	77.17	61.85	10.72
4.00	8.00	29.52	0.20	0.20	15.10	16.56	31.66	47.70	4.40
5.50	11.00	40.74	0.20	0.20	4.23	8.76	12.98	32.54	1.80
7.00	14.00	52.04	0.20	0.20	1.61	5.41	5.41	29.78	0.75
8.00	16.00	59.93	0.20	0.20	0.94	4.14	5.08	18.57	0.71

Table 5.3: *Summary of results from investigation into the influence of percentage of tension reinforcement*

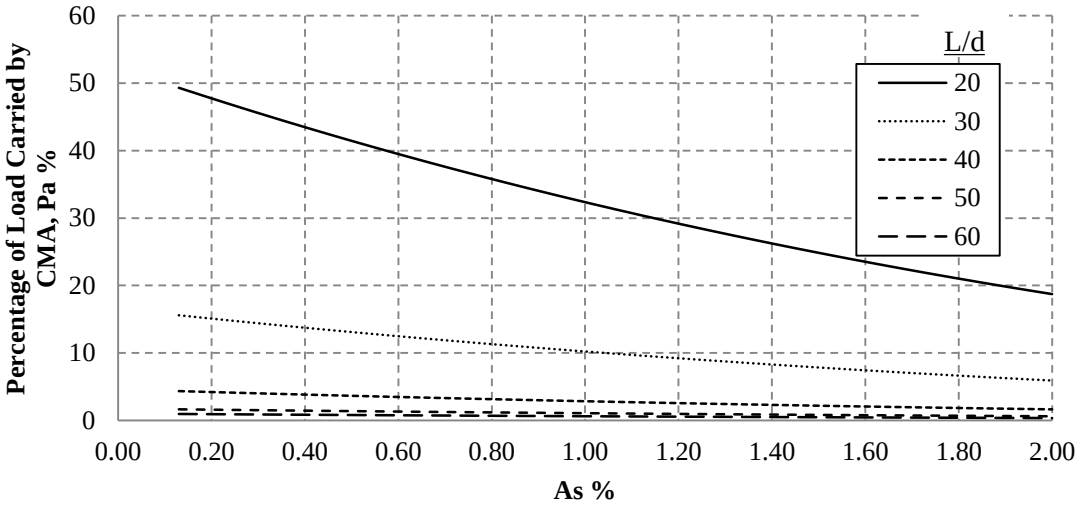

Figure 5.7: *Effect of reinforcement percentage on bending component of failure load at various span to depth ratios*

5.4 Influence of Restraint Stiffness

The review of Park & Gamble's prediction method in Chapter 2 demonstrated that the amount of outward movement at restraints has a significant effect on the amount of load that can be supported by CMA. The prediction method devised by Merola (2009), which is based on the Park & Gamble method, has been used to study the effects of restraint stiffness at span to depth ratios representative of double span conditions. A full description of Merola's original calculation procedure and an example calculation are given in Appendix A.10.

The longitudinal restraint stiffness at the end support, S, varies depending on the physical properties of the support. To allow quantification of the magnitude of restraint stiffness and for direct comparisons to be made Merola defined an axial restraint stiffness ratio, k_1. This is the ratio between the longitudinal restraint stiffness provided at the slab strip supports and the axial stiffness of the beam, allowing restraint stiffness to be normalised and non-dimensionalised:

$$k_1 = \frac{SL}{E_c bh} \tag{5.1}$$

$$E_c = 4730\sqrt{f'_c} \tag{5.2}$$

It should be noted that when the double span scenario is considered L should be taken as the span after the loss of the column.

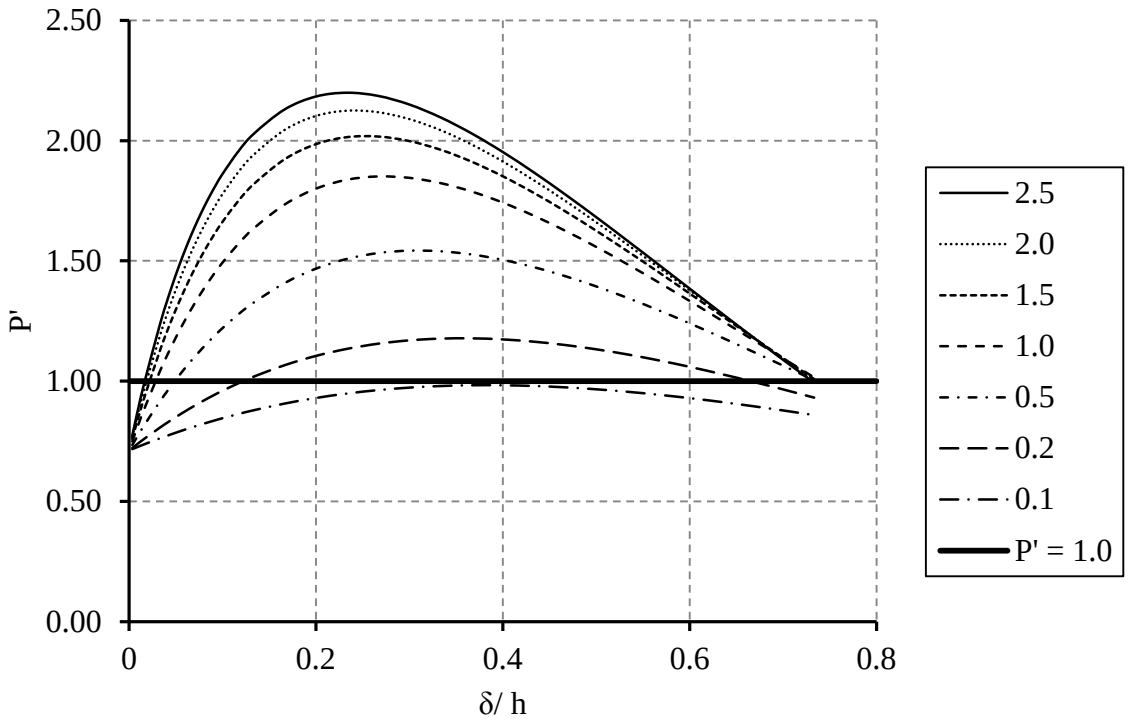

Figure 5.8: *Effect of varying k_1 on P' when L/d = 50.*

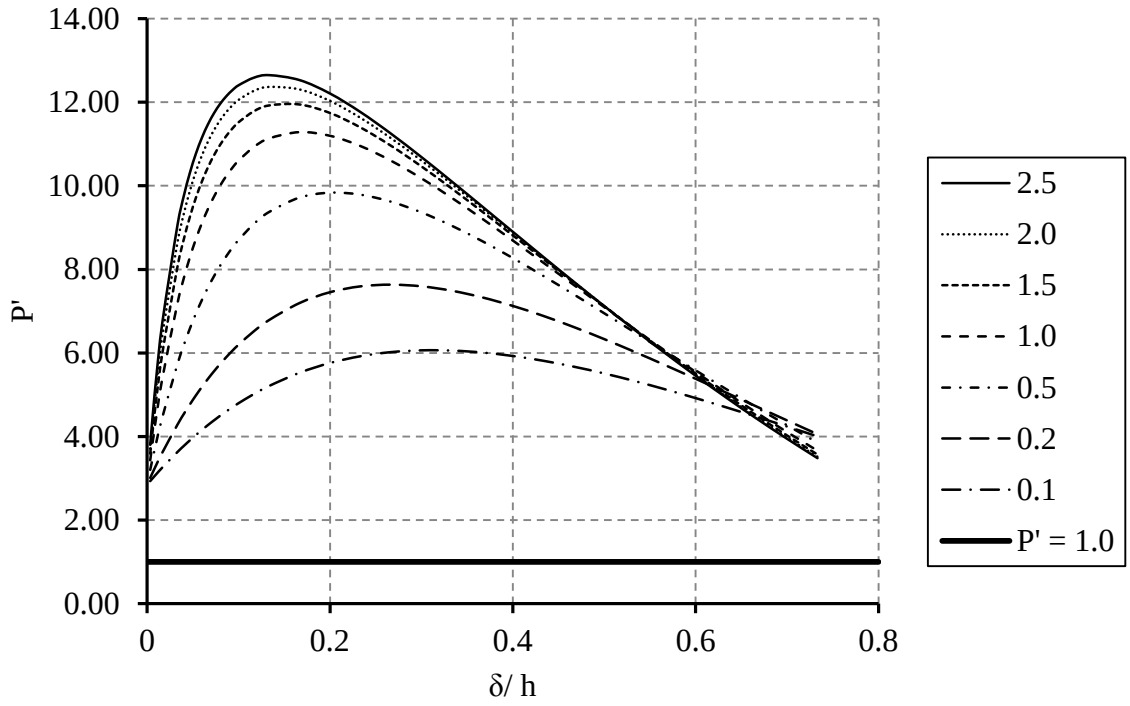

Figure 5.9: *Effect of varying k_1 on P' when L/d = 25.*

	Span to depth ratio L/d	
k_1	25	50
0.10	6.06	0.98
0.20	7.63	1.18
0.50	9.84	1.54
1.00	11.28	1.85
1.50	11.95	2.02
2.00	12.37	2.12
2.50	12.65	2.20

Table 5.4: *Maximum P' for varying stiffness k_1 for span to depth ratios 25 and 50.*

To investigate the effect restraint stiffness has on CMA in the double span conditions the enhancement factor P' has been calculated for various values of k_1 at increasing values of vertical deflection δ (expressed non-dimensionally as δ/h, where h is the specimen thickness) for a slab strip with constant span to depth ratios of 25 and 50. The results are illustrated in Figure 5.8 and Figure 5.9. The effect of varying the restraint stiffness is illustrated as each line represents a different value of k_1, while material and section properties have been kept constant. It should be noted that when k_1 is equal to 1.0 the restraint stiffness is equal to the

axial stiffness of the beam. The results are summarised for the maximum P' recorded at each increment of k_1 in Table 5.4.

The slab strip is shown to be capable of supporting at least its self weight for all values of restraint stiffness considered with the exception of when k_1=0.1 and L/d = 50. (In all the tests reported in Chapters 3 and 4 failure occurred at values of δ/h greater than 0.52) It can be seen that increasing the restraint stiffness by a factor of 10, from 0.1 to 1.0 for example, provides an increase of 50% in the enhancement through CMA for both span to depth ratios considered. Increasing restraint stiffness has a very beneficial effect on the enhancement factor P′. It is also shown that there is more to be gained from an increase in the restraint stiffness at higher span to depth ratios. Table 5.4 demonstrates that a doubling of the restraint stiffness results in an increase of 9% for a span to depth ratio of 25 and 15% for a span to depth ratio of 50. This effect is to be expected as at higher span to depth ratios with shallower arches outward movement will have a more significant effect on the point of snap through (CMA failure). These results for the double span conditions confirm those of Park and Gamble (2000) presented in the Literature Review (Chapter 2) on the sensitivity to outward movement.

The influence of span to depth ratio on the enhancement factor is further demonstrated in Figure 5.10 when the restraint stiffness is equal to the axial stiffness of the beam (k_1 = 1.0). It can be seen that with increasing span to depth ratio, at constant restraint stiffness, the enhancement factor falls. However the results indicate that the self-weight can be supported for all the span to depth ratios considered when k_1=1.0.

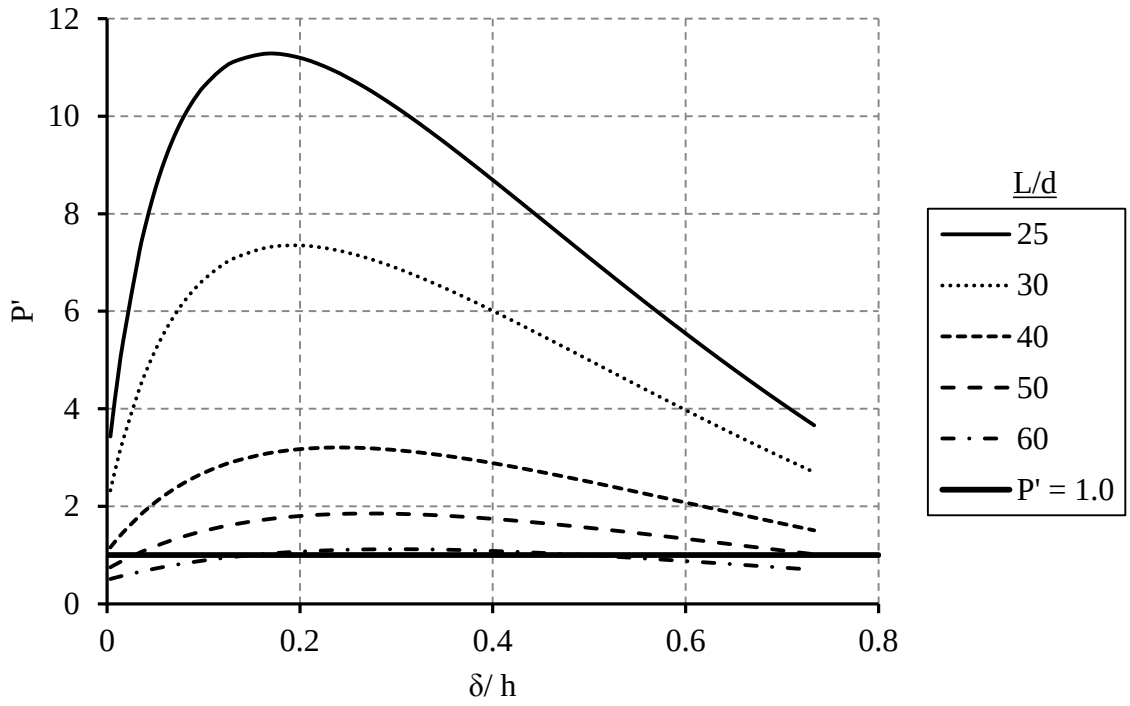

Figure 5.10: *Comparison of P' at varying L/d when k_1=1.0.*

The magnitude of the longitudinal restraint stiffness has a significant influence on the development of CMA and must be quantified in any analysis of membrane action in RC slabs. The longitudinal restraint of the test rig used for the tests reported in this thesis was calculated in section 3.5 to be 105 kN/mm, giving values of k_1 between 0.20 and 0.73. The issue of determining the longitudinal restraint stiffness that is mobilized in a damaged state scenario in a real structural frame has been considered in the next chapter of the thesis.

5.5 **Parametric Study of Slab Strips**

A parametric study focussing on span to depth ratio was carried out using the Merola prediction method. The following section and material properties have been used in the study:

f_{cu} =	55 N/mm^2	h =	300 mm
f'_c =	44 N/mm^2	d =	270 mm
f_y =	530 N/mm^2		

The span was increased incrementally and the study was carried out for two reinforcement percentages, 0.2% and 0.4%. The span to depth ratio was calculated using the span, L, after the central column had been lost. The longitudinal restraint stiffness was also varied in order to keep k_1=1.0. The results are shown graphically in Figure 5.11 and Figure 5.12. The maximum values of P' are summarised in Table 5.5 and shown in Figure 5.13.

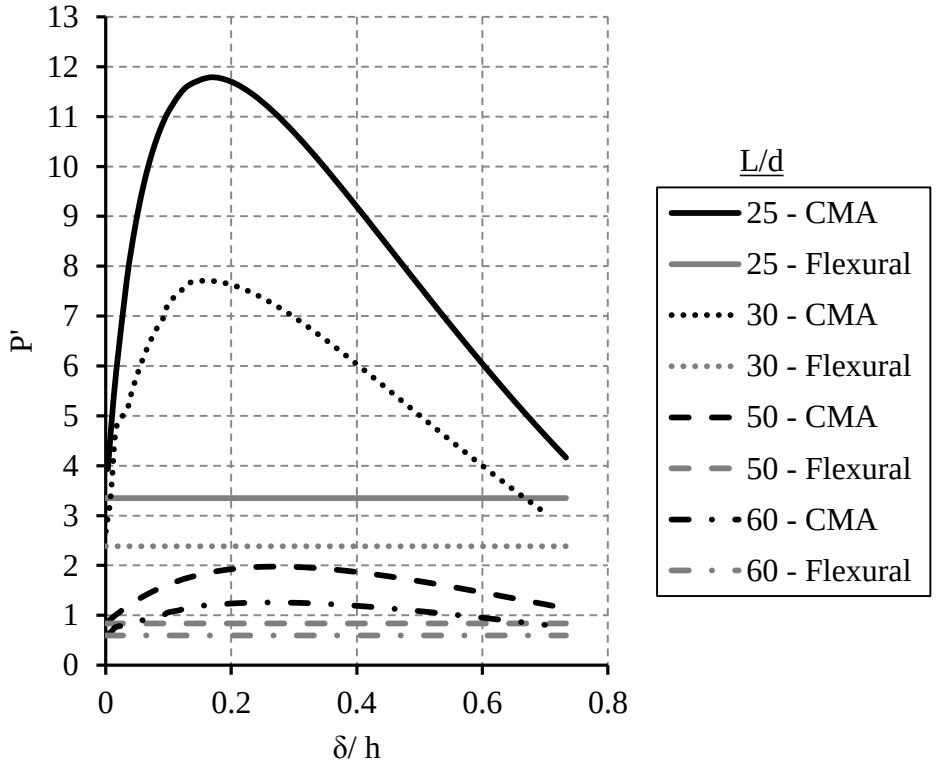

Figure 5.11: *Effect of L/d on enhancement when ρ=0.2.*

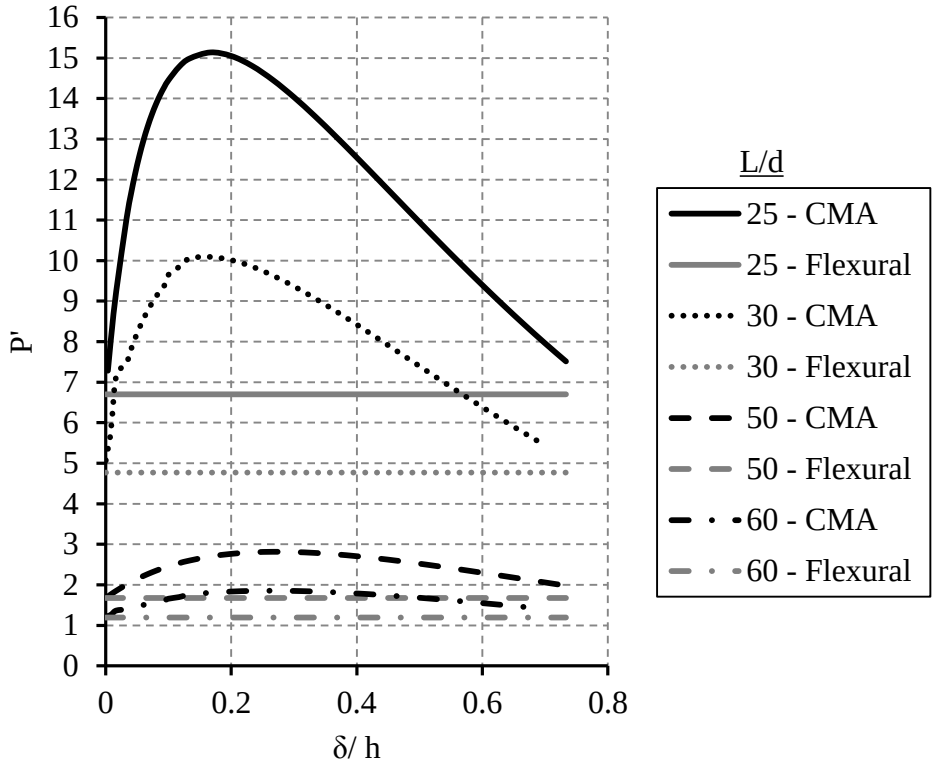

Figure 5.12: *Effect of L/d on enhancement when ρ=0.4.*

	Maximum P' inclusive of CMA		Maximum P' from flexure alone	
L/d	**0.2 [%]**	**0.4 [%]**	**0.2 [%]**	**0.4 [%]**
25	11.79	15.14	3.35	6.70
30	7.71	10.09	2.39	4.77
50	1.98	2.81	0.84	1.68
60	1.26	1.85	0.60	1.19

Table 5.5: *Summary of results from parametric study*

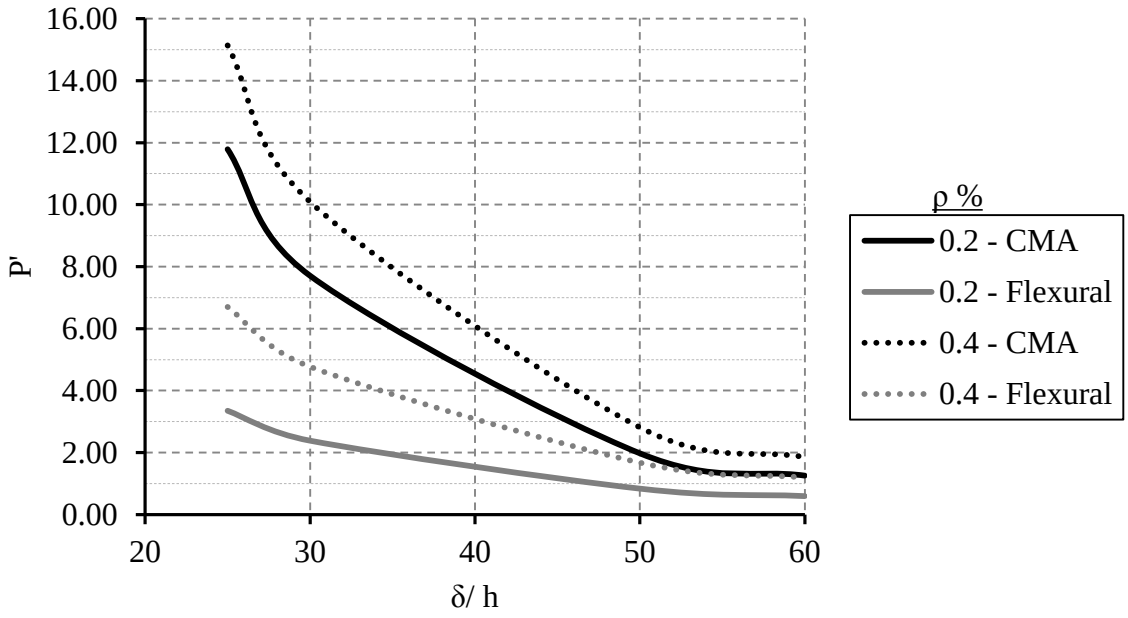

Figure 5.13: *Maximum values of P' at various percentages of reinforcement*

For both percentages of reinforcement the predicted load capacity followed a similar trend as the span to depth ratio was increased. The maximum value of the enhancement factor P' occurred at the lowest span to depth ratio, it then decreased until the span to depth ratio reached 55 as shown in Figure 5.13. At this point the enhancement factor P' plateaued as the enhancement above flexural action reached a minimum. The results show that for the section properties considered with k_1=1.0, enhancement from CMA could be obtained for span to depth ratios up to 60.

When the percentage of tensile reinforcement was set to 0.4% the highest value of P' was found. This effect is to be expected as a higher flexural strength allows for a higher load carrying capacity. With regards to enhancement through CMA results indicated that more can be achieved at a lower percentage of reinforcement. The amount of load supported above the flexural strength alone, shown in Figure 5.11 & Figure 5.12, was greater for a percentage of reinforcement of 0.2% than 0.4%. The benefit to enhancement from a low percentage of reinforcement was further demonstrated at the highest span to depth ratio considered of 60, where the restrained specimen with 0.2% reinforcement supported more load through the enhancement of CMA than the specimen with 0.4% through flexural action alone.

5.6 **Conclusions**

The influences of key factors at high span to depth ratios have been investigated and relationships described in the Literature Review have been confirmed. It has been found that by increasing the percentage of tension reinforcement the ability of the section to benefit from CMA reduces. By utilizing the method of Rankin and Long (1997) to examine the double span scenario it was shown that the percentage of total load contributed from arching action reduces by approximately half when the span was doubled. The effect of the double span, doubling the span to depth ratio and also the self weight, on the enhancement factor P' was closer to a four-fold reduction. Results indicated that at high span to depth ratios better load carrying capacity could be achieved by increasing the flexural strength of the section. Hence it can be concluded that lower values of reinforcement allow for more contribution from CMA and thus enhancement, but at the highest span to depth ratio considered (L/d = 60) it would be more beneficial to support loading in emergency conditions by an increase in the bending moment capacity of the section.

When assessing the inherent CMA available in a structure to support loading in emergency loading conditions the percentage of reinforcement is a parameter defined in the design process and so it should be kept in mind that as a general rule slabs with less reinforcement will induce more CMA thus promoting CMA as an alternative load path.

The longitudinal restraint stiffness ratio defined by Merola (2009) was introduced to allow normalised comparisons of the effect of variation in the outward movement at the ends of the specimen (which depends on the restraint stiffness). It was confirmed that samples at high span to depth ratios are sensitive to reduced restraint stiffness and benefit greatly from increased restraint stiffness. Sufficient restraint stiffness was found to be provided when k_1=1.0 to give load enhancement even at a span to depth ratio of 60. The longitudinal restraint stiffness ratio is key to load enhancement in emergency conditions, and quantifying the magnitude of the ratio that would be mobilized within a frame in the damaged state is discussed in depth in the next chapter.

To determine the most accurate means of predicting the behaviour of laterally restrained slab strips the CMA prediction methods were compared to the author's test results as well as to previously reported experimental data. The method proposed by Merola yielded the most accurate predictions and also provided the best correlation of results at the high span to depth ratios that are relevant to the double span scenario. However the method consistently underestimated the failure loads of the test specimens and therefore gives a conservative prediction of load capacity in the compressive membrane action phase of behaviour of restrained slabs. Since the Merola prediction method was the more accurate at high span to depth ratios it has been used to predict the ultimate loads of restrained samples in the event of losing a column. The initial parametric study of slab strips indicated that load enhancement from CMA was achieved at a span to depth ratio of 60 but significant load enhancement was limited to maximum span to depth ratios of 50. The parametric study also demonstrated sections with lower percentages of reinforcement provided more load enhancement over flexural action alone compared to sections with higher percentages of reinforcement.

The predictions made above were based on the use of the enhancement factor P', a value of $P' = 1.0$ indicating that the slab could carry only its' self weight. Values greater than 1.0 indicate that self weight and some imposed load could be carried. In practice only a portion of the imposed load would have to be supported in the damaged state. Consideration of full accidental loading has been made in the next chapter, Chapter 6.

Chapter 6: Frame Assessment

6.1 **Introduction**

The experimental programme reported earlier looked at the bending behaviour of reinforced concrete slab strips with large span to depth ratios. This extended the range of tested span to depth ratios and determined the extent of CMA at those large ratios. These large span to depth ratios could occur in a structural frame in the event of the accidental loss of a column. This chapter aims to make a realistic assessment of the feasibility of utilizing CMA in frames to support accidental loading conditions created in the abnormal event of losing a perimeter column. The loss of such a column would result in load being redistributed dynamically throughout the remaining structure. To account for this dynamic redistribution of load, dynamic load amplification factors have been considered. The Merola method, used in the previous chapter to predict the benefits of CMA, has been employed as a tool to predict the propagation of horizontal force across the structural bays affected by a column loss and effectively doubling the span of the concrete slab. This allowed the restraint stiffness provided to the double span to be determined by Finite Element Analysis (FEA) using the SAP2000 package. Using SAP2000 the linear elastic response of a typical frame has been determined for a variety of shear wall arrangements and grid sizes. Horizontal stiffness values for the double span slab have been used in conjunction with the Merola method to determine factors of safety (FOS) between calculated ultimate load and accidental loading. This allowed a parametric study to be carried out to determine the limitations of the ability of CMA to help redistribute load in damage situations.

It must be emphasised that the purpose of this chapter is to assess compressive membrane action in damaged structural frames, using the approach developed in the previous chapter. It is not intended as an accurate analysis of the whole structure using advanced finite element methods. It would have been appropriate to use a software package such as ANSYS for such an analysis but the approach presented in this chapter only requires a linear analysis elastic

approach, for which SAP 2000 is adequate. This follows the approaches set out in the various codes and guidelines

6.2 **Quantification of Accidental Loading**

International guidelines and codes of practice give requirements for loading on a structure in the event of localised damage and exceptional emergency load cases. The situation under consideration here is the removal of a perimeter column; in order to analyse the resulting structural behaviour the loading imposed on the structure after such an event must be quantified. Various suggested emergency loading conditions were reviewed in Chapter 2. The loading combination laid down in the British Standards (BS 8110:1997) has been used to define the accidental loading conditions.

An instantaneous column removal was assumed, the approach recommended in various codes of practice including guidelines developed by the United States General Services Administration, GSA 2003 and the Eurocodes EN 1991-1-7:2006. This allowed an assessment of the structure's ability to provide alternative load paths in the event of losing a primary structural element such as a perimeter column. The load redistribution would occur dynamically in response to the loss of a column and in a progressive collapse analysis the dynamic effects are an essential consideration in determining accurate structural behaviour (Ruth et al. (2006)). One method of considering dynamic effects whilst carrying out an equivalent static analysis is the use of a Dynamic Increase Factor, (DIF) sometimes referred to as a Dynamic Load Factor, (DLF). When using a linear elastic response the GSA 2003 and the document produced by the Unified Facilities Criteria in the USA applicable to new and existing Department of Defense (DoD) facilities, UFC 4-023-03 (2009) suggest a DIF of 2.0. An approach from other researchers such as Ruth et al. (2006) based on the work of Biggs (1964), equates the dynamic response of the damaged frame to simplified mass-spring systems using either single or multi-degree of freedom models. When assessing a linear elastic system results from these models match the suggested DIF from the GSA (2003) and UFC 4-023-03 (2009), with maximum deflection when the load is applied dynamically being double that from static analysis. The range of DIF is therefore between 1.0, where the response of the system is effectively static, and 2.0.

However the response of reinforced concrete under loading is elastic-plastic and as a consequence much of the dynamic energy will be absorbed through cracking of the concrete and plastic deformation of the steel reinforcement, meaning that a factor of 2.0 is likely to be conservative. It has been suggested by Ruth et al. (2006) that 2.0 is a conservative estimate and a factor of 1.5 is more realistic as the response of the structure is non-linear. Izzuddin et al. (2007) agreed with this, stating that for a non-linear elastic-plastic response a factor of 2.0 significantly overestimates the strength/deformation demands, and therefore does not offer a realistic assessment.

Yu and Tan (2011) employed the calculation method defined in UFC 4-023-03 to determine the DIF to be applied to static experimental test data. For a framed reinforced concrete structure the DIF was based on the rotational ductility and capacity of the RC members:

$$\mathrm{DIF} = 1.04 + \frac{0.45}{\theta_{pra} \Big/ \theta_y + 0.48} \qquad 6.1$$

The behaviour of a loaded reinforced concrete member can be equated to a simplified elastic plastic response. In the elastic phase rotation will continue until the extreme fibres reach their yield capacity, hence the elastic yield rotation (θ_y) corresponds with the end of the elastic phase. The yield rotation θ_y is determined using:

$$\theta_y = \left(\frac{M_y}{0.5 E_c I_g}\right)\frac{L_{cf}}{2} \qquad 6.2$$

Where L_{cf} defines the point of contraflexure as shown in Figure 6.1, which occurs at approximately L/4 when a beam is considered to be fixed at both ends and with a point load at mid-span

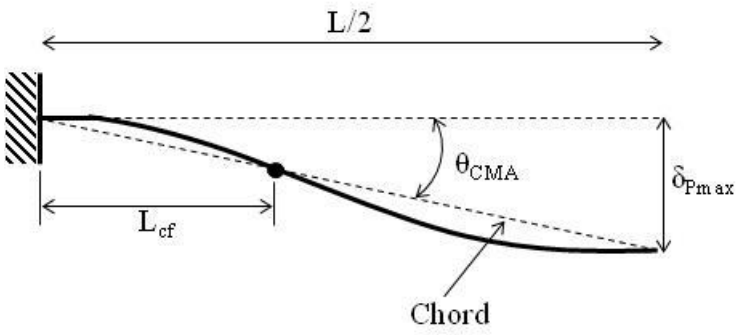

Figure 6.1: *Chord rotation of experimental testing at maximum load supported in the compressive phase.*

To determine the joint rotation once the response becomes plastic UFC 4-023-03 uses a simplified chord rotation approach, Figure 6.1. When considering a restrained slab strip, as in the experimental investigation (Chapter 3), the rotation in the plastic phase θ_{pra} is taken at the point of maximum applied load supported through arching action. As such the compressive membrane action joint rotation θ_{CMA} can be derived from:

$$\theta_{pra} = \theta_{CMA} = \frac{\delta_{Pmax}}{L/2} \qquad 6.3$$

Yu and Tan (2011) applied this method to give a DIF factor for test results of 1.1 for CMA. The same method was applied here to determine the DIF for the tests conducted by the author (Chapter 3), results are shown in Table 6.1. The average DIF for all test specimens was also found to be 1.1.

Specimen No.	Lo[mm]	h [mm]	b [mm]	Ec [N/mm2]	My [kNm]	δ/h P_{max}	I_g [cm^4]	θ_y	θ_{pra}	DIF
C1	2025.00	160.00	320.00	33549.20	15.73	0.54	1.09E+09	0.000	0.043	1.04
C2	2160.00	140.00	320.00	35418.19	10.74	0.70	7.32E+07	0.004	0.046	1.08
C3	2275.00	118.00	320.00	35184.76	6.15	1.05	4.38E+07	0.005	0.055	1.08
C4	2500.00	110.00	320.00	29069.30	5.72	1.12	3.55E+07	0.007	0.049	1.10
M2	2360.00	145.00	320.00	32080.42	5.62	0.52	8.13E+07	0.003	0.032	1.07
M3	1950.00	105.00	320.00	30381.61	2.82	0.52	3.09E+07	0.003	0.028	1.08
A	2500.00	90.00	275.00	31260.97	2.40	0.65	1.67E+07	0.006	0.024	1.14
S2	2500.00	90.00	275.00	35517.23	4.55	0.44	1.67E+07	0.010	0.016	1.25
S3	2500.00	90.00	275.00	29713.61	6.41	0.52	1.67E+07	0.016	0.019	1.31
E1	2500.00	175.00	225.00	34408.92	10.86	0.66	1.00E+08	0.004	0.046	1.08
E2	2500.00	175.00	225.00	27150.60	14.42	1.37	1.00E+08	0.007	0.096	1.07
E3	2500.00	175.00	320.00	31149.84	20.87	1.51	1.43E+08	0.006	0.106	1.06
								Average =		1.11

Table 6.1: *Summary of DIF calculations*

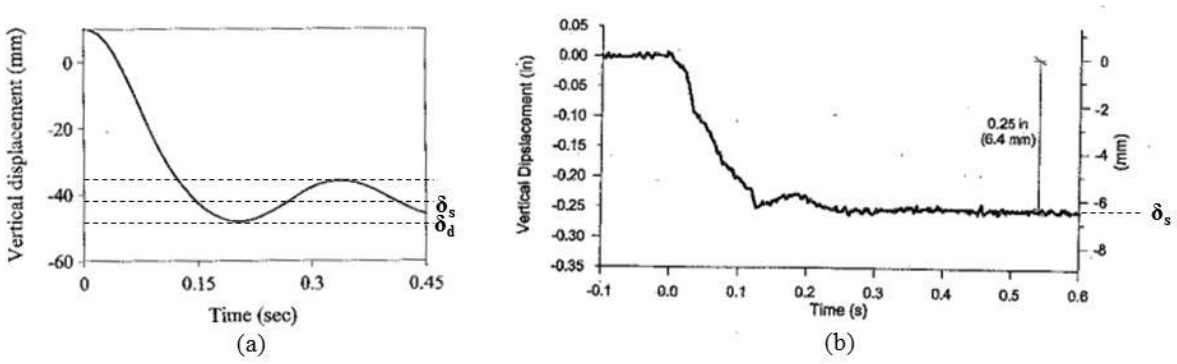

Figure 6.2: *(a) Time-vertical displacement curve for joint B6 Sasani (2011);(b)Time-vertical displacement graph for joint B5 located above failed column Sasani (2007)*

The testing reported by Sasani (2007) and Sasani (2011) provided an interesting insight into the actual behaviour of reinforced concrete frames when a column was removed. The measured vertical displacements directly above the removed column for both structures tested are displayed in Figure 6.2. It should be noted that Figure 6.2 (a) displays results from a structural prediction model and not the measured response, although the predicted displacements were found to be in reasonable agreement with the test results. In response to the dynamic removal of the column the system exhibited a large damping effect. It can be seen that the damping limited the maximum vertical deflection to only slightly more than the equivalent static deflection. The damping was attributed in part to the dissipation of energy

associated with large plastic deformation of the bowed out flexural reinforcing bars of the removed column along with the cracking and crushing of concrete. From the recorded dynamic response a DIF was calculated from the ratio of the dynamic deflection δ_d to the static deflection δ_s, using data obtained from the deflection-time graphs displayed in Figure 6.2 (a) and (b). The DIF for each was found to be 1.14 and 1.1 respectively which was in close agreement with the findings of Yu and Tan (2011).

In light of the above the DIF to be applied when considering the accidental loading has been taken as 1.1 and was used in Equation 2.5 (and repeated in Equation 6.4) to provide the accidental loading against which comparison of the ultimate load through CMA has been based.

$$ALS = 1.1(1.05G_k + 0.35Q_k) \quad 6.4$$

Where ALS = Accidental Loading State

In the parametric study the live loading was taken from Table 1 in BS 6399-1. It has been assumed that the building investigated was occupied for general office use and therefore, Q_k = 2.5 kN/m^2.

6.3 **Lateral Stiffness Assessment**

In considering a flat slab building that has lost a perimeter column it was assumed that at each level the slabs act independently to span the failed column and as such vertical displacement is equal on each floor. The amount of lateral restraint provided to each bay was quantified by the horizontal movement of the in-plane slab in the adjacent bays to the failed column that were assumed to be undamaged, as shown in Figure 6.3. The inherent restraint stiffness of a flat slab floor plate is an important parameter and an accurate value is required for realistic CMA predictions.

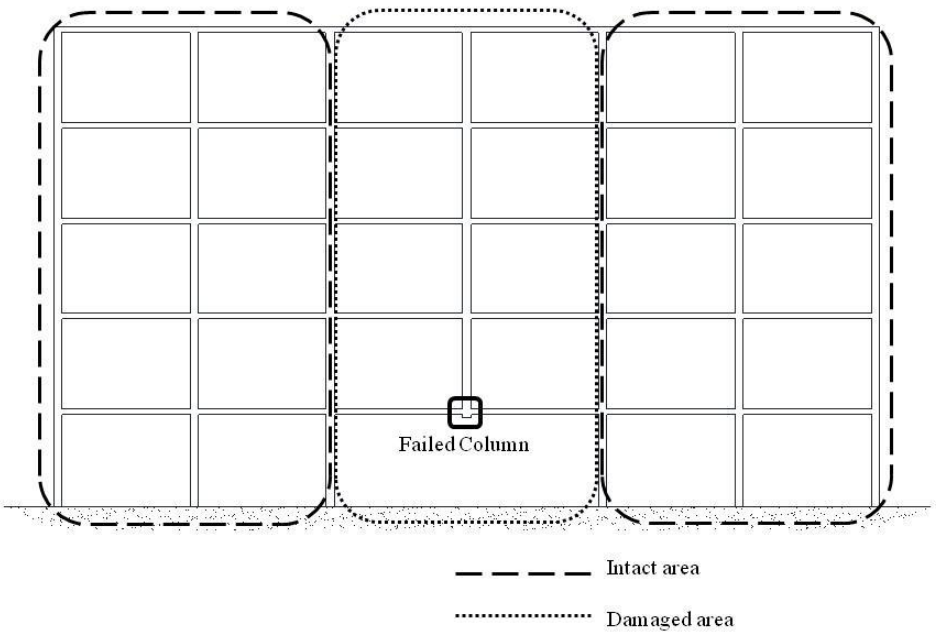

Figure 6.3: *Restraint stiffness provided by adjacent structural bays to failed column.*

When a column is lost and CMA is induced in the slab spanning the resulting double span a horizontal compressive thrust is exerted on the slab and reacted by the structural frame. It is the combined ability of the floor plate and frame to resist the outward movement that provides lateral stiffness. The response of the frame under horizontal loading from CMA is complex and to accurately model the global response of the in-plane floor plate and frame a Finite Element Analysis (FEA) was employed.

The nature of reinforced concrete (RC) produces added complexity to FEA. RC is comprised of two separate materials which each need to be characterised. Concrete deformations are influenced by creep and shrinkage which are time dependent. The full stress-strain relationship of steel reinforcement is non-linear and hence the behaviour of RC is also non-linear and is a function of many variables. The bond between concrete and steel must also be defined so that aspects such as bond slip can be taken into account. With the onset of cracking under load there is added complication as the structural system is continuously changing. Cracking reduces the overall flexural rigidity which increases deflections. With cracking rigidity varies along the member length and tension stiffening must also be taken into account.

However, modelling of the response to CMA horizontal forces allows for simplification of the analysis. Whilst slab cracking would be expected in the region around the failed column and at the ends of the slab, the damaged regions are localised and it is unlikely that cracking will occur in the rest of the slab. It was therefore assumed that the response of the adjacent floor plate and frame remains in the elastic phase, so that a linear elastic analysis could be carried out.

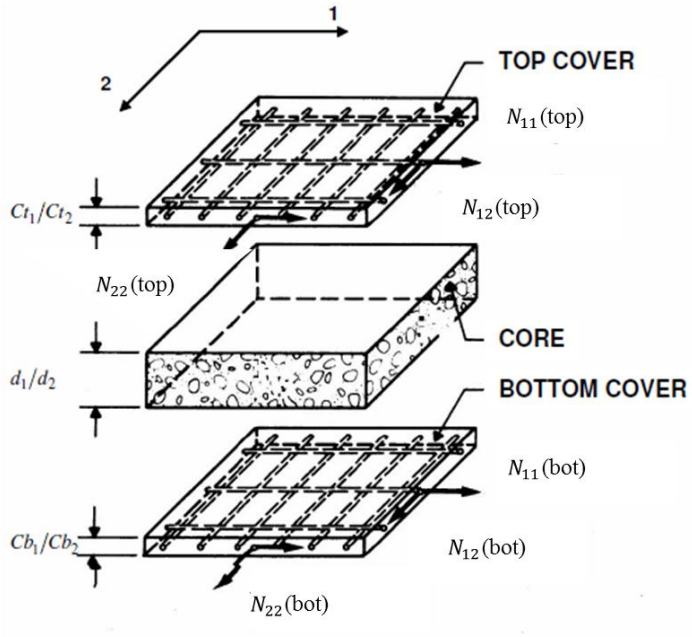

Figure 6.4: *Statics of Slab Element – Sandwich Model, SAP2000. Computers and Structures Inc (2006)*

In order to model floor plates SAP2000 utilises shell elements whose behaviour is based on the work of Brondum-Nielsen (1974) and Marti (1990). The more accurate four node quadrilateral elements were used. Reinforcement was taken into consideration by dividing the element into layers. Centred on the mid-planes of the top and bottom reinforcement are two outer layers which surround a middle layer of concrete, and the slab was therefore conceived as a "sandwich model", as shown in Figure 6.4. The shell element is generally subjected to eight stress resultants. The outer layers carry the three membrane force components f_{11}, f_{22}, and f_{12}; the two flexural moment components m_{11} and m_{22} and the twisting moment m_{12}. These are resolved into pure membrane forces N_{11}, N_{22} and N_{12} that act at the centre of the outer layers containing the reinforcement allowing for the lever arm to be taken as the distance

between the two outer layers. The thickness of the outer layers is defined as twice the cover from the face of the slab to the centre of the reinforcement. The cover to the reinforcement and the size of the steel reinforcement was defined in the setup of the model. The centre layer is assumed to take the two transverse shear force components V_{13} and V_{23}. Its thickness is defined as twice the distance from the centre of the slab to the centre of the outer reinforcement. The reinforcement forces, concrete principal compressive forces and stresses are then calculated by formulae from Brondum-Nielsen (1974). It should be noted that in shell elements the tensile strength of concrete is ignored.

A common assumption by Sasani (2011) amongst others is that in a flat slab structure the majority of the stiffness is provided through the in-plane strength of the floor plates as opposed to more conventional beam and slab frames where the stiffness is provided by beams and columns acting together as a frame. Therefore it was essential that a full 3D model was analysed so that the behaviour of the entirety of each floor plate was assessed. It also allowed for the summation of the contribution from each structural element at each storey height, to provide a global response of the structure.

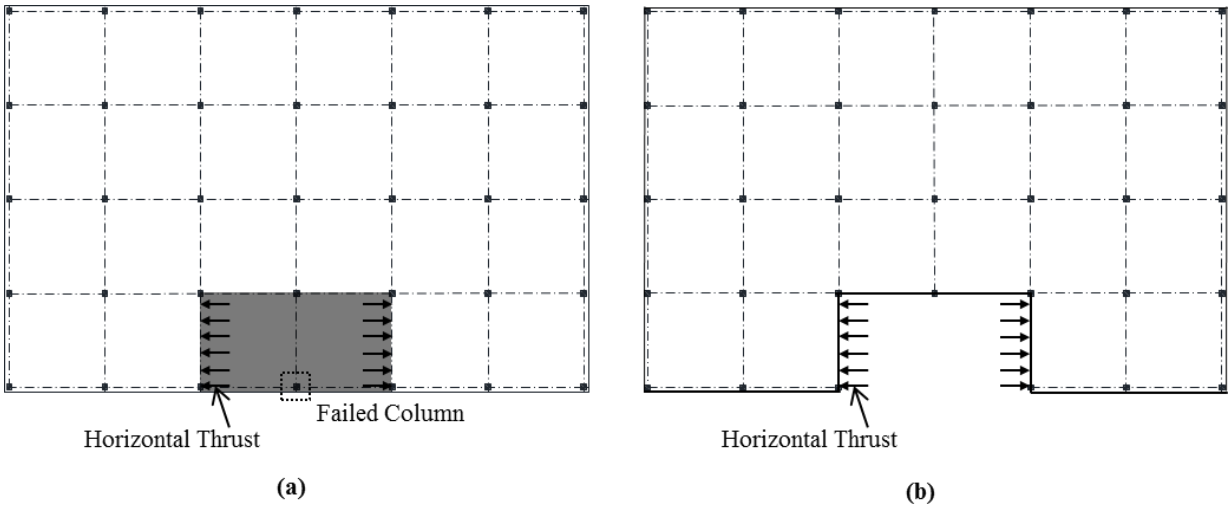

Figure 6.5: *Notional removal of double span, in the area of the failed column.*

A typical floor plate analysed in the FEA model is shown in Figure 6.5 (a). The failed column creates a double bay situation in which CMA develops and causes the adjacent structural bays to be subjected to horizontal thrust. In the FEA models the shaded area was removed from the structure as shown in (b) and the thrust was applied to the surrounding slabs. CMA puts the

double span slab into an overall state of compression with the slab pushing outwards. It was therefore assumed that it would provide no restraint to the outward movement of the surrounding floor plate. This is a conservative assumption because it is likely that continuity in tension reinforcement and the tensile strength of concrete between cracks will provide some stiffness .

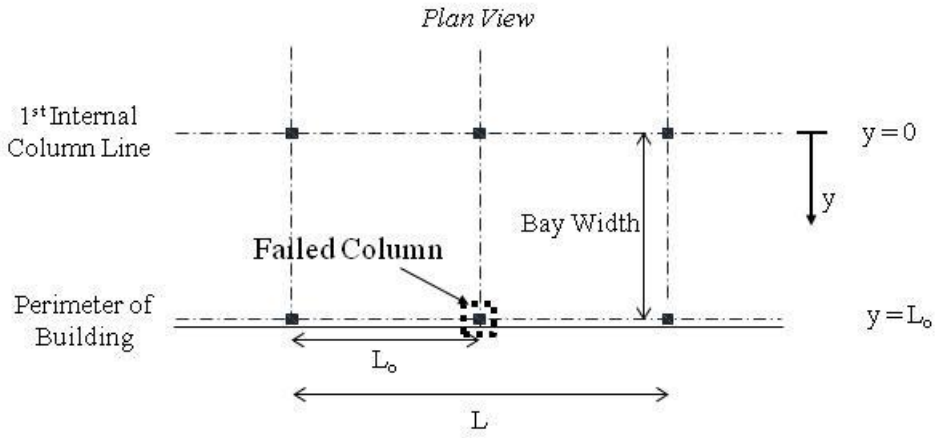

Figure 6.6: *Definition of bay width.*

A prerequisite to predicting the ultimate load using Merola's method was to first quantify the vertical deflection of the slab. At maximum deflection, the point of snap through, maximum compressive thrust is produced. The vertical deflected shape of the slab had therefore to be defined so that subsequently a horizontal loading pattern could be defined in order to conduct the FEA. Once the perimeter column had failed it was assumed that maximum mid-span deflection occurred at the point of the failed column and fell linearly to zero at the first internal column. The position under consideration across the bay width spanning between the first internal column and the perimeter column was defined by y (Figure 6.6), where y = 0 at the first internal column line and y = L_o at the perimeter of the building. To assess the accuracy of this assumption a flat slab subjected to a uniformly distributed load has been modelled using a linear elastic FEA. A plot of the deflected shape found from FEA is compared with a linear response in Figure 6.7. There is a good correlation between the two justifying the simplification of a linear vertical deflected shape.

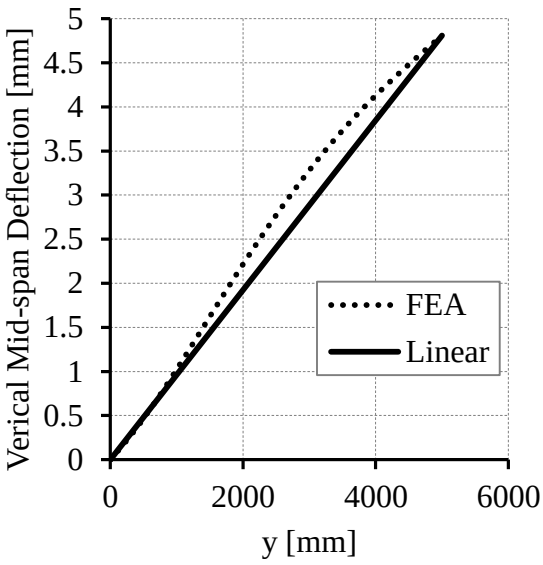

Figure 6.7: *Comparison of linear and FEA deflection*

The Merola's prediction method gives a value for the horizontal force in the slab which allows for quantification of thrust across the bay width through an iterative process. As the restraint stiffness was an input parameter for Merola's formulae it was set initially to be constant across the bay width. The calculated horizontal thrust varies across the panel width as the vertical deflection ranges from zero at the first internal column line to maximum at the perimeter of the panel. The maximum horizontal thrust occurs at the point of maximum defection. From the horizontal force the flexural and shear deflections of the adjacent flat slab (treated as a deep beam cantilever fixed at the 1st column line and free at the perimeter) were calculated. The calculated output restraint stiffness then replaced the initial constant value, and the process was iterated until both input and output stiffnesses were equal. At this stage the horizontal force distribution across the panel width was no longer linear but was curved with a maximum value at the perimeter column line. (The iterative process used to find this loading pattern is described further in Appendix A.11.) The final assumed behaviour of the slab when the perimeter column was lost is shown in Figure 6.8.

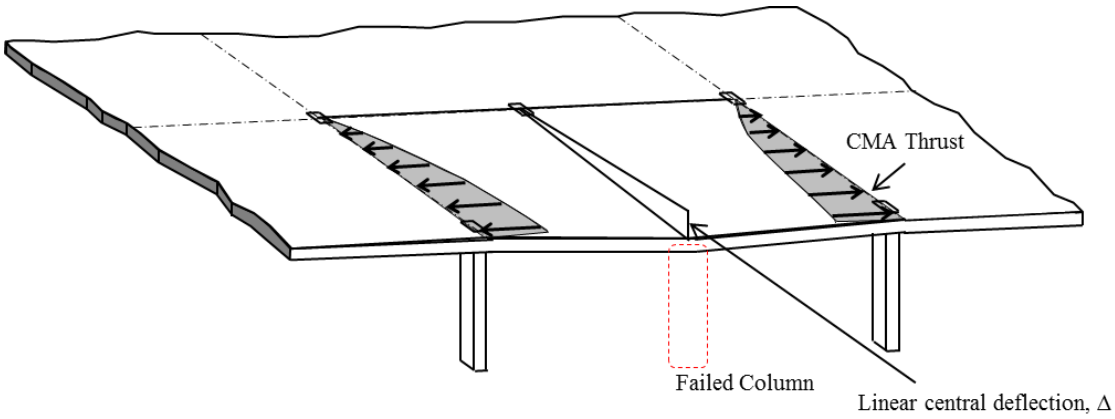

Figure 6.8: *Assumed linear mid-span deflection across bay depth when column fails and resulting CMA thrust distribution.*

6.4 Frame Design

It was important to ensure that the research was applicable to real structures by carrying out the analysis on realistic building layouts. To broaden the investigation into the effect of span length on CMA supporting accidental loading, a series of flat slab structures were designed to BS 8110 requirements. Square perimeter bays and external columns were designed for spans ranging from 5m to 9m in increments of 0.5m. The resulting reinforcement details were used in the FEA models and the analysis of CMA using the Merola method. Full details of the designs can be found in Appendix A.3.

6.5 FEA Parameters

Material properties based on C45/55 concrete were used in SAP2000 for all models, providing a cube strength of 55 N/mm^2, modulus of elasticity of 38000 N/mm^2 and a Poisson's ratio of 0.2. This concrete material was used as it provides cube strength close to the calculated 5 year concrete strength defined in Chapter 3. Steel reinforcement was defined to have a modulus of elasticity equal to 210 kN/mm^2 and a yield stress of 550 N/mm^2. These properties were similar to those found from tensile tests on the type 2 high strength steel reinforcement used in the experimental programme, and can be thought of as being comparable to reinforcement commonly used in construction in the UK today. Both the shell (slabs) and frame (columns) elements were meshed into quadrilateral elements. In slabs immediately adjacent to the damaged area a fine mesh was used and elements were defined as 250mm x 250mm. This allowed for direct compatibility with the Merola prediction method which was used to predict

behaviour of 250mm wide slab strips. The fine mesh was also employed in areas of the slab in contact with shear walls to ensure interaction behaviour was modelled accurately. Diaphragm joint constraints were applied at the common joints of slabs and shear walls to ensure connectivity to model a realistic response of the structure. The remainder of the slab away from shear walls and the damaged area were meshed more coarsely. The horizontal compressive thrust was applied in the form of a uniform pressure over the appropriate face of each 250mm wide element. The pressure was calculated sequentially to produce the curved loading pattern from the perimeter of the building to the 1st internal column line.

6.6 **Influence of Shear Wall Layout**

In order to resist wind loading the lateral strength of flat slab structures is usually provided through a series of shear walls, often configured as structural cores that carry stairwells and lifts. Shear wall arrangements can also provide restraint stiffness in damage situations that may be beneficial to the induction of CMA. It was in this light that the placement of structural cores was investigated. Five different arrangements, labelled A to E, were considered, as shown in Figure 6.9. It can be observed that in some cases the shear walls considered would not provide sufficient resistance to wind loading by themselves, in which case additional shear walls in the structure would be needed. The focus of this investigation was the effect of the structural cores on CMA. A constant core size of 4m in the x-direction by one full bay size in the y-direction was used. Walls were 200m thick with 16mm diameter reinforcement provided at 300mm spacing top and bottom in both directions.

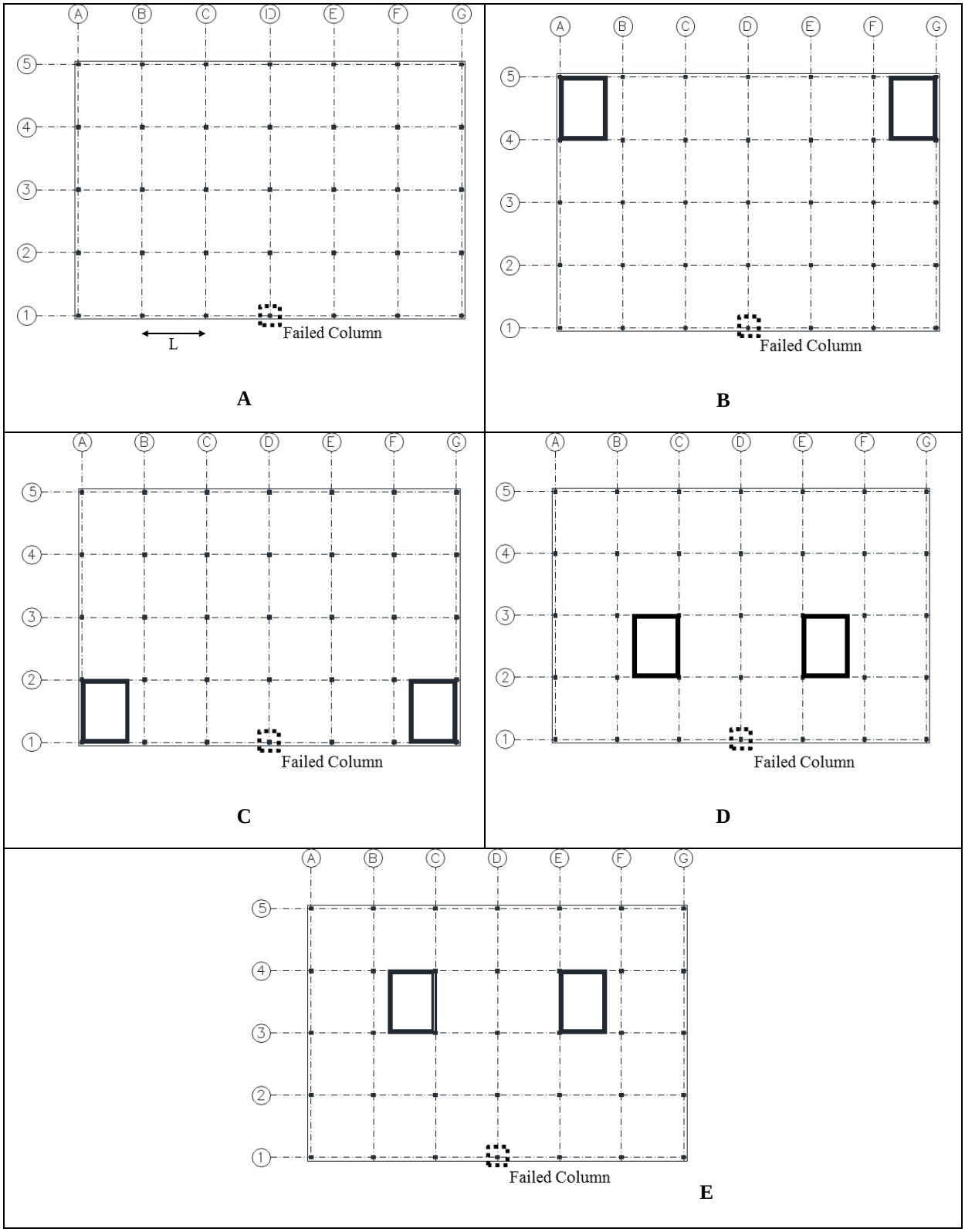

Figure 6.9: *Layouts of shear walls considered.*

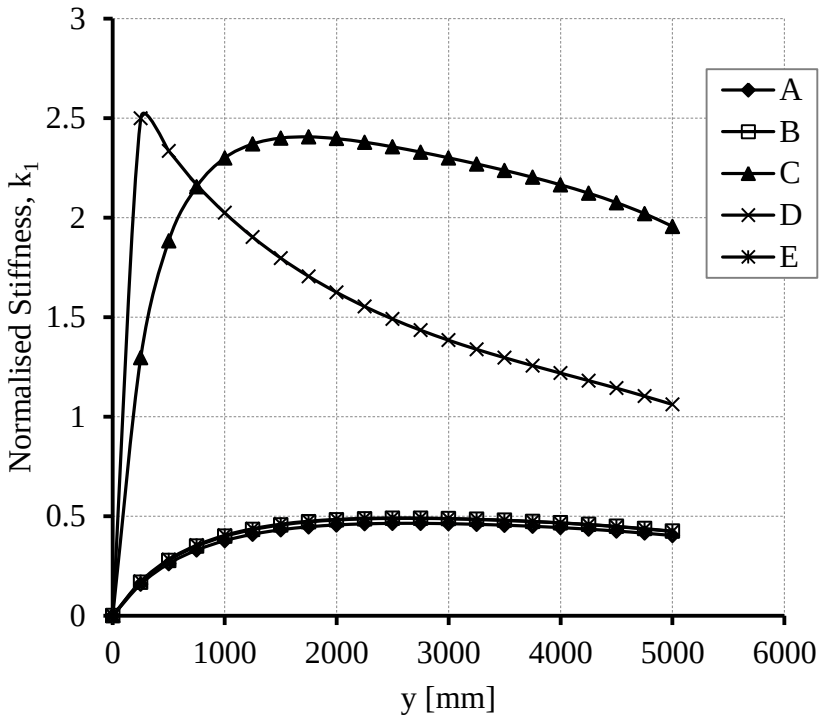

Figure 6.10: *Differences in CMA restraint stiffness provided by different shear wall arrangements.*

To highlight the effect that the position of shear walls has on the restraint stiffness a structure with 6x4 grid layout and 5m original span was analysed. Restraint stiffnesses across the width of the structural bay are displayed in Figure 6.10. Immediately it is clear that there is a significant difference in the stiffness provided by arrangements D and C compared to those from A, B and E. When shear walls are situated away from the damaged area they provide little improvement from when no shear walls are provided. However, when the core is in line with the compressive thrust (arrangement C) or when they act as a cantilever to the slab adjacent to the damaged area (arrangement D) there is considerable increase in restraint stiffness.

The differences in stiffness provided across the width of the bay for different shear wall arrangements can also be observed in Figure 6.10. It should first be noted that whilst the stiffness is shown to tend towards zero when y=0 this would not be the case in the actual structure. The effect of the assumed linear vertical deflected shape across the slab, with zero defection at y=0, means that no compressive thrust is induced when y=0 and so no horizontal

force is applied to the slab. For the shear wall arrangements A, B and E the peak stiffness occurs at around half the bay width but the peak is not great and the stiffness is close to constant across the bay width. The placement of structural cores in arrangement D effectively causes the adjacent slab to act as a cantilever. This is reflected in the shape of the stiffness curve which has a peak at the point of interaction with the core and is minimum at the perimeter. Arrangement C produces a similar peak but it is sustained across more of the bay width with the minimum still occurring at the perimeter. It is clear that the locations of shear walls has a significant effect on the variation of stiffness across the bay width.

6.7 **Frame Stiffness Analysis**

To determine the relative magnitude of restraint stiffness provided by the structural frame comparisons of the axial stiffness ratio (k_1) (defined in the previous chapter) have been made with the stiffness provided from experimental rigs used by previous authors. A range of values for each shear wall arrangement have been calculated for the perimeter strip at the range of spans considered, 5m to 9m.

Shear wall arrangements A, B and E provide values that are comparable with the test rig used by Taylor et al. (2001) and the test arrangement presented in this thesis. This indicates that these shear wall arrangements will provide moderate values of enhancement. Whilst testing by Taylor et al. (2001) was at very low span to depth ratios, the test specimens used by the author were designed to investigate behaviour at large span to depth ratios, as would occur in the double span damage scenario. It can be seen that the tests conducted by the author were undertaken with a realistic restraint stiffness, making the test results directly comparable to full scale structures.

Arrangements C and D are comparable with the stiffer rigs used by Su et al. (2009) and Christiansen (1963), further indicating that these placements of structural cores will provide the most advantageous restraint conditions for CMA.

The lateral restraint stiffness in the tests by Roberts (1969) was an order of magnitude higher than calculated in the frame analyses, which along with the low span to depth ratio used demonstrates the irrelevance of this testing to the damage scenario.

6.8 **Influence of Grid Size**

A comparison has been made between buildings with a 6x4 and 8x4 layout of structural bays with regard to the effect on stiffness with varying shear wall arrangements; the results of which are displayed in Figure 6.11. Stiffness is displayed against the distance (y) from the first internal column line. In all arrangements of cores excluding C there is a small increase in stiffness for 8x4 bays compared to 6x4 bays. In arrangement C (shown in Figure 6.9) the increase the number of bays between the damaged area and the cores reduces their effect in restraining the floor plates as more axial shortening takes place.

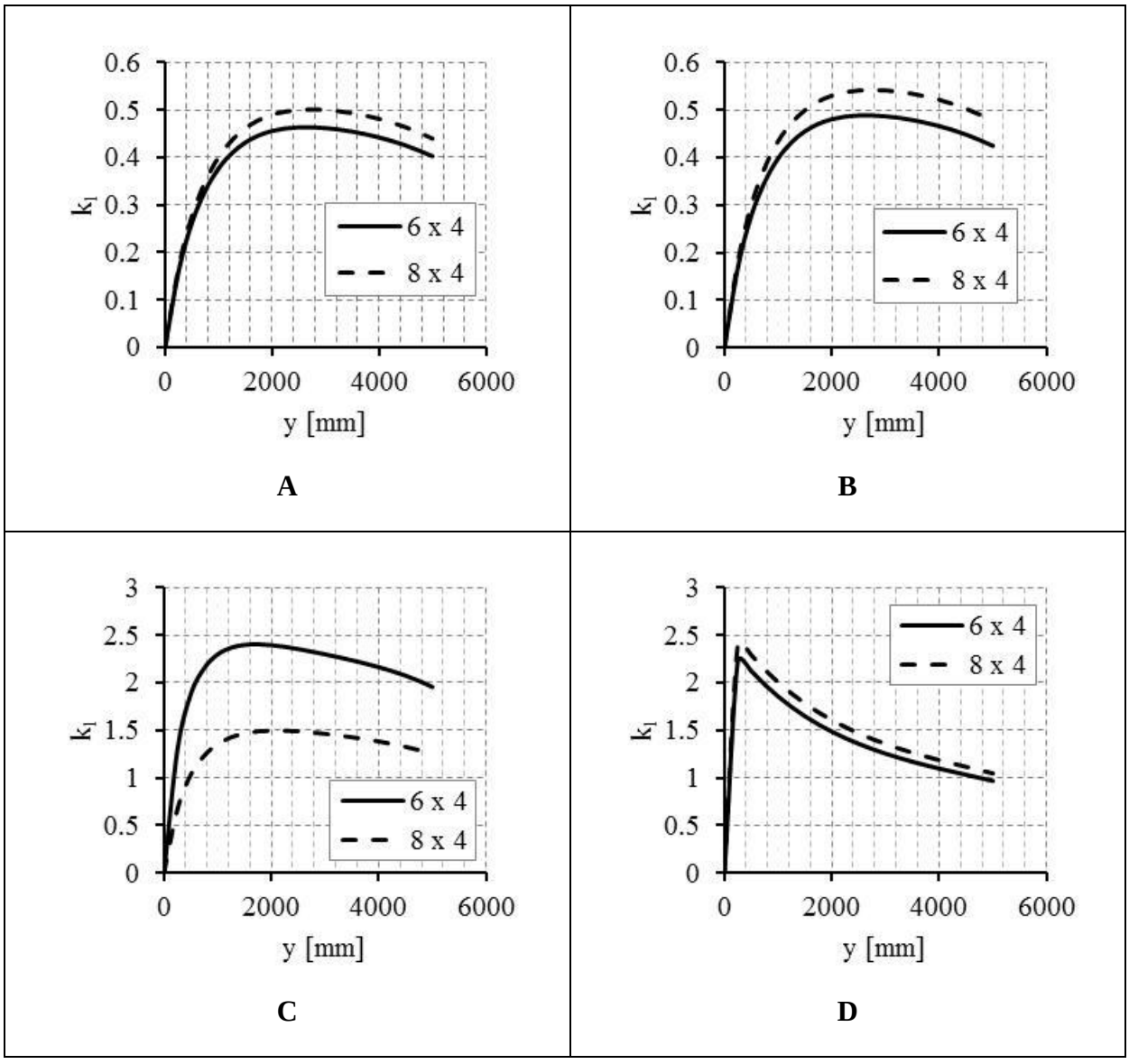

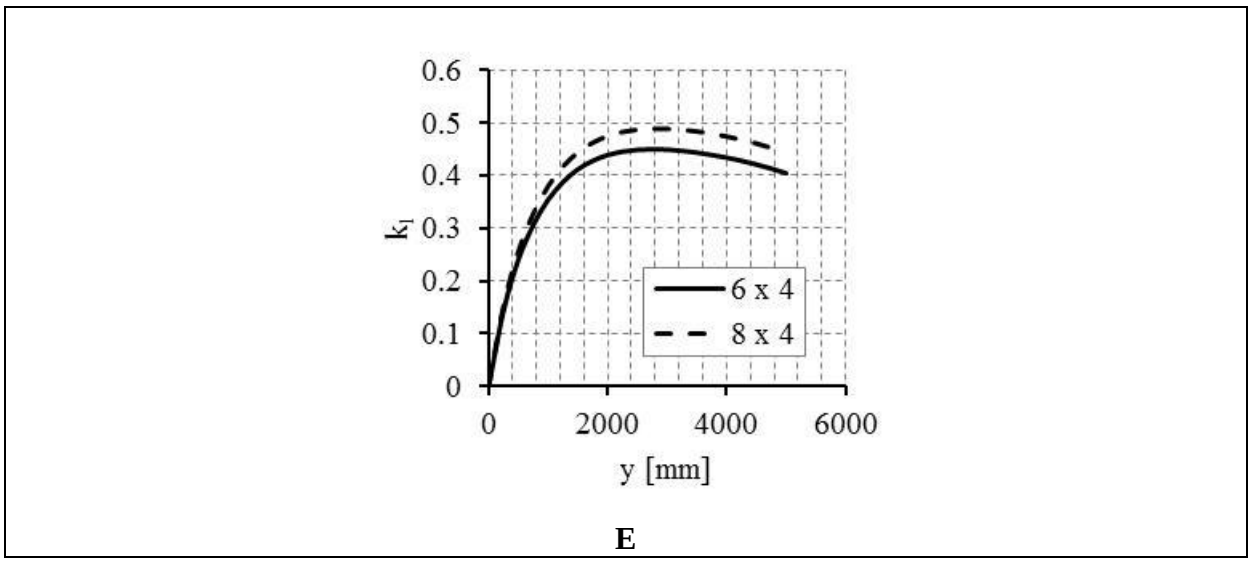

Figure 6.11: *Comparison of grid size for varying shear wall arrangements.*

6.9 Factor of Safety across the Bay Width

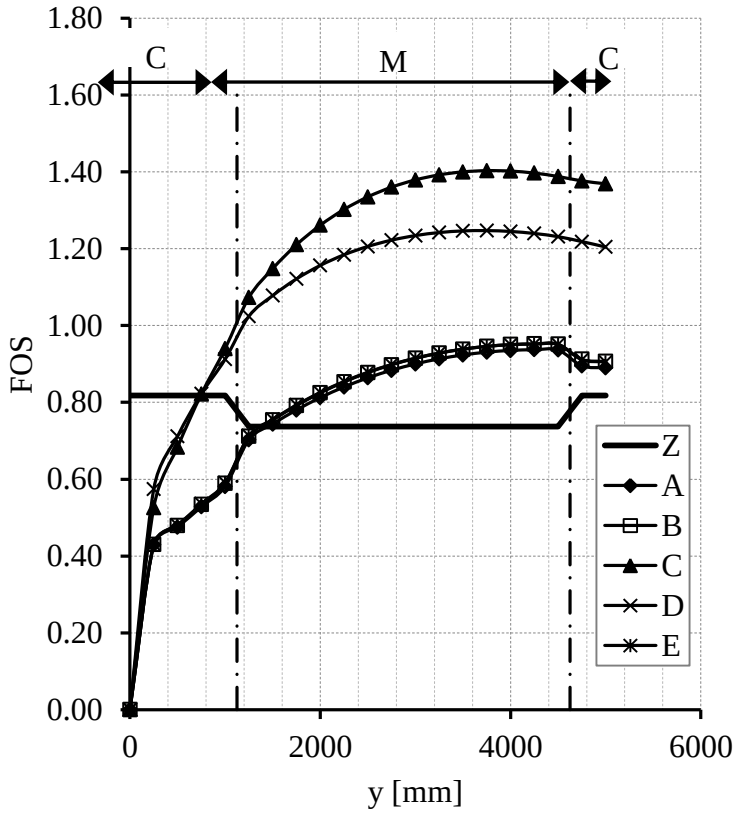

Figure 6.12: *Variation of FOS with distance from the 1st internal column line.*

The FOS, which can be considered as the ability the section through both flexure and arching action (CMA) combined to support accidental loading (defined in more detail later in this Chapter) has been plotted against the distance (y) from the 1st internal column line in Figure 6.12. The FOS is based on CMA being the only mechanism in supporting accidental loading at the perimeter of the building at the point of the failed column. This assumption is reasonable because to bridge the removed column the flat slab behaves as a series of one way spanning slab strips. The assumed linear vertical deflected shape across the slab width means that with zero deflection at the first internal column line no CMA is induced and hence a FOS of zero is predicted by the Merola method. However at the first internal column line with zero vertical deflection the slab supports load over the single design span and so is capable of supporting the accidental loading. In Figure 6.12 the FOS provided through flexural strength only in the double span conditions considering a one-way spanning slab strip has been denoted as Z. This provides a measure of minimum strength for the one way spanning slab strips and demonstrates that as deflection is increased closer to the perimeter of the building CMA enhances load carrying capacity. The strength through flexural action varies across the bay depth as the section properties change from column to middle strips.

When load carrying capacity is considered in one direction before arching action begins to support loading the critical portion of the slab is close to the first internal column line, however the flat slab will still span in two directions here which would have a significant influence. The slab would behave more like a plate with the surrounding slab creating twisting and cantilever effects. As such close to the first internal column line applied loading will be predominantly supported through mechanisms other than CMA. Since the ability to support accidental loading through arching action is the focus of this research other mechanisms which further supplement strength have not be considered.

Three main factors affect the shape of the graph; restraint stiffness, the assumed deflected shape and percentage of reinforcement. As vertical deflection increases the ability of arching action to supplement load resistance also increases. Whilst maximum deflection occurs at the perimeter, giving it the potential to support the maximum ultimate load, the peak FOS occurs at about $y=3L_o/4$ in most cases. This is partly due to the influence of restraint stiffness, which for each shear wall arrangement reaches its peak before the perimeter and then decreases as y

approaches L_o. This observation demonstrates that there is an optimum position for arching action in the bay width that produces sufficient deflection to induce CMA with the added benefit of increased restraint stiffness, indicating that the critical slab strip is at the perimeter of the building.

The shape of curves A to E can be explained by the influence of varying amounts of reinforcement in the section across the bay width. Flat slabs are divided into middle and columns strips, column strips effectively act as beams spanning between columns and are more heavily reinforced. This division across the bay depth is highlighted in Figure 6.12, with middle and column strips being represented by M and C respectively. The effect of the higher percentage of reinforcement in the column strip causes a decrease in arching action and consequently the load carrying capacity, this effect is most marked in the results for shear wall arrangements A, B and E. This further demonstrates that the perimeter strip, in this case between y = 4750mm and 5000mm, is under the most unfavourable condition for CMA to be beneficial as an alternative load path in the double span conditions. Because of this the focus of the parametric study was on the perimeter slab strip as this is the worst case scenario.

6.10 **Influence of Storey Height**

A 6x4 grid size of structural bays with 5m span has been used to examine the variation of horizontal deflection across the height of the structure. When a column is removed it is assumed that the vertical displacement of the slab on each floor in the damaged area is the same and consequently there is an equal compressive thrust produced; so that the same horizontal loading is applied in the FEA model at every storey. The surrounding slabs at higher storeys undergo more horizontal deflection as demonstrated in the calculated stiffness shown in Figure 6.13. This is to be expected as the vertical frame elements (columns and shear walls) exhibit more deflection under horizontal loading as the distance to the rigid restraint provided at ground level is increased. The difference is however quite moderate, over the height of the building the stiffness varies by only about 3%, resulting in a difference of FOS (method described later in this Chapter) of approximately 0.008. This demonstrates the concept that the floor plates provide the majority of the lateral stiffness to horizontal loading in flat slab structures. It can be concluded that, for a 5 storey structure at least, the height does not have a significant influence on restraint stiffness. For multi-storey structures the effect

could be amplified so it would be prudent to make a building specific assessment into the effect of storey height on restraint stiffness.

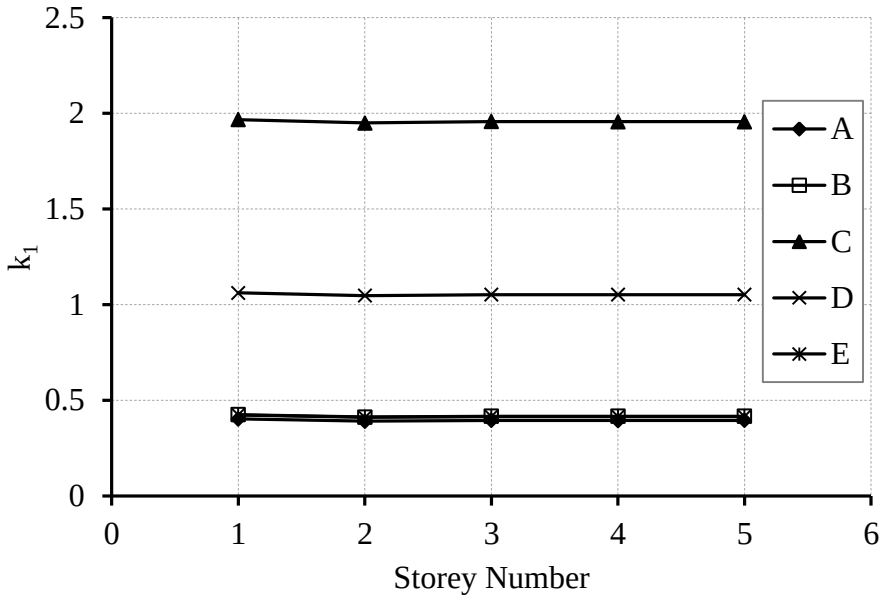

Figure 6.13: *Variation in stiffness over storey height*

6.11 **Parametric Study**

A parametric study using different grid sizes and shear wall arrangements was conducted to determine the effect of span size on the ability of CMA to support accidental loading. The parameter of interest was the grid span which was varied from 5m to 9m in increments of 0.5m hence producing double span scenarios of 10m to 18m. A factor of safety, defined as the ratio of the predicted uniform ultimate load from the Merola method w_F to the accidental loading w_{ALS}, defined using Equation 6.5, was employed to quantify results. The criterion for a slab being able to sustain accidental loading through arching action was determined initially as a value of FOS above 1.0. Values below this imply that CMA does not provide sufficient strength but does not necessarily indicate failure of the slab as other mechanisms such as tensile membrane action could prevent failure.

$$FOS = {}^{w_F}/_{w_{ALS}} \qquad 6.5$$

The methodology carried out to produce values of FOS was as follows:

1. Define grid size (6x4 or 8x4)
2. Define shear wall arrangement (A to E)
3. Set span size, to vary from 5m to 9m in increments of 0.5m.
4. Construct FEA models.
5. Apply horizontal loading to all floors to simulate CMA horizontal compressive thrust after losing a column.
6. Run model and output horizontal deflection of slab.
7. Calculate restraint stiffness provided by structure by dividing horizontal force by output deflection.
8. Input the calculated restraint stiffness across the bay width together with all slab parameters into the Merola prediction method.
9. Determine the ultimate load that the slab strip can sustain with the inclusion of CMA and hence define the F.O.S.

The results of the parametric study for the 6x4 grid layout are shown in Figure 6.14 for the perimeter 250mm slab strip. The differences in results for the larger 8x4 grid layout were shown in Section 6.7.

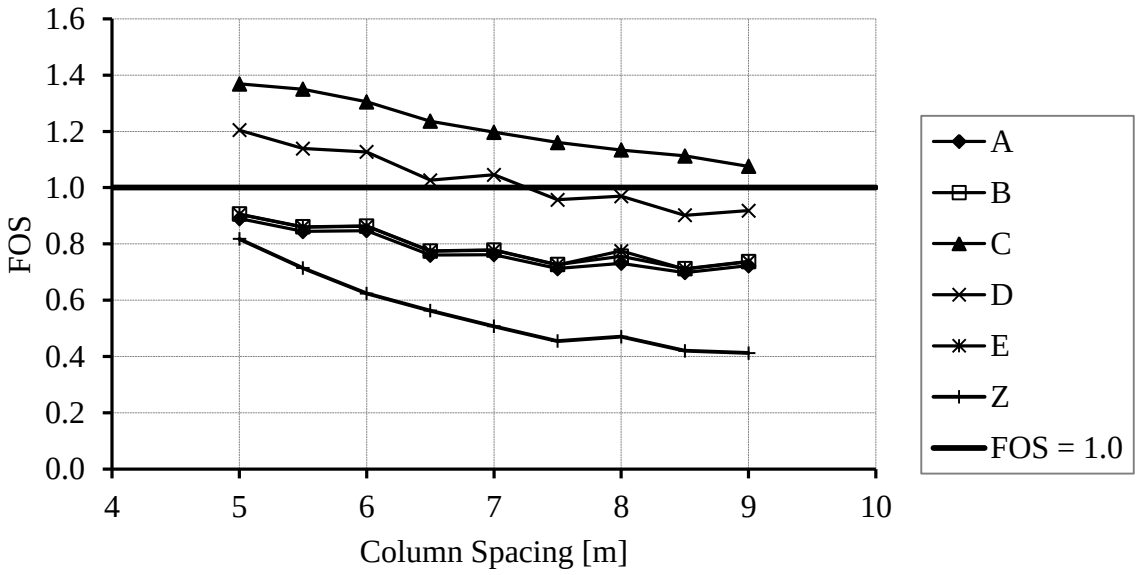

Figure 6.14: *FOS against column grid spacing for 6x4 layout.*

A clear and intuitively obvious trend can be observed that with increasing original span the FOS provided decreases. The effect ranges in reductions in the FOS by between approximately 0.1 and 0.4 as the column spacing increased from 5m to 9m. As found previously the shear wall arrangements C and D produced the most beneficial restraint conditions for arching action. Arrangement C produced the highest values of FOS and accidental loading was supported through CMA for all column spacings considered. The FOS falls below 1.0 at a column spacing just below 7.5m with arrangement D. All other arrangements failed to produce a FOS above 1.0 and accidental loading cannot be supported by CMA alone in the double span scenario.

In addition to the results from the 5 arrangements of shear walls considered the strength of the perimeter slab strip has been assessed based on flexural strength only, labelled Z in Figure 6.14. This allows for a comparison of the combined behaviour of the flexural strength inclusive of arching action against that of flexural strength alone. An assessment of the response through flexure has been made by an analysis of flexural moments induced using the moment distribution method verified against the Oasys GSA structural software. The results of the study demonstrate that the structure has a poor resistance to accidental loading in the event of losing a column. Comparisons with behaviour once CMA is considered indicate an increase in robustness for all scenarios, the highest being over a two-fold increase in robustness at the longest span considered.

6.12 **Conclusions**

Assuming a linear-elastic response for the frame has allowed FEA to be employed as a tool to predict the response of the frame from horizontal loading produced by arching action. In all previous Chapters it has been highlighted that the restraint stiffness is a significant parameter when predicting ultimate load inclusive of CMA. When assessing the inherent stiffness of a frame that has a realistic structural design an influential factor in the stiffness produced was found to be the placement of structural cores in relation to the damaged area under consideration. Two shear wall placements, C and D, have been clearly shown to provide the most beneficial conditions for CMA to support accidental loading. From the analysis conducted a clear conclusion can be made; the restraint stiffness provided is a complex parameter for which an accurate and detailed prediction method is required. FEA has been demonstrated to have the potential to provide this. The inherent restraint stiffness is unique to each structural frame and an assessment should be made on a case by case basis. No comprehensive solution to predict the restraint stiffness that applies to all structures can be made.

Further to this it has been found that storey height does not have a significant impact on the restraint stiffness and consequently the FOS and that the majority of horizontal in-plane stiffness in a flat slab structure is provided though the floor plate.

The robustness of the structure is improved by the inclusion of arching action when compared to the flexural response alone and the criterion to prevent failure by utilising CMA as an alternative load path was achieved for two of the shear wall arrangements considered. This indicates a significant underestimation of load capacity when membrane effects are neglected.

In all other arrangements insufficient enhancement from CMA was achieved with the FOS ranging between 0.7 and 0.9. However this may not mean failure of the slab under accidental loading and possible instigation of progressive collapse. The ability of flat slabs to span in two directions due to continuity of reinforcement over undamaged column lines has not been considered. Other alternative load paths in the structure provided through elements such as cladding and internal walls may also be mobilised to also support a portion of the accidental

loading. It should be further noted that the Merola prediction method used in the analyses of the damaged frames was shown in the previous chapter to be conservative consistently underestimating load capacity in comparison to test results.

Chapter 7: Conclusions

After the initial elastic behaviour in the flexural response of loaded prismatic RC elements the onset of cracking causes the neutral axis to move towards the compressive face. Codes of practice dictate design based on under-reinforced sections so that the section failure is dependent on yielding of the tension rebar allowing significant plastic deformation before fracture of the reinforcement occurs. As such the load capacity of the section is highly dependent on the percentage of reinforcement. With the introduction of longitudinal end restraint the in-plane expansion is restricted resulting in the formation compressive struts in the element producing an internal arch. This compressive arching action or compressive membrane action (CMA) supplements the flexural response and gives an increase in transverse load capacity over that from flexure alone.

It has been well documented by previous authors and confirmed by this research that the enhancement from CMA is dependent on the following three factors: span to depth ratio, restraint stiffness and percentage of reinforcement. With regards to the latter, the tensile force that is induced in the reinforcement is resisted by the compressive force in the concrete to ensure equilibrium about the neutral axis. As the tension reinforcement area is increased more of the concrete is mobilised to balance the section, resulting in less available concrete to form the compressive arch. Therefore, lightly reinforced beams have a greater capacity to generate CMA than more heavily reinforced sections.

The potential for CMA also reduces as the longitudinal restraint stiffness is reduced. It was found that samples at high span to depth ratios are particularly sensitive to outward movement as a result of reduced longitudinal restraint stiffness. However, it was also shown that enhancement can still be achieved even when the restraint stiffness is only equal to the longitudinal stiffness of the section under consideration.

The main focus of this research was to explore the potential for CMA to provide load enhancement in the ‘double span’ situation which would result from the instantaneous loss of

a column so the span to depth ratio is a particularly pertinent influencing factor. As the span to depth ratio is increased and the arch becomes shallow, the potential for load enhancement through CMA diminishes.

In recent years there has been a move towards the investigation of the importance of CMA as a robustness tool to provide an alternative load path when a structure is in a damaged state. However, previous analytical prediction methods used to determine the ultimate load inclusive of CMA were validated against experimental testing carried out at span to depth ratios less than 30. Since the double span condition for flat slab structures occurs at span to depth ratios from 40 to 60 it was not possible to use the existing prediction methods with confidence until they had been compared against appropriate testing at large span to depth ratios.

This thesis presents results from an experimental investigation conducted at these higher span to depth ratios. The aim of the testing was to model and quantify the behaviour of RC buildings in the situation where a column has been lost. The twelve specimens were designed to be representative of flat slab and conventionally framed structures providing a range of span to depth ratios from 30 to 66 and percentages of tension reinforcement between 0.2% and 0.7%. Initially three vertical supports were provided to the specimen by the rig (representing two perimeter structural bays in a typical structural frame) the double span scenario was then created by the removal of the central support. Vertical load was subsequently applied at mid-span using a hydraulic actuator in order to ascertain the collapse load of the specimen.

From the experimental investigation it was found that load is supported by two main components, firstly through the bending strength which is later supplemented by additional load capacity through arching action (CMA). Analysis of the specimens behaviour showed that snapthrough, the drop off in applied load at mid-span, occurred at $\delta/h = 0.58$ where δ was the vertical deflection at the applied load and h was the overall depth of the specimen. This was slightly higher than the values reported in the previous literature of 0.4 to 0.5. Results showed that for specimens at high span to depth ratios, L/d = 60 & 66, the changeover from compressive to tensile membrane action was gradual with no drop off in applied load. In these cases the snapthrough of the compressive arch occurred at an average $\delta/h = 0.67$.This indicates that when the thrust in the compressive arch is low the collapse of the arch does not cause the applied load to be reduced.

Significant load enhancement through CMA was limited to two specimens only, where enhancement factors of 2.4 and 1.9 was achieved. These had the lowest percentage of reinforcement considered, 0.2%, and span to depth ratios of 40 and 50 respectively. With one exception all other specimens reached the predicted ultimate load (from plastic bending analysis) but with an average enhancement of 17% did not significantly exceed it. Significant CMA was developed in the specimens but its benefits were offset by the extra bending moments from the P-Δ effect. Experimental results indicated that the percentage of reinforcement was more influential than the span to depth ratio and that significant load enhancement through CMA could still be achieved at a span to depth ratio of 50. Hence low levels of reinforcement provide the optimum conditions for CMA.

It was found that the peak applied load occurred before the peak bending moment, again due to the second order P-Δ effect caused by the axial force and the transverse deflection. At the end of the compressive membrane phase the specimens still had sufficient flexural strength to prevent a sudden failure from occurring.

The stiffness of the test rig used was compared to the restraint against in-plane movement provided by various RC flat slab structures designed to BS 8110. It was determined that the restraint stiffness of the test rig was similar to that of a frame with no additional lateral stiffness provided by shear walls. As such the test rig can be deemed to have provided a low level of stiffness, consequently if the restraint stiffness had been increased even moderately more load enhancement could have been expected.

The experimental results allowed for existing analytical methods to be compared with data representative of realistic structures in the double span condition for the first time. The prediction method developed by Merola proved the most accurate when compared with the test results at the high span to depth ratios that are relevant to the double span situation. However, it was found that the method consistently underestimated failure loads and consequently can be considered a conservative approach. The Merola method was selected and used for further parametric studies and in the subsequent frame assessment.

A parametric study of a series of flat slab structures has been conducted with the aim of making a realistic assessment of the feasibility of utilizing CMA to support accidental loading

in the double span condition. The column grid spacing was varied from 5m to 9m to investigate the influence of span to depth ratio, which would vary between 40 and 50 in the double span situation in realistic frames designed to industry standards.

When assessing the inherent restraint stiffness of a frame it was found that the placement of shear walls, often in the form of structural cores enclosing stairwells and lift cores, is highly influential. In total five different arrangements of structural cores were considered, including the omission of core shear walls. It was found that the scenario with the structural cores in the closest proximity to the damaged area was most beneficial for enhancement from CMA. It became clear that the restraint stiffness provided by the frame is a complex parameter that must be assessed on a case by case basis. FEA was shown to be an effective tool in assessing the frame stiffness. Storey height was found not to have significant influence on the restraint stiffness provided and consequently the calculated FOS against collapse in the damaged situation. Thus it can be concluded that the majority of the stiffness provided by a flat slab structure comes from the in-plane slab stiffness.

The arrangement of shear walls that produced the highest values of restraint stiffness across the structural bay was when cores were placed in direct interaction with the damaged area i.e. adjacent to and in-line with the direction of outward movement or at the first internal structural bay where the bay adjacent to the damaged area effectively cantilevered from the shear walls (arrangements C & D in Chapter 6). These arrangements provided around 5 times more stiffness than when the structural cores were far away from the damaged area or were omitted completely.

It was demonstrated for all arrangements of structural cores considered that an increase in FOS was produced by the inclusion of CMA over that from flexural strength alone. The highest FOS produced was for shear wall arrangement C, where the structural cores were positioned adjacent to the damaged area. A FOS above 1.0 was achieved in this instance for all column spacings considered. For arrangement D the FOS fell below unity at a column spacing of just below 7.5m. In all other arrangements the accidental loading could not be supported by enhancement from CMA in the double span scenario as the FOS ranged from 0.7 to 0.9. In all cases the robustness of the structure was improved by the consideration of CMA over the flexural response alone. This indicates a significant underestimation of load capacity in

conventional analysis when membrane forces are neglected. The cases where the FOS was found to be below 1.0 do not mean a failure of the slab under accidental loading. Additional strength would be provided in the transverse direction along with other mechanisms in the floor plate such as cantilever effects from the first internal column line. Hence collapse may be prevented through a combination of CMA and other mechanisms. Further to this tensile membrane action and other alternative load paths such as cladding or internal partitions (blockwork walls) could provide additional robustness.

A noticeable difference in performance was observed between column (edge beam) and middle (slab) strips. The more lightly reinforced middle strips produced higher load enhancement through CMA. Another reason for this was that the horizontal restraint provided by the slabs at each end of the damaged panels varied across the width of the damaged panels. It was lowest at the perimeter of the frame where the column was removed and increased along the edges of the damaged panels towards the adjacent undamaged column line. The parametric study also indicated that the higher percentage of reinforcement and thus higher flexural strength in the edge strips did not produce significant benefits. CMA is more effective in enhancing ultimate load. To achieve a similar level of load carrying capacity through flexure alone would require a significant increase in reinforcement. This would be very uneconomic because the cost of the extra steel would only be justified in the unlikely event of losing a column.

Many current guidelines across Europe and the USA recommend the notional removal of columns during progressive collapse analysis, where alternative load paths are highlighted as playing a significant role in redistributing load. There are however no clear guidelines on how to carry out such an analysis. This research has demonstrated that it is feasible to employ the Merola method to predict behaviour of slab strips in the damaged scenario inclusive of CMA. If this approach is used it is recommended that a linear static analysis is made. Since the nature of load redistribution once a column has been lost from a structure is dynamic, to equate this loading effect statically a dynamic load factor (DLF) must be applied. From theory of structural dynamics the DLF must lie between 1.0 and 2.0. Analytical work by Ruth et al. (2006) suggested a value of 1.5 should be applied, however from full scale testing by Sasani (2011) and the procedure used by Yu and Tan (2011) based on UFC 4-023-3 it was

determined that 1.1 is more representative of experimental behaviour and thus more applicable to realistic frames in the emergency condition. Hence if the Merola method utilised in this study is to be incorporated into a progressive collapse review, it is recommended that a linear static analysis is made was a DLF of 1.1 applied to accidental loading.

The findings from the research can be summarised into the following conclusions:

The review of previous literature indicated the potential for CMA to be used as a robustness tool but the lack of appropriate experimental data meant that prediction methods could not be employed with confidence for double span conditions. Experimental data equivalent to double span conditions has been produced for the first time by the author at high span to depth ratios allowing for comparisons with prediction methods.

In the experimental programme significant load enhancement was restricted to two specimens which had the low reinforcement percentage of 0.2% but at span to depth ratios of 40 and 50. It can be concluded that enhancement can still be achieved at the high span to depth ratios that are likely to occur in the double span situation but the percentage of reinforcement is the more important parameter. The level of restraint stiffness provided by the test rig had an influence on load enhancement. The test rig stiffness was shown to be similar to a framed structure with no shear walls present resulting in a low level of stiffness. Comparisons with the frame study indicated that if the longitudinal stiffness of the rig could be increased more load enhancement could be expected in experimental specimens with low levels of reinforcement.

From the comparison with experimental test data the prediction method of Merola was found to be the most accurate and yielded the best correlation at high span to depth ratios. This allowed it be applied with confidence in a parametric study of flat slab buildings. In combination with FEA (to determine in-plane restraint) it has been shown to be a feasible method of assessing the contribution of CMA in a structures ability to resist accidental loading in a damaged state.

The restraint stiffness provided by the frame to the damaged area once a column has been removed is highly dependent on structural form and must be determined on a case by case approach.

CMA has been shown to be a feasible method of supporting accidental loading in the abnormal double span condition. When sufficient restraint stiffness is provided it has been shown that span to depth ratio is not a restricting factor. Accidental loading was able to be supported at a span to depth ratio of 50 from an original column spacing of 9m. In all cases the robustness of a structure was increased by the inclusion of CMA when compared to flexural strength alone.

On the basis of the research presented in this thesis the following recommendations can be made for areas that require further work:

The longitudinal stiffness of the experimental test rig was shown to be comparable to the lowest frame stiffness values from the frame assessment in Chapter 6. This has contributed to the moderate levels of load enhancement found from the experimental programme. It is recommended that testing is conducted with a higher longitudinal restraint stiffness that is more comparable with structural frames in which structural cores provide significantly higher stiffness to the damaged area of a building.

The Merola method has been shown to provide a conservative prediction of load capacity. Further work is required to develop the method to provide a more accurate prediction method.

In the experimental and analytical work conducted the effect of the columns stub has been ignored. The column stub will have an effect on the deflected shape and consequently the compressive arch formed within the slab strip but its effect was considered to be small. Further investigations could be carried out to quantify the effect of column stubs on the load carrying capacity through CMA.

The use of finite element analysis as a tool to quantify stiffness provided by the frame needs to be validated against full scale testing to ensure accuracy as the restraint stiffness is such an influential parameter to enhancement. In particular the assumption of a linear elastic response of the intact portion of the frame needs further investigation to ascertain if the actual response is not a non-linear one. Full scale testing of frames would also be beneficial to clarify the dynamic load factor to be applied to static calculations.

The variance of restraint stiffness caused by the assumption of alternative positions of column loss needs further investigation. If the failed column was biased to one side of the structure each side of the compressive arch formed would have different levels of resistance to outward movement which will have implications to the magnitude of applied load that can be supported. Further to this the notion of a column being lost from the alternative side to the structure than that considered in this research will create a situation with a reduction in stiffness provided.

An assessment has been made of collapse mitigation through the mechanism of CMA alone; it is likely however that a portion of loading will be supported through other mechanisms. To achieve a full over sight and determine whether structures can sustain column loss the CMA analysis provided in this research needs to be integrated into a global response analysis, in which the behaviour of flat slabs in two directions is considered across the bay depth.

An investigation is required into whether the screeding or floor finishes may exhibit sufficient bond to the concrete to provide additional depth to the compressive arch which may lead to further load enhancement.

8 References

Allen, H. G. and P. S. Bulson (1980). Background to Buckling. London, McGraw-Hill

ACI 318-77 (1977). " Building Code Requirement for Reinforced Concrete". ACI Committee 318, American Concrete Institute, Detroit, Michigan.

ATF Car Bomb Table (2014) Bomb Basics: Why you neeed to know... Available at http://www.nationalhomelandsecurityknowledgebase.com/Research/International_Articles/Bomb_Basics.html

Bailey, C. B. (2001) "Membrane action of unrestrained lightly reinforced concrete slabs at large displacements" Engineering Structures **23**: 470-483

Baker, J. F., E. L. Williams and D. Lax (1948). "The civil engineer in war - Volume 3: Properties of materials structures, hydraulics, tunneling and surveying." Symposium of papers publised by the Institution of Civil Engineers, London.

Biggs, J. M. (1964). Introduction to Structural Dynamics. New York, McGraw-Hill.

Birke, H. (1975). "Kupoleffekt vid Betongplattor. Instituionen for Byggnadsstatik " Royal Technical University, Stockholm **Report no. 108 (in Swedish)**.

Braestrup, M. W. (1980). "Dome effect in RC slabs: Rigid-plastic analysis." Journal of the Structural Division ASCE **106**(ST6): 1237-1253.

Bramforth, P., D. Chisholm, J. Gibbs and T. Harrison (2008). Properties of Concrete for use in Eurocode 2. CCIP-029. **The Concrete Centre**.

BRE (1997). Design of normal conrete mixes. Watford, Construction Research Communication Ltd.

Brondum-Nielsen, T. (1974). "Optimum Design of Reinforced Concrete Shells and Slabs." Technical University of Denmark **Report NR. R 44**.

BSI (1997). BS 8110: Part 1: Structural Use of Concrete. BSI, London, UK.

BSI (1990) BS EN 1990:2002+A1:2005 UK National Annex for Eurcode - Basis of structural design. BSI, London, UK

BSI (2004) BE EN 1992-1-1:2004: Eurocode 2: Design of Concrete Structures. Part 1-1: General Rules and Rules for Buildings. BSI, London, UK.

BSI (2007) BS EN 1991-1-7: Eurocode 1: Actions on Structures: Part 1-7: Accidental Actions. BSI, London, UK.

Bussell, M. N. and A. E. K. Jones (2010). "Robustness and the relevance of Ronan Point today." The Structural Engineer **88**(7 December 2010).

Byfield, M. P. (2006). "Behaviour and Design of Commerical Multistory Buildings Subjected to Blast." Journal of Performance of Constructed Facilities **November 2006**: 324-329.

Chattopadhyay, B. (1981). "Compressive membrane action in reinforced concrete slabs." London, Polytechnic of Central London, PhD Thesis, December 1981.

Christiansen, K. P. (1963). "The effect of membrane stresses on the ultimate strength of the interior panel in a reinforced concrete slab." The Structural Engineer **41**(8): 261-265.

Computers and Structures Inc (2006). SAP 2000: Concrete Shell Reinforcement Design: Technical Note, Design Information. Berkley, California.

Corley, G. W., P. F. Mlakar Sr., M. A. Sozen and C. H. Thornton (1998). "The Oklahoma City Bombing: Summary and Recomendations for Multihazard Mitigation." Journal of Performance of Constructed Facilities **August 1998, ASCE**: 100-112.

Dat, P. X and Hai. T. K (2011). "Membrane actions of RC slabs in mitigating progressive collapse of building structures". Engineering Structures **55**: 107-115

Department of Defense (2009). UFC 4-023-03: Design of buildings to resist progressive collapse, US Department of Defence.

Department of the Environment, Northern Ireland (1986) "Design of M-beam dridge decks", Amendment No.3 to the Bridge Design Code, Nothern Ireland Road Service Headquarters, March 1986, 11.1-11.5

Eyre, J. R. (1990). "Flow rule in elastically restrained one-way spanning RC slabs." Journal of Structural Engineers **116**(12): 3251-3267.

Eyre, J. R. (1997). "Direct assessment of safe strengths of RC slabs membrane action." Journal of Structural Engineers **123**(10): 1331-1338.

Eyre, J. R. (2000). "Membrane action in plain concrete slabs under concentrated loading." Proceedings of the Institution of Civil Engineers: Structures and Buildings **140**(3): 207-217.

FarhangVesali, N. Valipour, H. Samali, B. and Foster, S. (2013) "Devlopment of araching action in longitudinally-restrained reinforced concrete beams"Construction and Building Materials **47 (2013)** 7-19

Foster, S. J., C. G. Bailey, I. W. Burgess and R. J. Plank (2004). "Experimental behaviour of concrete floor slabs at large displacements." Engineering Structures **26**: 1231–1247.

Higgins, J. B. and B. R. Rogers (1998). Designed and detailed (BS 8110 : 1997), British Cement Association Publication 43.501.

Hognestad,E., Hanson, N.W and McHenry, D. (1956). "Concrete Stress Distribution in Ultimate Strength Design." Journal of the American Concrete Institute **52**, 455

Izzuddin, B. A., A. G. Vlassis, A. Y. Elghazouli and D. A. Nethercot (2007). "Assessment of progressive collapse in multi-storey buildings." Proceedings of the Institution of Civil Engineers: Structures and Buildings **160**(4 B): 197-205.

Janas, M. (1968). "Large plastic deformations of reinforced concrete slabs." International journal of Solids & Structures **4**: 61-74.

Johansen, K. W. (1972). Yield-line formulae for slabs. London, Cement and Concrete Association.

Kemp, K. O. (1967). "Yield of a square reinforced concrete slab on simple supports, allowing for membrane forces." The Structural Engineer **45**(7): 235-240.

Kemp, K. O., J. R. Eyre and H. M. Al-Hassani (1989). Plastic Flow Rules for use in the Analysis of Compressive Action in Concrete Slabs. Frame and Slab Structures. A. Moore. London, Butterworth & Co.**:** 175-193.

Kennedy, G. and C. H. Goodchild (2004). Practical Yield Line Design, The Concrete Centre.

Khabbazan, M. M. (2005). "Progressive Collapse." The Structural Engineer.

Kirkpatrick, J., Rankin, G.I.B. and Long, A.E. (1984). "Strength evaluation of M-beam bridge deck slabs." The Structural Engineer **Vol. 62B**(September 1984): 60-68.

Lahlouh, E. H. and P. Waldron (1992). "Membrane action in one-way slab strips." Proceedings of the Institution of Civil Engineers: Structures and Buildings **94**(Nov): 419-428.

Long, A. E. (1975). "A two-phase approach to prediction of punching strength of slabs." ACI Journal Proceeding **Vol. 72**(No.8, Feb.1975): 37-45.

Marti, P. (1990). "Design of Concrete Slabs for Transverse Shear." ACI Strcutural Journal **March-April 1990**.

Mattock, A. H., L. B. Kriz and E. Hognestad (1961). "Rectangular concrete stress distribution in ultimate strength deisgn." ACI **57**(No. 8): 875-926.

McDowell, E. L., McKee and E. Sevin (1956). "Arching action theory of masonry walls." ASCE Journal of Structural Engineering **82**(No.ST2): 915-918.

Merola , R. (2009). Ductility and Robustness of Concrete Structures Under Accidental and Malicious Load Cases. Department of Civil Engineering. Birmingham, The University of Birmingham. **Doctor of Philosophy**.

Mlakar, S., G. W. Corley, M. A. Sozen and C. H. Thronton (1998). "The Oklahoma City Bombing: Analysis of Blast Damage to the Murrah Building." Journal of Performance of Constructed Facilities **August 1998, ASCE**: 113-119.

Morley, C. T. (1967). "Yield-line theory for reinforced concrete slabs at moderately large deflexions." Magazine of Concrete Research **19**(61): 211-222.

Moy, S. S. J (1970). " Load-Deflexion Characteristics of Reinforced Concrete Slabs". Nottingham, University of Nottingham Department of Civil Engineering, PhD Thesis, November 1970.

Nair, S. R (2006) "Preventing Disproportionate Collapse" Journal of Performance of Constructed Facilities **November 2006, ACSE**, 309-314

National Institute of Standards and Technology NIST (2007). "Best Practices for reducing the potential for progressive collapse in buildings."

Neville, A. M. (1995). Properties of Concrete. Harlow, England, Longman Group Limited.

Ockleston, A. J. (1955). "Load tests on a three storey reinforced concrete building in Johannesburg." Structural Engineer **33**(Oct): 304-322.

Ockleston, A. J. (1958). "Arching action in reinforced concrete slabs." Structural Engineer **36**(6): 197-201.

Office of The Deputy Prime Minister (2004). The Building Regulations 2000 - Part A3 (Amendment No.3). Schedule 1 : Disproportionate Collapse. London (UK).

Ontario Ministry of Transport and Communications (1983) "Ontario Highway Bridge Design Code" Downview, Ontario, Canada, 1983, 175.

Osteraas, J. D. (2006) "Murrah Building Bombing Revisited: A Qualitative Assessment of Blast Damage and Collapse Patterns" Journal of Performance of Constructed Facilities **November 2006, ASCE** 330-335

Park, R. (1964a). "Tensile membrane behaviour of ultimate load rectangular reinforced concrete slabs with fully restrained edges." Magazine of Concrete Research **16**(No.46, March 1964): 39-44.

Park, R. (1964b). "Ultimate strength of rectangular concrete slabs under short-term uniform loading with edges restrained against lateral movement." Proceedings of the Institution of Civil Engineers **June**(28): 125-150.

Park, R. and W. L. Gamble (2000). Reinforced Concrete Slabs, 2nd ed. New York, John Wiley & Sons, Inc.

Pearson, C. and N. Delatte (2005). "Ronan Point apartment tower collapse and its effect on building codes." Journal of Performance of Constructed Facilities **19**(2): 172-177.

Peel-Cross, J., G. I. B. Rankin, S. G. Gilbert and A. E. Long (2001). "Compressive membrane action in composite floor slabs in Cardington LBTF." Proceedings of the Institution of Civil Engineers **May**(2): 217-226.

Punton, B. M., M. P. Byfield and P. P. Smith (2011). Load redistribution using compressive membrane action in reinforced concrete buildings. 3rd International Workshop on Performance, Protection and Strengthening of Structures under Extreme Loading, PROTECT2011, August 30, 2011 - September 1, 2011, Lugano, Switzerland, Trans Tech Publications.

Rankin, G. I. B. and A. E. Long (1987). "Predicting the enhanced punching strength of conventional slab-column specimens." ICE Proceeding - Structures and Buildings **No.82**(April 1987): 327-346.

Rankin, G. I. B. and A. E. Long (1997). "Arching action strength enhancement in laterally-restrained slab strips." Proceedings of the Institution of Civil Engineers: Structures and Buildings **122**(Nov.): 461 – 467.

Rankin, G. I. B., R. A. Niblock, A. S. Skates and A. E. Long (1991). "Compressive membrane action strength enhancement in uniformly loaded, laterally restrained slabs." The Structural Engineer **Vol. 69**(No.16): 287-295.

Roberts, E. H. (1969). "Load-carrying capacity of slab strips restrained against longitudinal expansion." Concrete **September**: 369-378.

Ruddle, M. E., G. I. B. Rankin and A. E. Long (2003). "Arching action-flexural and shear strength enhancements in rectangular and Tee Beams." Proceedings of the Institution of Civil Engineers **Feburary**(1): 63-74.

Ruth, P., K. A. Marchand and E. B. Williamson (2006). "Static Equivalency in Progressive Collpase Alternative Path Analysis: Reducing Conservatism Whilse Retaining Structural Integrity." Journal of Performance of Constructed Facilities **ASCE**(Novemember 2006).

Sasani, M. (2007). "Experimental and Anlytical Progressive Collpase Evaluation of Actual Reinforced Concrete Structure." ACI Strcutural Journal **November - December**.

Sasani, M. (2011). "Experimental and Analytical Evaluation of Progrssive Collpase Resistance of a Full-Scale Structure Following Sever Loss of Load Bearing Elements." Applied Mechanics and Materials **82**: 326-331.

Smith, P. P. (2014). "Robustness Assessment of Framed Buildings." Unpublished.

Smith, P. P., M. P. Byfield and D. J. Goode (2010). "Building robustness research during World War II." Journal of Performance of Constructed Facilities **24**(Compendex): 529-535.

Sozen, M. A., C. H. Thornton, W. G. Corley and P. F. Mlakar (1998). "The Oklahoma City Bombing: Structure and Mechanisms of Murrah Building." Journal of Performance of Constructed Facilities **August 1998, ASCE**: 120-136.

Su, Y., T. Tian and X. Song (2009). "Progressive Collapse Resistance of Axially-Restrained Frame Beams." ACI Structural Journal **106-S55**(September-October 2009).

Taylor, S. E. (2000). Compressive membrane action in high strength concrete bridge deck slabs. PhD Thesis. Belfast, Queen's University.

Taylor, S. E., G. I. B. Rankin and D. J. Cleland (2001). "Arching action in high-strength concrete slabs." Proceedings of the Institution of Civil Engineers **November**(4): 353-362.

TCC (2006). Concrete Framed Buildings. TCC/03/024. **The Concrete Centre, 2006**.

United States General Service Administration (2003). "Progressive collapse analysis and design guidelines for new federal office buildings and major modernization projects." Washington, D.C.

Valipour, H. FarhangVesali, N and Foster, N. (2013) " A generic model for investigation of arching action in reinforced concrete members" Construction and Building Materials **38 (2013)** 742-750

Wood, R. H. (1961). Plastic and elastic design of slabs and plates. London, Thames and Hudson.

Yi, W. Qing-Feng, H Yan, X and Sahsi, K. (2008) "Experimental study on preogressive collapse-resistant behaviour of reinforced concrete frame structures". ACI Structural Journal **2008;105(4)**

Yu, J. and K.-H. Tan (2011). "Experimental and numerical investigation on progressive collapse resistance of reinforced concrete beam column sub-assemblages."

Appendices

A.1 Photographs of Test Rig

Figure A.1.1: *Elevation view of end detail connection to specimen with load cell.*

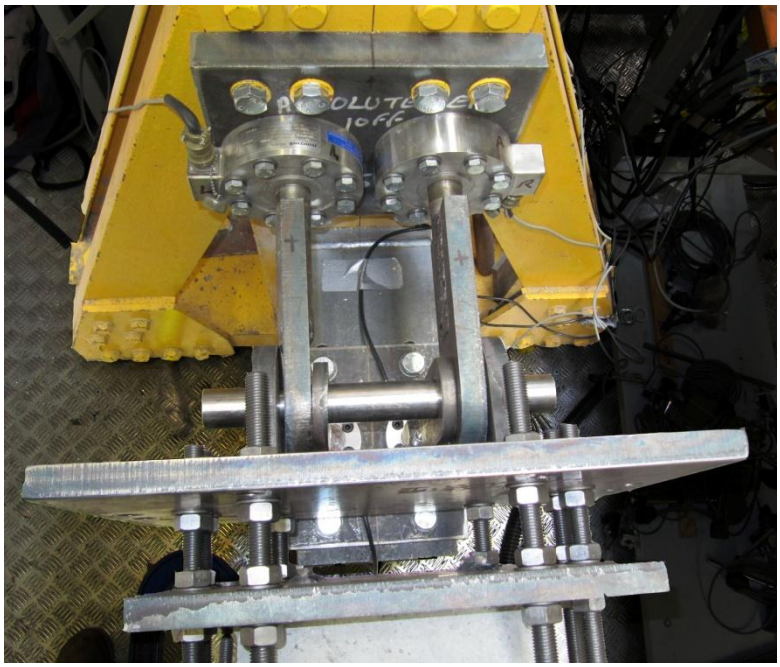

Figure A.1.2: *Plan view of end detail connection to specimen with load cell.*

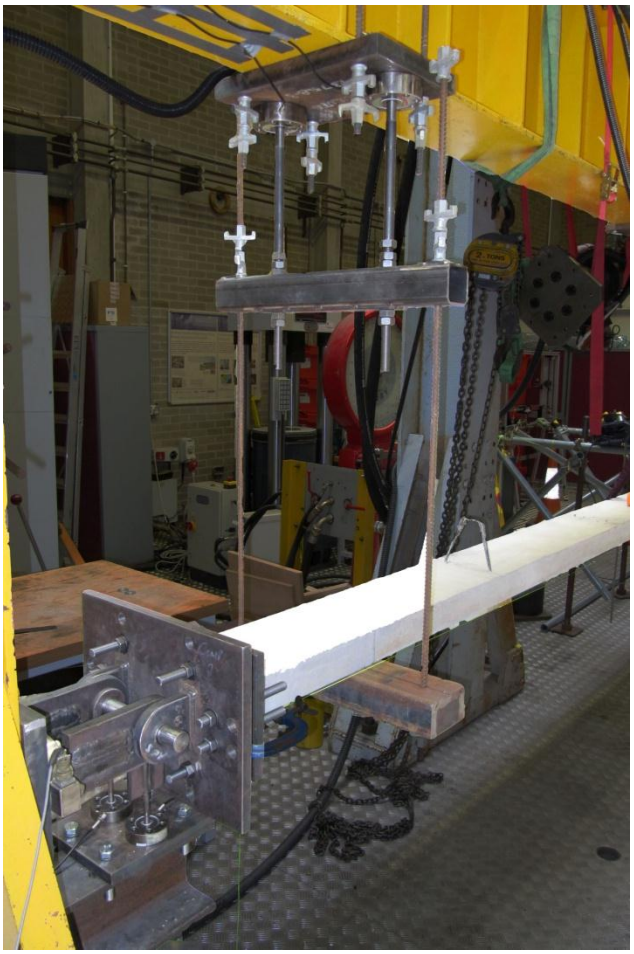

Figure A.1.3: *End detail and hanger support with load cells.*

Figure A.1.4: *End detail connection with no load cells, shown without concrete specimen connected.*

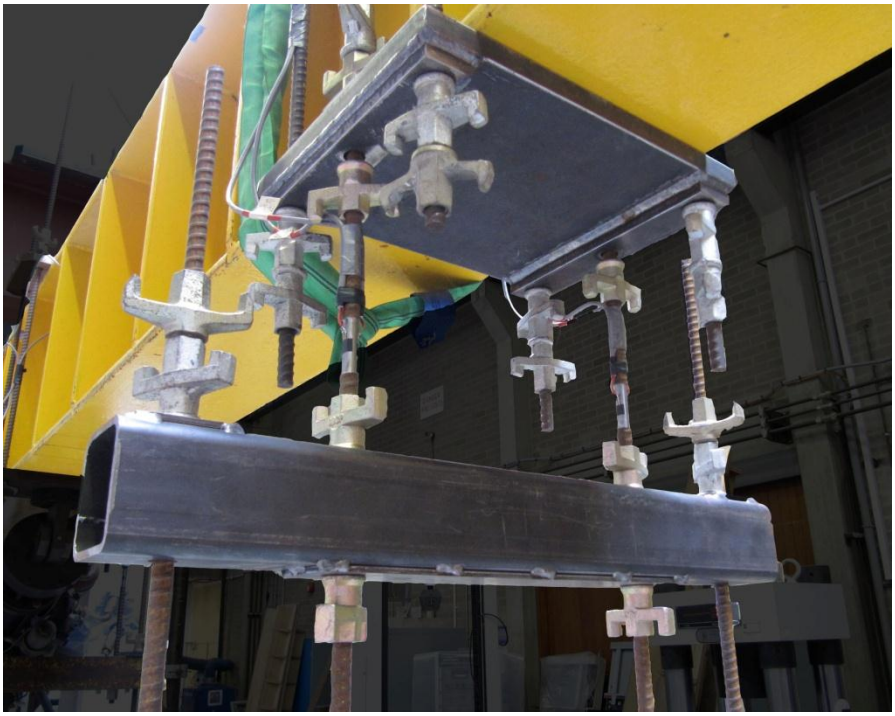

Figure A.1.5: *Hanger Detail with strain gauges.*

A.2 Concrete Mix Design

Imperative to understanding the procedure for designing a concrete mix is the definition of the characteristic concrete strength. The specified strength is termed as 'characteristic' rather than 'minimum' as the results from compressive concrete tests, either cube or cylinder, follow a normal distribution (Figure A.2.1) and so there is a possibility that the strength could fall below that specified. The percentage of defective samples that fall below the characteristic strength is defined as 5% in both BS8110 and EC2 (although the percentage can be altered if necessary in the design calculations). The cause of variation in strength results can be attributed to a number of factors. When using ready mix concrete delivered to site the quality of mix may vary in different deliveries due to inevitable inconsistencies at the plant which could be the differences in the grading and particle shape of the aggregate, which has a knock on effect on the water/cement ratio. Of more pertinence to the experimental procedure is the variation due to the process of sampling the concrete, casting, curing and testing of cubes. BRE (1997)

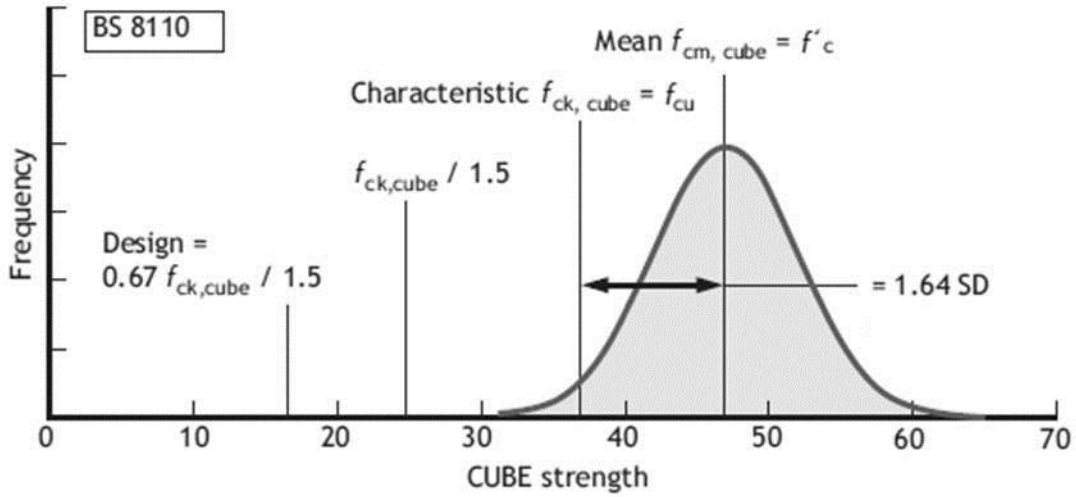

Figure A.2.1: *Normal distribution of compressive strength for strength class C30/37 in accordance with BS8110. Bramforth et al. (2008)*

It is common practice for the characteristic concrete strength to be specified at 28 days. The design compressive strength, f_{cd}, of the concrete can then be calculated in accordance with BS 8110, where the cube strength is used:

$$f_{cd} = \frac{0.67 f_{cu}}{\gamma_c} \qquad \text{A.1}$$

Where

$\gamma_c$is the partial safety factor for concrete.

The normal distribution of cube results as shown in Figure A.2.1 is symmetrical about the mean strength. The target mean strength is therefore required in the design process to account for the variation in results and is related to the specified characteristic strength by the standard deviation, equation A.2. The parameter k is defined in BS 5323 as 1.64 for 5% defective results. The margin between the characteristic and mean strength is defined as 10 N/mm^2 giving a standard deviation of 6.1N/mm^2. For a 5% defective occurrence it is safe to assume a standard deviation based on this calculation technique for all characteristic strengths above 20 N/mm^2. Below this the standard deviation increases as the specified characteristic strength increases.

$$f_{cm} = f_{cd} + k\sigma \qquad \text{A.2}$$

The standard deviation, σ, is dependent on the population that it is sampled from, the value of 6.1N/mm^2 is based on vast amounts of results from ready mix plants and so the probability errors are smaller. For the hand mixing procedure used in the experimental programme it was not possible to obtain a minimum of 20 results for each specimen and it was therefore recommended that a standard deviation of 8 N/mm^2 be used, BRE (1997). This gave a higher mean strength as shown in Table A.2.1.

Mix Designation	**C25/30**	**C30/37**	**C35/45**	**C40/50**	**C45/55**	**C50/60**	**C55/67**	**C60/75**
Characteristic cube strength f_{ck}	30	37	45	50	55	60	67	75
EC2 Target mean cube strength f_{cm}	40	47	55	60	65	70	77	85
Hand Mix Target mean cube strength $f_{cm,H}$	43.12	50.12	58.12	63.12	68.12	73.12	80.12	88.12

Table A.2.1: *Mean compressive cube strength for different strength classes.*

To determine the target mean strength to be used in the experimental programme, the effect of age on concrete had to be investigated. The concrete strength is a parameter that needs to be controlled throughout testing as it has an effect on the behaviour of the sample in the

compressive membrane stage. The structure was to be modelled in its damaged state in an accidental loading scenario; it was thought that this situation would not occur in the early stages of its life. It was therefore assumed herein that the structure had remained intact for 5 years and the sample in the experimental programme should be designed so that the concrete strength reflected that.

The type of cement used in a concrete mix has a direct effect on the rate of strength development beyond the 28 day period. Eurocode 2 gives a way of predicting concrete strength as it ages for different cement types with the following expression:

$$f_{cm}(t) = [\beta_{cc}(t)]f_{cm} \qquad \text{A.3}$$

$$\beta_{cc}(t) = exp\left\{s\left(\frac{28}{t}\right)^{0.5}\right\} \qquad \text{A.4}$$

Where $f_{cm}(t)$ is the mean compressive strength at t days and s is a coefficient that depends on the cement type. This expression has been plotted in Figure A.2.2 for a target mean strength (f_{cm}) of 55 N/mm^2, the three variants of s are represented by series A, B and C which correspond with strength class as follows:

A = 0.20 for cement of strength classes CEM 42.5R, CEM 52.5N and CEM 52.5R (Class R)

B = 0.25 for cement of strength classes CEM 32.5R, CEM 42.5N (Class N)

C = 0.38 for cement of strength class CEM 32.5N (Class S)

(Where Class R = high early strength; Class B = normal early strength; Class S = slow early strength), Neville (1995).

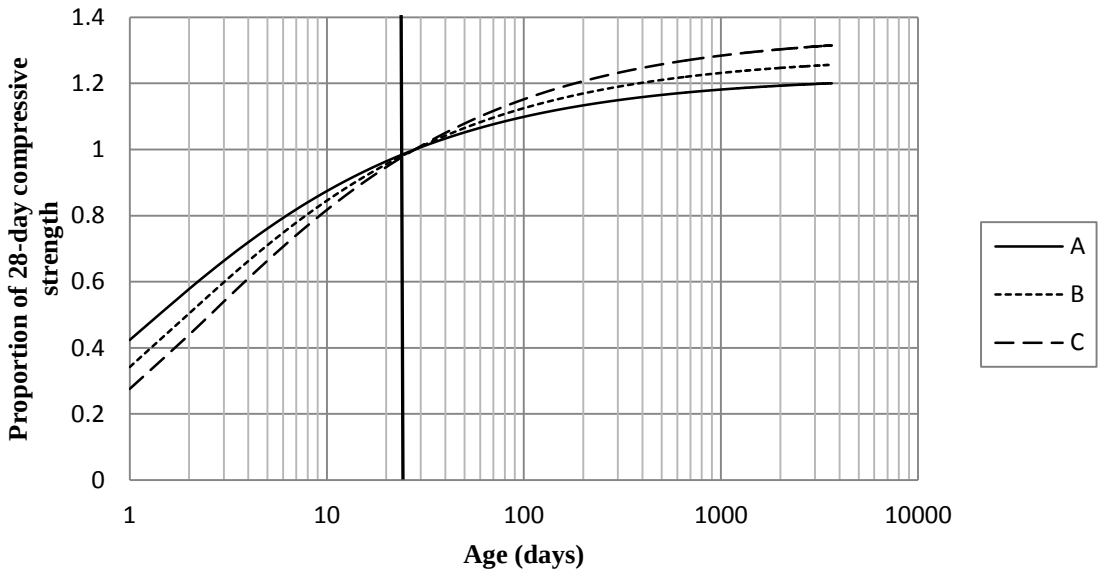

Figure A.2.2 : *Rate of compressive strength development at 20^{o}C for different cement strength classes.*

Depending on the cement type, the proportion of 28-day compressive strength increases by a factor of between 1.2 and 1.3 over a 5 year period. This is supported by Figure A.2.3 where curve I indicates the use of ordinary Portland cement and the factor is 1.3 for graph (a) and 1.28 for graph (b). Whilst it is hard to typify the type of cement that is commonly used on site, Figure A.2.2 indicates that the change in increase between types of cement used is not of great significance and the appropriate factor for the type of cement used in the experimental samples can be selected with confidence that it will give a realistic prediction of a 5 year old concrete strength.

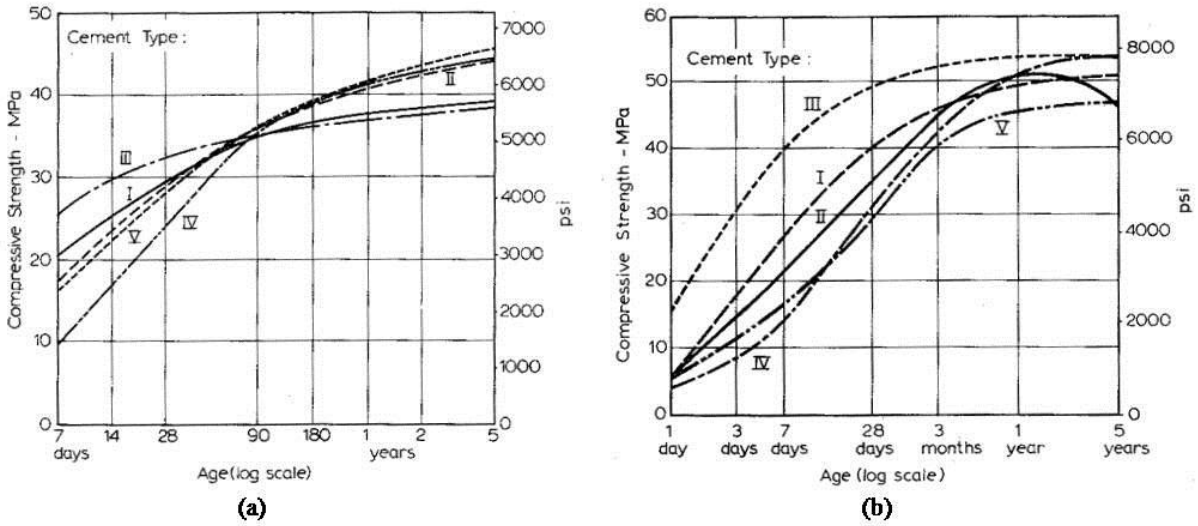

Figure A.2.3: *Development of concrete strength made with different cements (a) containing 335kg of cement per cubic metre (b) with a water / cement ratio of 0.49. Neville (1995)*

Further to this it is thought that the water/cement ratio used has an effect on the increase of strength with time. Figure A.2.4 indicates that with a lower water/cement ratio there is a greater increase in strength, however for the three values of water/cement ratio shown, the range of increase of the 28-day strength is in a similar region as Figure A.2.3, between 1.2 and 1.3.

It should be noted that all three charts (Figure A.2.3 and Figure A.2.4) are based on the assumption that the samples are cured at 20^{o}C and have the same ambient temperature. The temperature of the concrete plays a role in the development of strength but it is one factor that would be site specific and too difficult to model and predict therefore 20^{o}C has been assumed for the life of the structure to be modelled. Other factors that could be considered would be type of concrete, type of formwork and section thickness.

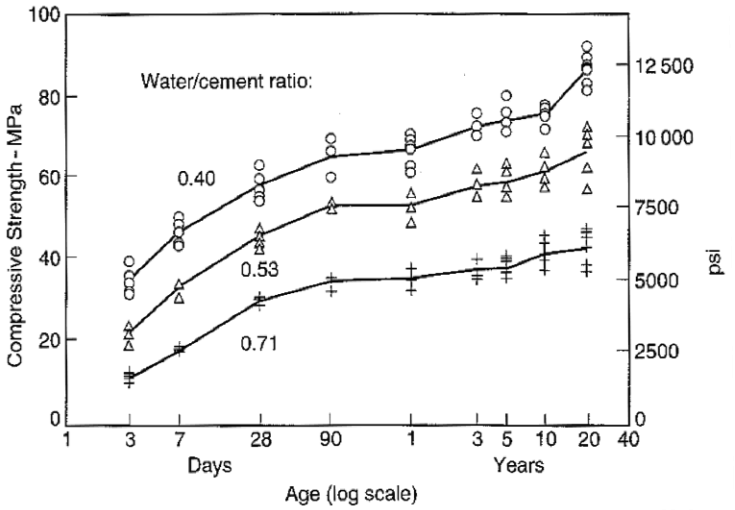

Figure A.2.4: *Development of strength of concrete over a period of 20 years; storage under moist conditions. Neville (1995)*

Mix Designation	C25/30	C30/37	C35/45	C40/50	C45/55	C50/60	C55/67	C60/75
Characteristic cube strength f_{ck}	30	37	45	50	55	60	67	75
Target mean cube strength f_{cm}	40	47	55	60	65	70	77	85
5 year mean strength $f_{cm,5}$	48	56.4	66	72	78	84	92.4	102

Table A.2.2*: Prediction of 5 year mean strength from 28 day target mean strength.*

As a conservative assumption the lower value from the range of enhancement of the 28-day strength at 5 years is used. Thus by using a factor of 1.2 the mean strength can be predicted for different strength classes, Table A.2.2. A mix designation of C30 concrete has been chosen, the target mean strength for the concrete to be poured in the experimental programme was that of the 5 year mean strength of C30 concrete hence creating a model of 5 year old concrete. It is not thought that the mean will be achieved with great accuracy due to the nature of mix design and the need to scale aggregate for scaled testing; 10mm aggregate has been used throughout. Cubes were tested on the day of specimen testing to ensure the strength of the specimen could be quantified. The success of achieving a 5 year concrete specimen could then be analysed. It should be noted that the curing time of the concrete varied in some instances due to the programming of the testing and in these cases the design mix was altered so that the strength when tested remained roughly constant. The full details of the mix design are as follows:

Concrete mix design form

Stage	Item		Reference or calculation	Values
1	1.1	Characteristic strength	Specified	45 N/mm² at 14 days; Proportion defective 5 %
	1.2	Standard deviation	Fig 3	..... N/mm² or no data 8 N/mm²
	1.3	Margin	C1 or Specified	(k = 1.64) 1.64 × 8 = 13.12 N/mm²; ..... N/mm²
	1.4	Target mean strength	C2	45 + 13.12 = 58.12 N/mm²
	1.5	Cement strength class	Specified	42.5/52.5
	1.6	Aggregate type: coarse Aggregate type: fine		Crushed/uncrushed (uncrushed) Crushed/uncrushed (uncrushed)
	1.7	Free-water/cement ratio	Table 2, Fig 4	0.375
	1.8	*Maximum free-water/ cement ratio*	*Specified*	..... Use the lower value: 0.375
2	2.1	Slump or Vebe time	Specified	Slump 10-30 mm or Vebe time ..... s
	2.2	Maximum aggregate size	Specified	10 mm
	2.3	Free-water content	Table 3	180 kg/m³
3	3.1	Cement content	C3	180 ÷ 0.375 = 480 kg/m³
	3.2	*Maximum cement content*	*Specified*	530 kg/m³
	3.3	*Minimum cement content*	*Specified*	..... kg/m³
				use 3.1 if ≤ 3.2 use 3.3 if > 3.1: 480 kg/m³
	3.4	Modified free-water/cement ratio		
4	4.1	Relative density of aggregate (SSD)		2.6 known/assumed
	4.2	Concrete density	Fig 5	2377 kg/m³
	4.3	Total aggregate content	C4	2377 − 480 − 180 = 1717 kg/m³
5	5.1	Grading of fine aggregate	Percentage passing 600 µm sieve	100 %
	5.2	Proportion of fine aggregate	Fig 6	26 %
	5.3	Fine aggregate content	C5	0.26 × 1717 = 446.42 kg/m³
	5.4	Coarse aggregate content	C5	1717 − 446.42 = 1270.58 kg/m³

Quantities	Cement (kg)	Water (kg or litres)	Fine aggregate (kg)	Coarse aggregate (kg) 10 mm	20 mm	40 mm
per m³ (to nearest 5 kg)	480	180	445	1270		
per trial mix of ..... m³						

Items in italics are optional limiting values that may be specified (see Section 7).
Concrete strength is expressed in the units N/mm². 1 N/mm² = 1 MN/m² = 1 MPa. (N = newton; Pa = pascal.)
The internationally known term 'relative density' used here is synonymous with 'specific gravity' and is the ratio of the mass of a given volume of substance to the mass of an equal volume of water.
SSD = based on the saturated surface-dry condition.

Figure A.2.5: *Concrete mix design for experimental samples, BRE (1997)*

A.3 Flat Slab Design

Job No:Design of Flat Slab Building with Varying Grid Spacing **Created By: BP**

Flat Slab Design to BS 8110

Input

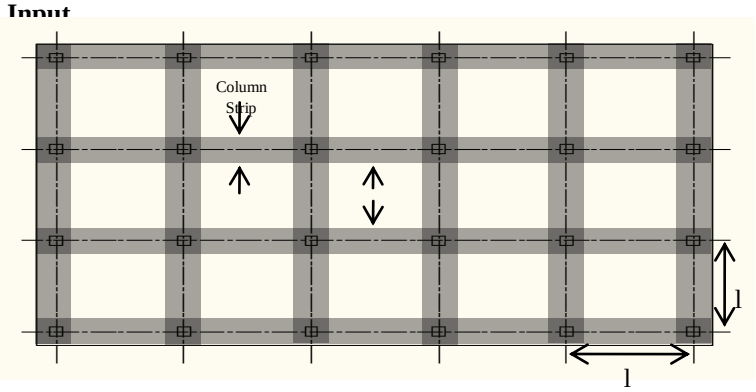

Building Usage
B - Office

Bay
Type
Edge

Storey Height
3.5 m

Concrete Cube Strength
40 N/mm2

Grid Spacing l, (m),from *5* to *9* in *0.5* increments

Grid Size *6* by *4* bays

Number of Stories
5

Tension Steel Reinforcement

Grid Spacing	5	Section Depth	200	mm	L/d	29.94

Bay No.	Column Strip As %			Middle Strip As %			
	Left Support	Mid Span	Right Support	Left Support	Mid Span	Right Support	
1	0.4816	0.2974	0.5351	0.2310	0.2974	0.2310	*Deflection Okay*
2	0.5351	0.2310	0.3824	0.2310	0.2310	0.2310	
3	0.3824	0.2310	0.4013	0.2310	0.2310	0.2310	
4	0.4013	0.2310	0.3824	0.2310	0.2310	0.2310	
5	0.3824	0.2310	0.5351	0.2310	0.2310	0.2310	
6	0.5351	0.2974	0.4816	0.2310	0.2974	0.2310	

Grid Spacing	5.5	Section Depth	225	mm	L/d	28.35

Bay No.	Column Strip As %			Middle Strip As %			
	Left Support	Mid Span	Right Support	Left Support	Mid Span	Right Support	
1	0.4028	0.2915	0.4664	0.2014	0.2915	0.2014	*Deflection Okay*
2	0.4664	0.2302	0.3887	0.2014	0.2302	0.2014	
3	0.3887	0.2302	0.3887	0.2014	0.2302	0.2014	
4	0.3887	0.2302	0.3887	0.2014	0.2302	0.2014	
5	0.3887	0.2302	0.4664	0.2014	0.2302	0.2014	
6	0.4664	0.2915	0.4028	0.2014	0.2915	0.2014	

Grid Spacing	6	Section Depth	250	mm	L/d	27.27

Bay No.	Column Strip As %			Middle Strip As %			
	Left Support	Mid Span	Right Support	Left Support	Mid Span	Right Support	
1	0.3443	0.2856	0.4633	0.1785	0.2856	0.1785	*Deflection Okay*
2	0.4633	0.2295	0.3570	0.1785	0.2040	0.1785	
3	0.3570	0.2295	0.3706	0.1785	0.2295	0.2856	
4	0.3706	0.2295	0.3570	0.1785	0.2295	0.1785	
5	0.3570	0.2295	0.4633	0.1785	0.2040	0.1785	
6	0.4633	0.2856	0.3443	0.1785	0.2856	0.1785	

Grid Spacing	6.5	Section Depth	275	mm	L/d	26.86

Bay No.	Column Strip As %			Middle Strip As %			
	Left Support	Mid Span	Right Support	Left Support	Mid Span	Right Support	
1	0.3090	0.3090	0.4635	0.1603	0.3090	0.1832	*Deflection Okay*
2	0.4635	0.2137	0.3693	0.1832	0.2060	0.1603	
3	0.3693	0.2318	0.3693	0.1603	0.2137	0.1603	
4	0.3693	0.2318	0.3693	0.1603	0.2137	0.1603	
5	0.3693	0.2137	0.4635	0.1603	0.2060	0.1832	
6	0.4635	0.3090	0.3090	0.1832	0.3090	0.1603	

Grid Spacing	7	Section Depth	300	mm	L/d	26.22

Bay No.	Column Strip As %			Middle Strip As %			
	Left Support	Mid Span	Right Support	Left Support	Mid Span	Right Support	
1	0.2327	0.3012	0.4675	0.1454	0.2803	0.1869	*Deflection Okay*
2	0.4675	0.2102	0.3765	0.1869	0.1939	0.1454	
3	0.3765	0.2327	0.3765	0.1454	0.2102	0.1454	
4	0.3765	0.2327	0.3765	0.1454	0.2102	0.1454	
5	0.3765	0.2102	0.4675	0.1454	0.1939	0.1869	
6	0.4675	0.3012	0.2327	0.1869	0.2803	0.1454	

Grid Spacing	7.5	Section Depth	325	mm	L/d	25.51

Bay No.	Column Strip As %			Middle Strip As %			
	Left Support	Mid Span	Right Support	Left Support	Mid Span	Right Support	
1	0.1923	0.3060	0.4590	0.1331	0.3060	0.1775	*Deflection Okay*
2	0.4590	0.2130	0.3443	0.1775	0.1923	0.1331	
3	0.3443	0.2295	0.3847	0.1331	0.2130	0.1521	
4	0.2940	0.2920	0.2920	0.1521	0.2130	0.1331	
5	0.3443	0.2130	0.4590	0.1331	0.1923	0.1775	
6	0.4590	0.3060	0.1923	0.1775	0.3060	0.1331	

Grid Spacing	8	Section Depth	350	mm	L/d	25.60

Bay No.	Column Strip As %			Middle Strip As %			
	Left Support	Mid Span	Right Support	Left Support	Mid Span	Right Support	
1	0.1773	0.3171	0.4727	0.1227	0.3171	0.1773	*Deflection Okay*
2	0.4727	0.2114	0.3545	0.1773	0.1963	0.1402	
3	0.3545	0.2364	0.3927	0.1402	0.2114	0.1402	
4	0.3927	0.2364	0.3545	0.1402	0.2114	0.1402	
5	0.3545	0.2114	0.4727	0.1402	0.1963	0.1773	
6	0.4727	0.3171	0.1773	0.1773	0.3171	0.1227	

Grid Spacing	8.5	Section Depth	375	mm	L/d	24.85

Bay No.	Column Strip As %			Middle Strip As %			
	Left Support	Mid Span	Right Support	Left Support	Mid Span	Right Support	
1	0.1461	0.3636	0.4107	0.1680	0.3288	0.1680	*Deflection Okay*
2	0.4107	0.2277	0.3636	0.1680	0.2192	0.1680	
3	0.3636	0.2277	0.3919	0.1301	0.2192	0.1461	
4	0.3919	0.2277	0.3636	0.1461	0.2192	0.1301	
5	0.3636	0.2277	0.4107	0.1680	0.2192	0.1680	
6	0.4107	0.3636	0.1461	0.1680	0.3288	0.1680	

Grid Spacing	9	Section Depth	400	mm	L/d	24.66

Bay No.	Column Strip As %			Middle Strip As %			
	Left Support	Mid Span	Right Support	Left Support	Mid Span	Right Support	
1	0.1213	0.3652	0.3443	0.1565	0.3385	0.1565	*Deflection Okay*
2	0.3443	0.2452	0.3443	0.1565	0.2435	0.1565	
3	0.3443	0.2452	0.3443	0.1362	0.2435	0.1362	
4	0.3443	0.2452	0.3443	0.1362	0.2435	0.1362	
5	0.3443	0.2452	0.3443	0.1565	0.2435	0.1565	
6	0.3443	0.3652	0.1213	0.1565	0.3385	0.1565	

Job No:Design of Flat Slab Building with Varying Grid Spacing **Created By: BP**

Flat Slab Design to BS 8110 Assumed cover 25 mm

Loading Assumed fixed dead load 2.5 kN/m^2

Span	h [m]	Dead Load [kN/m2]	Imposed Load [kN/m2]	Max Load [kN/m^2]	Min Load [kN/m^2]	F
5	0.2	7.3	4	16.62	7.3	415.5
5.5	0.225	7.9	4	17.46	7.9	528.165
6	0.25	8.5	4	18.3	8.5	658.8
6.5	0.275	9.1	4	19.14	9.1	808.665
7	0.3	9.7	4	19.98	9.7	979.02
7.5	0.325	10.3	4	20.82	10.3	1171.125
8	0.35	10.9	4	21.66	10.9	1386.24
8.5	0.375	11.5	4	22.5	11.5	1625.625
9	0.4	12.1	4	23.34	12.1	1890.54
NA	0.3	NA	NA	NA	NA	NA
NA	0.3	NA	NA	NA	NA	NA

Job No:Design of Flat Slab Building with Varying Grid Spacing **Created By: BP**

Flat Slab Design to BS 8110

Moments Calculated from Moment Distribution

Negative Moments

Span	Support 1	Support 2	Support 3	Support 4	Support 5	Support 6	Support 7
5	-37.807	-101.884	-80.851	-82.147	-80.851	-101.884	-37.80735
5.5	-42.305	-142.176	-110.828	-113.599	-110.828	-142.176	-42.304782
6	-46.299	-192.490	-148.086	-153.243	-148.086	-192.490	-46.299251
6.5	-49.866	-254.273	-193.692	-202.360	-193.692	-254.273	-49.865618
7	-53.081	-329.120	-248.818	-262.304	-248.818	-329.120	-53.081259
7.5	-56.017	-418.760	-314.728	-334.509	-314.728	-418.760	-56.017489
8	-58.736	-525.047	-392.775	-420.489	-392.775	-525.047	-58.735993
8.5	-61.288	-552.960	-484.398	-521.845	-484.398	-552.960	-61.287987
9	-63.715	-580.608	-580.608	-580.608	-580.608	-580.608	-63.714838
NA							
NA							

Positive Moments

Span	Mid Span 1	Mid Span 2	Mid Span 3	Mid Span 4	Mid Span 5	Mid Span 6
5	82.088	65.699	67.822	67.822	65.699	82.08784919
5.5	118.308	90.103	94.103	94.103	90.103	118.3075685
6	164.851	120.468	127.273	127.273	120.468	164.8509846
6.5	223.250	157.706	168.413	168.413	157.706	223.250342
7	295.134	202.809	218.676	218.676	202.809	295.1337749
7.5	382.235	256.846	279.284	279.284	256.846	382.2353258
8	486.400	320.957	351.531	351.531	320.957	486.4001632
8.5	651.060	425.502	436.786	436.786	425.502	651.0604287
9	846.678	571.440	571.440	571.440	571.440	846.6777905
NA						
NA						

Job No:Design of Flat Slab Building with Varying Grid Spacing **Created By: BP**

Flat Slab Design to BS 8110

Example Reinforcement Calculation 500

Span 1 **5**

Column Strip							cover	
		Support 1		Mid Span		Support 2	assumed	bar size
M	kNm	-37.80735		82.087849		-101.8844	assumed d	
βb		1		1.078013		0.8	fy	
be	m	0.5625		1.5		1.5		
b								
Mtmax	kNm	94.125375		251.001		251.001		
						-		
M	kNm	-28.355512		45.148317		76.413297		
d	m	0.167		0.167		0.167		
K'		0.156		0.156		0.156816		
K		0.0451879		0.026981		0.0456651		
		COMP NOT REQ		COMP NOT REQ		COMP NOT REQ		
z	m	0.1581457		0.15865		0.1580466		
x	m	0.0196763		0.0185556		0.0198965		
As req	mm2/m	796.49041		474.05982		805.40729		
As prov	mm2/m	804.24772		502.65482		893.60858		
Bar size	mm2/m	16		12		16		
Spacing	mm	250		225		225		
d	m	0.167		0.169		0.167		
As%	%	0.4815855	DEF OK	0.2974289	DEF OK	0.535095	DEF OK	

Middle Strip							
		Support 1		Mid Span		Support 2	
M	kNm	-37.80735		82.087849		-101.8844	
βb		1		1.078013		0.8	
be	m	2.1875		1.25		1.25	
b							
Mtmax	kNm	0.8		209.1675		0.8	
M	kNm	-9.4518374		36.939532		-25.471099	
d	m	0.167		0.167		0.167	
K'		0.156		0.156		0.156816	
K		0.0038732		0.0264904		0.0182661	
		COMP NOT REQ		COMP NOT REQ		COMP NOT REQ	
z	m	0.15865		0.15865		0.15865	
x	m	0.0185556		0.0185556		0.0185556	
As req	mm2/m	68.053587		465.44055		320.93753	
As prov	mm2/m	392.69908		502.65482		392.69908	
Bar size	mm	10		12		10	
Spacing	mm	200		225		200	
d	m	0.17	29.41176471	0.169	29.585799	0.17	29.411765
As%	%	0.2309995		0.2974289		0.2309995	

A.4 Reinforcement Layout Drawings

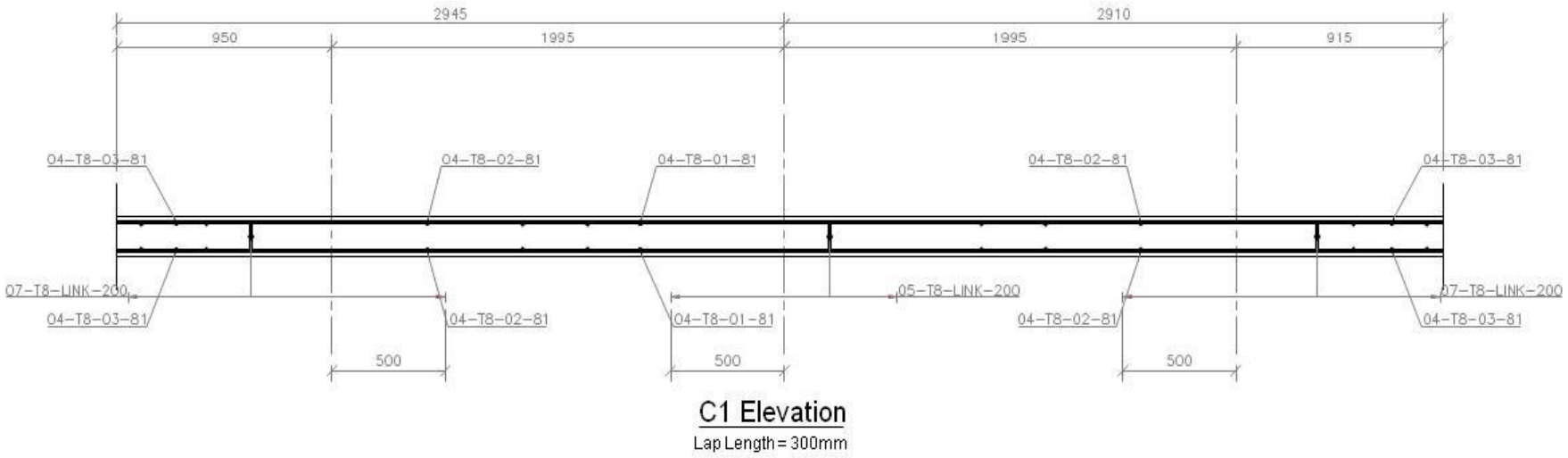

Figure A.4.1: *Elevation of reinforcement detailing of sample C1.*

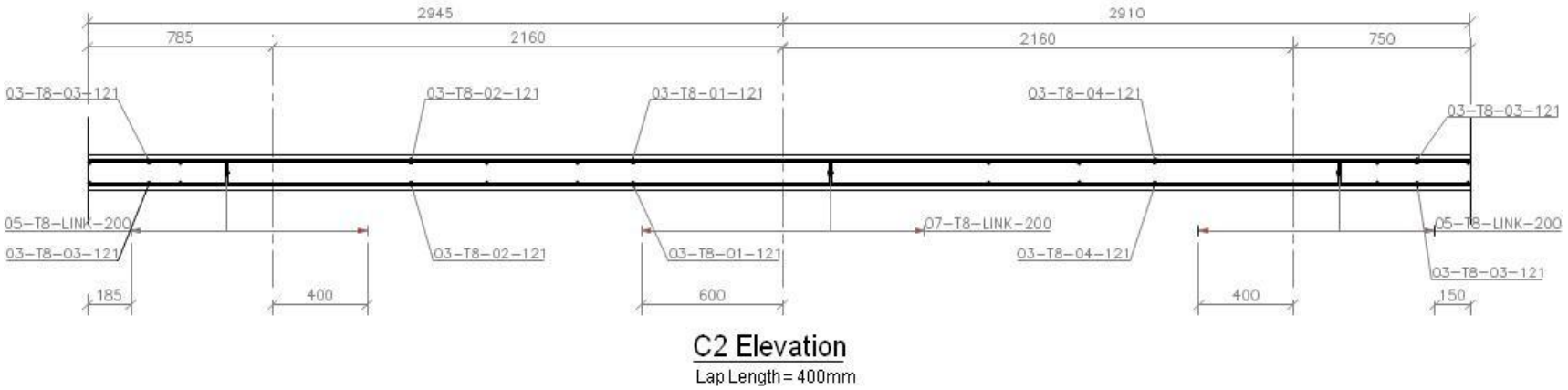

Figure A.4.2: *Elevation of reinforcement detailing of sample C2.*

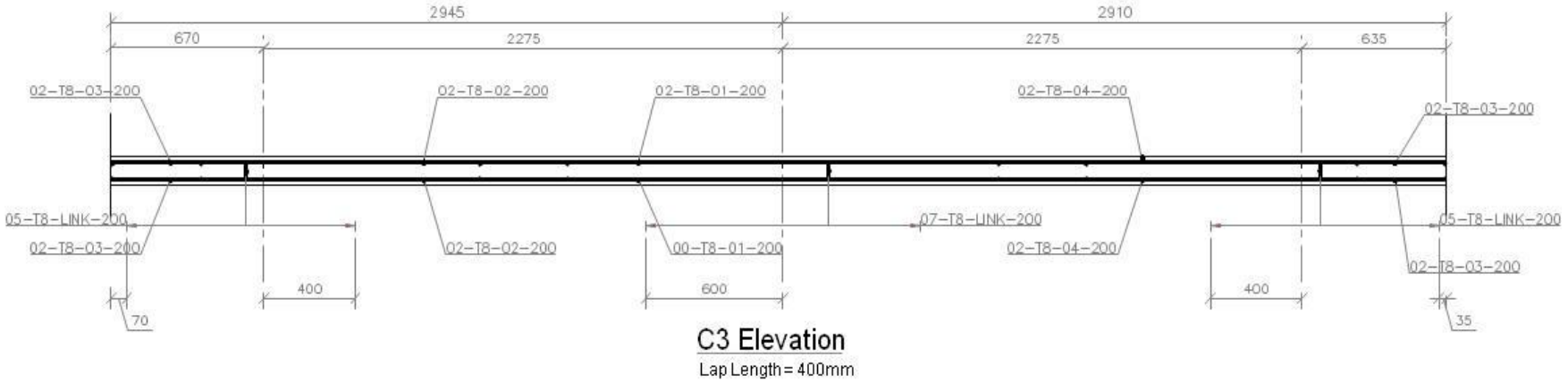

Figure A.4.3: *Elevation of reinforcement detailing of sample C3.*

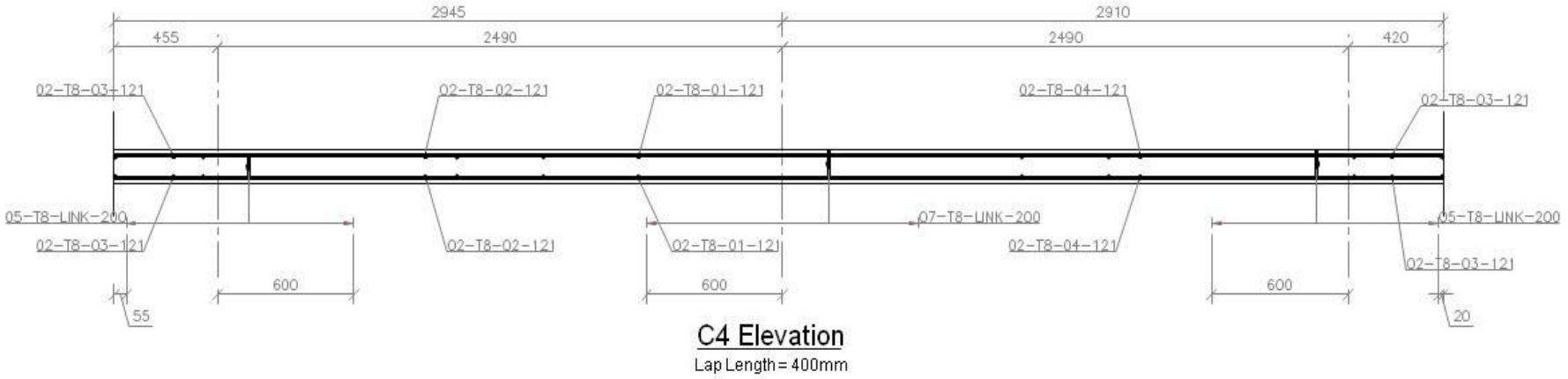

Figure A.4.4: *Elevation of reinforcement detailing of sample C4.*

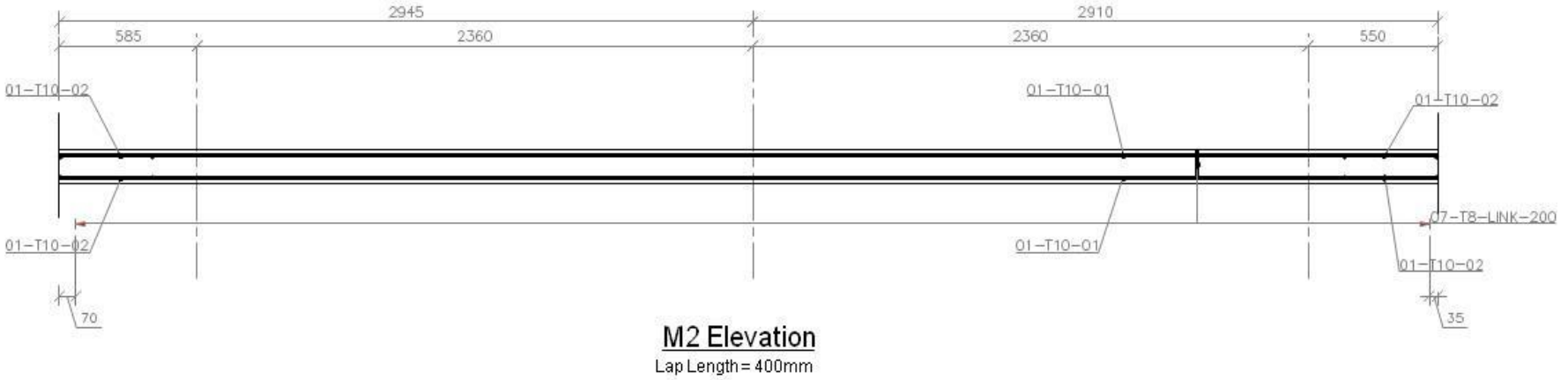

Figure A.4.5: *Elevation of reinforcement detailing of sample M2.*

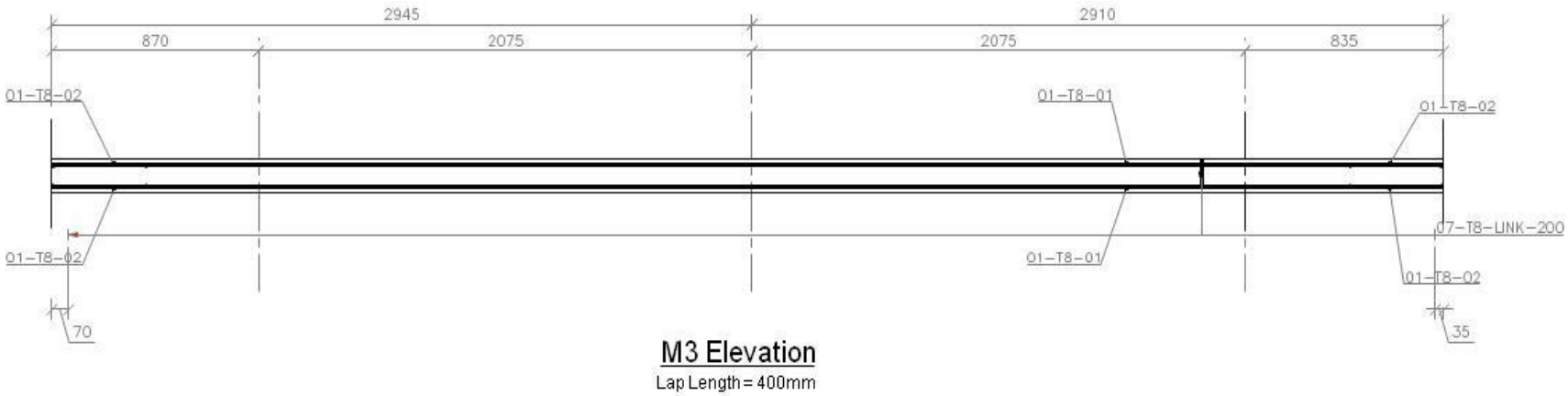

Figure A.4.6: *Elevation of reinforcement detailing of sample M3.*

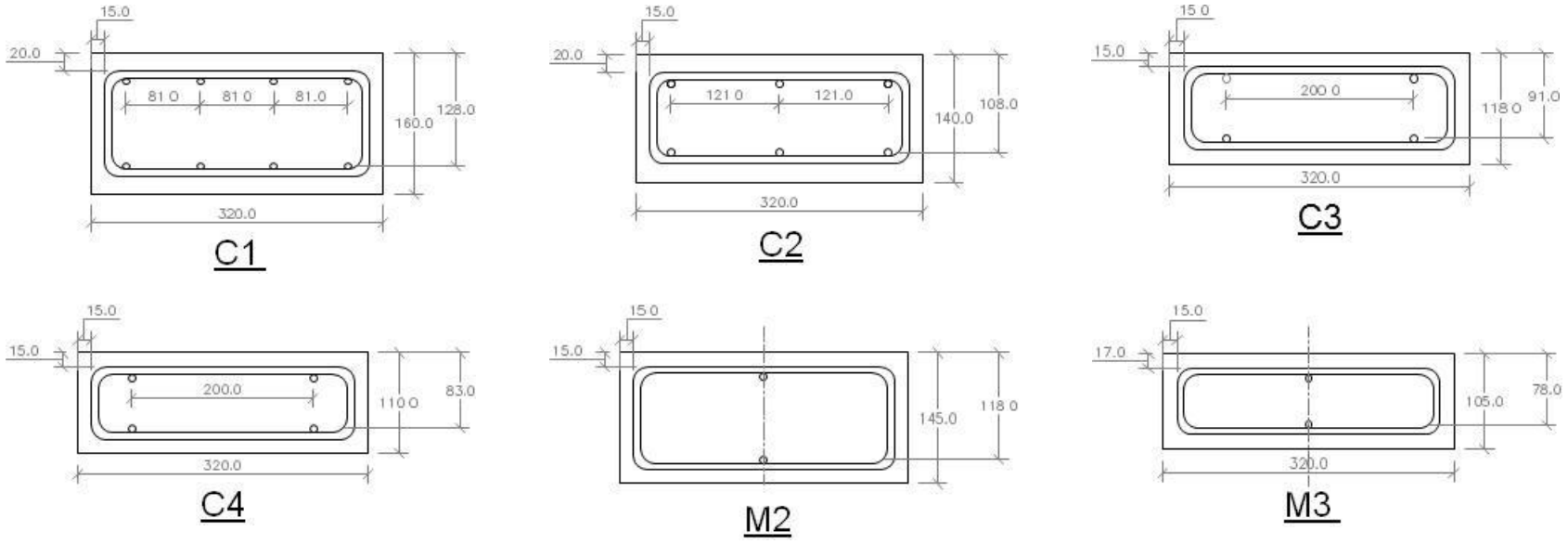

Figure A.4.7: *Cross section of reinforcement detailing for all samples.*

A.5 Experimental Results

A.5.1 Sample C1

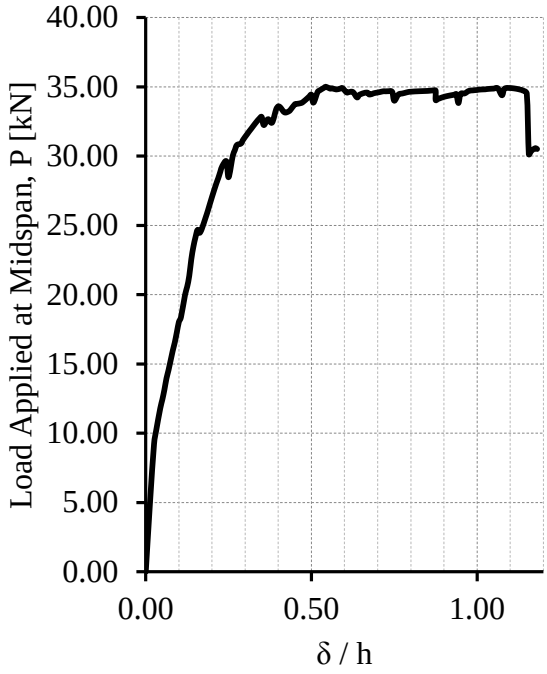

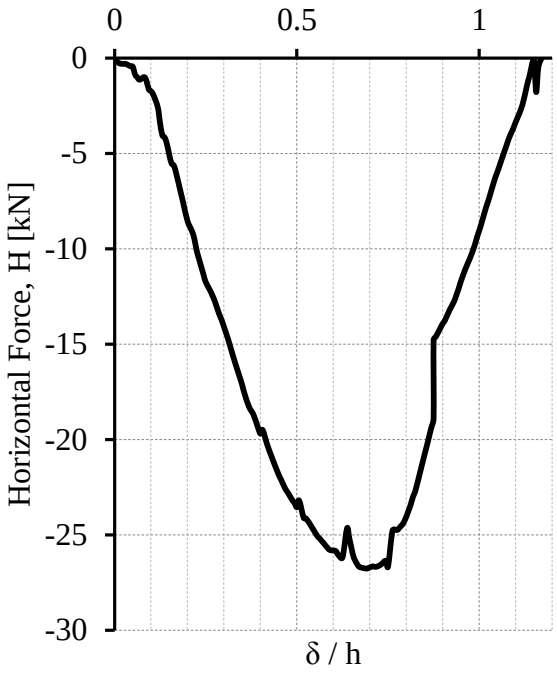

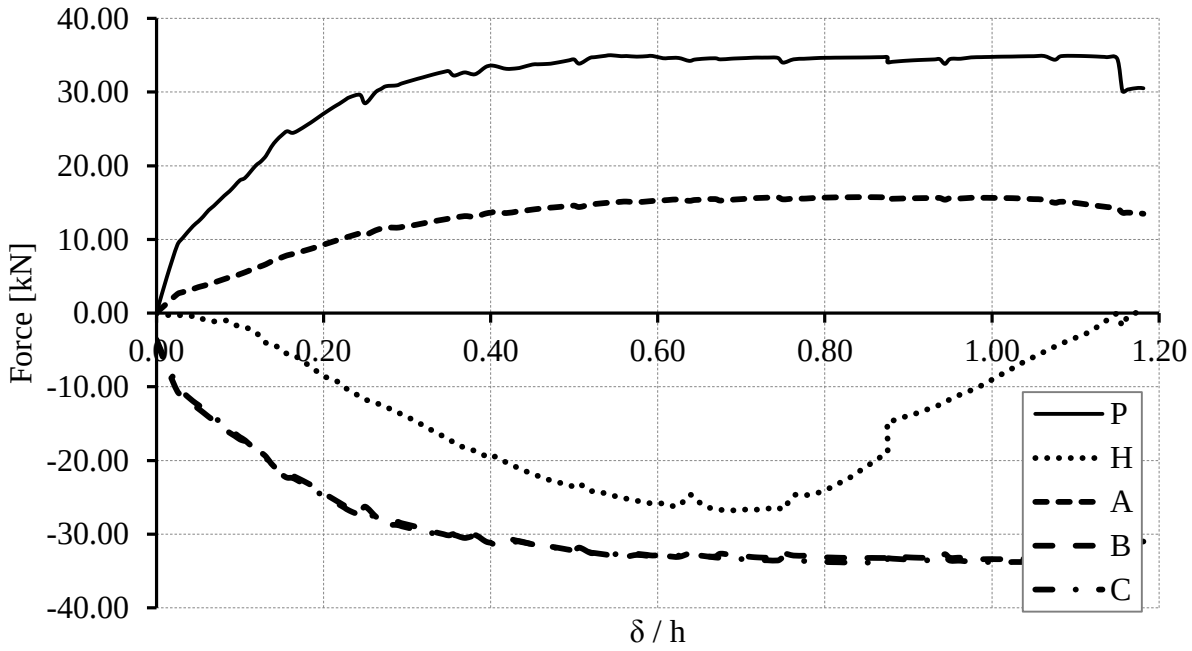

Where P = Applied Load at mid-span; H = Horizontal Force; A = Vertical reaction at end detail; B and C are vertical reactions at supports; called R_A, R_B and R_C in the main text.

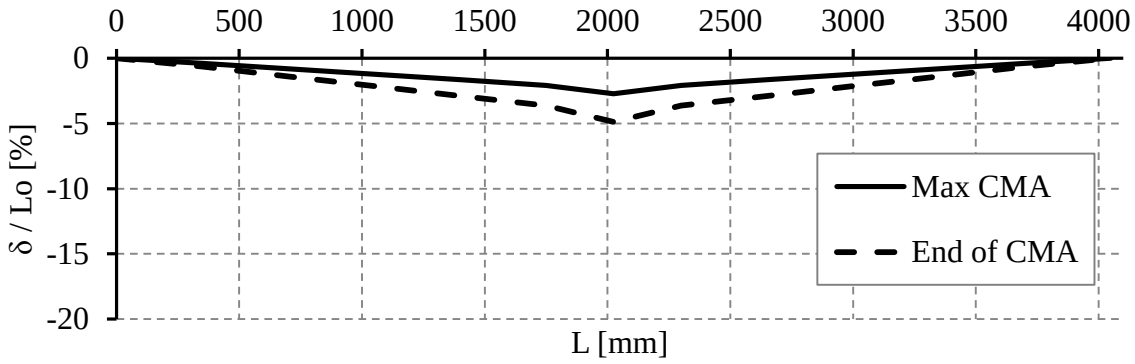

Section Properties

L_1	4050	mm		**A_s**	**A'_s**
h	160	mm	**Bar**	4 T8	4 T8
b	320	mm	**Area [mm^2]**	201.06	201.06
d	128	mm	**%**	0.49	0.49
L/d	31.64		**f_{cu}**	62.89	N/mm^2
M_{cap}	18.13	kNm	**ρ**	2244.44	kg/m^3
M'_{cap}	18.13	kNm	**E_c**	33549.20	N/mm^2

Observations in compressive phase

- The maximum compressive horizontal load of 26.686 kN occurred at a value of mid-span deflection over the section height of 0.69. The applied load at this point was 34.56 kN.
- The applied load then rose by a small amount to 35.00 kN at a value of normalised deflection of 1.15 where the bottom steel fractured at mid-span.

A.5.2 Sample C2

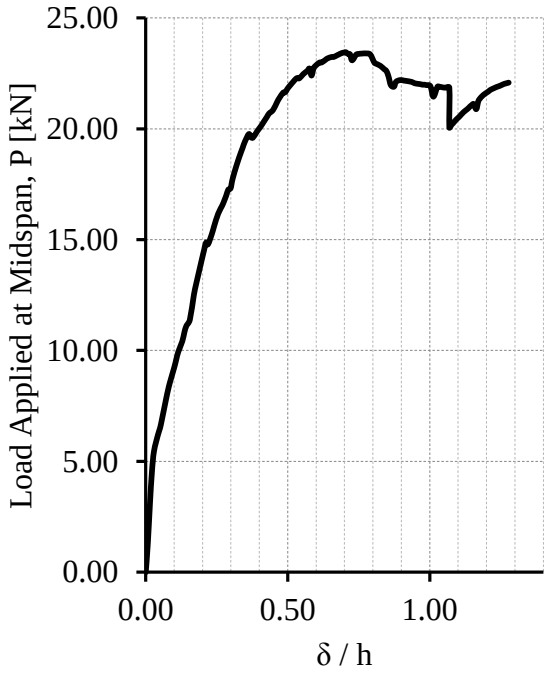

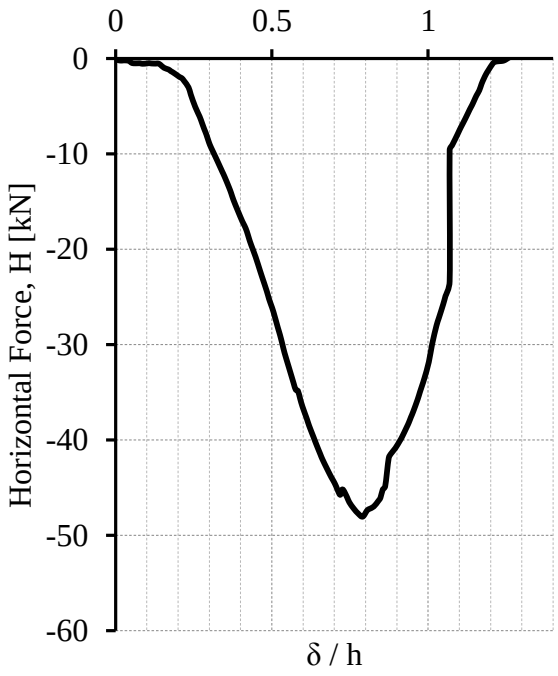

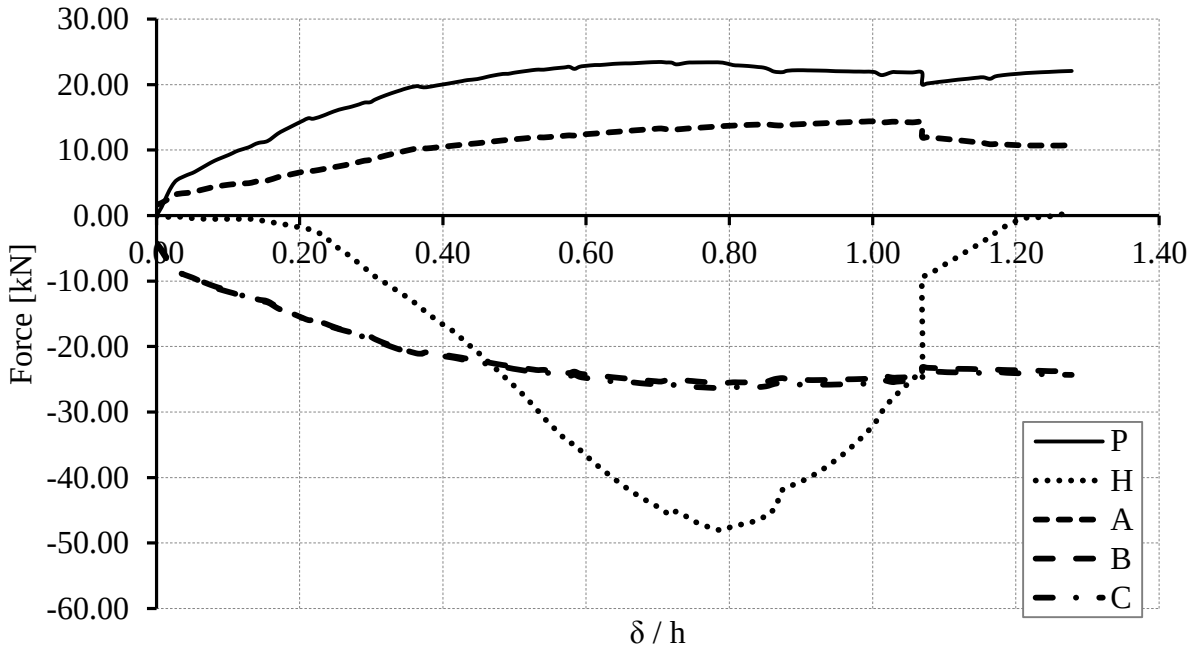

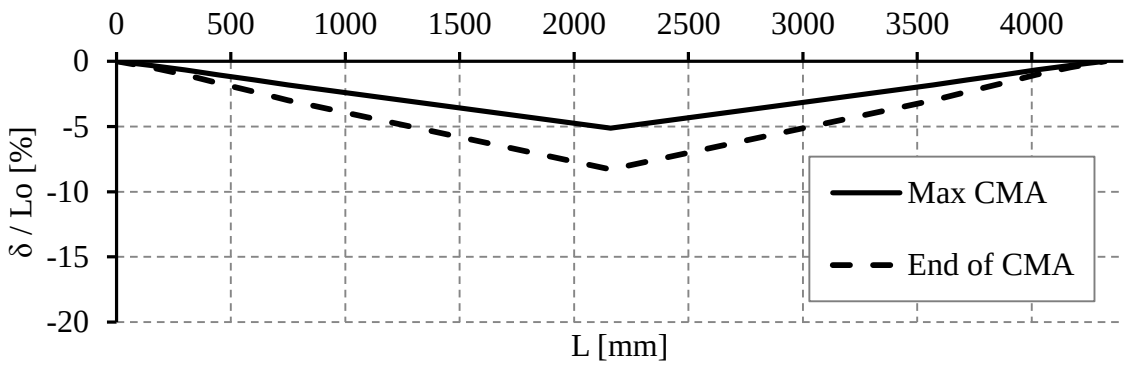

Section Properties

L_1	4320	mm		**A_s**	**A'_s**
h	140	mm	**Bar**	3 T8	3 T8
b	320	mm	**Area [mm^2]**	150.80	150.80
d	108	mm	**%**	0.44	0.44
L/d	40		**f_{cu}**	70.09	N/mm^2
M_{cap}	12.40	kNm	**ρ**	2246.81	kg/m^3
M'_{cap}	12.40	kNm	**E_c**	35418.20	N/mm^2

Observations in compressive phase

- The maximum compressive horizontal load of 48.13 kN occurred at a value of mid-span deflection over the section height of 0.79. The applied load at this point was 23.34 kN.
- The peak applied load was 23.45 kN at a value of normalised deflection of 0.70.
- Drop off in applied load at δ/h = 1.1 due to packing of load actuator.

A.5.3 Sample C3

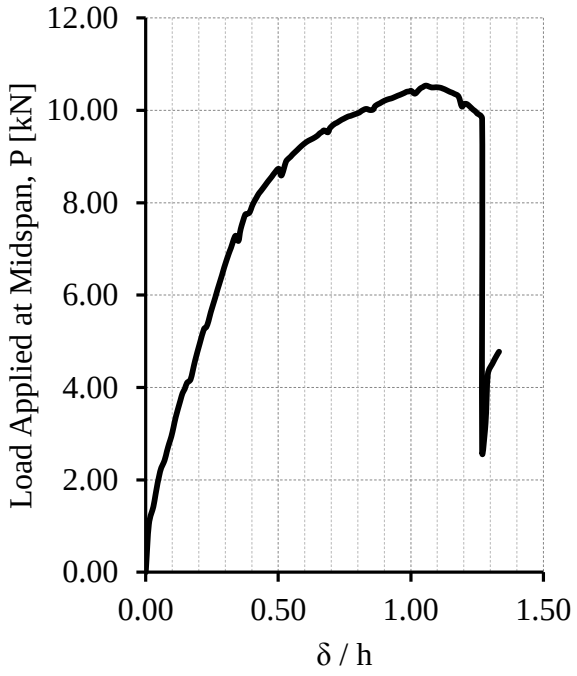

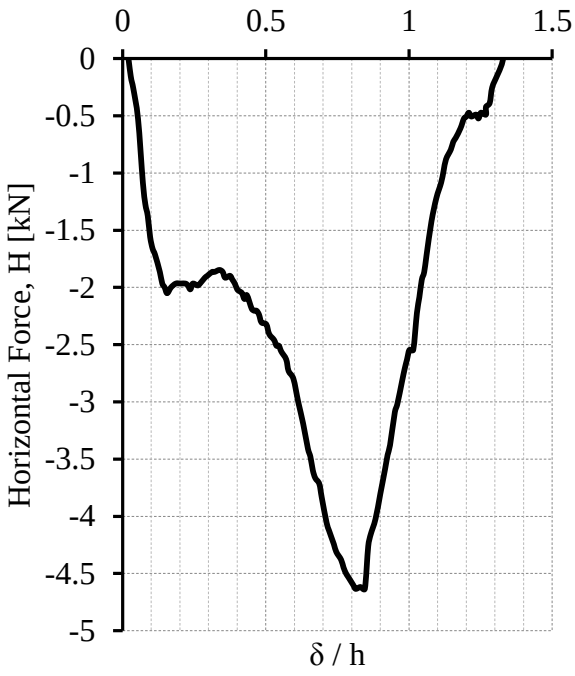

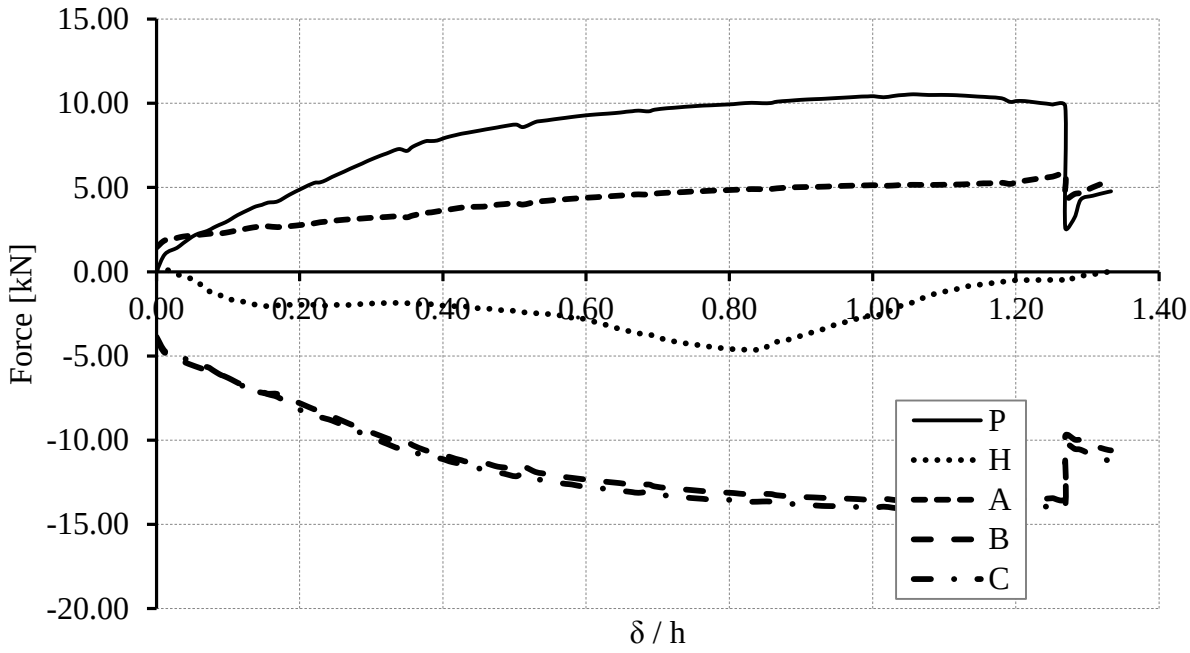

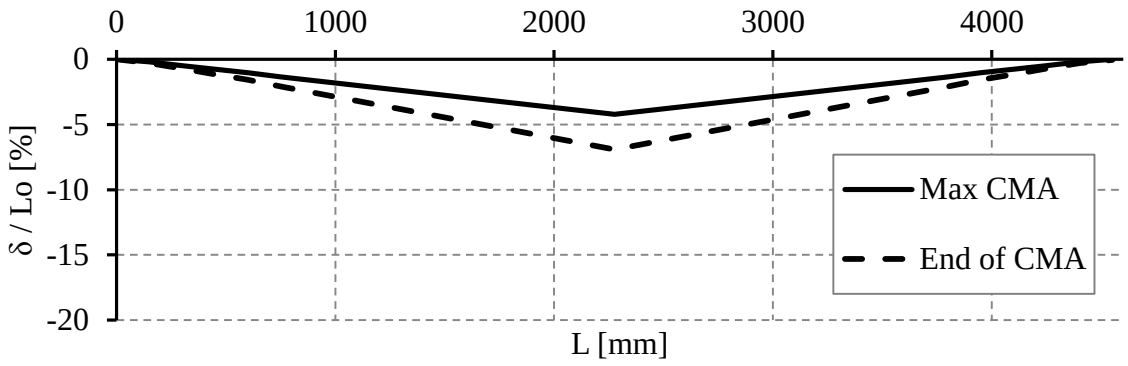

Section Properties

L_1	4550	mm		**A_s**	**A'_s**
h	118	mm	**Bar**	2 T8	2 T8
b	320	mm	**Area [mm^2]**	100.53	100.53
d	91	mm	**%**	0.35	0.35
L/d	50		**f_{cu}**	69.17	N/mm^2
M_{cap}	7.26	kNm	**ρ**	2237.27	kg/m^3
M'_{cap}	7.26	kNm	**E_c**	35184.76	N/mm^2

Observations in compressive phase

- The maximum compressive horizontal load of 4.64 kN occurred at a value of mid-span deflection over the section height of 0.81. The applied load at this point was 9.98 kN.
- The peak applied load was 10.52 kN at a value of normalised deflection of 1.05.
- Bottom rebar failed at mid-span during packing of load actuator coinciding with the end of the compressive phase.

A.5.4 Sample C4

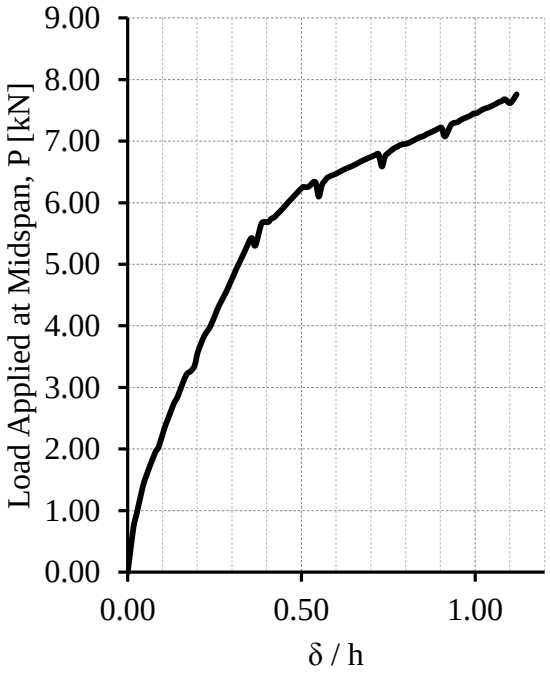

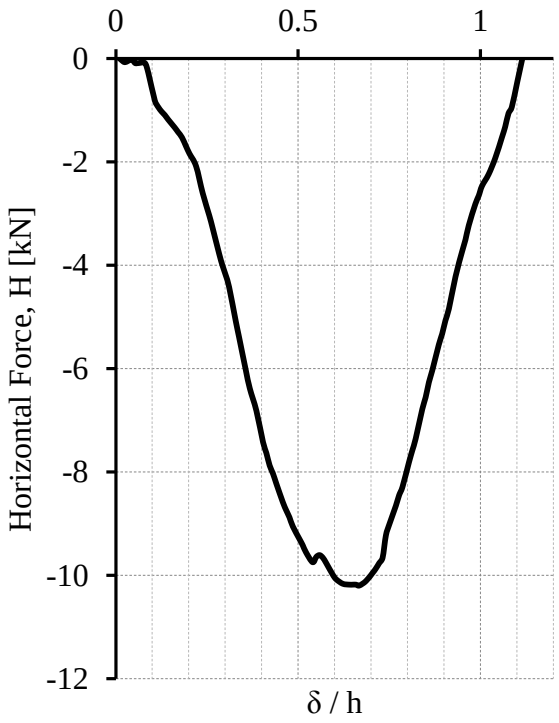

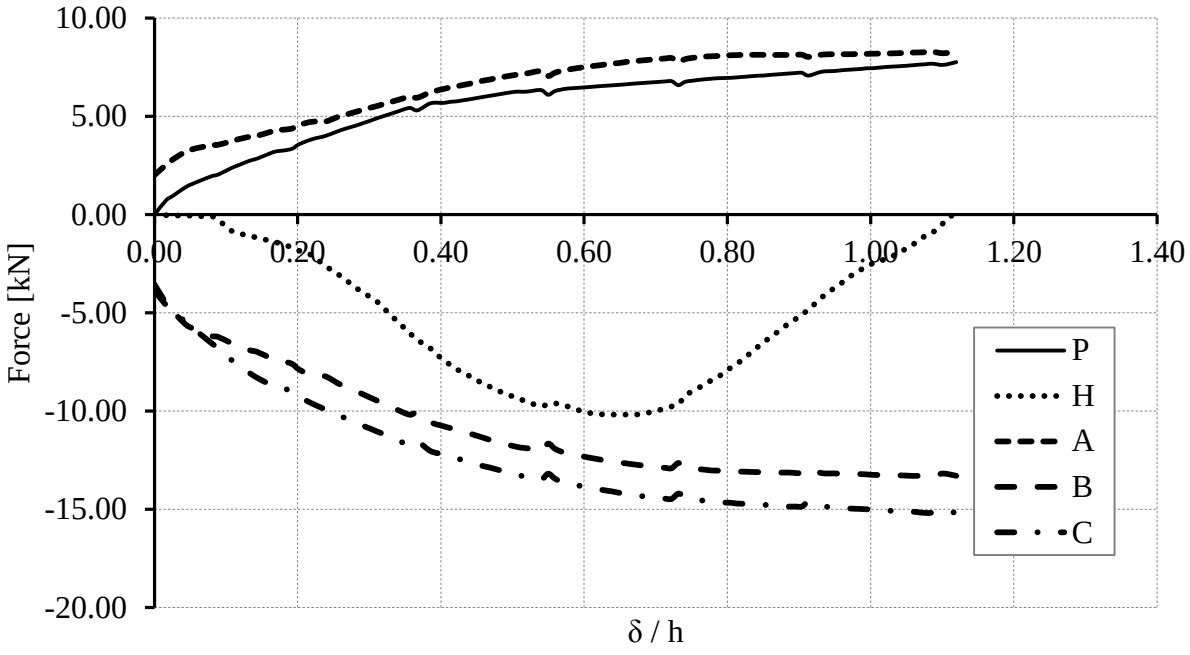

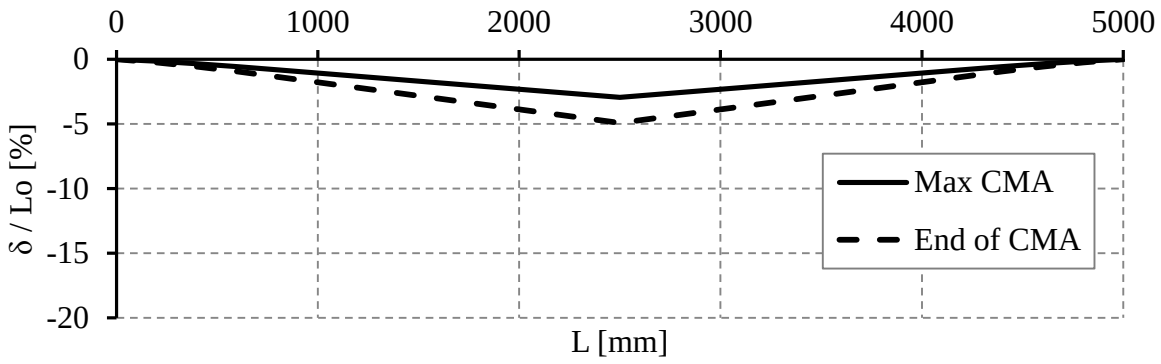

Section Properties

L_1	5000	mm		**A_s**	**A'_s**
h	110	mm	**Bar**	2 T8	2 T8
b	320	mm	**Area [mm^2]**	100.53	100.53
d	83	mm	**%**	0.38	0.38
L/d	60		**f_{cu}**	47.21	N/mm^2
M_{cap}	6.72	kNm	**ρ**	2286.86	kg/m^3
M'_{cap}	6.72	kNm	**E_c**	29069.00	N/mm^2

Observations in compressive phase

- The maximum compressive horizontal load of 10.20 kN occurred at a value of mid-span deflection over the section height of 0.67. The applied load at this point was 6.66 kN.
- The peak applied load was 7.76 kN at a value of normalised deflection of 1.12.

A.5.5 Sample M2

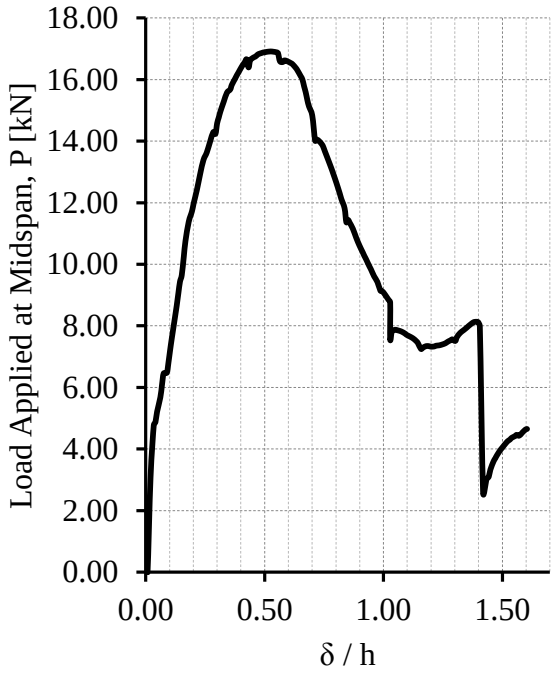

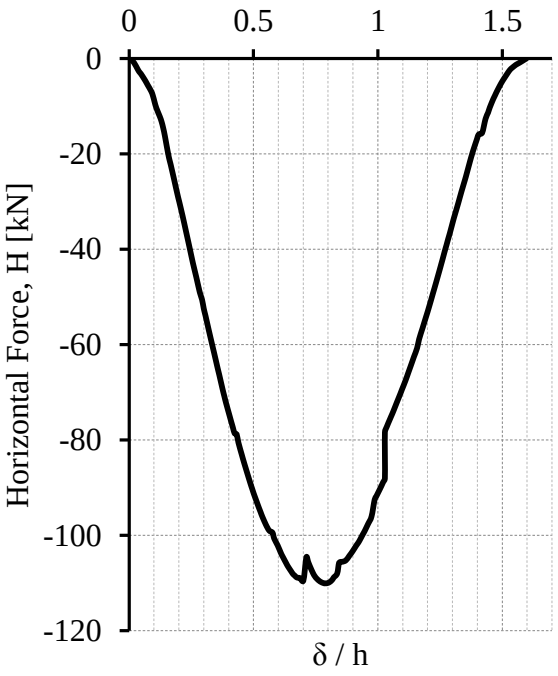

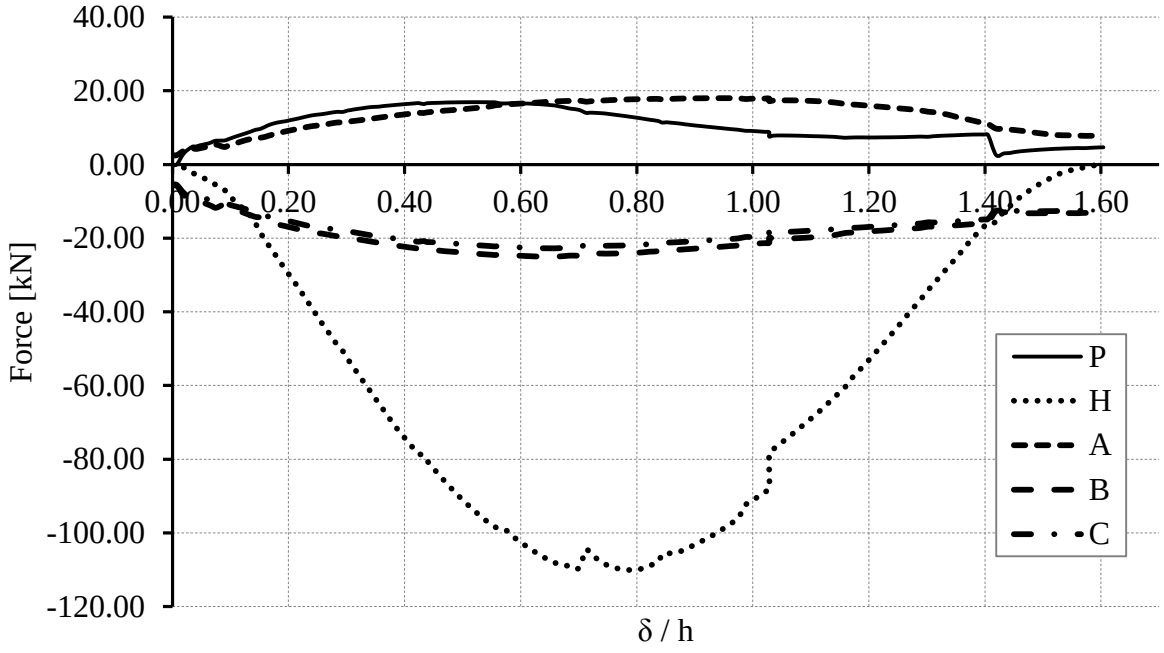

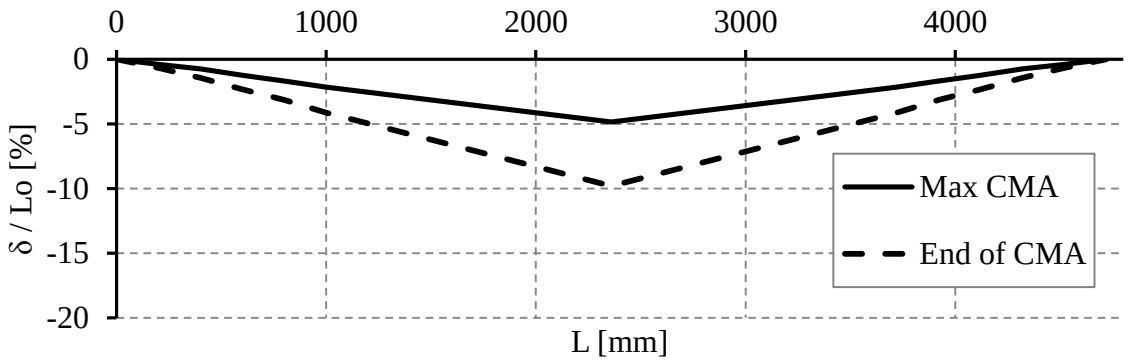

Section Properties

L_1	4720	mm		**A_s**	**A'_s**
h	145	mm	**Bar**	1 T10	1 T10
b	320	mm	**Area [mm^2]**	78.54	78.54
d	118	mm	**%**	0.21	0.21
L/d	40		**f_{cu}**	57.50	N/mm^2
M_{cap}	7.21	kNm	**ρ**	2320.49	kg/m^3
M'_{cap}	7.21	kNm	**E_c**	32081.61	N/mm^2

Observations in compressive phase

- The maximum compressive horizontal load of 110.07 kN occurred at a value of mid-span deflection over the section height of 0.80. The applied load at this point was 12.64 kN.
- The peak applied load was 16.90 kN at a value of normalised deflection of 0.52.
- Slight drop off in applied load due to packing of load actuator.
- The bottom steel fractured at mid-span at a value of normalised deflection of just over 1.4.

A.5.6 Sample M3

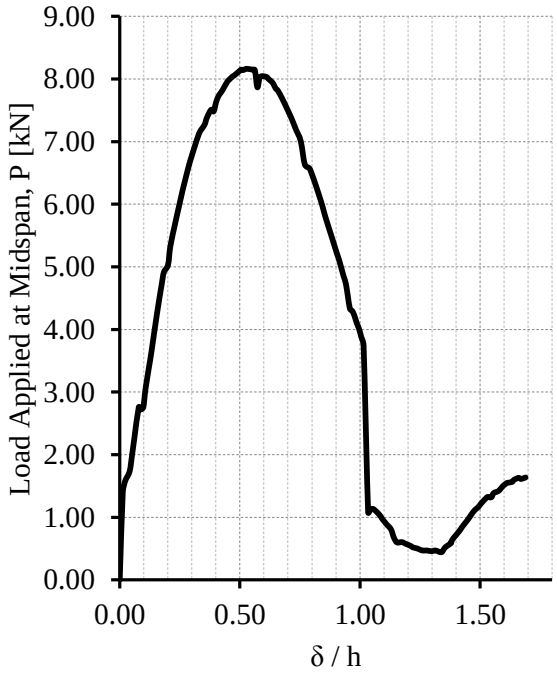

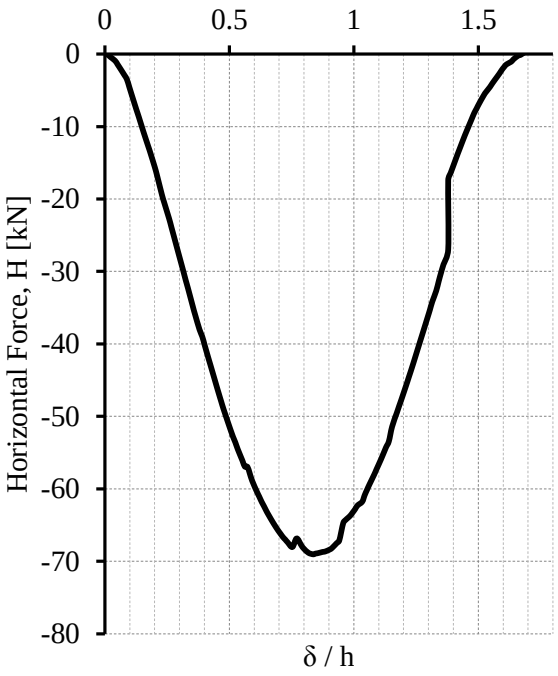

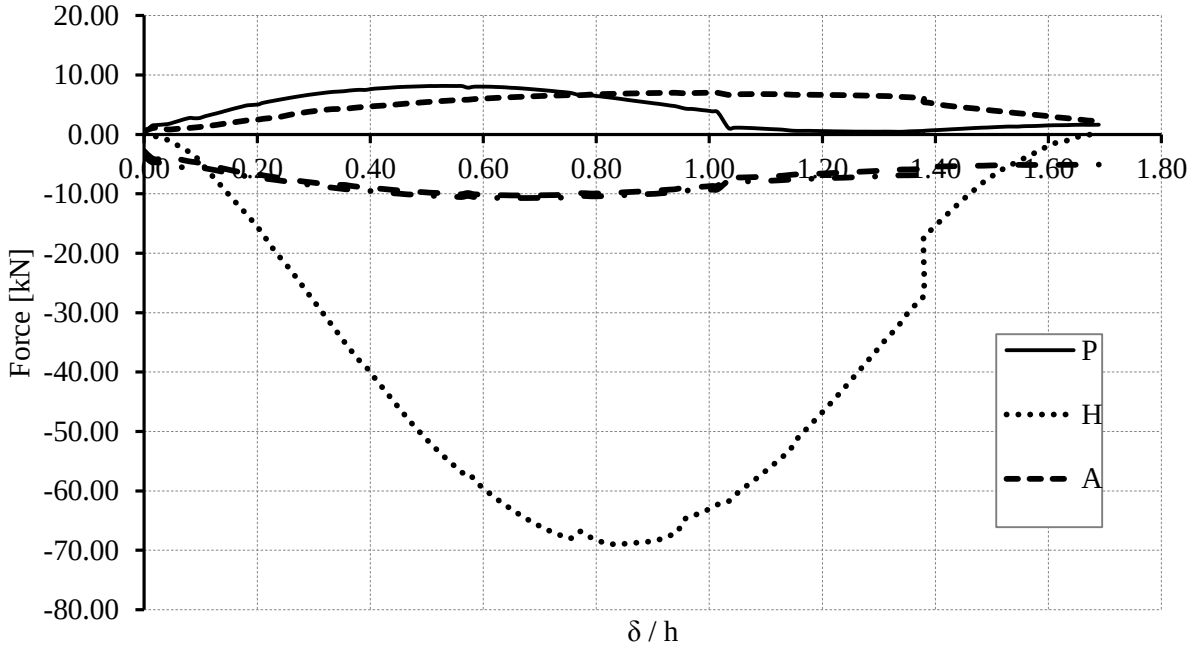

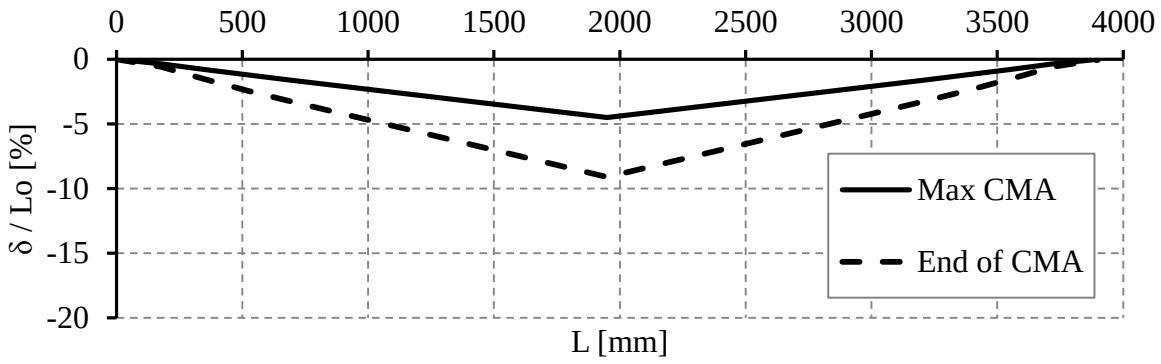

Section Properties

L_1	3900	mm		**A_s**	**A'_s**
h	105	mm	**Bar**	1 T8	1 T8
b	320	mm	**Area [mm^2]**	50.27	50.27
d	78	mm	**%**	0.20	0.20
L/d	50		**f_{cu}**	51.57	N/mm^2
M_{cap}	3.36	kNm	**ρ**	2334.37	kg/m^3
M'_{cap}	3.36	kNm	**E_c**	30381.61	N/mm^2

Observations in compressive phase

- The maximum compressive horizontal load of 69.03 kN occurred at a value of mid-span deflection over the section height of 0.84. The applied load at this point was 6.06 kN.
- The peak applied load was 8.16 kN at a value of normalised deflection of 0.52.
- The bottom steel fractured at mid-span at a value of normalised deflection of just over 1.0.

A.5.7 Sample A

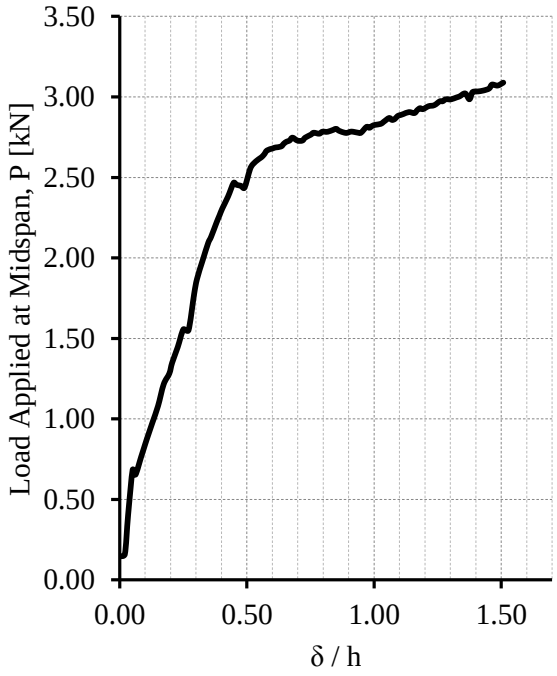
Load Applied at Midspan, P [kN]
3.50
3.00
2.50
2.00
1.50
1.00
0.50
0.00
0.00
0.50
1.00
1.50
δ / h

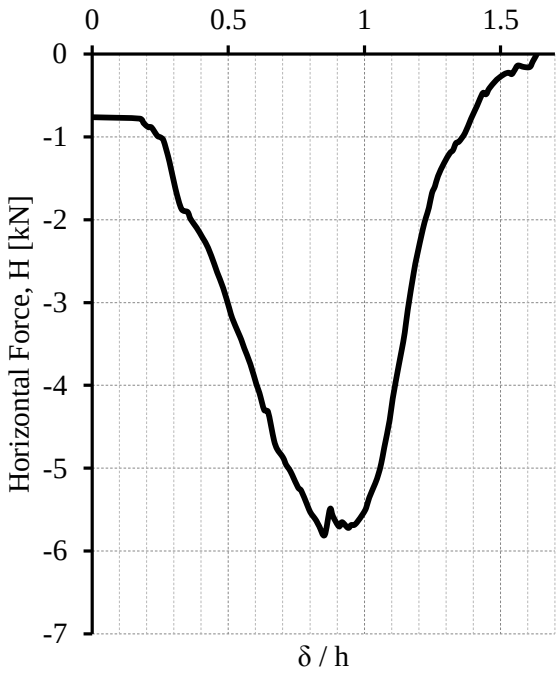
Horizontal Force, H [kN]
0
0.5
1
1.5
0
-1
-2
-3
-4
-5
-6
-7
δ / h

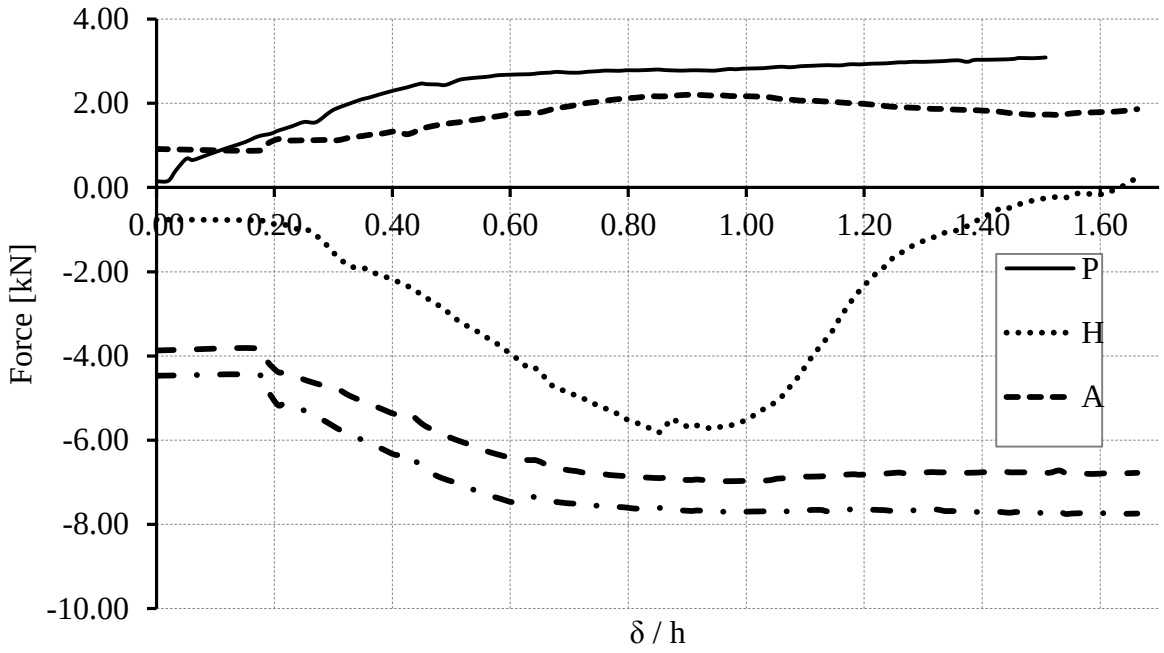
Force [kN]
4.00
2.00
0.00
-2.00
-4.00
-6.00
-8.00
-10.00
0.00
0.20
0.40
0.60
0.80
1.00
1.20
1.40
1.60
δ / h
P
H
A

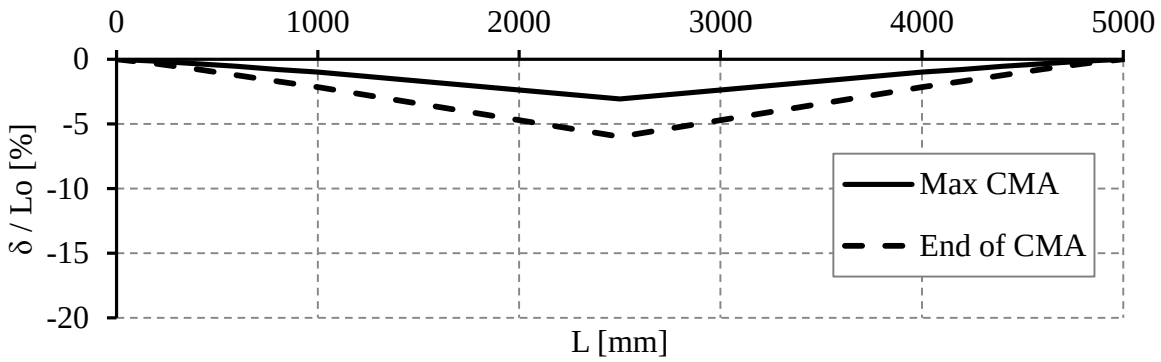

Section Properties

L_1	5000	mm		**A_s**	**A'_s**
h	90	mm	**Bar**	1 T8	1 T8
b	275	mm	**Area [mm^2]**	50.27	50.27
d	75	mm	**%**	0.24	0.24
L/d	66.67		**f_{cu}**	54.60	N/mm^2
M_{cap}	2.86	kNm	**ρ**	2324.83	kg/m^3
M'_{cap}	2.86	kNm	**E_c**	31260.97	N/mm^2

Observations in compressive phase

- The maximum compressive horizontal load of 5.81 kN occurred at a value of mid-span deflection over the section height of 0.85. The applied load at this point was 2.72kN.
- The peak applied load was 3.08 kN at a value of normalised deflection of 1.66.

A.5.8 Sample S2

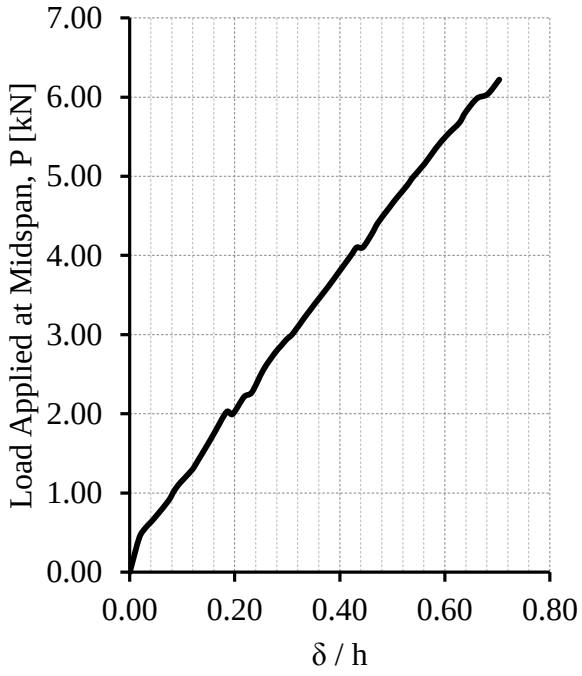

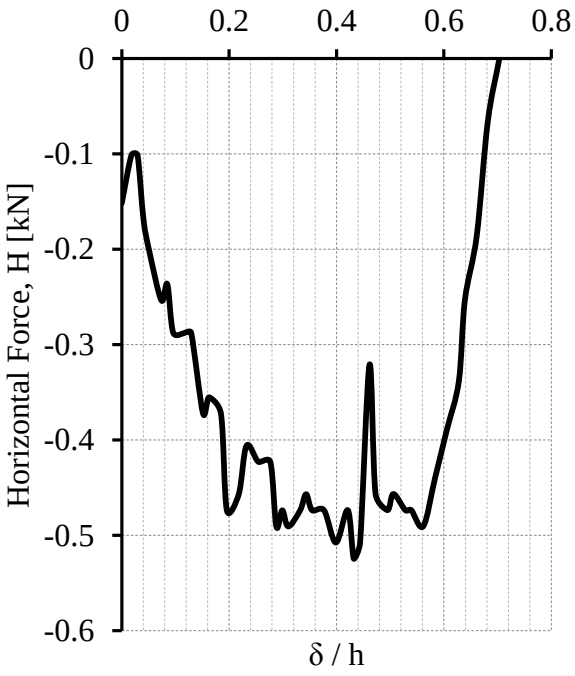

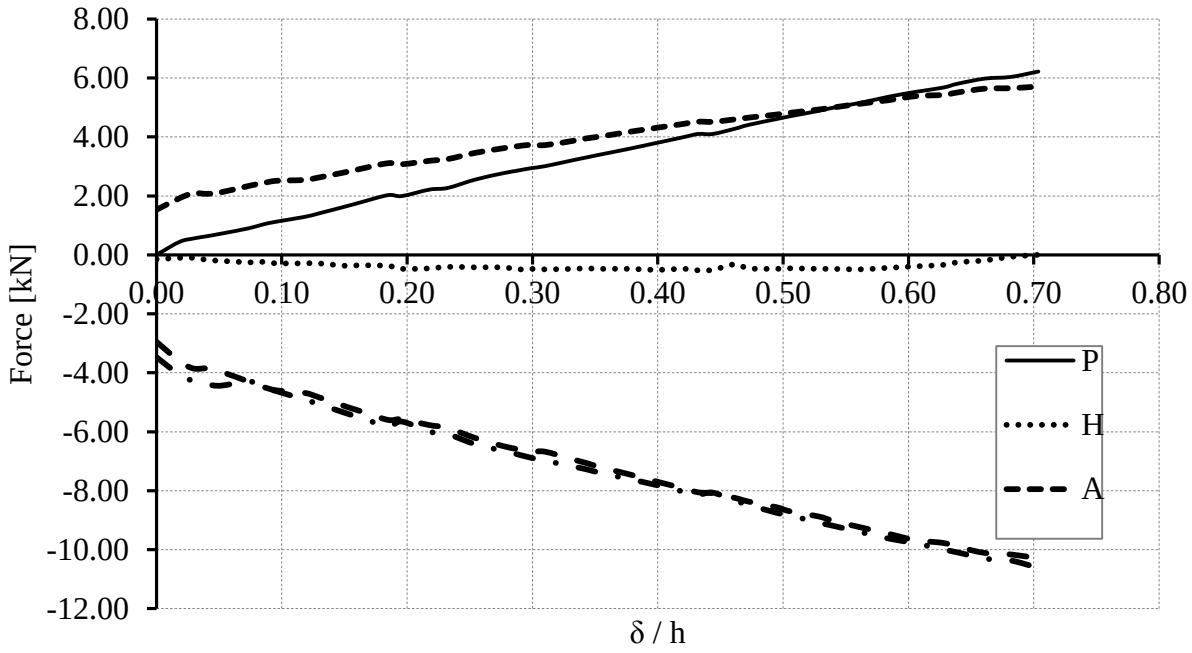

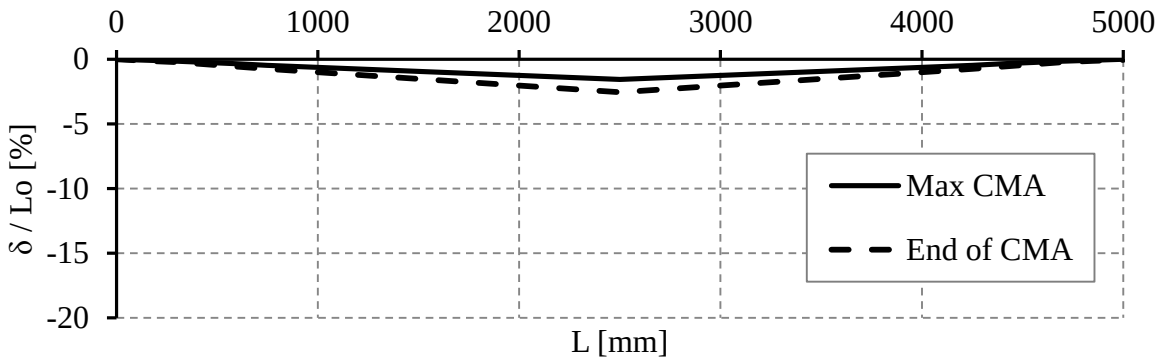

Section Properties

L_1	5000	mm		**A_s**	**A'_s**
h	90	mm	**Bar**	2 T8	2 T8
b	275	mm	**Area [mm^2]**	100.53	100.53
d	75	mm	**%**	0.49	0.49
L/d	66.67		**f_{cu}**	70.48	N/mm^2
M_{cap}	5.21	kNm	**ρ**	2228.42	kg/m^3
M'_{cap}	5.21	kNm	**E_c**	35517.23	N/mm^2

Observations in compressive phase

- The maximum compressive horizontal load of 0.52 kN occurred at a value of mid-span deflection over the section height of 0.43. The applied load at this point was 4.10 kN.
- The peak applied load was 6.22 kN at a value of normalised deflection of 0.70.

A.5.9 Sample S3

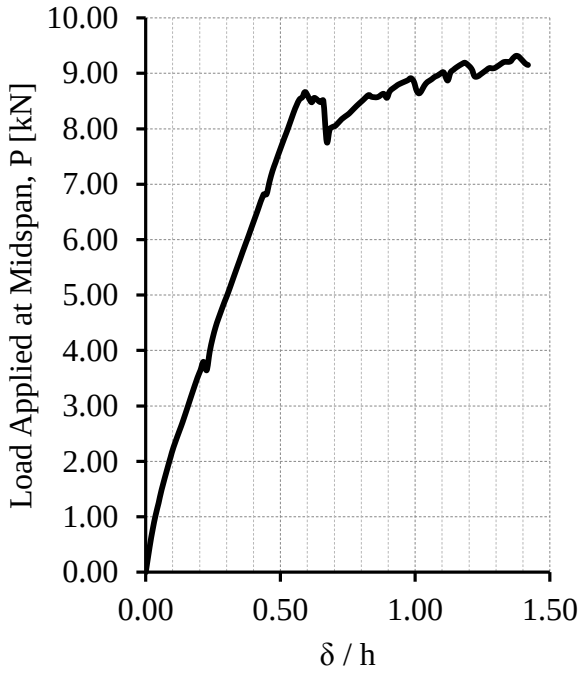

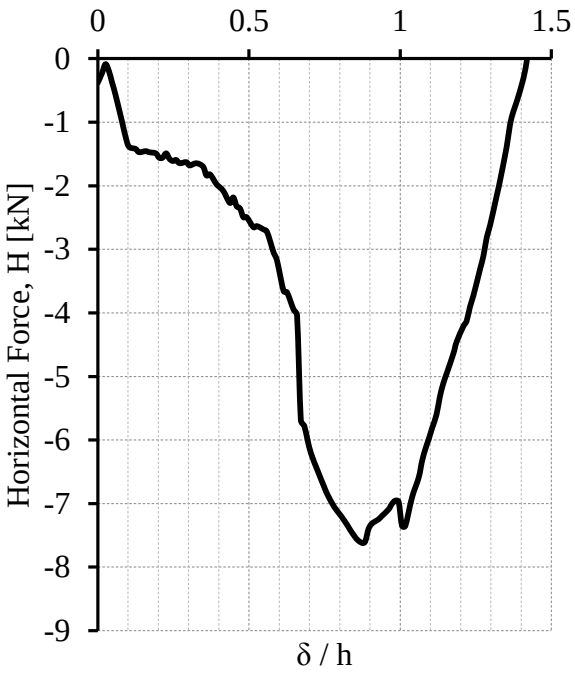

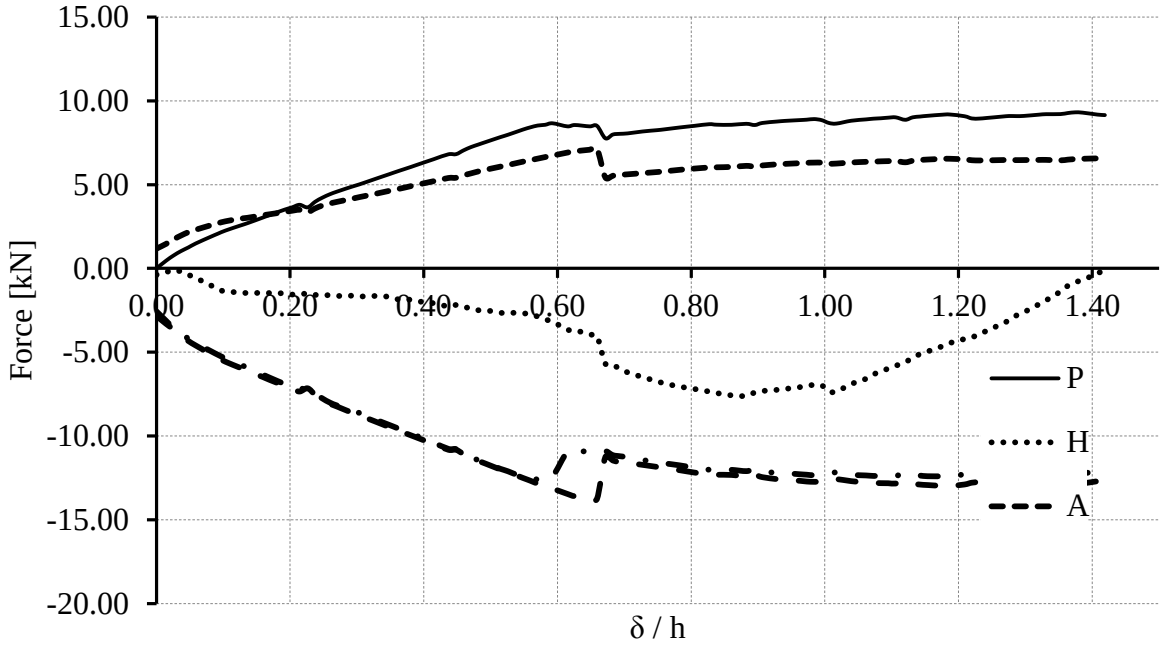

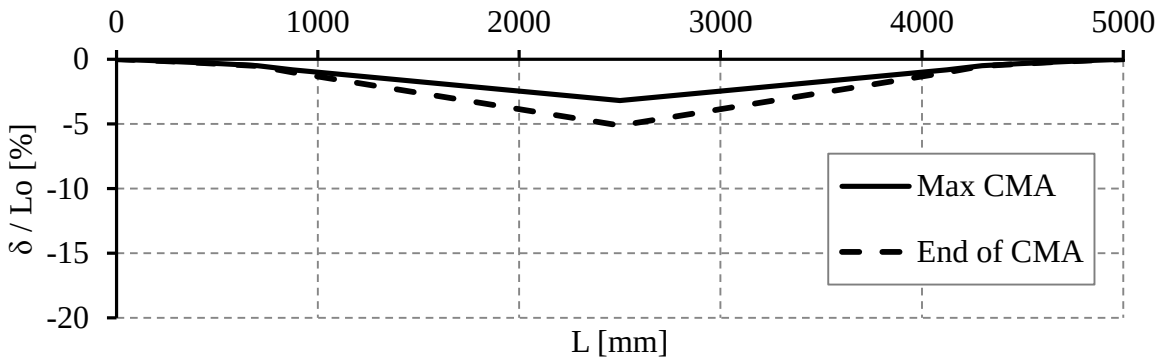

Section Properties

L_1	5000	mm		**A_s**	**A'_s**
h	90	mm	**Bar**	3 T8	3 T8
b	275	mm	**Area [mm^2]**	150.80	150.80
d	75	mm	**%**	0.73	0.73
L/d	66.67		**f_{cu}**	49.33	N/mm^2
M_{cap}	7.37	kNm	**ρ**	2320.54	kg/m^3
M_{cap}	7.37	kNm	**E_c**	29713.61	N/mm^2

Observations in compressive phase

- The maximum compressive horizontal load of 7.61 kN occurred at a value of mid-span deflection over the section height of 0.88. The applied load at this point was 8.64 kN.
- The peak applied load was 9.32 kN at a value of normalised deflection of 1.37.
- At d/h of 0.67 significant concrete cracking occurred at the end of top steel at support causing a drop off in applied load.

A.5.10 Sample E1

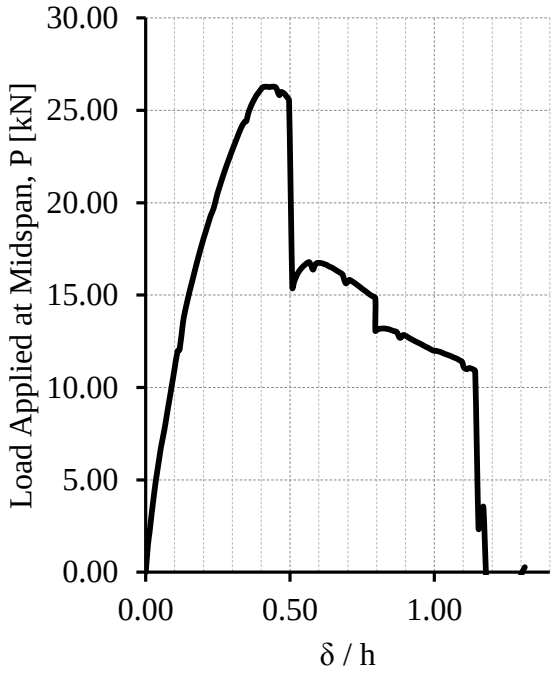

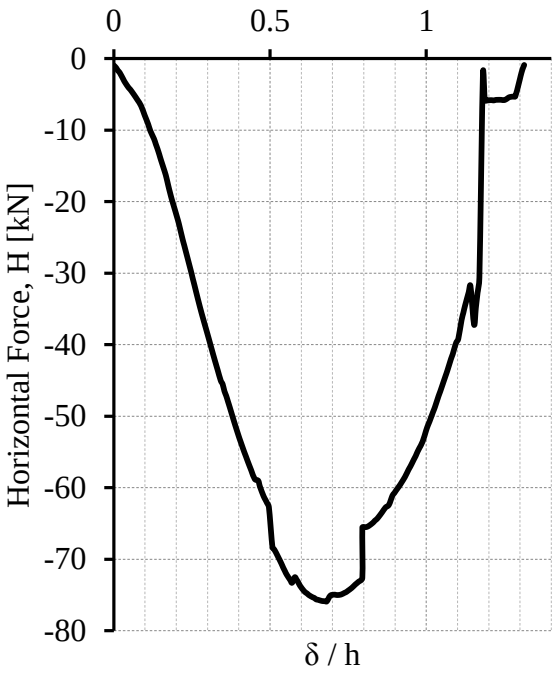

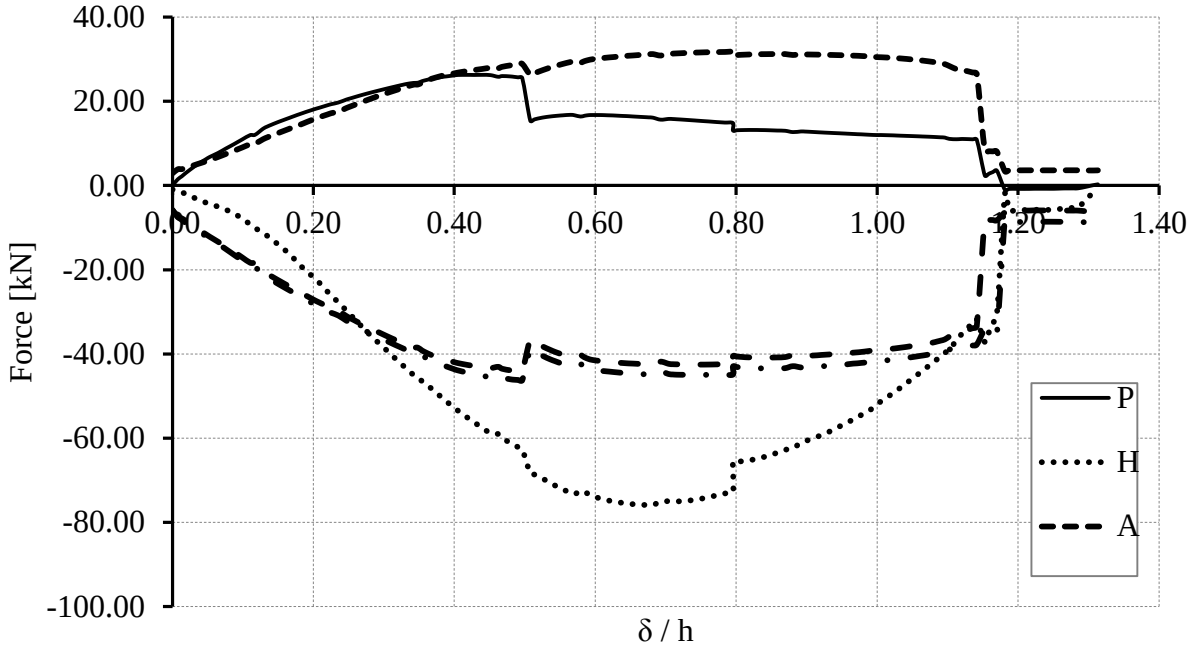

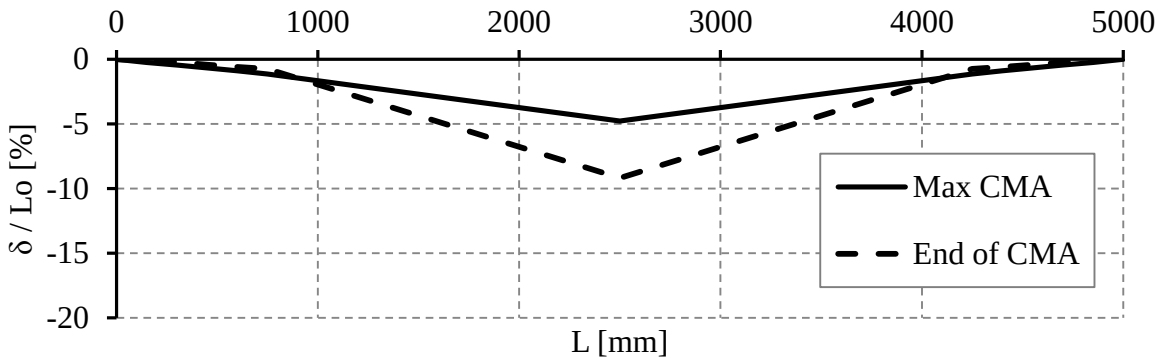

Section Properties

L_1	5000	mm		**A_s**	**A'_s**
h	175	mm	**Bar**	2 T8	2 T12
b	225	mm	**Area [mm^2]**	100.53	226.19
d	143	mm	**%**	0.31	0.70
L/d	34.965		**f_{cu}**	66.15	N/mm^2
M_{cap}	12.28	kNm	**ρ**	2249.41	kg/m^3
M'_{cap}	21.76	kNm	**E_c**	34408.92	N/mm^2

Observations in compressive phase

- The maximum compressive horizontal load of 75.90 kN occurred at a value of mid-span deflection over the section height of 0.68. The applied load at this point was 16.12 kN.
- The peak applied load was 26.28 kN at a value of normalised deflection of 0.44.
- At d/h of 0.5 bottom rebar fractured at mid-span.
- At d/h of 0.8 applied load dropped off due to packing of load actuator.
- At d/h of 1.15 top rebar fractured at support R_B.

A.5.11 Sample E2

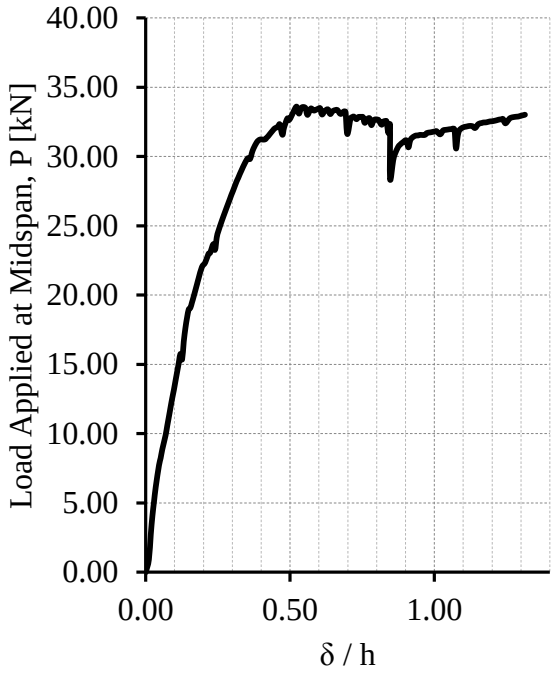

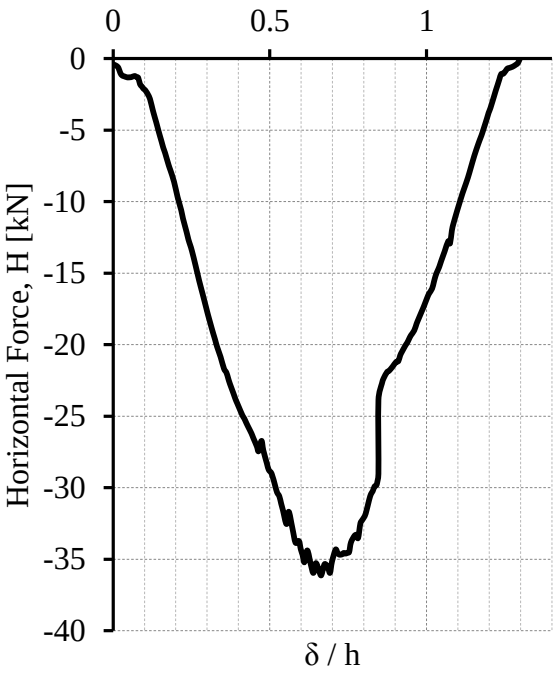

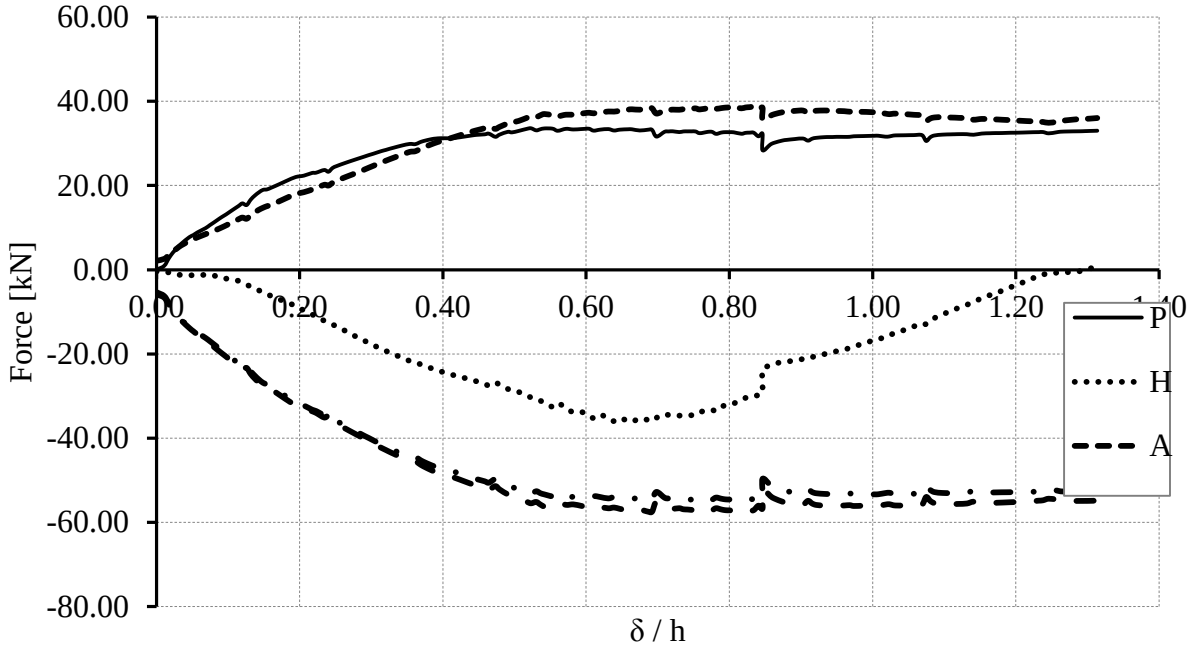

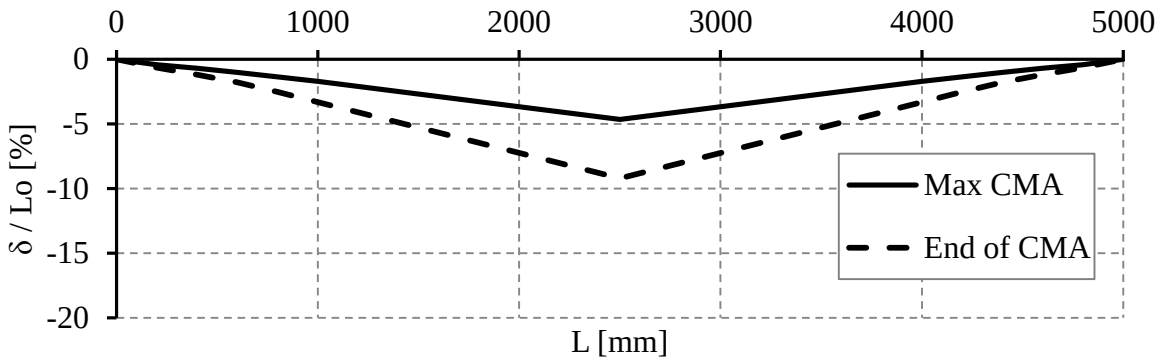

Section Properties

L_1	5000	mm		**A_s**	**A'_s**
h	175	mm	**Bar**	3 T8	3 T12
b	225	mm	**Area [mm^2]**	150.80	339.29
d	143	mm	**%**	0.47	1.05
L/d	34.965		**f_{cu}**	41.19	N/mm^2
M_{cap}	16.56	kNm	**ρ**	2297.40	kg/m^3
M'_{cap}	31.06	kNm	**E_c**	27150.60	N/mm^2

Observations in compressive phase

- The maximum compressive horizontal load of 36.26 kN occurred at a value of mid-span deflection over the section height of 0.66. The applied load at this point was 33.34 kN.
- The peak applied load was 33.6 kN at a value of normalised deflection of 0.52.
- Packing of load actuator at d/h = 0.85.

A.5.12 Sample E3

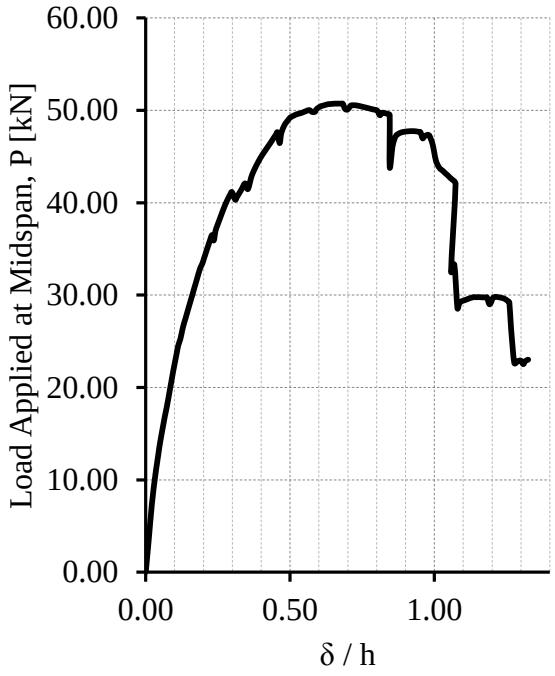

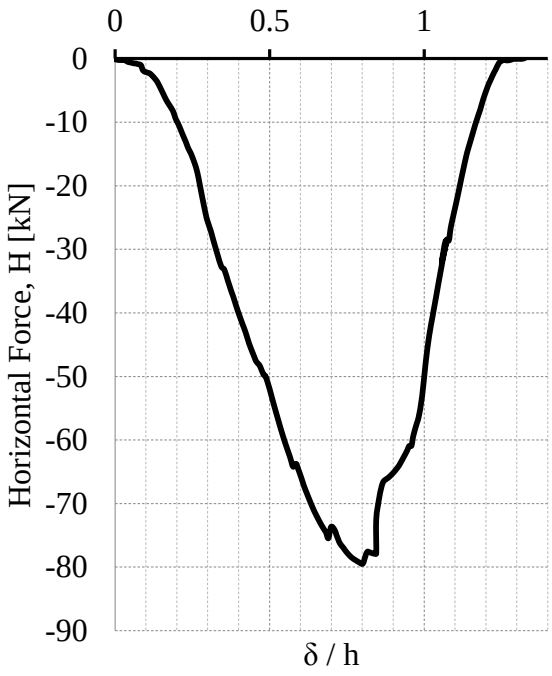

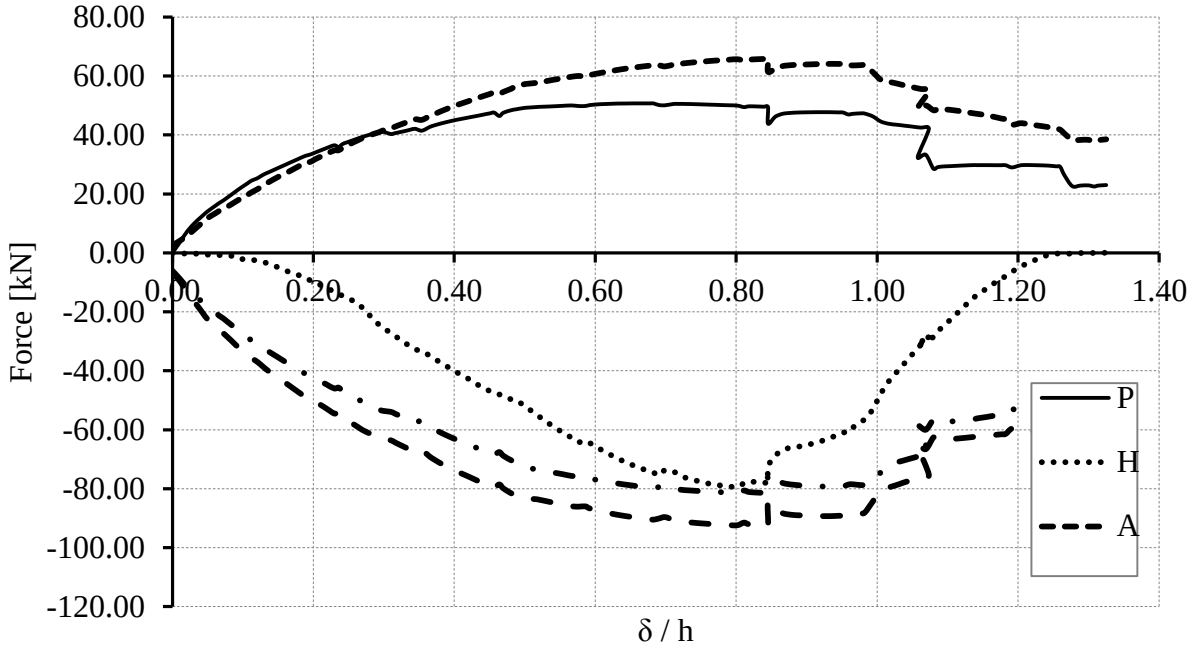

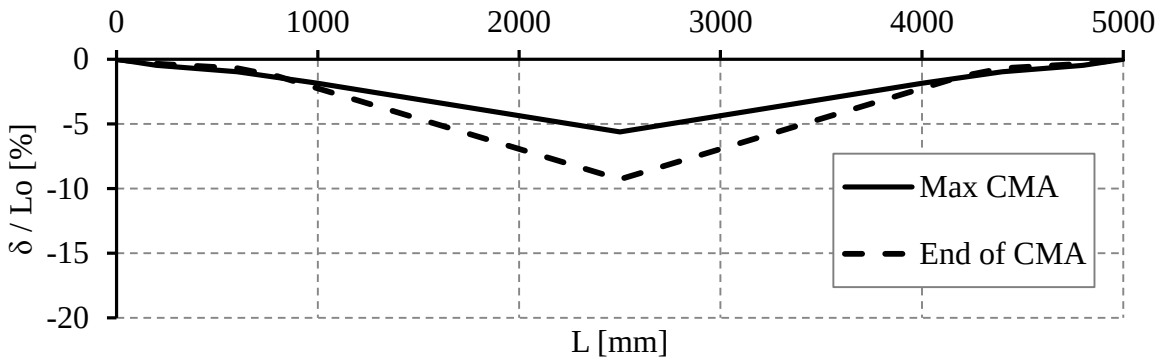

Section Properties

L_1	5000	mm		**A_s**	**A'_s**
h	175	mm	**Bar**	3 T10	3 T16
b	320	mm	**Area [mm^2]**	235.62	603.19
d	144	mm	**%**	0.51	1.31
L/d	34.722		**f_{cu}**	54.21	N/mm^2
M_{cap}	23.44	kNm	**ρ**	2316.55	kg/m^3
M_{cap}	54.03	kNm	**E_c**	31149.84	N/mm^2

Observations in compressive phase

- The maximum compressive horizontal load of 79.45 kN occurred at a value of mid-span deflection over the section height of 0.80. The applied load at this point was 49.96 kN.
- The peak applied load was 50.72 kN at a value of normalised deflection of 0.65.
- Packing of load actuator at δ/h = 085.
- At δ/h = 1.06 applied load reduced due to cracking at support B.
- At δ/h = 1.3 bottom rebar at mid-span fractured.

A.6 Photos of Samples

Sample C1

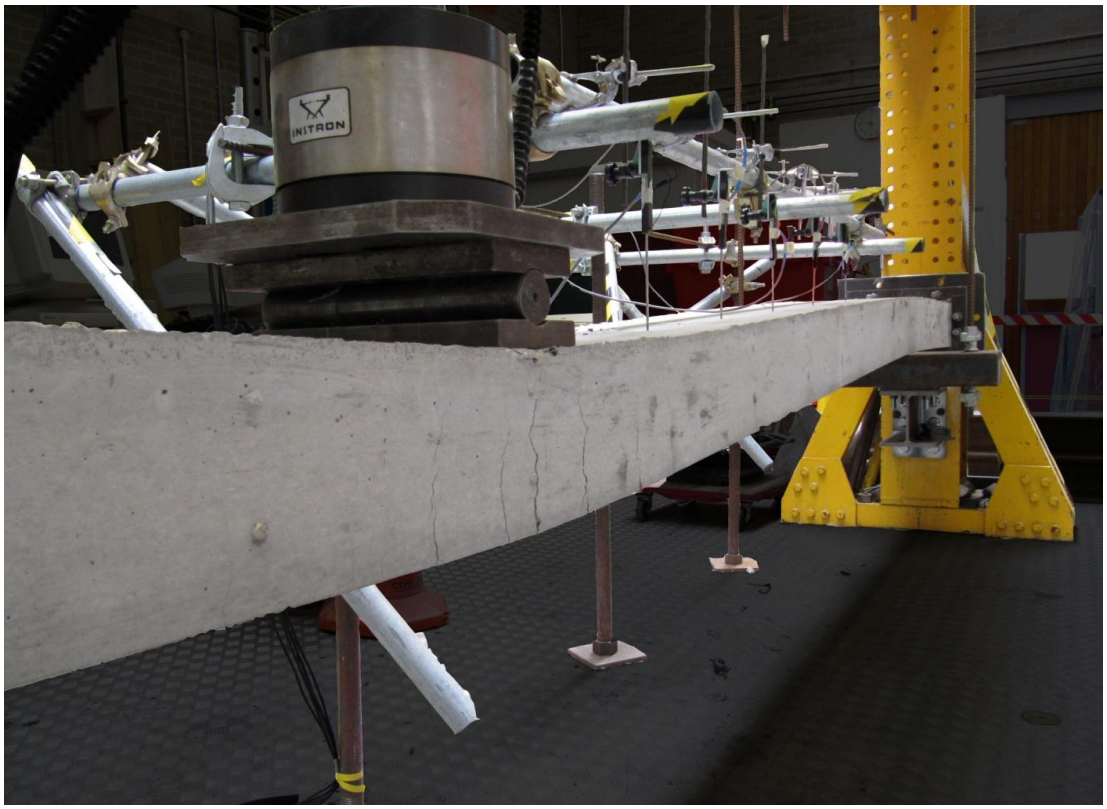

Figure A.6.1: *Loaded sample view from mid-span to hanger C at approximately H_{max} (δ=100mm).*

Figure A.6.2: *Mid-span crack pattern of underside of sample at approximately H_{max} (δ=100mm).*

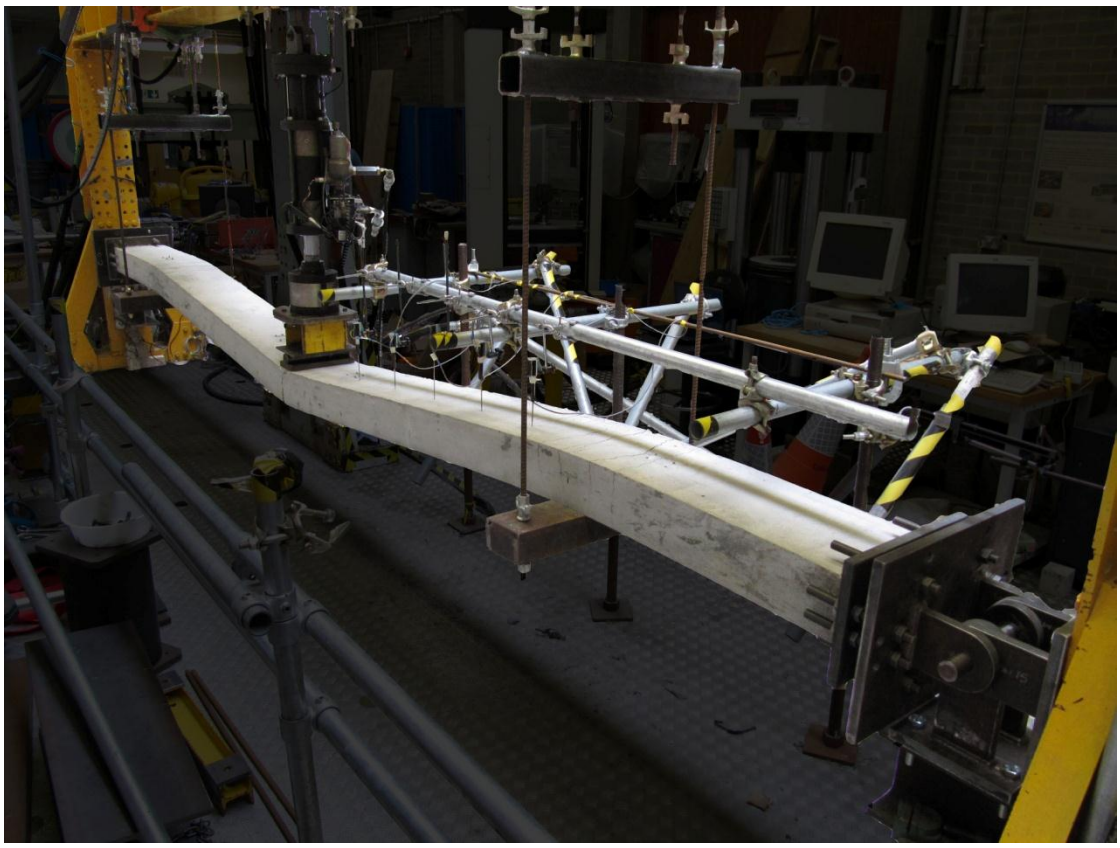

Figure A.6.3: *Loaded sample view at approximately the end of CMA phase (δ=200mm).*

Figure A.6.4: *Mid-span crack pattern of underside of sample at approximately end of CMA (δ=200mm).*

Sample E1

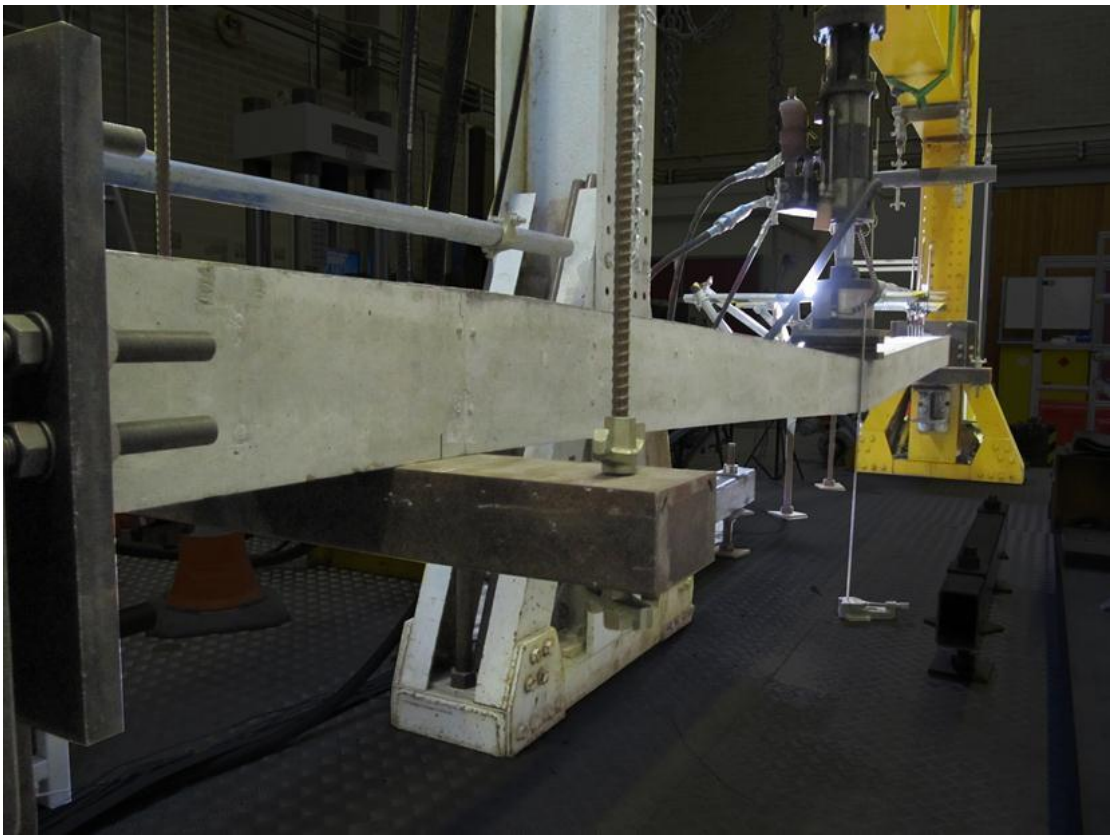

Figure A.6.5: *Full view of loaded sample at approximately H_{max} (δ=100mm).*

Figure A.6.6: *Mid-span crack pattern of underside of sample at approximately H_{max} (δ=100mm).*

Figure A.6.7: *Full view of loaded sample at end of CMA phase (δ=200mm).*

Figure A.6.8: *Crack pattern at support C at approximately end of CMA (δ=200mm).*

Figure A.6.9: *Mid-span crack pattern of underside of sample at approximately end of CMA (δ=200mm).*

A.7 Moment Capacity Calculations

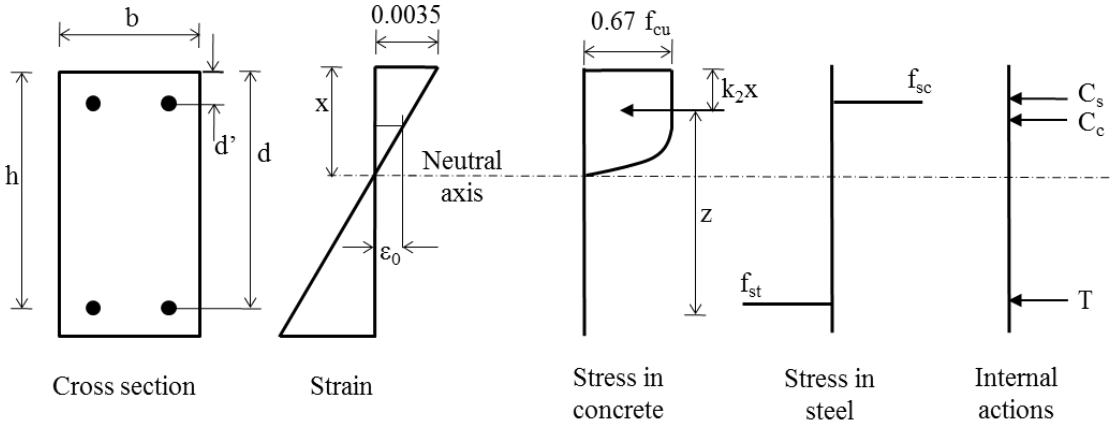

Figure A.7.1: *Conditions of stress and strain assumed at the ultimate limit state (BS 8110-3:1985 Appendix A Figure 1)*

To determine the moment of resistance of a doubly reinforced concrete section when the tension reinforcement reaches its yield stress (M_y) and when it reaches ultimate stress (M_u) the parabolic concrete stress block from BS:8110-3 has been assumed, Figure A.7.1.

Equilibrium of axial forces is found from:

$$N = C_c + C_s + T \qquad \text{A.5}$$

$$N = k_1 bx + A'_s f_{sc} + A_s f_{st} \qquad \text{A.6}$$

Where the concrete compressive force C_c at failure is given by:

$$\frac{0.67 f_{cu} bx}{0.0035}\left(0.0035 - \frac{\varepsilon_0}{3}\right) = k_1 bx \qquad \text{A.7}$$

Where ε_0 can be taken as:

$$\varepsilon_0 = 2.4 \times 10^{-4}\sqrt{f_{cu}} \qquad \text{A.8}$$

The equilibrium of moments, M, is found from:

$$M = k_1 bx\left({}^{h}/_{2} - k_2 x\right) + A'_s f_{sc}\left({}^{h}/_{2} - d'\right) + A_s f_{st}\left({}^{h}/_{2} - d\right) \qquad \text{A.9}$$

Where:

$$\left[\frac{\left(2-{}^{\varepsilon_0}/_{0.0035}\right)^2+2}{4\left(3-{}^{\varepsilon_0}/_{0.0035}\right)}\right]x = k_2 x \qquad \text{A.10}$$

The compressive and tensile stress of concrete can be determined from the strain once a value of neutral axis, x, has been assumed:

$$\varepsilon_{sc} = \frac{0.0035}{x}(x - d') \qquad \text{A.11}$$

$$\varepsilon_{st} = \frac{0.0035}{x}(d - x) \qquad \text{A.12}$$

$$f_{sc} = \varepsilon_{sc} E_s \qquad \text{A.13}$$

$$f_{st} = \varepsilon_{st} E_s \qquad \text{A.14}$$

When M_y is required $f_{st} = f_y$ and f_{sc} is limited to f_y, when M_u is required $f_{st} = f_{ult}$ and f_{sc} is limited to f_{ult}.

The neutral axis is determined by trial and error so that Equation A.6 is equal to 0.

A.8 Test Data and Predictions

Author	Slab No.	d [mm]	b [mm]	h [mm]	L [mm]	f_y [N/mm^2]	f_{cu} [N/mm^2]	f'_c [N/mm^2]	Ec [N/mm2]	A_s [%]	A'_s [%]	K [kN/mm]	L/d	Ultimate Load [kN]
Taylor	S1	104.00	475.00	150.00	1415.00	500.00	31.20	24.96	23631.07	0.68	0.68	414.74	13.61	135.00
	S2	104.00	475.00	150.00	1415.00	500.00	40.80	32.64	27023.17	0.68	0.68	414.74	13.61	145.00
	S3	104.00	475.00	150.00	1415.00	500.00	64.50	51.60	33977.08	0.68	0.68	414.74	13.61	175.00
	S4	104.00	475.00	150.00	1415.00	500.00	82.20	65.76	38356.77	0.68	0.68	414.74	13.61	187.00
	S5	104.00	475.00	150.00	1415.00	500.00	101.10	80.88	42538.45	0.68	0.68	414.74	13.61	192.00
Su et al	A1	274.00	150.00	300.00	2700.00	350.00	32.30	25.84	24044.04	0.55	0.55	1000.00	9.85	168.00
	A2	274.00	150.00	300.00	2700.00	350.00	35.30	28.24	25135.84	0.83	0.83	1000.00	9.85	221.00
	A3	273.00	150.00	300.00	2700.00	340.00	39.00	31.20	26420.34	1.13	1.13	1000.00	9.89	246.00
	A4	273.00	150.00	300.00	2700.00	340.00	28.80	23.04	22704.00	0.38	0.55	1000.00	9.89	147.00
	A5	274.00	150.00	300.00	2700.00	350.00	33.10	26.48	24339.98	0.55	0.83	1000.00	9.85	198.00
	A6	273.00	150.00	300.00	2700.00	340.00	35.80	28.64	25313.23	0.75	1.13	1000.00	9.89	226.00
	B1	273.00	150.00	300.00	4200.00	340.00	23.20	18.56	20377.46	1.13	1.13	1000.00	15.38	125.00
	B2	273.00	150.00	300.00	5600.00	340.00	24.10	19.28	20768.96	1.13	1.13	1000.00	20.51	82.90
	B3	273.00	150.00	300.00	5600.00	340.00	26.40	21.12	21737.43	0.75	1.13	1000.00	20.51	74.70
	C1	174.00	100.00	200.00	2700.00	350.00	19.90	15.92	18872.64	1.30	1.30	1000.00	15.52	60.90
	C2	174.00	100.00	200.00	2700.00	350.00	21.00	16.80	19387.23	1.30	1.30	1000.00	15.52	64.90
	C3	174.00	100.00	200.00	2700.00	350.00	20.40	16.32	19108.26	1.30	1.30	1000.00	15.52	68.60
Christiansen	1	66.70	152.40	76.20	1828.80	485.00	34.27	27.41	24765.31	0.62	NA	370.00	27.42	11.25
	2	66.70	152.40	76.20	1524.00	485.00	32.27	25.81	24031.92	0.62	NA	370.00	22.85	14.15
	3	79.40	152.40	88.90	1524.00	485.00	28.20	22.56	22466.08	0.62	NA	370.00	19.19	17.66
	4	79.40	152.40	88.90	1524.00	485.00	39.02	31.22	26428.58	0.62	NA	370.00	19.19	19.57
Roberts	RB10	43.30	229.00	51.00	1436.00	241.50	50.40	40.32	30034.57	0.56	NA	5198.00	33.16	28.39
	RB11	43.30	229.00	51.00	1436.00	241.50	24.70	19.76	21025.90	0.56	NA	5198.00	33.16	17.90
	RB12	43.30	229.00	51.00	1436.00	241.50	32.80	26.24	24229.42	0.74	NA	5198.00	33.16	24.45
	RB13	43.30	229.00	51.00	1436.00	241.50	30.20	24.16	23249.29	0.74	NA	5198.00	33.16	19.72
	RB14	43.30	229.00	51.00	1436.00	241.50	49.70	39.76	29825.27	0.74	NA	5198.00	33.16	28.11
	RB15	43.30	229.00	51.00	1436.00	241.50	24.10	19.28	20768.96	0.93	NA	5198.00	33.16	20.67
	RB17	43.30	229.00	51.00	1436.00	241.50	53.30	42.64	30886.57	0.93	NA	5198.00	33.16	25.57

	RB18	68.30	229.00	76.00	1436.00	241.50	27.00	21.60	21983.05	0.58	NA	5198.00	21.02	32.78
	RB19	68.30	229.00	76.00	1436.00	241.50	28.70	22.96	22664.55	0.58	NA	5198.00	21.02	40.12
	RB20	68.30	229.00	76.00	1436.00	241.50	47.90	38.32	29280.19	0.58	NA	5198.00	21.02	52.99
	RB21	68.30	229.00	76.00	1436.00	241.50	18.10	14.48	17998.88	0.92	NA	5198.00	21.02	30.39
	RB22	68.30	229.00	76.00	1436.00	241.50	30.20	24.16	23249.29	0.92	NA	5198.00	21.02	37.97
	RB23	68.30	229.00	76.00	1436.00	241.50	56.30	45.04	31743.90	0.92	NA	5198.00	21.02	56.49
Punton & Smith	C1	128.00	320.00	160.00	4050.00	500.00	62.89	50.31	33549.20	0.49	0.49	60.31	31.64	17.50
	C2	108.00	320.00	140.00	4320.00	500.00	70.09	56.07	35418.19	0.44	0.44	60.31	40.00	11.73
	C3	91.00	320.00	118.00	4550.00	500.00	69.17	55.33	35184.76	0.35	0.35	60.31	50.00	5.26
	C4	83.00	320.00	110.00	5000.00	500.00	47.21	37.77	29069.30	0.38	0.38	60.31	60.24	3.88
	M2	118.00	320.00	145.00	4720.00	500.00	57.50	46.00	32080.42	0.21	0.21	60.31	40.00	8.45
	M3	78.00	320.00	105.00	3900.00	500.00	51.57	41.26	30381.61	0.20	0.20	60.31	50.00	4.08
	A	75.00	275.00	90.00	5000.00	500.00	54.60	43.68	31260.97	0.24	0.24	60.31	66.67	1.54
	S1	75.00	275.00	90.00	5000.00	500.00	70.48	56.38	35517.23	0.49	0.49	60.31	66.67	2.99
	S2	75.00	275.00	90.00	5000.00	500.00	49.33	39.46	29713.61	0.73	0.73	60.31	66.67	4.66
	E1	143.00	225.00	175.00	5000.00	500.00	66.15	52.92	34408.92	0.31	0.70	60.31	34.97	13.14
	E2	143.00	225.00	175.00	5000.00	500.00	41.19	32.95	27150.60	0.47	1.05	60.31	34.97	16.80
	E3	144.00	320.00	175.00	5000.00	500.00	54.21	43.37	31149.84	0.51	1.31	60.31	34.72	25.36

Table A.8.1: *Sample properties and ultimate load of experimental data.*

Author	Slab No.	L/d	Actual [kN]	Rankin & Long [kN]	Merola [kN]	R&L Pt/Pp	Merola Pt/Pp
Taylor	S1	13.61	135.00	124.30	142.25	1.09	0.95
	S2	13.61	145.00	135.30	160.74	1.07	0.90
	S3	13.61	175.00	151.90	197.37	1.15	0.89
	S4	13.61	187.00	159.60	210.69	1.17	0.89
	S5	13.61	192.00	166.98	219.43	1.15	0.87
Su et al	A1	9.85	168.00	204.11	233.98	0.82	0.72
	A2	9.85	221.00	267.42	303.35	0.83	0.73
	A3	9.89	246.00	335.31	362.96	0.73	0.68

	A4	9.89	147.00	177.95	204.47	0.83	0.72
	A5	9.85	198.00	233.72	267.75	0.85	0.74
	A6	9.89	226.00	289.42	329.58	0.78	0.69
	B1	15.38	125.00	118.58	204.29	1.05	0.61
	B2	20.51	82.90	60.36	151.80	1.37	0.55
	B3	20.51	74.70	55.47	137.75	1.35	0.54
	C1	15.52	60.90	53.27	100.41	1.14	0.61
	C2	15.52	64.90	54.34	102.00	1.19	0.64
	C3	15.52	68.60	53.76	101.14	1.28	0.68
Christiansen	1	27.42	11.25	10.34	9.51	1.09	1.18
	2	22.85	14.15	12.91	11.71	1.10	1.21
	3	19.19	17.66	17.87	14.77	0.99	1.20
	4	19.19	19.57	19.97	17.73	0.98	1.10
Roberts	RB10	33.16	28.39	19.14	19.31	1.48	1.47
	RB11	33.16	17.90	14.37	11.37	1.25	1.57
	RB12	33.16	24.45	19.95	14.77	1.23	1.66
	RB13	33.16	19.72	19.35	13.93	1.02	1.42
	RB14	33.16	28.11	22.99	19.90	1.22	1.41
	RB15	33.16	20.67	19.93	12.72	1.04	1.62
	RB17	33.16	25.57	25.98	21.71	0.98	1.18
	RB18	21.02	32.78	34.39	31.61	0.95	1.04
	RB19	21.02	40.12	35.68	33.06	1.12	1.21
	RB20	21.02	52.99	48.59	48.64	1.09	1.09
	RB21	21.02	30.39	31.93	27.88	0.95	1.09
	RB22	21.02	37.97	41.85	38.26	0.91	0.99
	RB23	21.02	56.49	59.02	56.30	0.96	1.00
Punton & Smith	C1	31.64	17.50	23.84	24.45	0.73	1.43

	C2	40.00	11.73	14.35	21.53	0.82	1.09
	C3	50.00	5.26	6.96	11.16	0.76	0.94
	C4	60.24	3.88	5.11	7.03	0.76	1.10
	M2	40.00	8.45	7.09	15.12	1.19	1.12
	M3	50.00	4.08	3.48	7.50	1.17	1.09
	A	66.67	2.99	4.80	6.17	0.62	1.01
	S1	66.67	4.66	7.35	8.23	0.63	1.13
	S2	66.67	1.54	1.87	3.50	0.82	0.88
	E1	34.97	13.14	18.17	25.61	0.72	1.03
	E2	34.97	16.80	25.16	32.05	0.67	1.05
	E3	34.72	25.36	43.23	35.70	0.59	1.42

Table A.8.2: *Comparison of experimental data and predicted values.*

A.9 Rankin and Long (1997) Example Calculation

An example prediction of ultimate strength for a 1m wide slab strip with a span to depth ratio of 37 with the following properties is give n in this section:

f_{cu} =	40 N/mm^2	h =	300 mm
f'_c =	32 N/mm^2	d =	270 mm
f_y =	460 N/mm^2	L =	10 m
ρ =	0.001309	L_E =	5 m

Bending Capacity

$$M_b = 0.001309 \times 460 \times 270^2 \left(1 - 0.59\frac{0.001309 \times 460}{32}\right)$$

$$= 43.41\text{kNm}$$

$$k = \frac{8}{L} = 0.8$$

$$Pb = k(M_b + M'_b) = 69.45\text{kN}$$

Area of Concrete Available to Arching

$$2d_1 = 300 - (0.001309 + 0.001309)\frac{460 \times 270}{0.85 \times 32}$$

$$d_1 = 144.023\text{ mm}$$

Half Span of Equivalent Rigidly-Restrained Strip

$$E_c = 4730\sqrt{32} = 26756.921\ (\text{N/mm}^2)$$

$$K = \frac{26756.921 \times 144.023}{5} = 770{,}722$$

$$\alpha = 1.0$$

$$L_r = 5000\left[\frac{26756.921 \times 144.023 \times 0.845 \times 1000}{770722 \times 5000} + 1\right]^{1/3}$$

$$= 6132.47\text{mm}$$

Geometric and Material Property for Arching

$$e_c = (-400 + 60 \times 32 - 0.33 \times 32^2) \times 10^{-6} = 0.0011821$$

$$R = \frac{e_c \times 6132.47^2}{4 \times 144.023^2} = 0.536$$

Arching Deflection Parameter

$$R > 0.26 \ \therefore u = 0.31$$

Contact Depth

$$\alpha = 1 - \frac{0.31}{2} = 0.845$$

$$\alpha d_1 = 121.699$$

When u is constant at 0.31 no iterations are needed

Arching Capacity

R>0.26

$$M_r = \frac{0.3615}{0.5355} = 0.675$$

$$M_a = \frac{0.675 \times 0.85 \times 32 \times 144.023^2}{4} \times \frac{5000}{6132.47} = 77.62\text{kNm}$$

$$M_{ar} = \frac{0.675 \times 0.85 \times 32 \times 144.023^2}{4} = 95.21\text{kNm}$$

$$\frac{M_a}{M_{ar}} = 0.815$$

$$P_a = kM_a = \frac{8}{10} \times 77.62 = 62.096\text{kN}$$

Enhanced Ultimate Load

$$P_p = P_b + P_a = 131.546\text{kN}$$

$$= 13.15\text{kN/m}$$

A.10 Merola (2009) Example Calculation

An example prediction of ultimate strength for a 1m wide slab strip with a span to depth ratio of 37 with the following properties is give n in this section:

f_{cu} =	40 N/mm^2	h =	300 mm
f'_c =	32 N/mm^2	d =	270 mm
f_y =	460 N/mm^2	L =	10 m
A_s =A'$_s$=	351 mm^2/m	L_o =	5 m

Stiffness Parameters

$$E_c = 4730\sqrt{32} = 26756.92 \text{ N/mm}^2$$

$$S = \frac{bhE_c}{L_o} = \frac{1000 \times 300 \times 26756.92}{5000} = 1605415.2 \text{ N/mm}^2$$

Forces

$$C_1 + F'_{s1} - F_{s1} = C_2 + F'_{s2} - F_{s2}$$

Where $\gamma_s = 1$

$$F_{s1} = F_{s2} = 351 \times \frac{460}{1} = 161460 \text{ N}$$

$$F'_{s1} = F'_{s2} = 351 \times \frac{460}{1} = 161460 \text{ N}$$

$$\beta_1 = 0.85 - \big((32 - 30) \times 0.008\big) = 0.834$$

Where $\alpha_{cc} = 0.85$ and $\gamma_c = 1.2$ (Accidental loading state)

$$f_{cd} = \frac{0.85 \times 32}{1.2} = 22.67 \text{ N/mm}^2$$

Where η =1 and $\lambda = 0.8$

$$C_1 = 1 \times 22.67 \times 0.8 \times 1000 \times x_1 = 18133.33x_1$$

$$C_2 = 1 \times 22.67 \times 0.8 \times 1000 \times x_2 = 18133.33x_2$$

As previously stated the procedure requires increments of deflection δ to be assumed, for the purpose of this example calculation a values of $\delta = 10$ will be taken.

$$\left(\frac{1}{\mathrm{bhE_c}} + \frac{2}{\mathrm{LS}}\right) = \left(\frac{1}{1000 \times 300 \times 26756.9} + \frac{2}{10000 \times 1605415.2}\right)$$
$$= 2.5 \times 10^{-10}$$

$$\left[\frac{\mathrm{h}}{2} - \frac{\delta}{4} - \frac{\mathrm{F_{s1}} - \mathrm{F_{s2}} - \mathrm{F'_{s1}} + \mathrm{F'_{s2}}}{\eta \mathrm{f_{cd}} \lambda \mathrm{b}}\right]$$
$$= \left[\frac{300}{2} - \frac{10}{4} - \frac{161460 - 161460 - 161460 + 161460}{1 \times 22.67 \times 0.8 \times 1000}\right] = 147.5$$

$$\varepsilon + \frac{2\mathrm{t}}{\mathrm{L}} = \frac{2.5 \times 10^{-10} \times \{1 \times 22.67 \times 0.8 \times 1000 \times [147.5]\}}{1 + (2.27 \times 10^{10} \times 2.5 \times 10^{-10})}$$
$$= 1.00 \times 10^{-4}$$

$$\mathrm{x_1} = 147.5 - \left(\frac{0.5 \times 10000^2}{4 \times 10} \times 1.0 \times 10^{-4}\right) + 0 = 22.5\mathrm{mm}$$

$$x_1 = x_2 = 22.5mm$$

Hence:

$$\mathrm{N_{u2}} = \mathrm{N_u} = 18133.33 \times 22.5 + 161460 - 161460 = 408\ \mathrm{kN}$$

$$\mathrm{M_{u1}} = \mathrm{M_{u2}} = 18133.33 \times 22.5\left(150 - 0.5\frac{0.8}{2}22.5\right)$$
$$+ 161460(150 - 30) + 161460(150 - 30)$$
$$= 98.11\ \mathrm{kNm}$$

The sum of moments about the mid depth at one side of yield section is, for a point load:

$$\mathrm{P} = 8\ \times \frac{(98.11 \times 10^6 + 98.11 \times 10^6 - 408 \times 10^3 \times 10)}{10^2}$$
$$= 15.4\mathrm{kN/m}$$

A.11 Iterative process used to define horizontal loading pattern

1. *Definition of Maximum Deflection*

The short sides of the structural bay (the double bay after the removal of the column) are split into 250mm wide strips. The perimeter (free edge) strip is then assessed with a constant initial input stiffness, K1, equal to when k_1 =1.0 as described in Chapter 4. The peak enhanced load from CMA is highlighted and the corresponding mid span deflection, δ_{max}, noted (Figure A.11.1). This can be considered the maximum midspan deflection before snap-through occurs.

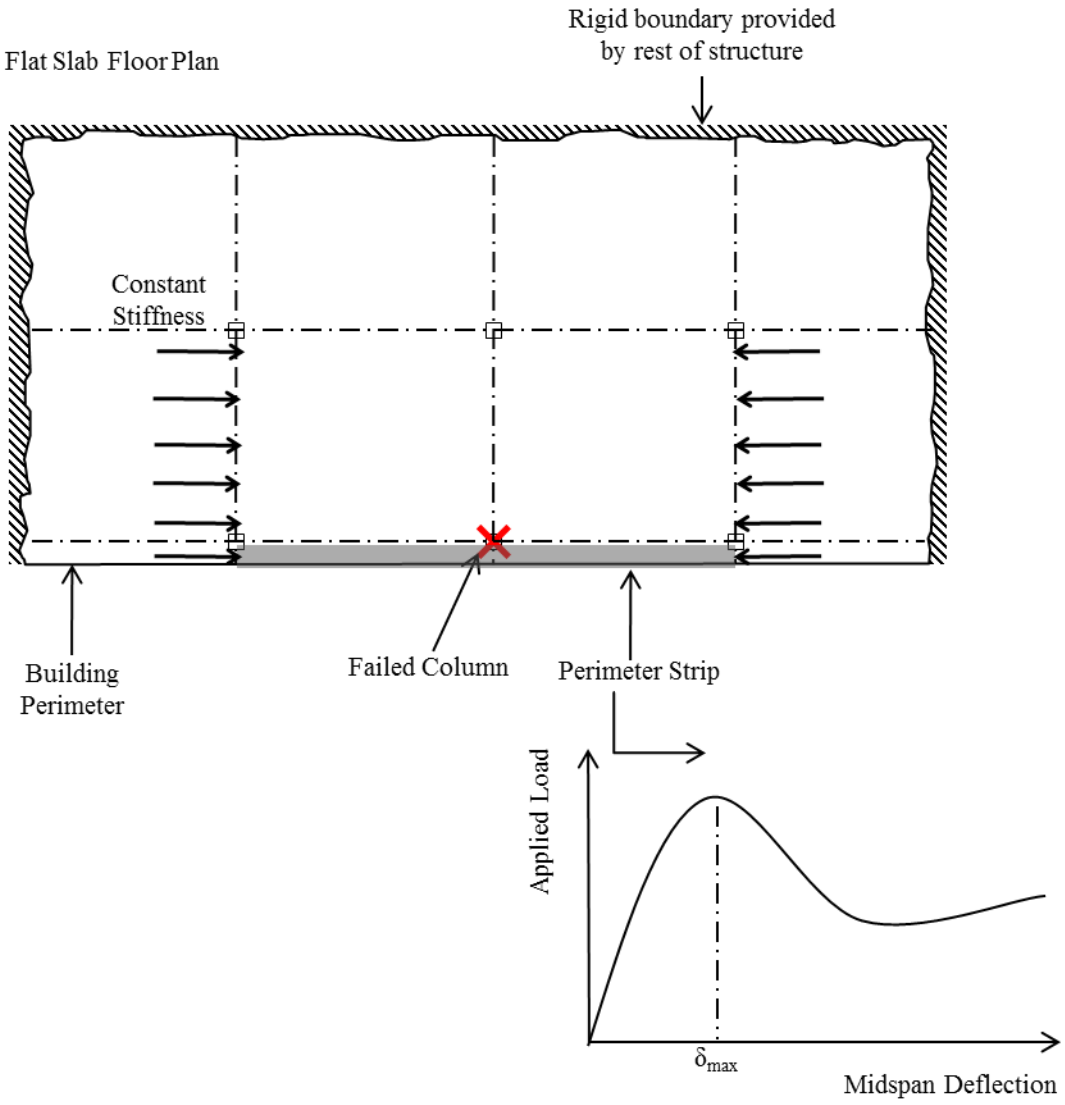

Figure A.11.1: *Applied constant stiffness to determine maximum mid-span deflection.*

2. *Calculation of Deep Beam Cantilever Deflection*

The short sides from y = L_o to y = 0 and divided into 250mm wide sections is then investigated. The deflection of the perimeter strip is set to δ_{max} and a linear relationship is then assumed across the slab depth to zero deflection at x = 0, as in Figure A.11.2

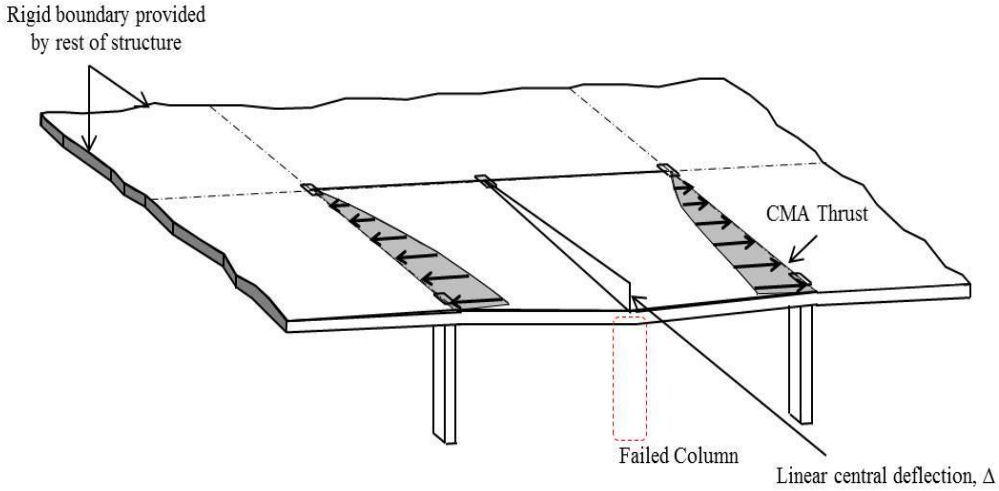

Figure A.11.2: *Assumed linear mid-span deflection across depth of bay when column fails.*

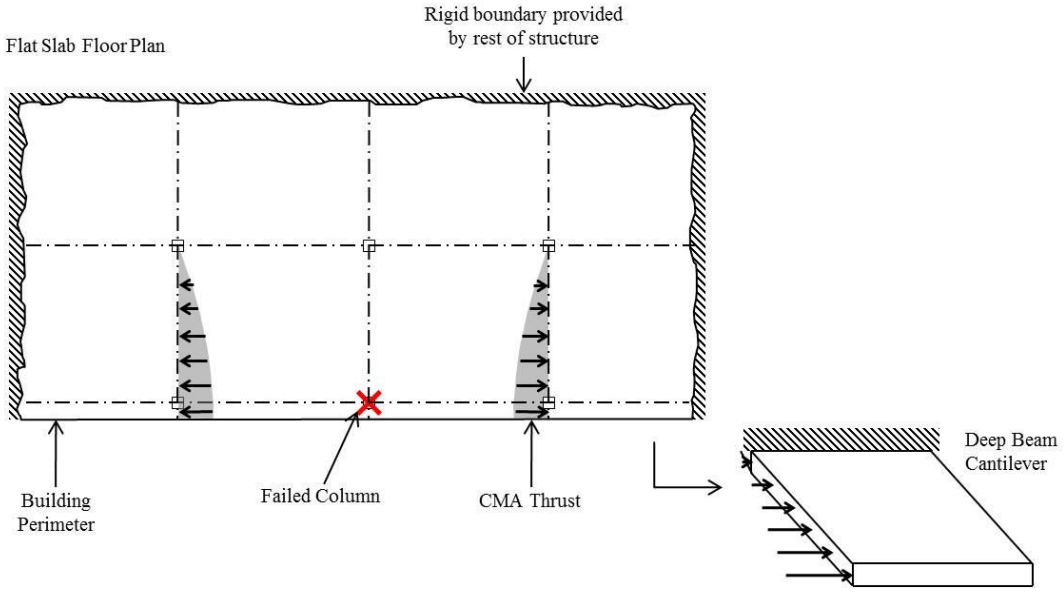

Figure A.11.3: *Deep beam cantilever assumption of flat slab restraint stiffness.*

The compressive horizontal thrust creates a distribution of load in the form of a curve with maximum at the perimeter (removed) column line. This is applied in a deep beam cantilever analysis of the adjacent structural bay, Figure A.11.4. The deflection of the cantilever is calculated in two components; flexure and shear.

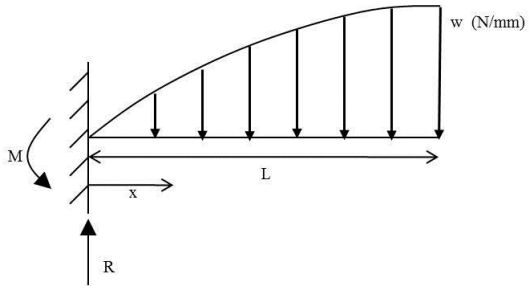

Figure A.11.4: *Curved load distribution on cantilever.*

Flexural Deflection

The curve can be defined as a 4th order polynomial, $f(x) = Ax^4 + Bx^3 + Cx^2 + Dx$.The reaction force R is equal to the area under the curve, $\int_0^L f(x)dx$ .The fixed end moment M can be found from $R\bar{x}$ where $\bar{x}$ is the centroid of the area under the curve. An expression can easily be developed for the moment M_x at point x on the cantilever. Double integration can then be used to find the flexural deflection, Δ_f:

$$\Delta_f = -\frac{1}{EI}\left(\left(\frac{AL^5x^3}{30}+\frac{BL^4x^3}{24}+\frac{CL^3x^3}{18}+\frac{DL^2x^3}{12}\right)-\left(\frac{AL^6x^2}{12}+\frac{BL^5x^2}{10}+\frac{CL^4x^2}{8}+\frac{DL^3x^2}{6}\right)-\left(\frac{Ax^8}{280}+\frac{Bx^7}{168}+\frac{Cx^6}{90}+\frac{Dx^5}{40}\right)+\left(\frac{Ax^8}{336}+\frac{Bx^7}{210}+\frac{Cx^6}{120}+\frac{Dx^5}{60}\right)\right) \quad \text{A.15}$$

A, B, C and D are constants depending on the shape of the curve to be determined from solving a set of simultaneous equations.

Shear Deflection

The effect of shear deflection is often neglected in elastic calculations however with deep beams under significant loading the contribution from shear deflections will be significant. From the parameters used in this analysis the shear deflection contributes approximately 25% of the total deflection.

$$\Delta_s = F\int \frac{Vv}{AG}dx$$

Where $V = \frac{wx^2}{2L}$

v is the vertical shear due to a unit load acting at the section where the deflection is required

$$= F\int \frac{wx^2}{2LAG}dx$$

$$\Delta_s = \frac{1}{6}F\frac{wx^3}{LAG} \quad \text{A.16}$$

Where A is the cross sectional area, $b \times d$

F is a factor depending on the form of the cross section and for a rectangular cross section $F = \frac{6}{5}$

and

$$G = \frac{E}{2(1+v)} \qquad \text{A.17}$$

Poisons ratio v is assumed to be 0.2

Thus the total deflection Δ_t is calculated by summing the flexural and shear deflections:

$$\Delta_t = \Delta_f + \Delta_s \qquad \text{A.18}$$

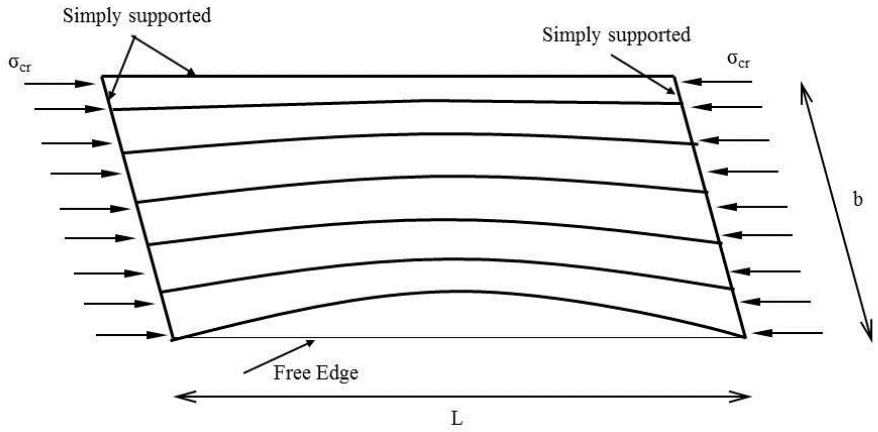

Figure A.11.5: *Buckling pattern of a plate free along one edge*

To ensure the slab does not fail due to buckling under the load from CMA the critical buckling stress has been calculated assuming for simplicity the boundary condition depicted in Figure A.11.5. The slab is treated as a plate element under uniform compression with one free edge representing the perimeter of the flat slab. The critical buckling stress σ_{cr} is calculated from, Allen and Bulson (1980) :

$$\sigma_{cr} = \frac{\pi^2 E}{12(1-v^2)} \frac{k_b}{\left(b/t\right)^2} \qquad \text{A.19}$$

Where t is the slab thickness and $k_b$is the buckling coefficient found from:

$$k_b = 0.425 + \left(\frac{b}{L}\right)^2 \qquad \text{A.20}$$

When $b = L$

$$k_b = 1.425 \quad \text{A.21}$$

Therefore as long as the stress produced by CMA is less that the critical buckling stress the slab will not buckle, hence;

$$if\ \frac{w}{b} < \sigma_{cr} \quad \therefore slab\ safe\ from\ buckling \quad \text{A.22}$$

3. *Output Stiffness Calculation*

The stiffness provided by each slab strip can be calculated from dividing the compressive thrust by the deflection, providing an output stiffness K_2.

4. *Iterative Stiffness Process*

The output stiffness K_2 can then be used as the input stiffness i.e. $K_1 = K_2$. An iterative process is then used until the input and output stiffness are equal and the final stiffness, K, of each slab strip is given i.e. $K_1=K_2=K$.

A.12 Investigation into the age of buildings at the time of attack

	Building	Year Built	Year of attack on building	Age of building at time of attack
1	Murrah Building, Oklahoma	1974	1995	21
2	WTC 1&2, New York	1970	2001	31
3	Khobar Towers, Saudi Arabia	1979	1996	17
4	99 Bishopsgate, London	1976	1993	17
5	WTC, New York	1970	1993	23
6	HSBC Bank, Turkey	1990	2003	13
			Average age =	**20**

Table A.12.1: *Summary of building age at the time of attack*

References

1 Osteraas, J. D. (2006) "Murrah Building Bombing Revisited: A Qualitative Assessment of Blast Damage and Collapse Patterns" Journal of Performance of Constructed Facilities November 2006, ASCE 330-335

Sozen, M. A., C. H. Thornton, W. G. Corley and P. F. Mlakar (1998). "The Oklahoma City Bombing: Structure and Mechanisms of Murrah Building." Journal of Performance of Constructed Facilities August 1998, ASCE: 120-136.

2 National Institute of Standards and Technology NIST (2007). "Best Practices for reducing the potential for progressive collapse in buildings."

3 "Khobar Towers" - Available at http://www.globalsecurity.org/military/facility/khobar.htm

4 "The Bishopsgate Bombing" - Available at http://www.independent.co.uk/news/the-bishopsgate-bomb-one-bomb-pounds-1bn-devastation-man-dead-after-city-blast--two-more-explosions-late-last-night-1457397.html, http://en.wikipedia.org/wiki/1993_Bishopsgate_bombing

5 National Institute of Standards and Technology NIST (2007). "Best Practices for reducing the potential for progressive collapse in buildings.", "Remembering the 1993 World Trade Centre Bombing" - Available at http://www.history.com/news/remembering-the-1993-world-trade-center-bombing

6 "Istanbul rocked by double bombing" Available at http://news.bbc.co.uk/1/hi/world/europe/3222608.stm, "HSBC Bank Turkey" Available at http://en.wikipedia.org/wiki/HSBC_Bank_(Turkey)